Taylor, B., Huchon, P., Klaus, A., et al., 1999
Proceedings of the Ocean Drilling Program, Initial Reports Volume 180

9. SITE 1115[1]

Shipboard Scientific Party[2]

SITE 1115

Hole 1115A (APC [advanced hydraulic piston corer]):
9°11.389′S, 151°34.450′E; 1149.6 mbsl (meters below sea level)
0–4.40 mbsf cored; 4.43 m recovered (101%)
Hole 1115B (APC/XCB [extended core barrel]):
9°11.382′S, 151°34.437′E; 1148.8 mbsl
0–293.10 mbsf cored; 286.84 m recovered (98%)
Hole 1115C (RCB [rotary core barrel]):
9°11.383′S, 151°34.422′E; 1148.7 mbsl
0–283.5 mbsf drilled without coring; 283.2–802.5 mbsf cored; 291.63 m recovered (56%)

The objectives of our study at Site 1115 were to determine the sedimentology, biostratigraphy, and vertical motion history of the Woodlark Rise (the northern, upper plate margin to the Moresby detachment fault), including the prerift history of the Trobriand forearc basin sequence. The site was located ~35 km to the north of Site 1109 to (1) better characterize the slope sediments and provide widely spaced data from shallower water depths for flexural subsidence models, (2) avoid the thick dolerite that prevented sampling of the prerift forearc sequence at Site 1109, and (3) sample the upper ~150 m of section that has been eroded by a submarine channel further south.

From bottom to top, the sedimentary succession cored at Site 1115 shows (1) a shoaling and coarsening upward, middle Miocene forearc sequence, unconformably below (2) a late Miocene nonmarine coastal (fluvial?) and lagoonal succession, and (3) a shallow marine, then progressively deepening and fining upward, latest Miocene (5.54 Ma) to Pleistocene sequence related to the subsidence of the margin during the rifting of the Woodlark Basin. The synrift sequence is undeformed, with

[1]Examples of how to reference the whole or part of this volume.
[2]Shipboard Scientific Party addresses.

Ms 180IR-109

bedding dips <10° throughout, whereas the forearc sequence below exhibits a few normal, reverse, and strike-slip faults.

We cored the upper ~230 m of the >2-km-thick Trobriand forearc basin sequence. This section was deposited at >135 m/m.y. and is older than 12.1 Ma and younger than 15.1 Ma. The sequence comprises turbiditic sands, silts, and clays derived from calc-alkaline arc sources including distinctive clinopyroxene-phyric basic extrusives. The turbidites below 615 mbsf were deposited in upper bathyal depths (150–500 m). The turbidites above 659 mbsf were joined by redeposited neritic carbonates and deposits marked by sediment instability, possibly related to local channeling and/or regional tectonism. Benthic foraminifers indicate a change to neritic deposition (50–150 m) above 615 mbsf and by 13.6 Ma. The sediments record substantial input of shallow-water carbonate. The upward shallowing of the forearc sequence may be attributed to both filling of the basin and tectonic uplift.

An unconformity and hiatus at 574 mbsf resulted from the emergence of the forearc sequence. The unconformity is seismically imaged throughout the Trobriand forearc basin and is younger than 9.63 Ma at the Nubiam-1 well ~100 km to the northwest. At Site 1115, the unconformity is older than 5.54 Ma, by which time sediments younger than 8.6 Ma had accumulated to 513 mbsf at rates >13 m/m.y. The basal sediments above the unconformity are nonmarine (fluvial?) conglomerate (to 566 mbsf), topped by an organic-rich silty claystone (inner lagoonal), and capped by a siltstone with common to abundant shell fragments (open-marine lagoonal).

Margin subsidence is recorded by inner neritic (<50 m) sandy siltstone (to 475 mbsf) passing upward to silty sandstone (to 417 mbsf) deposited on an open shelf (50–150 m) influenced by traction currents. Sedimentation rates from 4.0–5.5 Ma averaged 45 m/m.y.

From 4.0 to 3.0 Ma, the average sediment accumulation dramatically increased to ~284 m/m.y. This resulted in undercompaction and anomalously high measured porosities between ~420 and ~300 mbsf. Above 417 mbsf, turbidites were deposited in deeper water, upper bathyal (150–500 m), and they fine upward from sandy silty claystone to silty claystone. Volcaniclastic sand and silt horizons, originating from a calc-alkaline arc source, remain little changed throughout the Pliocene section. The pelagic carbonate component increases above 300 mbsf with $CaCO_3$ concentrations increasing from ~20 to ~75 wt% at the seafloor.

Since 3.0 Ma the sedimentation rate markedly slowed, initially to ~79 m/m.y. (to 2.0 Ma) and then ~59 m/m.y. (to 0.5 Ma) and ~34 m/m.y. thereafter. The marked change in the sediment supply to the area corresponds in part to a decrease in the volcaniclastic sand deposited by turbidity currents. Above 169 mbsf (2.58 Ma), the input of fine metamorphic detritus marked by the presence of illite to 520 mbsf also ends. By this time and since then, the sedimentation rate was much slower than the margin subsidence and the surface deepened to upper middle bathyal (500–1150 m) depths. No record of the last 120 k.y. is preserved, and this may be responsible for the low porosities (65%–70%) near the surface. Pleistocene sedimentation was dominated by nannofossil ooze with volcanic ash. The Pleistocene volcanic ash fallout layers and middle–late Pliocene volcanogenic turbidites record a marked increase in explosive Trobriand Arc volcanism since 3.7 Ma.

The thermal gradient determined from five temperature measurements between 26 and 227 mbsf is $28°C \cdot km^{-1}$, yielding a heat flow of $28\ mW \cdot m^{-2}$ given the average thermal conductivity measured on cores from this interval of $1\ W \cdot m^{-1} \cdot °C^{-1}$.

The magnetostratigraphic record of the upper 400 m is very good. The Brunhes/Matuyama/Gauss/Gilbert polarity transitions, and the Jaramillo, Olduvai, and Kaena Subchrons are identified, as are the Cobb Mountain and Reunion events. Very low magnetic susceptibilities characterize the intervals 210–410 mbsf and 480–550 mbsf, without apparent correlation to grain size, lithology, or sedimentation rate. The variation of susceptibility with depth observed at Site 1115 between 120 and 550 mbsf is similar to that observed at Site 1109 between 80 and 705 mbsf, and the susceptibility boundaries at both sites are time correlative.

Hole 1115C was successfully logged above 784 mbsf with triple combo geophysics and FMS-sonic tool strings. The well seismic tool was used to record check shots near the base of the hole, allowing depth correlation with seismic reflection lines.

The longest profile to date of the deep subseafloor biosphere was made at this site. Bacteria were present in the deepest sample analyzed (801 mbsf) and both dividing and divided cells were present to 775 mbsf. The persistence of apparently living microbial life into indurated sedimentary rock ~15 m.y. old and to 801 mbsf extends the limit of the biosphere whose base remains undefined. Methane is present at levels above 1000 ppm from 250 to 450 mbsf and above 20,000 ppm from 572 to 802 mbsf. The C_1/C_2 ratios generally exceed 1500 and 3000 over the same intervals, and broad maxima in ammonia are found within 200–450 mbsf and at the base of the hole. These observations are consistent with a biogenic origin for the volatile hydrocarbons and the presence of a significant amount of bacteria at depth.

High-resolution pore-water sampling (63 whole rounds) comprehensively documents the interstitial water chemical variations. In the upper 300 mbsf of the cored section, pore-water variations primarily reflect the oxidation of organic matter and the concomitant early diagenesis of biogenic carbonate (including aragonite) leading to precipitation of dolomite, as well as alteration of detrital, mostly volcanic, matter. Further downhole, most of the pore-water variations are controlled largely by the alteration of volcanic minerals and the formation of clays and zeolites. Silicification appears to be a dominant process below 500 mbsf. The formation of calcite cements is significant in sediments of the forearc sequence.

OPERATIONS

Transit to Site 1115 (ACE-15A)

After the ~36 nmi (~3.75 hr) transit to Site 1115 (ACE-15A), a positioning beacon was deployed at the Site 1115 GPS coordinates at 1145 hr on 16 July 1998.

Hole 1115A

After preparing an advanced hydraulic piston corer (APC) coring assembly and lowering it to the seafloor, we spudded Hole 1115A at 1510 hr on 16 July. The single APC core taken in Hole 1115A recovered 4.43 m; therefore, the seafloor was 1149.6 meters below sea level (mbsl) (Tables T1, T2). The bit was pulled clear of the mudline immediately ending Hole 1115A, Core 1H was recovered, and the pipe was spaced out for spudding Hole 1115B.

T1. Coring summary, p. 163.

T2. Coring summary by section, p. 166.

Hole 1115B

At 1540 hr, Hole 1115B was spudded and Core 1H recovered 7.14 m establishing the seafloor depth at 1148.8 mbsl. Cores 1H through 23H were taken to 216.2 mbsf. Core orientation (tensor tool) was performed on Cores 4H–23H and Adara temperature measurements were taken while obtaining Cores 3H (26.2 mbsf), 5H (45.2 mbsf), 7H (64.2 mbsf), and 9H (83.2 mbsf). The APC coring was suspended after Core 23H when 70,000-lb overpull was required to extract the core barrel from the formation. The APC core recovery was 225.67 m (104%).

Use of the extended core barrel (XCB) began with Core 24X and continued through Core 31X to a depth of 1453.4 m or 293.1 mbsf. A single Davis-Villinger Temperature Probe (DVTP) temperature measurement was taken after Core 23X at a depth of 225.7 mbsf. Hole conditions remained excellent as did the rate of penetration (ROP), which averaged 19.2 and 38.4 m/hr, respectively, on the last two cores. Recovery for the XCB portion of the hole was 80%. The hole was terminated after Core 31X because the formation had become indurated enough for successful rotary core barrel (RCB) coring, and because this section would have to be drilled again in Hole 1115C. Total recovery for the hole was 286.84 m (98%).

The drill string was pulled clear of the seafloor at 1415 hr on 17 July and the bit cleared the rig floor at 1615 hr that same day, ending Hole 1115B.

Hole 1115C

While we assembled the RCB bottom-hole assembly (BHA), the ship was offset 30 m to the west. The drill string was lowered to the seafloor and Hole 1115C was spudded at 2130 hr on 17 July. A seafloor depth of 1148.7 mbsl was established based on a reduction in drill string weight. With a center bit in place, the hole was drilled without coring to 283.2 mbsf. The hole was flushed clean and the center bit recovered, preparing the way for RCB coring.

The RCB coring began at 0400 hr on 18 July 1998 and continued through Core 54R to 802.5 mbsf. Coring was terminated when the scientists considered that the primary scientific objectives had been achieved. Two zones of low recovery were encountered: 7% from 523.0 to 542.2 mbsf and 1%–2% from 628.8 to 657.8 mbsf. Bentonite gel mud sweeps (30 bbl each) were pumped every third core, and hole conditions remained excellent throughout the coring operations. Penetration rates were quite variable, ranging from 5.8 m/hr to 57.6 m/hr and averaged 18.0 m/hr. Total RCB core recovery was 291.63 m (56.2%).

A wiper trip, up to 99.7 mbsf and then back to the bottom, identified tight spots at 701.7 and 762.7 mbsf where the driller observed 40,000 lb overpull. The bit encountered 15 m of fill in the bottom of the hole, which we decided not to spend the time washing, reaming, and circulating out of the hole. The bit was released, the hole displaced with 215 bbl of sepiolite mud, and the drill pipe positioned at 99.7 mbsf in preparation for logging.

We began rigging up for logging at 0500 hr on 21 July and the first logging run consisted of the triple combo. The suite of tools reached a depth of 783.7 mbsf, which was 4.0 m above where the bit was released. The second tool string (Formation MicroScanner [FMS] sonic) also reached the same depth. Two logging passes were made with the FMS before pulling it out of the hole. The third logging string run was with

the ultrasonic borehole imager (UBI). This tool was put aboard ship by Schlumberger in lieu of a second borehole televiewer (BHTV) tool. The UBI is another form of borehole imager used extensively in industry, but this was the first time this tool had been deployed for the Ocean Drilling Program (ODP). The tool reached the same depth as the previous tool runs but, unfortunately, did not function correctly. It was recovered without obtaining any data. The final logging run was with the well seismic tool (WST), but it failed to pass a bridge at 564.7 mbsf (probably because of its light weight). An air gun was deployed using the aft port side crane and several stations were successfully occupied until the logging run had to be aborted because of an expected helicopter landing. During helicopter landings, the cranes must not be deployed for safety reasons. At 0600 hr, the WST was pulled up inside the pipe, the air gun was rigged down, and the crane used to deploy the air gun was retracted. The helicopter was bringing out a reporter from the Australian Broadcasting Commission (ABC) and a roustabout who had recovered from illness after having been evacuated from the ship earlier in the leg. We were notified by the ship's agent in Papua New Guinea (PNG) that the helicopter would depart Alotau at ~0630 hr on 22 July and would arrive on location within 30 min. By 0730 hr the helicopter had still not arrived and the radio officer made several unsuccessful attempts to contact the helicopter via radio. He was able to hear conversations between other airborne helicopters, but was not able to contact the helicopter destined for the *JOIDES Resolution*. At ~0845 hr the ship received a phone call from the agent that the helicopter had gone to the wrong site coordinates. Unable to locate the ship the helicopter had returned to Alotau. At ~0900 hr we resumed vertical seismic profile (VSP) logging operations. Subsequent VSP stations were not as successful as those earlier because of an unidentified source of noise in the system. After attempts to isolate and fix the cause of the noise, the VSP was terminated. The WST was pulled out of the hole and the air guns rigged down. All logging operations were completed and the tools rigged down by 1345 hr on 22 July.

The open-ended drill pipe was lowered to 483.7 mbsf, and the hole was displaced with 100 bbl of 10.5-ppg weighted gel mud. The drill string was pulled clear of the seafloor at 1630 hr and the positioning beacon was recovered at 1745 hr. After recovering the drill string, the BHA drill collars and associated subs were subjected to the routine end of leg inspection for cracks (none were identified). Once the BHA inspection was completed, the final thruster was raised and we began the transit to Site 1116 (proposed site ACE-16A) at 2230 hr on 22 July 1998.

LITHOSTRATIGRAPHY

The succession cored at Site 1115 consisted of 802.5 m of sediments, including an inferred late Miocene–Pleistocene rift succession and underlying Miocene forearc unit. Twelve lithostratigraphic units are recognized on the basis of sediment or rock type, grain size, sedimentary structures, color, smear slides, thin sections, bulk mineralogy (by X-ray diffraction [XRD]), and calcium carbonate content (Fig. **F1**). In certain areas in which grain size varies markedly over short intervals (Fig. **F2**) the mineral composition as determined by XRD in fine-grained sediments proved useful in helping to define unit boundaries. In addition, geophysical logs including FMS data were used to help reconstruct

F1. Lithologic units recovered at Site 1115, **p. 64.**

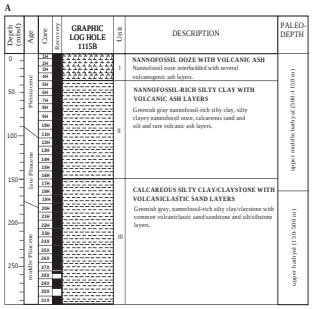

F2. Grain-size trend for units in Hole 1115B, **p. 66.**

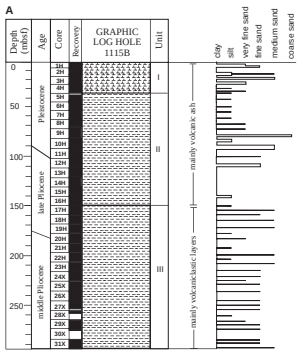

parts of the succession that were poorly recovered, especially conglomeratic intervals.

Lithostratigraphic Unit I

Description: nannofossil ooze and clay, with volcanic ash interbeds
Interval: Cores 180-1115A-1H; Cores 180-1115B-1H through 4H
Depth: 0–4.4 mbsf (Hole 1115A); 0–35.7 mbsf (Hole 1115B)
Age: Pleistocene

The uppermost 4.4 m of the unit were cored in Hole 1115A. In addition, the whole of Unit I was recovered from Hole 1115B.

Unit I is composed of the following main types of unconsolidated sediment: nannofossil ooze, nannofossil-rich silty clay, calcareous silty clay/claystone, and volcanic ash. Volcanic ash layers are present throughout the whole of Unit I. Details of these different lithologies are as follows:

Nannofossil Ooze and Nannofossil-Rich Silty Clay

The nannofossil ooze is light yellowish brown, with numerous planktonic foraminifers, scattered colorless glass shards (e.g., Section 180-1115A-1H-1), wood fragments (1H-2), rare small pumice clasts, numerous shell fragments (1 cm × 0.5 cm × 0.5 cm; e.g., Section 180-1115A-1H-4, 80 cm) and occasional pteropods. In some intervals slightly more clay-rich laminae (i.e., nannofossil-rich clay) are present within clay-rich nannofossil ooze (e.g, Section 180-1115B-2H-3), and some partings within these intervals are graded.

Discontinuous lamination is commonly defined by concentrations of planktonic foraminifers (e.g., Section 180-1115A-1H-4). Individual laminae exhibit sharp bases and diffuse tops (e.g., Cores 1H and 2H). Occasionally, the foraminifer-rich intervals represent distinct beds with graded bases and diffuse tops (e.g., interval 180-1115B-1H-CC, 0–10 cm). Sulfide mottling is commonly present. From ~12 mbsf downward the sediment tends to be slightly more clay rich and is termed nannofossil-rich silty clay.

Smear slides indicate that the component grains are quartz, feldspar, volcanic glass, calcite, nannofossils, foraminifers, bioclasts, sponge spicules, and radiolarians (see **"Site 1115 Smear Slides,"** p. 86). In addition, XRD analysis shows that calcite predominates with minor quartz and aragonite (Table **T3**). In agreement, calcium carbonate values range from 62 to 77 wt% (see **"Organic Geochemistry,"** p. 45).

T3. XRD analysis of fine-grained sediments, **p. 181.**

Volcanic Ash

Volcanic ash is present as multiple thin beds over narrow, discrete intervals and as isolated laminae and thin beds. The main types are as follows:

Seven thin beds/laminae are present within interval 180-1115A-1H-4, 89–105 cm. These are divided into three sediment types: (1) volcanic ash (silt) composed of silt-sized platy and bubble-wall shards, (2) volcanic ash (fine- to medium-grained sand), mainly composed of pipe-vesicle glass, and (3) volcanic ash (fine to very fine grained sand), made up of volcanic glass mixed with nannofossils. Elsewhere, individual glass-rich laminae are present. These exhibit sharp bases and diffuse tops (e.g., Section 180-1115A-1H-4, 85–110 cm; Fig. **F3**).

F3. Nannofossil ooze with volcanic ash layers, **p. 68.**

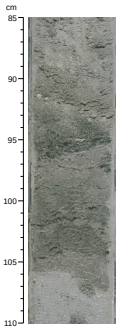

An ash layer of similar composition was recognized in interval 180-1115B-1H-3, 75–93 cm. Of the seven layers identified in Section 180-1115A-1H-4, four of their counterparts in Hole 1115B are much less well preserved, a result of bioturbation of the thinner ash layers.

An ash layer in interval 180-1115B-1H-6, 6–22 cm (fine-grained sand) is dominated by bubble-wall shards and rare pipe-vesicle shards, also rare detrital quartz and ferromagnesian grains. The base of the layer is sharp, whereas the top is diffuse. This ash layer was not observed in Hole 1115A.

In the interval 180-1115B-2H-3, 15–25 cm, two thin ash beds are juxtaposed. The lower bed, ~5 cm thick, grades from fine-grained sand to silt and includes organic material and detrital grains, passing up into mainly green, silt-sized glass. By contrast, the upper bed is composed of very fine silt sized glass, grading into silt.

A further volcanic ash layer comprises a lower interval of medium- to fine-grained sand, passing up into fine-grained sand. Both of these sedimentary intervals exhibit sharp bases and sharp tops. In places, "ghosts" of volcanic ash layers are present that are rarely recognizable after bioturbation. For example, within the intervals 180-1115B-2H-4, 8–10 and 18–19 cm, remnants of volcanic ash laminae are preserved.

A discrete ash lamina is present in the interval 180-1115B-2H-5, 0–1 cm.

Volcaniclastic Silt

Discrete interbeds of graded silt (with sharp bases) appear at ~12 mbsf (e.g., interval 180-1115B-2H-3, 72–70 cm). This sediment is composed of thin to medium beds of volcaniclastic silt. Individual beds exhibit sharp bases and diffuse tops, and grade from very fine silt to clay and ooze (e.g., interval 180-1115B-3H-1, 8–15 cm). The XRD analysis reveals the presence of amphibole in addition to calcite and quartz.

Volcaniclastic Sand

The volcaniclastic sands form thin to medium beds that grade from coarse-grained sand to clay. Bioturbation becomes more abundant at the top. The sand is rich in foraminifer tests and detrital grains. Smear slides reveal the presence of feldspar, rock fragments, volcanic glass, nannofossils, and planktonic foraminifers (see **"Site 1115 Smear Slides,"** p. 86).

Interpretation

Lithostratigraphic Unit I accumulated at upper middle bathyal depths during the Pleistocene at estimated sedimentation rates of 34–59 m/m.y. (see **"Sediment Accumulation Rate,"** p. 34). The background pelagic sediment is dominated by biogenic material (nannofossils, planktonic foraminifers, radiolarians, and shell fragments), accounting for much of the observed mineralogy (calcite, quartz, and aragonite). Some of the fine-grained sediment also might be interpreted as mud turbidites. In addition, mainly siliceous volcanic glass is interpreted as primary air-fall tuff derived from volcanoes related to the Trobriand Arc and/or per-alkaline volcanoes of the Dawson Strait (Davies et al., 1984; Smith, 1976; Stolz et al., 1993). The volcaniclastic silts rich in amphibole and sands are interpreted as epiclastic deposits from turbidity currents.

Lithostratigraphic Unit II

Description: nannofossil-rich silty clay with volcanic ash layers
Interval: Cores 180-1115B-5H through 16H
Depth: 35.7–149.7 mbsf
Age: late Pliocene–Pleistocene

This unit is marked by a transition from mainly ooze, to clay as the background fine-grained sediment. Volcanic ash layers (interpreted as air-fall tuff) are less abundant than in Unit I, but numerous volcanogenic layers of epiclastic origin are present. The following lithologies are present.

Nannofossil-Rich Silty Clay

This greenish gray sediment is intergradational with silty nannofossil ooze (see **"Silty Clayey Nannofossil Ooze,"** p. 8). Numerous burrows are filled with volcaniclastic sand that is locally glass rich (e.g., Section 3H-4). Sulfide mottling is widespread. Thin partings are commonly rich in foraminifers, whereas clay-rich zones (i.e., nannofossil clay) are often homogeneous with few foraminifers (e.g., interval 180-1115B-3H-CC, 0–4 cm). Scattered shell fragments, pteropods, whole or broken foraminifers, and grains of ferromagnesian minerals are commonly observed.

Smear slides reveal quartz, feldspar, volcanic glass, nannofossils, foraminifers, and sponge spicules (**"Site 1115 Smear Slides,"** p. 86). The XRD analysis revealed calcite, quartz, and plagioclase (Table **T3**). Calcium carbonate values range from 35 to 64 wt% (see **"$CaCO_3$, Sulfur, Organic Carbon, and Nitrogen,"** p. 45).

Calcareous Clay

Lower in the unit the nannofossil clays become more consolidated and contain fewer nannofossils. These sediments are classified as calcareous clay (e.g., Section 8H-5). Otherwise the clay is highly burrowed, with little sign of preserved primary sedimentary structures. Smear slides of the calcareous clay contain quartz, feldspar, volcanic glass, calcite, nannofossils, foraminifers, and organic material (**"Site 1115 Smear Slides,"** p. 86). The XRD analysis reveals calcite and minor amounts of quartz, aragonite, and plagioclase (Table **T3**). Calcium carbonate contents range from 50 to 65 wt%.

Calcareous Silt

Thin to very thin beds and laminae strongly disrupted by bioturbation are present (e.g., intervals 180-1115B-3H-6, 69–70 cm, and 3H-7, 43–44 cm). They exhibit sharp bases and tops and are clearly graded from silt to clay (e.g., intervals 180-1115B-4H-3, 20–20.5 cm, and 5H-2, 97–100 cm).

Silty Clayey Nannofossil Ooze

This minor lithology, more typical of Unit I (see **"Lithostratigraphic Unit I,"** p. 6) is greenish gray, strongly burrowed, with few visible primary sedimentary structures. Sulfide mottling is widespread. Burrows are commonly infilled with sand (e.g., interval 180-1115B-4H-1, 10–145

cm). A number of foraminifer-rich beds grade from very fine sand to silt and then silty clay (e.g., interval 180-1115B-4H-1, 121–128 cm).

Calcareous, Siliceous, and Volcaniclastic Sand

These layers are characterized by mixtures of volcanic glass, rock fragments, quartz, and feldspar (e.g., interval 180-1115B-9H-2, 0–3 cm). Unusually, a lower thin bed of volcanic ash (5 cm thick) is overlain by a second thin bed of fine- to medium-grained volcaniclastic sand (interval 180-1115B-10H-4, 48–66 cm; Fig. F4) comprising volcanic glass, mica, quartz, feldspar, and lithic fragments, based on smear-slide analysis ("Site 1115 Smear Slides," p. 86).

F4. Pyroclastic and epiclastic volcanogenic layers, p. 69.

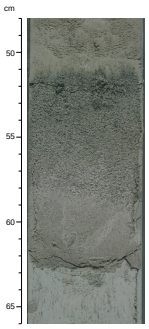

Volcanic Ash

Rare, very thin beds are present within nannofossil clay. Individual layers are sharp based and graded (e.g., interval 180-1115B-5H-7, 61–66.6 cm). In addition, three volcanic ash layers (each 1 cm thick) were observed in Sections 6H-7 and CC. The ash is mixed with detrital grains and foraminifers. Another occurrence of repeated thin volcanic ash beds is in the interval 180-1115B-10H-1, 126–129 cm. Each of three very thin beds (<2 cm in thickness) is normal graded from medium-grained sand to silty clay. Another ash bed (2 cm thick) is present in the interval 180-1115B-12H-2, 37–39 cm. Beneath Core 15H discrete volcanic ash layers were not observed. However, white acidic pumice fragments were noted in the interval 180-1115B-15H-2, 62 cm, and a thin bed of silty volcanic ash is present in the interval 180-1115B-15H-4, 142–145.5 cm. The sharp base of this ash was considerably disrupted by bioturbation. This bed contains mainly platy and bubble-wall and rare pipe-wall shards. Another similar thin bed is present in the interval 180-1115B-15H-5, 86–89 cm. Core 16H contains minor volcaniclastic sediment appearing as a graded volcaniclastic bed in the interval 180-1115B-16H-5, 10–13 cm.

Interpretation

Unit II accumulated in the late Pliocene–Pleistocene in upper to middle bathyal depths (500–1150 m). The average sedimentation rate was 59–79 m/m.y. (see "Sediment Accumulation Rate," p. 34, for details on depth zonation). The depositional processes and provenance of Unit II are similar to those of Unit I, but for increased input of epiclastic silt and sand, interpreted as turbidites. The amount of volcanic ash of inferred air-fall origin is less, but the character and possible origins remains the same (see "Volcanic Ash," p. 9).

Lithostratigraphic Unit III

Description: calcareous silty clay/claystone with volcaniclastic sand/sandstone layers
Interval: Cores 180-1115B-17H through 31X and Cores 180-1115C-1R through 11R
Depth: 149.7–293.1 mbsf (Hole 1115B); 283.2–388.5 mbsf (Hole 1115C)
Age: middle Pliocene

Lithostratigraphic Unit III is characterized by the appearance of discrete thin, graded beds of volcaniclastic sand/sandstone within calcare-

ous silty clay/claystone. It is the thickest stratigraphic unit (~240 m) at Site 1115. Calcium carbonate values in fine-grained sediments show a general decrease from >30 wt%, to around 20 wt% below 250 mbsf, with a few exceptions (see **"$CaCO_3$, Sulfur, Organic Carbon, and Nitrogen,"** p. 45). Volcaniclastic beds are mainly present above Core 180-1115B-22H (206.7 mbsf). The first well-indurated sediment was in Section 180-1115B-28X-CC (256.55 mbsf). Volcaniclastic sands/sandstones are present sporadically throughout the unit and are greatly affected by burrowing until near the base of the unit (below Core 180-1115C-6R). Rarely, bedding is tilted (e.g., interval 180-1115B-17H-3, 121–124 cm), and small high-angle normal faults occasionally are present (e.g., interval 180-1115B-18H-2, 40–49 cm) (see **"Structural Geology,"** p. 29).

The following lithologies are present in decreasing order of abundance:

Nannofossil-Rich Silty Clay/Claystone and Calcareous Clay/Claystone

These lithologies have similar counterparts in Units I and II (see **"Lithostratigraphic Unit I,"** p. 6, and **"Lithostratigraphic Unit II,"** p. 8). However, the sediment becomes more consolidated downward. The sediment is highly bioturbated (*Chondrites,* with rare *Zoophycos;* e.g., interval 180-1115C-4R-2, 138 cm). Smear slides revealed quartz, feldspar, mica, calcite, nannofossils, planktonic foraminifers, sponge spicules, and volcanic glass (**"Site 1115 Smear Slides,"** p. 86). The XRD analysis reveals major amounts of calcite, also minor quartz, plagioclase, chlorite, and illite. Foraminifer tests are locally concentrated in small burrows, also scattered small shell fragments, very rare gastropods, and rare echinoderm fragments were observed (e.g., interval 180-1115C-1R-CC, 37 cm). Sulfide mottling is common and pyrite framboids are locally concentrated in burrows.

In the lower part of Unit III, the claystone is slightly more silty with scattered angular sand-sized grains of ferromagnesian minerals, feldspar, biotite, quartz, and shell fragments (Fig. **F5**). Lower still, the calcareous silty claystone contains abundant detrital grains of up to granule size (e.g., intervals 180-1115B-29X-3, 12–14 cm, 47–49 cm, 106–110 cm, and 115–120 cm). Discrete shell-rich laminae rarely are near the base of the unit (interval 180-1115C-10R-4, 104 cm). The calcareous claystones include occasional dark silt- or clay-rich layers up to several cm thick (e.g., interval 180-1115B-18H-CC, 8–10 cm). Very rarely, woody, carbonaceous fragments were observed (i.e., intervals 180-1115B-29X-6, 16–18 cm, and intervals 180-1115C-7R-2, 60–61 cm, 9R-1, 81.5 cm, 10R-73 cm, and 10R-4, 64 cm).

Analysis of a small number of impregnated thin sections revealed the presence of a predominantly clay-rich and micritic matrix with variable amounts of detrital quartz, plagioclase, hornblende, biotite, lithic volcanics, organic matter, shell fragments, pyrite, and planktonic foraminifers (**"Site 1115 Thin Sections,"** p. 89). In one thin section, shell fragments and primary micritic matrix are replaced by blocky calcite spar (interval 180-1115C-2R-1, 17–19 cm). In another, micrite is replaced by microspar (interval 180-1115C-6R-2, 17–19 cm). Foraminifers are commonly infilled with pyrite.

The XRD analyses of the silty clays reveal quite variable compositions. The typical composition is calcite, with quartz, plagioclase, illite, sporadic chlorite, and rare ankerite. More volcaniclastic-rich samples include amphibole and clay. Pyrite is consistently present in samples

F5. Silty claystone with unaltered detrital grains, **p. 70.**

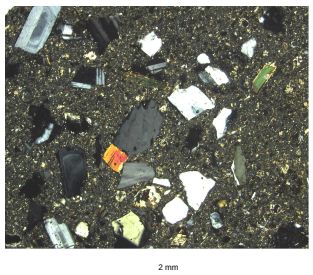

from below 285 mbsf. One sample of Core 180-1115B-26X contains dolomite as the major phase (Table T3).

Volcaniclastic Sand/Sandstone and Silt/Siltstone

Graded volcaniclastic sand/sandstone beds, typically <8 cm thick, mainly exhibit sharp, scoured bases and grade upward into silty clay to clay (up to 4 per section; e.g., Section 180-1115B-17H-2). The thicker beds are slightly coarser grained, especially at the base, where concentrations of detrital or volcanic-glass grains (Fig. F6), or small lithic fragments (e.g., interval 180-1115C-18R-3, 0–3 cm) are present. Parallel laminations were observed very rarely (e.g., 0.2 cm within interval 180-1115B-31X-5, 27–31 cm).

The volcaniclastic material is locally reduced to a few-mm-thick layers rich in silt-sized glass with sharp upper and lower contacts. Elsewhere, diffuse crystal-rich layers define a weak normal grading. In addition, many ghosts of volcaniclastic sandstone beds are present, marked by a concentration of sand grains, particularly within burrows (intervals 180-1115B-25X-2, 9–11 cm, and 27X-5, 84–105 cm).

Toward the base of the unit, sharp-based, graded volcaniclastic sandstones again become abundant, with less evidence of burrowing (e.g., Core 180-1115C-6R). Also, at the base of the unit, acidic extrusive rock fragments are scattered throughout (Cores 180-1115C-9R and 10R).

Thin sections of volcaniclastic sandstone and siltstone revealed the presence of unaltered (and also altered) plagioclase, quartz, hornblende, biotite, muscovite, plagioclase and hornblende phyric basalt, chloritized basalt, colorless glass shards, and bioclasts ("Site 1115 Thin Sections," p. 89).

F6. Sharp based, normally graded volcaniclastic sand layer, p. 71.

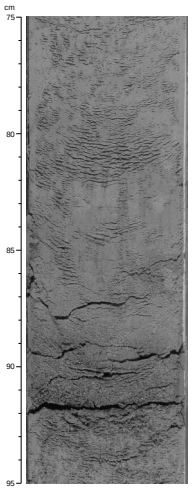

Volcanic Ash

Rare beds of volcanic ash were observed. Smear slides show that these contain variable amounts of volcanic glass, together with quartz, feldspar, mica, rock fragments, calcite, nannofossils, and foraminifers ("Site 1115 Smear Slides," p. 86). These thin beds are similar to those of Unit II (see "Lithostratigraphic Unit II," p. 8), with sharp bases and graded tops, and commonly include concentrations of ferromagnesian minerals. These beds are strongly disrupted by burrowing (e.g., intervals 180-1115B-19H-5, 91–93 cm and 19H-6, 137–145 cm).

Examples of graded volcanic ash include the following: intervals 180-1115B-19H-7, 1–10 cm; 20H-2, 132–134 cm; 21H-6, 72–73 cm; 26X-2, 72.5–75 cm; 27X-2, 113–114 cm; and 27X-5, 37–40 cm; also in intervals 180-1115C-8R-4, 85–86 and 130–132 cm, and 12R-5, 59–61 cm. In addition, patches of volcanic ash dispersed by burrowing organisms were seen occasionally (e.g., intervals 180-1115B-25X-5, 35–41 cm; 26X-3, 34–38 and 109–109.5 cm; 29X-1, 26, 106–110, and 112–112.5 cm; 29X-2, 20–21, 40, 142, and 147 cm; and 29X-7, 26–28 cm), and fragments of pumice? were observed in the intervals 180-1115B-27X-CC, 24–26 cm, and 10R-3, 48–53 cm.

Interpretation

Unit III continues the same general type of sedimentation as in Units I and II. Deposition mostly took place at upper bathyal depths (150–500 m) during middle Pliocene time. Sedimentation was very rapid, at ~284 m/m.y., decreasing to ~79 m/m.y. above 190 mbsf (see

"Sediment Accumulation Rate," p. 34). There is a marked decrease in magnetic susceptibility at 210 mbsf (Core 180-1115B-23H; see "Magnetic Susceptibility," p. 35). However, no obvious changes in the facies, or composition as determined by smear slides or XRD are observed here, and it is not identified as a lithostratigraphic unit boundary. In addition, the geophysical logs indicate the presence of a rather uniform muddy succession throughout Unit III, with some thin sandy intervals.

Interpretation of the photoelectric effect suggests the presence of a thin dolomite-rich layer at 291–292 mbsf (see "Lithologic Analysis," p. 53). The XRD of a sample from 292.1 mbsf (interval 180-1115C-2R-1, 9–11 cm) confirms the presence of dolomite.

The FMS images (static and dynamic normalized) indicate that the succession is relatively muddy, with occasional thin (<5 cm), bright, resistive layers that are interpreted as sands (e.g., at 154.5, 155.7, 158.3, 160.5, and 161.3 mbsf). The succession is locally more sandy at ~245 mbsf with ~5- to 10-cm-thick inferred sands occurring on average every 20–40 cm. In general, the succession becomes slightly more resistive downward, suggesting it is becoming more silty.

The core evidence shows that the graded volcaniclastic silts/siltstone and sands/sandstone, interpreted as deposits from turbidity currents, become markedly more abundant downward. However, some of these sediments could be outer shelf deposits that were extensively bioturbated in view of the inferred water depth. On the other hand, definite volcanic ash interpreted as air-fall tuff is rare. The abundance of volcaniclastic beds was probably originally greater than that visible in the cores, because many beds were so strongly bioturbated they remain only as disseminated silt or sand grains. A number of intervals are relatively rich in volcanic glass. However, this is mainly reworked with lithic and biogenic material. In Unit III we witnessed the first significant appearance of illite below 169 mbsf, which indicates a significant input of fine-grained sediment derived by continental erosion. Also, the relative abundance of pyrite suggests that subseafloor conditions were anoxic.

Lithostratigraphic Unit IV

Description: calcareous sandy silty claystone
Interval: Cores 180-1115C-12R through 14R
Depth: 388.5–417.30 mbsf
Age: early Pliocene

Lithostratigraphic Unit IV recognition is based on a slight change in grain size and increasing lithification from mainly silty claystone, to uniform dark greenish gray claystone, admixed with siltstone and claystone, termed calcareous sandy silty claystone. Shell fragments become more abundant, whereas only minor fine-grained volcaniclastic sandstone is present. The following lithologies are observed in decreasing order of abundance:

Calcareous Sandy Silty Claystone

This is a poorly sorted, mixed sediment that is typically highly bioturbated with scattered volcaniclastic detrital grains and foraminifer fragments. Many burrows are infilled with fine- to medium-grained sandstone, often rich in ferromagnesian minerals. Shell fragments are

locally common (e.g., interval 180-1115C-13R-3, 90–95 cm) and intact shells are also present (e.g., interval 1115C-14R-1, 124 cm). Plant debris is rarely observed (interval 180-1115C-14R-4, 58 cm). Possible *Teichichnus* trace fossils were noted locally.

Smear slides indicate the presence of quartz, plagioclase, volcanic glass, rare biotite, amphibole, calcite, and biogenic components including sponge spicules (**"Site 1115 Smear Slides,"** p. 86). The XRD analysis of this interval shows that the composition is little changed from Unit III, with calcite, quartz, and plagioclase as major minerals, and illite, amphibole, and pyrite as minor minerals (Table **T3**). Calcium carbonate values are similar to those in the lower part of Unit III, above (i.e., ranging from ~18 to 30 wt%; see **"$CaCO_3$, Sulfur, Organic Carbon, and Nitrogen,"** p. 45.

Volcaniclastic Sandstone/Siltstone and Silty Claystone/Claystone

Thin interbeds of volcaniclastic sandstone and siltstone are rarely present in this unit (mainly in Section 12R-5). Thin sections of these rare volcaniclastics indicate the presence of quartz, plagioclase, acidic extrusive rock fragments (with hornblende and plagioclase microphenocrysts, zoned plagioclase, glassy basalt, chloritized basalt, shell fragments, benthic foraminifers, and echinoid fragments) set in a micritic matrix (**"Site 1115 Thin Sections,"** p. 89). In addition, medium-grained lithoclasts rich in hornblende are present (Fig. **F7**). This unit includes pumice with abundant hornblende set in a glassy matrix (Fig. **F8**).

F7. Sandy silty claystone with various fragments and grains, **p. 72.**

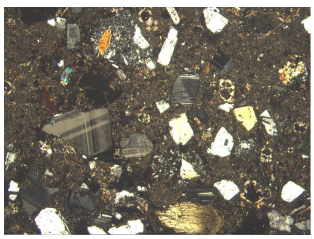

F8. Pumaceous rock with hornblende phenocrysts, **p. 73.**

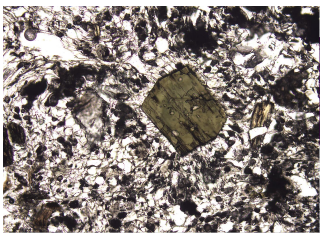

Interpretation

The main significance of Unit IV is that it marks a drastic decrease in the volcaniclastic sand input by turbidity currents. The geophysical logs are interpreted to indicate the presence of a mainly muddy succession (see **"Downhole Measurements,"** p. 52). This interpretation is supported by the FMS data that indicate this unit is relatively uniform and nonresistive. Some of the sediments of Unit IV may have been deposited under the influence of currents in an outer shelf setting. However, bioturbation has extensively modified the original sedimentary structures, which makes it almost impossible to interpret depositional processes. The composition of this sand indicates a calc-alkaline–type source and remains similar to Unit III. Sedimentation continued at upper bathyal depths (150–500 m) during early Pliocene time. However, the lowermost 5 m of the unit accumulated in outer neritic water depths (50–150 m). Average sedimentation rates were ~155 m/m.y. (see **"Sedimentation Accumulation Rate,"** p. 34).

Lithostratigraphic Unit V

Description: mixed silty sandstone
Interval: Cores 180-1115C-15R through 20R
Depth: 417.3–474.9 mbsf
Age: early Pliocene

Lithostratigraphic Unit V recognition is based on an increase in grain size from mainly sandy and silty claystone to predominantly mixed fine- to medium-grained silty sandstone, as follows:

Silty Sandstone

Individual beds are sharp based, with concentrations of calcium carbonate and volcaniclastic grains, and occasional parallel laminations and low-angle (<10°) cross laminations (e.g., intervals 180-1115C-15R-4, 27–28 cm; 17R-1, 4–8 cm; 17R-1, 36–40 cm; and 18R-1, 20–50 cm; Fig. F9). Individual laminations are defined by slightly coarser grains (e.g., interval 180-1115C-20R-1, 6–17 cm). The lower parts of some sandstone beds are well cemented by calcite spar, whereas the upper parts of beds are less well cemented and highly burrowed. Shell fragments are locally very abundant (e.g., intervals 180-1115C-15R-3, 87–150 cm and 16R-1, 56–60 cm). Fragments of organic matter were rarely observed (e.g., interval 180-1115C-18R-2, 52 cm).

In many intervals only vague parallel laminations, or low-angle inclined laminations, are visible (interval 180-1115C-15R-6, 100–116 cm) in the lower part of the beds. Where bioturbation is very extensive, no primary sedimentary structures were observed (e.g., Section 17R-1). Lower in the unit (Section 18R-2) burrowing is less intense. As in Units III and IV, some intervals exhibit concentrations of detrital grains that could have originated as discrete beds (e.g., interval 180-1115C-13R-2, 90–100 cm).

F9. Cross-bedded sandstone with ripple-laminated sand, p. 74.

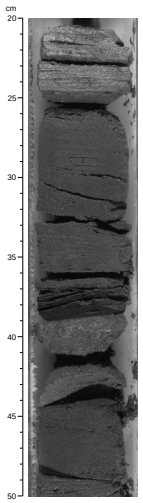

Graded Sandstone

Many thin beds are graded, with sharp bases rich in planktonic foraminifers. As in other units (i.e., Units I–IV), these beds grade upward from medium- to fine-grained sandstone to calcareous silty claystone (Fig. F10). A thin section shows that these sandstones are rich in both benthic and planktonic foraminifers, subrounded basic and intermediate igneous rock fragments, ferromagnesian minerals, quartz, and feldspar (Fig. F11; "Site 1115 Thin Sections," p. 89).

F10. Sandstone rich in foraminifers and shell fragments, p. 75.

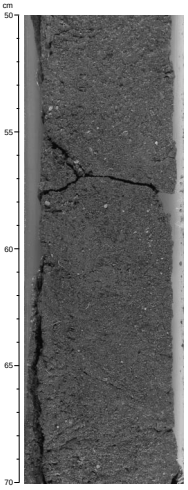

Siltstone/Claystone

Minor amounts of siltstone and claystone are present, commonly near the top of graded beds. In smear slides quartz, plagioclase, rare biotite, rock fragments, volcanic glass, amphibole, bioclasts, and pyrite are present ("Site 1115 Smear Slides," p. 86). The XRD analysis revealed a relative decrease in calcite compared to Unit III (see "Lithostratigraphic Unit III," p. 9) with plagioclase and quartz being the major minerals (Table T3). Calcite, illite, pyrite, and minor amphibole, aragonite, and chlorite are also present. Calcium carbonate contents in the fine-grained sediments range from 14 to 52 wt%. A thin section siltstone (see "Site 1115 Thin Sections," p. 89) was seen to comprise a recrystallized microspar calcite cement with planktonic foraminifers, shell fragments, and with common detrital grains of felsic volcanics, hornblende, and biotite, also some brown altered basaltic glass (palagonite), and coarse plagioclase of possible intrusive origin.

F11. Sandstone with various fragments in a micritic cement, p. 76.

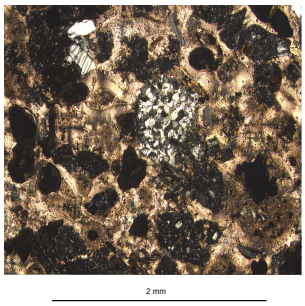

Packstone

Several thin beds of limestone are present. A thin section revealed that one is a packstone dominated by planktonic foraminifers, with well-preserved shell fragments, quartz, acidic volcanic rock, glass shards, minor recrystallized quartz (polycrystalline), rare aphyric basalt,

and rare coarse plagioclase (of possible intrusive origin) ("Site 1115 Thin Sections," p. 89).

Interpretation

Lithostratigraphic Unit V accumulated in outer neritic depths (50–150 m) in early Pliocene time. Average sedimentation rates were initially ~155 m/m.y., as in the base of Unit IV, but greatly decreased downward to ~45 m/m.y. (see "Biostratigraphy," p. 31, for details of depth zonation). Unit V is largely made up of detrital material from a volcanic source. Acidic volcanic rock is abundant in this unit and a minor amount of plutonic igneous rock fragments may be present in addition.

The natural gamma–ray logs indicate that the K/Th ratio is relatively suggestive of the presence of a volcaniclastic component of distinctive composition (see "Downhole Measurements," p. 52). Otherwise, the log response is indicative of a mixed sandy and silty succession, becoming more clay rich near the base. The FMS images reveal a sharp change to more resistive, inferred more silty and sandy near the top of this unit at 415.0 mbsf. Occasional, thin very bright layers at 424.0, 430.4, 434.1, and 436.2 mbsf are interpreted as sandstones <15 cm thick. Near the base (467.0–472.0 mbsf), a less resistant, inferred more muddy unit is present.

Despite the limited core recovery in this unit (<20%) the facies recovered show a transition from poorly sorted, highly bioturbated sandstone in the lower part of the unit to a cross-bedded, parallel- and wavy-laminated sandstone in the middle part of this unit. Recovery in the upper part is very poor. The transition in sedimentary structures suggests an increase in current effects through time.

The laminated and cross-bedded, fine-grained sandstone may represent part of a shelf, or bar, or ridge that was formed under the influence of wave or current action. Tidal currents may also have played a role, although there is little sedimentary evidence of this (e.g., herringbone cross lamination). Also, a storm influence cannot be ruled out for sediments that may have accumulated at shallow-water depths.

Lithostratigraphic Unit VI

Description: sandy siltstone and silty sandstone
Interval: Cores 180-1115C-21R through 24R
Depth: 474.9–513.4 mbsf
Age: earliest Pliocene

Lithostratigraphic Unit VI is distinguished by a decrease in grain size from mainly mixed silty sandstone to more heterogeneous mixed sediment. Calcium carbonate values range from 10 to 25 wt% (see "$CaCO_3$, Sulfur, Organic Carbon, and Nitrogen," p. 45). A number of related lithologies are interbedded to produce a heterogeneous succession as follows:

Calcareous Siltstone with Foraminifers

The lithology comprises structureless, bioturbated foraminifer-rich siltstone with abundant shell fragments (e.g., intervals 180-1115C-21R-4, 23 and 44.5 cm) and volcaniclastic grains. Smear slides reveal the presence of quartz, feldspar, rare plagioclase, biotite, rare amphibole

and pyroxene, and volcanic glass ("Site 1115 Smear Slides," p. 86). Nannofossils are abundant, and planktonic foraminifers are rare to common. The XRD analysis additionally shows the presence of calcite, plagioclase, quartz, and illite, with minor chlorite and amphibole (Table T3).

Calcareous and Clayey Siltstone

This contains fewer planktonic foraminifers. Vague traces of inclined bedding are locally visible (e.g., interval 180-1115C-21R-3, 123 cm). Shell fragments are locally abundant (e.g., interval 180-1115C-21R-3, 82–95 cm). The clayey siltstone contains scattered small shell fragments, detrital grains, and planktonic foraminifers.

Sandy Siltstone

This facies, lower in the unit (Section 22R-1) contains abundant shell fragments and detritus (including disarticulated bivalves and gastropods), mainly ferromagnesian grains, foraminifers, and rare carbonaceous grains. Bioturbation is extensive. Shells are rarely aligned, imparting a very weak bedding. Thin sections indicate that this unit is rich in plagioclase, hornblende, biotite, benthic and planktonic foraminifers, and subrounded basalt rock fragments (Fig. F12; "Site 1115 Thin Sections," p. 89).

Clayey Siltstone-Sandstone

This is a mixed deposit composed of bioturbated sediment, rich in foraminifers, showing parallel to wavy lamination and including large thin-shelled bivalves (4 cm × 2 cm in size; e.g., interval 180-1115C-23R-1, 86–110 cm; Fig. F13). The XRD analysis revealed the same composition as within the siltstones (see "Calcareous Siltstone with Foraminifers," p. 15; "Calcareous and Clayey Siltstone," p. 16; and "Sandy Siltstone," p. 16), with the addition of aragonite and pyrite. In addition, several thin sections revealed sandstones and siltstones to contain mixed bioclastic grains (i.e., shell fragments, benthic foraminifers, calcareous algae, echinoderm plates and spines, and rare planktonic foraminifers), and detrital grains (i.e., quartz, plagioclase, hornblende, basalt, and acidic volcanics), micritic and chloritic grains, rare microcline, and also pyrite. The grains of basalt are rounded to well rounded ("Site 1115 Thin Sections," p. 89)

Interpretation

The whole of Unit VI accumulated in an inner neritic setting (<50 m) at an estimated sedimentation rate of 45 m/m.y. (see "Sediment Accumulation Rate," p. 34). The unit is dated as latest Miocene to earliest Pliocene on the basis of nannofossils. A shallow-water setting is supported by the abundance of reworked neritic carbonate, including calcareous algae. High uranium log values are consistent with the presence of abundant reduced organic matter. Otherwise, the geophysical logs indicate the succession is mainly sandy (based on the gamma ray, neutron porosity, and density logs; see "Downhole Measurements," p. 52). This is confirmed by the FMS data that show a sharp increase in resistivity near the boundary with the overlying unit (at 472.2 mbsf).

F12. Siltstone with detrital minerals, grains, and foraminifer fragments, p. 77.

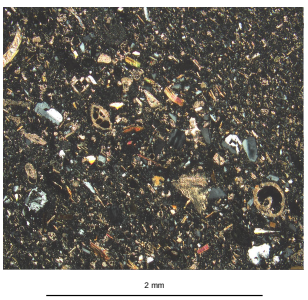

F13. Bioturbated foraminifer- and shell-fragment-rich silty sandstone, p. 78.

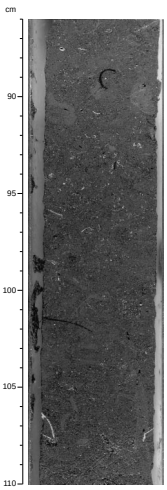

The frequent marked changes in grain size and sedimentary structures, including rarely preserved wavy as well as parallel laminations, suggest the unit accumulated in a coastal or shoal setting, affected to some extent by wave or current activity. Although less intense than in open, unprotected coastal areas, wave activity can also play an important role in more restricted (e.g., lagoonal) deposits, especially in transport of fine-grained sediments. The very well rounded basaltic grains possibly originated in a high-energy coastal, or fluvial setting, and were then reworked offshore by waves or currents, and interbedded with finer grained sediments containing planktonic foraminifers and nannofossils. Provenance from mainly volcanic-related setting(s) remained largely unchanged from Unit V, with a minor contribution from plutonic, as well as volcanic rocks.

Lithostratigraphic Unit VII

Description: siltstone
Interval: Cores 180-1115C-25R through 28R
Depth: 513.4–551.8 mbsf
Age: late Miocene

Lithostratigraphic Unit VII is recognized on the basis of a change from relatively coarse grained heterogeneous sediments, to still mixed, but finer grained, mainly silty facies. In contrast to Unit VI, in which calcite is predominant, plagioclase and aragonite are important in Unit VII, based on XRD data (Table T3). Calcium carbonate values range from ~10 to 41 wt%, with only one sample being very depleted (0.3 wt%; see "$CaCO_3$, Sulfur, Organic Carbon, and Nitrogen," p. 45). In common with Unit VI, a number of lithologies are interbedded, as follows:

Sandy Siltstone

This is dark greenish gray and has abundant shell fragments and foraminifers, bivalves, and gastropods (disarticulated). Shells are rarely aligned, imparting a weak bedding. Traces of organic matter are locally present. Rare articulated bivalves and gastropods are present. Several types of burrows were observed (including *Zoophycos*), some filled with detrital sand grains, others with silty clay. The burrows are commonly rendered visible by traces of black monosulfide.

Silty Sandstone

These intervals are very similar to the sandy siltstone beds, but are coarser, up to granule size (e.g., Section 28R-1), with common shelly fragments, foraminifers, and sand-sized detrital grains (i.e., ferromagnesian minerals, biotite, plagioclase, and rock fragments; Fig. F14). Burrows are infilled with detrital sand grains and small shell fragments. Rare concentrations of detrital grains define vague intervals between 13 and 20 cm thick with weakly defined top and bottom contacts to the laminae. Rare carbonaceous detritus and pyrite are also present.

Thin-section study revealed the sandstone to contain quartz, plagioclase (fresh and altered), zoned plagioclase, biotite, pyroxene, hornblende, palagonite, altered basaltic grains, plagioclase and hornblende phyric acidic volcanics, and microcline set in a calcareous and micritic matrix (Fig. F15; "Site 1115 Thin Sections," p. 89). The sandstone contains the following bioclasts: shells, calcareous algae, shell fragments,

F14. Sandstone with abundant shells and shell fragments, p. 79.

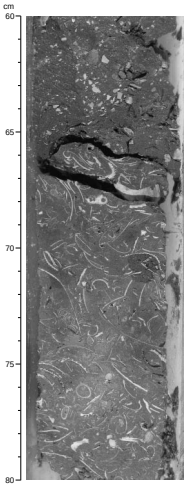

F15. Sandstone with a micritic cement containing grains and fragments, p. 80.

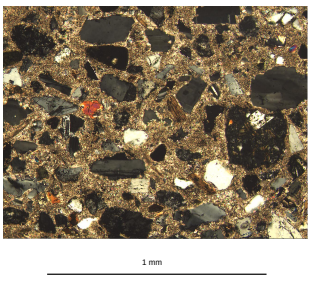

and echinoderm fragments, in addition to the detrital grains mentioned above. Many of the grains are moderately to well rounded.

Silty Claystone

This forms a very minor component of Unit VII as thin beds or isolated laminae. In addition, some calcareous silty claystones, which are structureless and rich in shell fragments and foraminifers, are present.

Smear slides reveal the presence of quartz, plagioclase, rare volcanic glass, accessory minerals (amphibole), calcite, and pyrite ("Site 1115 Smear Slides," p. 86). Nannofossils were only noted in a few samples; planktonic foraminifers are rare or absent. The XRD analysis revealed the presence of plagioclase, calcite, quartz, illite, chlorite, aragonite, and pyrite (Table T3).

Interpretation

Unit VII is dated as late Miocene on the basis of calcareous nannofossils. A relatively low sedimentation rate of >13 m/m/y. is inferred (see "Sediment Accumulation Rate," p. 34). In addition, foraminifers indicate inner neritic water depths (0–50 m). In common with Unit VI, Unit VII accumulated in a shallow-water setting. The increase in shelly bioclasts and volcaniclastic material, the decrease in average grain size, and the decrease in observed presence of planktonic foraminifers are all consistent with a relatively low energy setting, possibly a marine lagoon. However, some shell-rich beds may represent shell lags that resulted from reworking from wave or tidal activity in a lagoonal setting. The high gamma-ray logs are again suggestive of reduced organic matter in the upper part of the unit (above 526 mbsf) as in Unit VI (see "Lithostratigraphic Unit VI," p. 15). Beneath this, hole conditions were poor and the low gamma-ray response is suggestive of the presence of abundant soft nonresistive material, possibly organic-rich (coaly?) material, as inferred for Site 1109 (see "Downhole Measurements," p. 52). The FMS images reveal a mainly muddy succession with rare, thin-bedded (~10 cm) resistive inferred sandstones (e.g., at 528.6 mbsf). In addition, the mainly volcanic-related provenance remained unchanged from Unit VI, again with some input of plutonic rock. In addition, a few grains of possible metamorphic rock were also noted.

Lithostratigraphic Unit VIII

Description: organic-rich silty claystone and bioclastic limestone
Interval: Core 180-1115C-29R through Section 30R-4
Depth: 551.8–565.7 mbsf
Age: late Miocene

This unit is distinguished by the appearance of darker, organic-rich, finer grained sedimentary rocks and bioclastic limestone. Calcium carbonate values vary drastically from 0.3 wt% in organic-rich sediment (with 3.84% carbon), to ~53 wt% in limestone (see "$CaCO_3$, Sulfur, Organic Carbon, and Nitrogen," p. 45). Lithologies present are as follows:

Organic-Rich Silty Claystone

Organic-rich silty claystone is present either as massive, finely disseminated material; scattered particles (0.5–0.7 mm in size; interval

180-1115C-30R-3, 108–137 cm); or discrete thin laminae (coal like; e.g., interval 180-1115C-30R-3, 0–20 cm; Fig. F16). Dark greenish gray, less organic rich claystone is present near the base of the unit. Smear slides revealed typical detrital fragments, as in the overlying Unit VII. Bioclasts are restricted to rare planktonic foraminifers ("Site 1115 Smear Slides," p. 86). In addition, XRD analysis allowed the recognition of plagioclase, quartz, K-feldspar, pyrite, amphibole, and probably smectite in different samples (Table T3).

F16. Claystone with interbeds of organic-rich siltstone, p. 81.

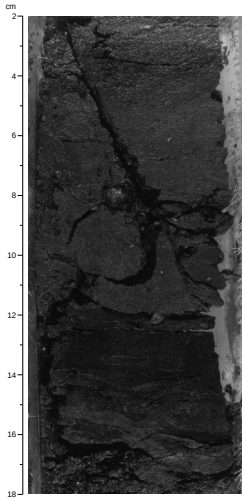

Siltstone and Medium- to Fine-Grained Sandstone

Rare occurrences of this lithology were sampled for study in thin sections (Table T3). A medium-grained sandstone is texturally mature with well-rounded grains cemented by sparry calcite (Sample 180-1115C-29R-1, 72–73 cm). The grains include acidic volcanics, altered basalt (locally chloritized), plagioclase, biotite, pyroxene, hornblende, polycrystalline quartz, and rare microcline (Fig. F17). A fine-grained siltstone contains a similar range of detrital grains, together with benthic foraminifers and shell fragments set in a micritic matrix (interval 180-1115C-29R-1, 82–83 cm).

F17. Sandstone with calcite cement containing fragments and grains, p. 82.

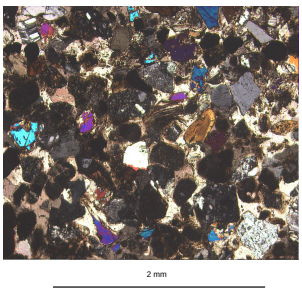

Limestone

Rarely, near the top of the unit, several isolated clasts of bluish gray limestone were recovered. These contain shell fragments, burrows infilled with black volcaniclastic sediment, and veins of calcite (intervals 180-1115C-29R-2, 28–32 and 62–65 cm; and 29R-3, 32–34 cm; and Section 29R-CC).

Interpretation

Sediments of Unit VIII accumulated in a marine, inner neritic setting (<50 m) during late Miocene time. The sedimentation rate is estimated as >13 m/m.y. (see "Sediment Accumulation Rate," p. 34). The abundance of plant-rich material, including coaly laminae, suggests accumulation in a quiet-water, lagoonal setting adjacent to a vegetated land area. This is again supported by the low response of the gamma-ray log that is interpreted to suggest the presence of coaly layers up to 2 m thick (see "Downhole Measurements," p. 52). The FMS images of most of this unit are difficult to interpret as a result of numerous washouts. In addition, micritic carbonate is a common constituent of marine lagoons, in which the source of calcium carbonate could be detrital and/or biogenic (e.g., from breakdown of calcareous algae, or even direct precipitation).

Lithostratigraphic Unit IX

Description: sandstone, siltstone, and conglomerate
Interval: Sections 180-1115C-30R-5 through 31R-1, 90 cm
Depth: 565.7–571.9 mbsf
Age: late Miocene

This unit is distinguished by a marked increase in grain size, with alternations of sandstone, siltstone, and conglomerate. A single calcium carbonate value within rare claystone yielded a value of ~41 wt% (see

"$CaCO_3$, Sulfur, Organic Carbon, and Nitrogen," p. 45). Details of the lithologies are as follows:

Conglomerate

Conglomerate is made up of well-rounded clasts (up to 4.0 to 0.3 cm), mainly basalt (e.g., intervals 180-1115C-31R-1, 8–87 cm, and 30R-5, 45–70 cm; Fig. F18). Individual clasts exhibit varying extents of alteration with onion-skin weathering observed. A matrix between the clasts is composed of coarse-grained sand and granules of the same material, in turn cemented by calcite spar. A possible vertical root trace (0.4 cm wide × 4 cm deep) was observed in one instance (interval 180-1115C-30R-CC, 6–9 cm). Where matrix is abundant, the fabric is more matrix supported than clast supported (interval 180-1115C-31R-1, 8–87 cm).

F18. Pebble and granule matrix-supported conglomerate, p. 83.

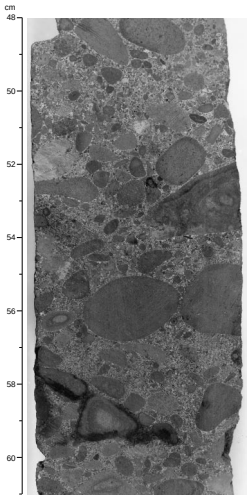

Sandstone/Siltstone

The sandstone is structureless, medium grained, poorly sorted, and well cemented (by calcite), with scattered subrounded sand grains. Greenish gray clay-rich material is present between grains. Small (1.5 cm) radiating veinlets are filled with calcite in one case (interval 180-1115C-30R-5, 28 cm). A single sample of siltstone contains only calcite and plagioclase, by XRD study (Table T3).

Two thin sections of sandstone contain the following detrital components: basalt (with feldspar microphenocrysts), chloritized basalt, variolitic glassy basalt, altered acidic volcanic, schist, plagioclase, hornblende, perthitic feldspar (mermikitic), microcline, pyroxene, minor chalcedonic quartz, as well as various bioclasts (including coral), all set in calcite spar cement. Many of the lithic grains are well rounded (Fig. F19; "Site 1115 Thin Sections," p. 89).

F19. Sandstone containing fragments and subangular grains, p. 84.

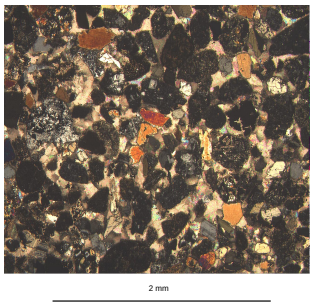

Interpretation

The well-rounded nature of the conglomerate clasts is suggestive of prolonged sediment transport or reworking in a high-energy setting (i.e., littoral, beach, or fluvial). The geophysical logs are interpreted to indicate the presence of conglomerate between 574 and 567 mbsf. The elevated photoelectric effect is explicable by the presence of a calcite spar cement, as observed in the cores (see "Downhole Measurements," p. 52). The FMS images indicate the presence of a very bright resistive unit from 570 to 576 mbsf. In detail, discrete resistive beds 10–30 cm thick are separated by less resistive (muddy) intervals, individually 20–30 cm thick. Several factors favor a fluvial setting: (1) marine fossils are absent; (2) the presence of interstitial sand and granules within the conglomerate is consistent with a fluvial setting; (3) the clasts show alteration suggestive of subaerial weathering; (4) a probable root trace was observed; and (5) a calcium carbonate nodule, possibly incipient caliche is present. Diagenetic processes include precipitation of minor amounts of (spherulitic) chalcedonic quartz and extensive calcite spar. The porous and permeable poorly sorted, texturally mature sands probably acted as conduits for fluid flow after deposition.

Lithostratigraphic Unit X

Description: sandstone, siltstone, claystone, and conglomerate
Interval: interval 180-1115C-31R-1, 90 cm, through Section 34R-3

Depth: 571.9–603.85 mbsf
Age: middle Miocene

This unit is recognized by the appearance of well-graded intervals, including sandstone, siltstone, and minor granule conglomerate. Levels of calcium carbonate in fine-grained sediment are generally low (<2 wt%), with the exception of a single more calcareous sample with about 9 wt% calcium carbonate (see "$CaCO_3$, Sulfur, Organic Carbon, and Nitrogen," p. 45). Details of the component lithologies are as follows:

Graded Sandstone

Many of the sandstones are reddish brown, in contrast to the mainly greenish and grayish colors of the entire overlying succession. A few sandstones exhibit sharp, scoured bases (e.g., interval 180-1115C-32R-3, 54–68 cm; Fig. F20). Normal grading is common, and in one case inverse-to-normal grading was observed (Section 32R-1). Several relatively thick (0.35 m), normal-graded beds also exhibit local inverse grading in their basal few centimeters (e.g., interval 180-1115C-32R-3, 75–96 cm). Parallel lamination is also well developed, but largely obliterated by burrowing. In one case a massive sandstone bed includes a large mud clast (8 cm wide). A poorly sorted, medium- to coarse-grained sandstone with abundant rounded mud clasts was observed locally (Fig. F20). Small shell fragments are rarely present (interval 180-1115C-33R-2, 127–140 cm). Shell fragments and calcium carbonate material become more abundant lower in the unit (e.g., interval 180-1115C-34R-1, 19–80 cm). Near the base of the unit, fine sand-sized shelly material forms faint thin layers (0.2–0.3 cm). Bedding is mainly flat, but inclined bedding planes were rarely observed (interval 180-1115C-34R-1, 80–135 cm).

Thin sections of the sandstone reveal grains of pyroxene phyric basalt, glassy basalt, palagonite, and flow-banded well-crystallized basalt, together with fresh pyroxene and subordinate plagioclase, all set in a minor calcite spar cement (Fig. F21; "Site 1115 Thin Sections," p. 89).

Conglomerate-Sandstone-Siltstone

A small number of thick beds up to 50–80 cm thick have lower parts composed of granule conglomerate that is usually <10 cm thick that graded upward to medium-grained sand with siltstone or claystone rip-up clasts comprising irregularly laminated siltstone and burrowed claystone (i.e., intervals 180-1115C-32R-3, 0–58.5 cm, and 33R-1, 32 cm). In addition, a few thin beds were noted with sharp bases grading from very fine grained sandstone with parallel lamination (interval 180-1115C-32R-1, 12–22 cm), or convolute lamination, passing into siltstone and claystone. Furthermore, in several sections contorted and irregular beds of calcareous sandstone interfinger with clay-rich sandstone (Fig. F22).

Siltstone/Claystone

This siltstone is greenish gray, weakly indurated, mainly structureless, poorly sorted, homogeneous, and weakly burrowed, with scattered sandy grains. In places, the siltstone is highly calcareous and very well cemented (interval 180-1115C-31R-1, 91–108 cm; "Site 1115 Thin Sec-

F20. Sandstone with mud clasts in upper part, p. 85.

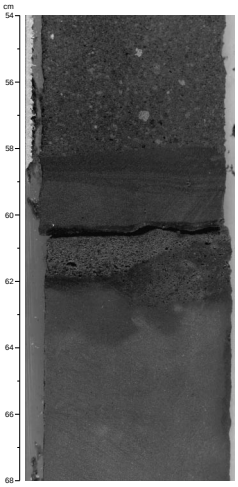

F21. Sandstone containing detrital grains and rock fragments, p. 86.

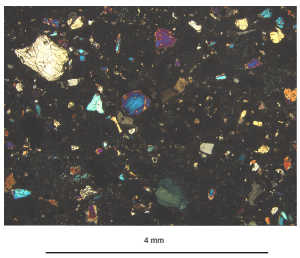

F22. Sandstone structures resulting from soft-sediment deformation, p. 87.

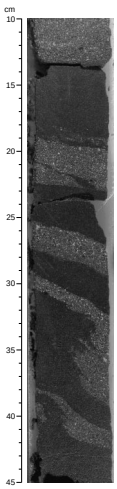

tions," p. 89). The siltstone is clay rich and rarely exhibits convolute lamination (e.g., interval 180-1115C-32R-1, 8–12 cm), or parallel lamination (e.g., Section 32R-1). In addition, siltstone also constitutes the upper parts of individual graded beds (of which the bases were probably not recovered).

The XRD analysis of fine-grained sediment revealed an unusual mineralogy, with pyroxene as a major mineral, and minor constituents including amphibole, hematite, and illite (Table T3).

Interpretation

Unit X is interpreted to have accumulated in middle Miocene (Serravallian) time in an outer neritic setting, based on the combined presence of neritic fossils and planktonic microfossils. The sedimentation rate is poorly defined, based on limited biostratigraphical control, but could be similar to or slightly less than the unit below (>135 m/m.y.; see "Biostratigraphy," p. 31). The geophysical logs, including FMS, suggest the unit as a whole is relatively sandy with thin- to medium-bedded sandstones <15 cm thick on the average of every 0.5–1.0 m. The neritic shells were derived from a shallow-water setting, possibly a calcium carbonate–influenced coastline or shoal. Also, the reddish color may suggest a well-oxidized depositional setting. The fine-grained clastic sediments clearly accumulated largely from suspension. In view of the thick-graded units, including large rip-up clasts, the coarser grained sediments either accumulated entirely from turbidity currents, or in part as storm deposits (i.e., tempestites). For example, the shallow-water carbonate was possibly swept offshore by storm currents. An origin mainly as high-density turbidites, is, however, favored by the absence of obvious ripple lamination typical of storm deposits. Also, there is little evidence of current reworking as in the two overlying units (Units VIII and IX).

The provenance was mainly from pyroxene phyric basalt, or basaltic andesite. The relative uniformity of the source lithology without strong alteration is suggestive of a relatively local source. In view of the abundance of altered basalt present, it is likely that the unusual zeolite is detrital, possibly following low-grade alteration of a volcanic rock.

Lithostratigraphic Unit XI

Description: sandstone, packstone, siltstone, and silty claystone
Interval: Cores 180-1115C-34R-CC through 39R
Depth: 603.85–657.8 mbsf
Age: middle Miocene

This unit is distinguished by the presence of sandstones and packstones, interbedded with siltstones and claystones and minor conglomerate. Calcium carbonate was determined as <2 wt% in two samples of claystone (see "$CaCO_3$, Sulfur, Organic Carbon, and Nitrogen," p. 45). However, routine testing of core samples with dilute HCl and the results of thin-section analysis show that some lithologies (e.g., packstone) are much more calcareous than this.

Sandstone/Packstone

This lithology is coarse-grained sandstone, with abundant shell fragments (Fig. F23). Upper and lower bed contacts are sharp (e.g., interval

F23. Carbonate sandstone/pebbly packstone overlying silty claystone, p. 88.

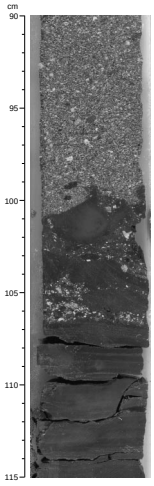

180-1115C-35R-1, 133–135 cm). Coarse-grained beds are pebbly at the base, with shell fragments, mud, and silty rip-up clasts (3–5 cm × 2–3 cm), also some carbonate clasts. In one normal-graded bed there is a decrease in the size of clasts from small pebbles (0.5–1.0 cm) to granules at the top. Otherwise, no fabric is seen in this bed (interval 180-1115C-35R-3, 93–145 cm). In another bed (which lacks a preserved base) large elongate clasts (4 cm × 2 cm) are present (interval 180-1115C-35R-2, 16–18 cm). Some individual siltstone and claystone clasts exceed the core diameter (intervals 180-1115C-35R-3, 20–30 and 85–90 cm). Rarely, these clasts are well rounded. In addition, a single, very thick graded bed (>2 m) spanning several sections was observed (Sections 34R-3 and 34R-CC). This bed grades from coarse-grained sand to silt. The lower interval contains rip-up clasts of silty clay and a variety of volcanic rock fragments.

The most calcium carbonate–rich beds were observed in Section 35R-4, as a very coarse grained packstone composed of bioclastic carbonate, with centimeter-sized intraclasts of greenish gray clayey siltstone (interval 180-1115C-35R-4, 0–20 cm). Slightly lower in the unit, sporadic packstones are composed of well-sorted, slightly normal graded bioclastic calcarenite. In thin section, the packstone contains benthic foraminifers, echinoderm debris, planktonic foraminifers (filled with pyrite), calcareous algae, bivalve shell fragments, bryozoans, and coral fragments (Fig. F24). In addition, detrital grains include pyroxene, hornblende, quartz, plagioclase, pyroxene, and rarely, olivine phyric basalt, acidic volcanics, limestone, very rare chloritic schist, micaceous calc-schist, and iron oxide.

F24. Sandstone with fossil and mineral fragments, p. 89.

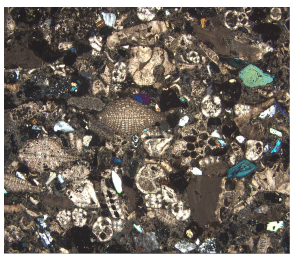

Clayey Siltstone

Greenish clayey siltstone contains scattered small bioclastic grains (e.g., interval 180-1115C-35R-4, 38–40 cm). Locally, lamination (including fine convolute lamination) is inclined at up to 50° and the rock is cut by anastomosing cracks (interval 180-1115C-35R-4, 50–76 cm). In places the siltstone changes to a reddish brown color (interval 180-1115C-35R-4, 86–105 cm). These red siltstone intervals exhibit dipping laminae, small-scale convolute lamination, synsedimentary microfaults, dark gray clayey siltstone rip-up clasts, and occasional rhodoliths. Elsewhere, rhodoliths are again observed (interval 180-1115C-35R-4, 10–12 cm). Some individual fragments are rich in microfossils cemented by calcite (Section 39R-CC).

Silty Claystone

Interbeds are parallel laminated, with sharp basal and upper contacts (interval 180-1115C-35R-1, 106–135 cm). Locally, the siltstone is dark gray, parallel laminated, lacks bioturbation, and appears to be rich in organic matter (e.g., Fig. F25).

F25. Claystone with very thin silt- and clay-rich laminae, p. 90.

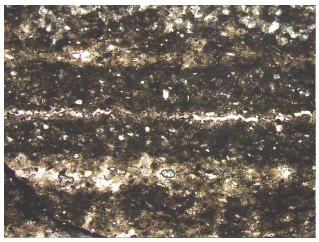

Matrix-Supported Conglomerate

There is a single interval of reddish brown clayey siltstone, with subrounded pebbles of dark gray siltstone and bioclastic pebbles (i.e, algal oncolites). A single clast of derived conglomerate was noted in interval 180-1115C-35R-4, 86–105 cm.

In addition, a single conglomerate clast was recovered from the lower part of the unit. This is composed mainly of small (0.5–1.5 cm), suban-

gular to rounded calcium carbonate or limestone pebbles, also very well rounded siltstone and claystone clasts (interval 180-1115C-37R-CC, 3–6 cm).

Interpretation

Unit XI accumulated rapidly in an upper bathyal to outer neritic setting (~150 m) during middle Miocene time at an estimated sedimentation rate of >135 m/m.y. (see **"Sediment Accumulation Rate,"** p. 34). The carbonate rock (packstone) and associated volcaniclastic sediment were redeposited from a neritic setting, presumably by high-density turbidity currents. The source area included pyroxene phyric basalt, as in the overlying unit. A continental slope setting is inferred from the abundance of sedimentary structures indicative of sediment instability, including soft-sediment deformation, evidence of slumping or sliding, and dewatering. Specifically, one internally deformed unit is interpreted as part of a small slide block that partially broke up during transport. It is likely that slope instability characterized a wide area of the inferred slope environment. However, it is also possible that the site lay within a submarine channel, with only very localized slumping of soft sediment from the banks of the channel. In addition, the isolated clast was possibly transported within a debris flow. A relatively uniform sandy and silty succession is present, based on the gamma-ray, resistivity, neutron porosity, and density logs (see **"Downhole Measurements,"** p. 52). The FMS data further indicate that a particularly resistive layer is present near the top of the unit from 607 to 614 m that may correspond to the presence of calcite-cemented sandstone in the cores. Conversely, one of several thin, relatively muddy intervals is present from 614.2 to 614.5 mbsf. The FMS data further suggest that unusual lithologies are present between 640 and 650 mbsf, an interval of minimal recovery.

Lithostratigraphic Unit XII

Description: sandy siltstone and silty sandstone
Interval: Cores 180-1115C-40R through 54R
Depth: 657.8–802.5 mbsf
Age: middle Miocene

This lowest unit in Hole 1115C is marked by a change from heterogeneous, variably calcareous sedimentary rocks of the overlying unit to a much more homogeneous, finer grained, less calcareous succession of sandy siltstone alternating with silty sandstone and rare silty claystone. Levels of calcium carbonate vary within a narrow range, 5–10 wt% (see **"$CaCO_3$, Sulfur, Organic Carbon, and Nitrogen,"** p. 45).

Silty Sandstone

Dark gray, bioturbated, calcareous sandstone (with mainly *Chondrites* and rare *Zoophycos*), is present mainly near the top of the unit, with scattered fragments of shells and planktonic foraminifers. Planar lamination and cross lamination are locally preserved (e.g., intervals 180-1115C-41R-2, 17–18 and 29–31 cm; and 41R-4, 35–45 cm). Bioturbation varies in different beds from minor to intense. Darker, apparently more organic-rich beds are generally less bioturbated. In places, burrowing is so intense that primary lamination is largely obscured. Below 670 mbsf

sandstone largely disappears other than as rare intercalations. Exceptionally, in the interval 180-1115C-47R-2, 0–15 cm, a sandstone grades into siltstone, marked by a very irregular base, parallel or inclined lamination, and unusual thin (mm) clay-rich veins.

In thin sections, the sandstones are compositionally quite constant (**"Site 1115 Thin Sections,"** p. 89). Samples studied are fine-grained arkosic sandstones, with plagioclase, quartz, planktonic foraminifers (pyrite filled), acidic volcanic fragments, and rare chloritic grains. In general, there is a high ratio of individual mineral grains to rock fragments (>80%). Also, organic matter is common.

Sandy Siltstone

From 670 mbsf downward, there is a slight decrease in average grain size from silty sandstone to dark gray and pale gray sandy siltstone, with occasional silty sandstone interbeds (e.g., interval 180-1115C-41R-CC, 12–22 cm). Otherwise, the composition and sedimentary structures remain unchanged from above. Individual intervals of sandy siltstone (0.1–0.4 cm thick) are calcareous and very highly bioturbated, with parallel or slightly wavy lamination (Fig. **F26**). Sandy siltstones are present near the base of the hole, in Section 54R-5, as thick laminae to thin beds with sharp bases and tops, which are commonly erosional based. Small bioclastic fragments include possible echinoderms. Locally, a small (<0.5 cm) lensoidal structure is infilled with sandstone. Small, synsedimentary mud clasts are present between 65 and 75 cm.

Calcareous Siltstone

From 710 mbsf downward, the sand content further decreases and the lithology is calcareous siltstone. Otherwise, there is little change. The rocks are burrowed throughout, with scattered planktonic foraminifers and rare sand-sized shelly fragments. Thin-section study indicates the presence of abundant biotite, feldspars, clinopyroxene, rare quartz, and subrounded basalt fragments (Fig. **F27**; **"Site 1115 Thin Sections,"** p. 89). Parallel and convolute lamination are vaguely preserved. In places, thin (3–5 cm) beds grade from very fine grained sandstone to siltstone at the base, to uniform silty clay at the top (e.g., five such intervals are present in Section 46R-1, and another in Section 47R-1; Fig. **F28**). In other cases similar very thin beds exhibit both sharp upper and lower boundaries (e.g., interval 180-1115C-46R-2, 10–107 cm). Inverse-to-normal grading is also locally visible on a scale of several centimeters (e.g., Section 48R-1).

The graded beds are commonly less burrowed than the adjacent lithologies, and some intervals are more or less devoid of burrowing (e.g., Section 47R-7). Commonly, bioturbation is concentrated in 3- to 5-cm-wide zones (e.g., Section 47R-1). Small shell fragments are locally present (e.g., interval 180-1115C-46R-5, 124–127 cm). In this lower part, only rare intervals of fine, calcareous sandstone are present, with scattered planktonic foraminifer tests and very rare benthic foraminifers (e.g., interval 180-1115C-47R-7, 26 cm).

The XRD analysis of the fine-grained sedimentary rocks revealed a relatively constant composition with plagioclase, and sometimes calcite, pyroxene, and quartz as major constituents, and smectite? and zeolite (clinoptilolite?) as minor components (Table **T3**).

F26. Siltstone with bioturbation and planar lamination, **p. 91.**

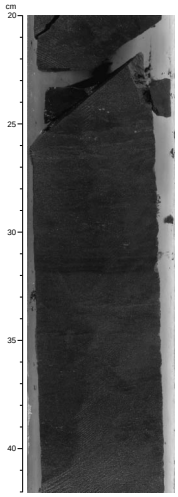

F27. Siltstone with grains of minerals, foraminifers, and rock fragments, **p. 92.**

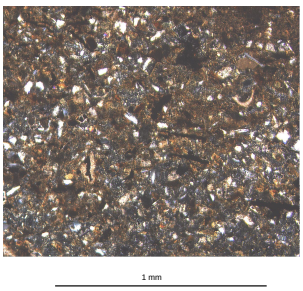

F28. Sandstone with sharp contacts and little bioturbation, **p. 93.**

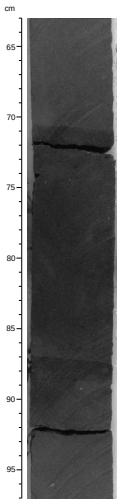

Silty Claystone and Claystone

Downward in the unit finer grained silty claystone begins to appear, first as thin laminae (Section 42R-5), then as discrete very thin beds, 1–2 cm thick (e.g., intervals 180-1115C-45R-1, 10, 75, and 105 cm). Several such thin claystone intercalations are seen in intervals 180-1115C-45R-4, 44–46 and 100–107 cm. Rare dewatering structures are evident (i.e., small subvertical dewatering conduits infilled with sand; interval 180-1115C-45R-5, 0–10 cm).

Smear slides of the finer grained sediment indicate the presence of common quartz and feldspar, coupled with sporadic biotite, accessory minerals (pyroxene), rock fragments, calcite, and pyrite. Bioclasts present are nannofossils, planktonic foraminifers, and rare sponge spicules (**"Site 1115 Smear Slides,"** p. 86). The XRD analysis of the fine-grained sediments of Unit IX indicates an abundance of plagioclase, with subordinate calcite, quartz, pyroxene, smectite? and zeolite (Table **T3**).

Volcaniclastic Sandstone

A medium- to coarse-grained ash-rich volcaniclastic layer with sharp upper and lower contacts was observed in the interval 180-1115C-45R-3, 107–108 cm.

Interpretation

Unit XII accumulated in the middle Miocene at an upper bathyal depth (150–500 m) at a rapid average sedimentation rate of >135 m/m.y., unchanged from Unit XI above (see **"Biostratigraphy,"** p. 31). However, interpretation of conventional logs shows that the succession is made up of relatively constant alternations of sandstone and siltstone, based on the gamma-ray, resistivity, neutron porosity, and density logs (see **"Downhole Measurements,"** p. 52). The FMS images further reveal a very homogenous succession, with occasional thin (<5 cm), more resistant, inferred sandstone layers. Possible cross bedding is imaged between 677 and 679 mbsf.

The sandy siltstone and silty sandstone probably underwent extensive bioturbation of original discrete beds. The predominance of bioturbation points to well-oxygenated bottom conditions, although the abundance of organic matter particles seen in thin sections suggests that there was a high input of terrestrial organic matter. The siltstones and sandstones were largely deposited from suspension and are interpreted as deposits from turbidity currents in view of the water depth below wave base, as inferred from paleontological evidence. Relative to Unit XI above, there is less evidence of sediment instability, which is consistent with a relatively stable, tectonic setting. After lithification, the succession was locally faulted.

The provenance of Unit XII was from a calc-alkaline magmatic suite, assumed to be from the Trobriand volcanic arc to the southwest. During the middle–late Miocene, Site 1115 is inferred to have formed part of a submerged forearc ~70 km northeast of the front of the Trobriand Arc (see **"Hanging Wall and Northern Margin Sites,"** p. 17, in the "Leg 180 Summary" chapter).

Depositional History

The depositional history at Site 1115 can be divided into three sequences: (1) a mainly deep-water forearc succession culminating in a relative regression; separated by an erosional unconformity from (2) a nonmarine to fluvial, lagoonal, coastal succession; and (3) a shallow- to deep-marine succession related to rifting of the Woodlark Basin.

Sequence 1

Unit XII accumulated mainly by deposition of turbidity currents during the middle Miocene in an upper bathyal (150–500 m) forearc basin to the northeast of the Miocene calc-alkaline Trobriand Arc (Davies et al., 1984; Johnson et al., 1978; Lock et al., 1987; Smith and Milsom, 1984; and Stolz et al., 1993). The source material included distinctive pyroxene phyric basic extrusives. Comparison with the seismic stratigraphic record suggests that the cored interval represents only the top of a very thick (>2 km) forearc succession. Unit XI, also late Miocene in age, represents a similar provenance and shoaling water depths. The presence of redeposited neritic carbonate indicates additional input of shallow-water deposits. Marked sediment instability is recorded, related either to local channeling or regional tectonic movements. Subsequently, Unit X records a more shallow-water setting (50–150 m), with accumulation at a similar or possibly somewhat reduced sedimentation rate with substantial input of shallow-water carbonate. Alternative explanations for the shallowing are that the forearc basin simply overfilled and became emergent, or, more probably, that the basin was tectonically uplifted, possibly as a result of regional compression. Sequence 1 culminated in emergence with a resulting uncomformity and a hiatus.

Sequence 2

Based on the biostratigraphy of Site 1115 and the Nubian-1 well, the time span of this hiatus is shorter than 5.54–9.93 Ma (see **"Site 1115,"** p. 1). Units IX to VII accumulated during part of this time, after 8.6 Ma. A subaerial to fluvial environment (Unit IX) was transgressed by the sea, giving rise to a low-energy inner lagoonal setting with a high organic-matter content (Unit VIII), then to a more open-marine lagoonal setting (Unit VII).

Sequence 3

Since 5.54 Ma the area of Site 1115 subsided. A shallow-marine setting (Unit VI) became an open-shelf setting influenced by traction currents (Unit V). Sediment deposition accelerated, but subsidence was even faster: turbidity currents deposited Unit IV during the early Pliocene at ~155 m/m.y. in water depths of ~150 m. The provenance of volcaniclastic sandstone was from a calc-alkaline arc source that remained little changed throughout the Pliocene. During middle and earliest late Pliocene time (Unit III), rapid deposition (393 m/m.y. until 3.11 Ma) was followed by reduced accumulation (79 m/m.y.) all in an upper bathyal setting (150–500 m). Calcium carbonate increases generally upward, which correlates with a general increase in pelagic carbonate component. Graded volcaniclastic sandstones deposited by turbidity currents are common, whereas volcanic glass-rich units are

interpreted as air-fall tuff (see "Record of Ash Eruption," p. 28). The basin at Site 1115 deepened during late Pliocene– Pleistocene time to upper middle bathyal depths (Unit II). The relative amount of volcaniclastic sand deposited by turbidity currents decreased (Unit II), and also the overall sedimentation rate decreased to 63 m/m.y. Pleistocene deposition (Unit I) was dominated by nannofossil ooze with volcanic ash (see paragraph below), and sedimentation slowed further (34 m/m.y.), post 0.5 Ma.

Record of Ash Eruption

The sedimentary succession recovered at Site 1115 contains 161 volcanogenic ash layers. They total 474 cm in thickness and, therefore, represent about 0.5% of the 802.5 m section. The thickness of individual layers ranges from 0.5 cm to 18 cm. The stratigraphic distribution and number of volcanogenic ash layers observed per core, as well as the total thickness of ash observed per core, are shown in Figure **F29.** The highest frequency of layers per core is 19, constituting up to 5.6% of the total recovered thickness of the single core (Core 180-1115B-29X).

The distribution of volcanic ash layers through time is as follows:

Only one volcaniclastic ash layer was recovered in the middle Miocene section (>13.6 Ma; see "Biostratigraphy," p. 31). No volcanogenic ash layers were recovered from the uppermost middle Miocene to lowermost Pliocene. Beginning in the middle Pliocene sediments at ~385 mbsf (3.58 Ma; see "Paleomagnetism," p. 34) and extending to 150 mbsf (~2.55 Ma; see "Paleomagnetism," p. 34, and "Biostratigraphy," p. 31) the amount of volcanogenic material dramatically increased. Within this interval, volcanogenic material is dominantly in the form of volcaniclastic sandstone layers. Several volcanic ash layers (i.e., ash fallout) happened during this interval, but its volumetric contribution was minor compared with that supplied by volcaniclastic turbidites.

Volcaniclastic ash layers are relatively rare in the uppermost Pliocene and in the Quaternary (<1.95 Ma; see "Biostratigraphy," p. 31). The influx of volcanogenic material was delivered predominantly by ash fallout. Some of the ash fallout layers are associated with volcaniclastic sand beds that, together, are interpreted as primary pyroclastic material (e.g., Carey and Sigurdsson, 1980; Fisher and Schmincke, 1984).

The discovery of ash fallout layers and associated volcaniclastic turbidites at Site 1115 has important implications for the volcanic-tectonic evolution of the Trobriand Arc and eastern Papua (Smith, 1976; Davies et al., l984; Johnson et al., 1978; Lock et al., 1987; Smith and Milsom, 1976; and Stolz et al., 1993).

Taken together, the above types of volcanogenic deposits indicate a relatively local, at least partly subaerial, volcanic source. The stratigraphic distribution of volcanogenic ash layers indicates that local volcanism extends at least to the early Pliocene (3.58 Ma). Given the proximity of the Amphletts Islands, Egum Atoll, Fergusson Island, and Goodenough Island, it seems likely that the record of volcanogenic deposits reflect regional volcanic-tectonic activity. For example, volcanic rocks from these islands have been dated at 6.3 Ma to Holocene (see Smith and Milsom, 1984, and references therein).

F29. Volcanogenic ash layers and ash thickness per core, p. 94.

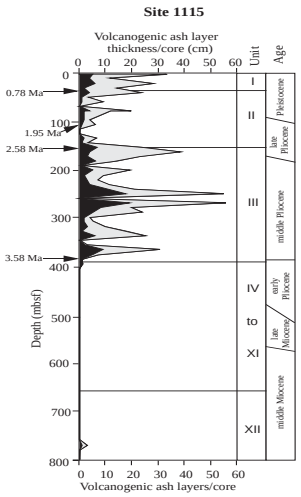

STRUCTURAL GEOLOGY

Introduction

The 802.5-m-long middle Miocene to Pleistocene sedimentary succession cored at Site 1115 is relatively undeformed. The only evidence of deformation is in the lowermost part of the section where three discrete fault zones alternate with undeformed zones. Undeformed zones, referred to Domain I, extend from the seafloor to 551.8 mbsf (Subdomain Ia), from 566.1 to 603.85 mbsf (Subdomain Ib) and from 689.8 to 724.9 mbsf (Subdomain Ic). Domain II consists of three fault zones that form Subdomains IIa (551.8 to 566.7 mbsf), IIb 609.4 to 696.5 mbsf) and IIc (725.4 to 802.5 mbsf). They are labeled FZ1, FZ2, and FZ3 in Figure **F30.** In general, bedding dips are very shallow, with a mode between 0° and 5°. The few steep dips (50° and 60°) shown in Figures **F30** and **F31A** are inferred to be mostly related to soft-sediment deformation. The fault network identified at Site 1115 displays a relatively large range of dips, as illustrated on the histogram of Figure **F31B,** which shows three maxima at 45°–50°, 70°–75°, and 85°–90°, respectively.

F30. Structural features at Site 1115, **p. 95.**

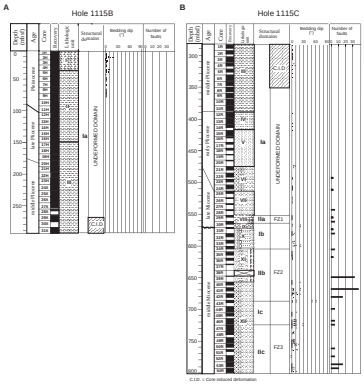

F31. Bedding and fault dips, **p. 96.**

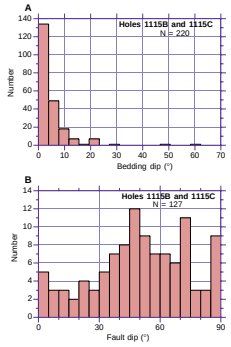

Domain I: Undeformed Zones

Subdomain Ia

Subdomain Ia extends from the seafloor to 551.8 mbsf and is composed of unconsolidated and weakly indurated late Miocene to Pleistocene oozes and silty clays of lithostratigraphic Units I to VII (see **"Lithostratigraphy,"** p. 5). Bedding is generally horizontal (Fig. **F30**), but some gentle dips up to 10° are locally observed. At interval 180-1115B-17H-3, 121–125 cm (153.91–153.95 mbsf), strata are exceptionally inclined at 15°, probably as the result of slope instability. Additional evidence is suggested by a minor high angle (75°–80°) normal fault filled with greenish clayey material, and inferred to be an early compaction-induced feature (Section 180-1115B-18H-2 [160.7–162.2 mbsf]).

In Core 180-1115B-29X (264.3–273.9 mbsf), the silty material becomes more lithified, and exhibits drilling-induced brittle deformation especially in Cores 180-1115B-29X to 180-1115C-9R (264.3 to 369.5 mbsf). Two types of coring-induced deformation are observed. Steep individual fractures ~10 cm long, cut through the central part of cores. In addition boudinlike structures are formed by regularly spaced (5–10 cm) silty pieces separated by more clay-rich horizons along which rotation has preferentially occurred during coring. This coring-induced fabric is in the interval from Section 180-1115C-1R-2 to Core 11R (284.6–388.5 mbsf), and is particularly well developed in Section 8R-2 (351.4 to 352.9 mbsf).

Subdomain Ib

Subdomains Ib and Ic are located within the middle Miocene forearc sequences forming lithostratigraphic Units X and XII, respectively, although the former straddles the major unconformity identified in Section 180-1115C-31R-1 at 571.87 mbsf (see **"Lithostratigraphy,"** p. 5).

Subdomain Ib extends from 566.01 to 603.85 mbsf (Sections 180-1115C-30R-5 to 34R-3), and is characterized by almost horizontal bed-

ding, dipping from 0° to 7°–8° (Fig. F30). The highest dips (9°–20°) measured in Section 180-1115C-34R-3 correspond to slump structures marked by thin layers of medium- to coarse-grained sandstones injected into underlying clays (see "Lithostratigraphy," p. 5). Evidence for fracturing is documented in intervals 180-1115C-31R-1, 90–95 cm; 31R-3, 8–10 cm; and 31R-CC, 0–5 cm, by very few mm-thick calcite-filled veins lying in either horizontal or vertical positions. In addition, Section 180-1115C-31R-4 is cut throughout most of its length (interval 180-1115C-31R-4, 15–95 cm) by a vertical, 1-mm-thick quartz-filled vein.

Subdomain Ic

This subdomain is present from 689.8 to 724.9 mbsf (Sections 180-1115C-43R-3 to 46R-7). Bedding is nearly horizontal everywhere with only a few beds dipping between 0° and 12° (Fig. F30). Weak brittle deformation is expressed by either minor steeply dipping normal faults or coring-induced structures (boudinlike features in Section 180-1115C-43R-3 [689.8 to 691.0 mbsf]).

Domain II: Fault Zones

Subdomain IIa

Subdomain IIa represents a discrete fault zone (FZ1 in Fig. F30), extending from Sections 180-1115C-29R-3 to 30R-4 (554.3–565.7 mbsf) and corresponds to lithostratigraphic Unit VIII (see "Lithostratigraphic Unit VIII," p. 18). Ten minor faults, including three shallow dip-slip slickensided fault surfaces, exhibit dips ~20°–40°. Figure F30 shows that bedding remains nearly horizontal throughout FZ1, with no marked change with respect to the two bounding undeformed zones. The few moderate bedding dips (20°) measured in interval 180-1115C-30R-3, 10–40 cm, are bounded on top and bottom by horizontal strata, and they are, therefore, assigned to local soft-sediment deformation.

Subdomain IIb

This domain (FZ2) constitutes the most significant fault zone at Site 1115 (Fig. F30) and extends from 609.4 to 696.5 mbsf (Cores 180-1115C-35R to 43R). Within the fault zone, bedding is still nearly horizontal (Figs. F30, F32A). A few steep beds, dipping at 50°–60°, are present in interval 180-1115C-43R-2, 45–100 cm, and because their overlying and underlying strata are horizontal, they may represent intraformational slump features. Soft-sediment deformation is also observed in interval 180-1115C-40R-4, 90–100 cm.

The fault system of Domain IIb displays almost the same dips as the total fault population, with a mode of 40°–60° with another peak at 90° (Fig. F32B). Some shallow-dipping faults are occasionally associated with scaly fabrics in fine-grained silts, as in interval 180-1115C-41R-3, 135–140 cm. Most of the steepest fractures are usually filled with fine-grained material similar to the clay-rich host rock in interval 180-1115C-43R-2, 50–90 cm. They are, therefore, inferred to be early brittle structures formed during sediment compaction. The histogram of Figure F32C illustrates the composite nature of the Domain IIb fault network, including dip-slip, oblique-slip, and strike-slip faults. Dip-slip faults are dominant, with either extensional or reverse sense of motion. In intervals 180-1115C-40R-4, 40–50 cm, and 42R-3, 90–130 cm, the

F32. Structural measurements of Fault Zone 2, p. 97.

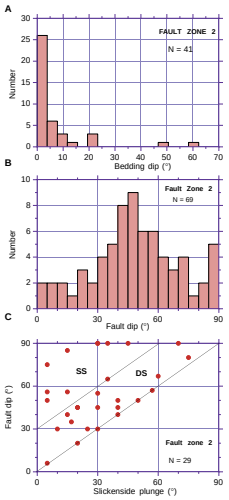

reverse displacements systematically take place along almost vertical and sigmoidal surfaces, in close association with normal faults. Since steeply dipping faults are likely to be early structures, generated during compaction, the reverse motions are not interpreted as true compressional structures, but are the result of slightly varying dip angle of the nearly vertical curved normal fault.

Subdomain IIc

Subdomain IIc forms the third fault zone within Cores 180-1115C-47R to 54R (725.4–802.45 mbsf). Bedding dips are similar to those of the above-mentioned structural domains, with a mode between 0° and 10°, and maximum values between 15° and 28° (Figs. **F30, F33**). Faults are generally steep, dipping on the average of 70°–90°, and they include both strike-slip and pure dip-slip structures. Most of the dip-slip faults are extensional; however, reverse structures are present in intervals 180-1115C-47R-6, 95–103 cm, and 48R-2, 55–60 cm, with offsets a few millimeters long. The reverse motions can be explained in the same way as those discussed above.

The comparative analysis of the histograms of Figure **F34** clearly shows that there is no major contrast in bedding dips on both sides of the intra-Miocene unconformity, which is in accord with the local strata pattern imaged by reflection seismic (see **"Vertical Seismic Profile and Depth Conversion,"** p. 59).

F33. Bedding dips in Fault Zone 3, **p. 98.**

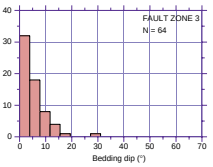

F34. Bedding dip measurements in synrift and forearc sequences, **p. 99.**

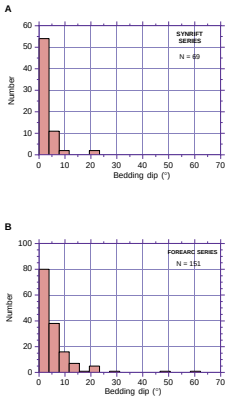

BIOSTRATIGRAPHY

Calcareous Nannofossils

Abundance and Preservation

Nannofossils are abundant and well preserved in Sample 180-1115A-1H-CC, and common to abundant and well preserved in Samples 180-1115B-1H-CC to 27X-CC. Nannofossils are common and preservation is moderate in Samples 180-1115B-28X-CC to 31X-CC, with the exception of 30X-CC, which is barren.

In Hole 1115C, Samples 180-1115C-1R-CC to 15R-CC contain common nannofossils with moderate to good preservation. Nannofossils are still common from Sample 180-1115C-16R-CC down to 23R-CC, but preservation is moderate to poor. Few to rare, mostly poorly preserved nannofossils are present in Samples 180-1115C-24R-CC to 36R-CC, with the exception of Samples 180-1115C-30R-CC, 31R-CC, 34R-CC, and 35R-CC, which are barren or almost barren of nannofossils. Nannofossil numbers increase and their degree of preservation improves below Sample 180-1115C-37R-CC, with nannofossils becoming few to common and preservation moderate from Sample 180-1115C-37R-CC to 41R-CC. Sample 180-1115C-42R-CC is nearly barren. Nannofossils in Samples 180-1115C-43R-CC to 54R-CC are few to common in abundance and preservation is moderate or poor (mostly moderate).

Zonation

Sample 180-1115A-1H-CC is in Zone NN20/21, based on the presence of rare *Emiliania huxleyi* and lack of *Pseudoemiliania lacunosa* (Fig. **F35;** Table **T4**).

F35. Biostratigraphic units and ages, **p. 100.**

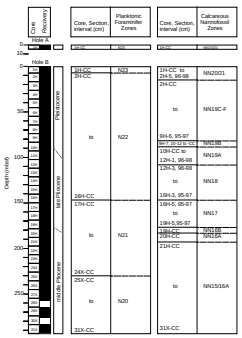

T4. Distribution of calcareous nannofossils, **p. 183.**

Samples 180-1115B-1H-CC to 2H-5, 96–98 cm are also in Zones NN20/21. We assign Samples 180-1115B-2H-CC through 9H-6, 95–97 cm, to the Subzone NN19C-NN19F interval because of the presence of *Pseudoemiliania lacunosa* and *Helicosphaera sellii,* and lack of *Calcidiscus macintyrei*. *Calcidiscus macintyrei* is present in Samples 180-1115B-9H-7, 10–12 cm, to 9H-CC, together with some small forms of *Gephyrocapsa oceanica*. We assign this interval to Subzone NN19B. Samples 180-1115B-10H-CC to 12H-1, 96–98 cm, lack *G. oceanica* and are therefore in Subzone NN19A. The last occurrence (LO) of *Discoaster brouweri* in Sample 180-1115B-12H-3, 96–97 cm, marks the Zone NN18/Subzone NN19A/B boundary. The LO of *D. pentaradiatus* in Sample 180-1115B-16H-5, 95–97 cm, marks the Zone NN17/NN18 boundary, and the LO of *D. surculus* in Sample 180-1115B-19H-CC marks the Subzone NN16B/Zone NN17 boundary. The LO of *D. tamalis* in Sample 180-1115B-20H-CC in this hole defines the Subzone NN16B/NN16A boundary.

The difficulty of recognizing the true Zone NN15/NN16 boundary in low latitudes is discussed in **"Biostratigraphy,"** p. 43, in the "Site 1109" chapter. In Hole 1115B, the LO of *Sphenolithus* spp. (the secondary species approximating the boundary) appears to be anomalously high in the section when compared to the first occurrence (FO) of the foraminifer *Globorotalia tosaensis*. We are not sure of the cause of this relationship, but because of it we have not separated Zone NN15 and Subzone NN16A in this hole. Instead, we assign Zone NN15/Subzone 16A undifferentiated to Samples 180-1115B-21H-CC through 31X-CC.

In Hole 1115C, undifferentiated Zone NN15/16A ranges from Sample 180-1115C-1R-CC to 16R-CC. The upper boundary of Zone NN14 is marked by the last common occurrence (LCO) of *Reticulofenestra pseudoumbilicus* in Sample 180-1115C-17R-CC. *Discoaster asymmetricus* is rare in these samples, and we could not confirm its first common occurrence (FCO), which defines the Zone NN13/NN14 boundary. *Ceratolithus rugosus,* whose FO defines the Zone NN12/NN13 boundary, is rare in these samples. *Ceratolithus rugosus* is present in Sample 180-1115C-19R-CC. However, the LO of *C. acutus,* which also is present at the Zone NN12/NN13 boundary, is in Sample 180-1115C-21R-1, 40–42 cm, and we consider this to be the top of Zone NN12. The LO of *D. quinqueramus* is in Sample 180-1115C-25R-CC, which defines the Zone NN11/NN12 boundary. We, therefore, assign all samples from Sections 180-1115C-17R-CC to 20R-CC to Zone NN13-NN14 undifferentiated, and assign Samples 180-1115C-21R-1, 40–42 cm, through 25R-1, 89–91 cm, to Zone NN12. *Discoaster quinqueramus* is present from Sample 180-1115C-25R-CC through 29R-CC, indicating Zone NN11. Samples 180-1115C-30R-CC through 33R-CC are barren or contain only a rare, middle to late Miocene assemblage. Samples 180-1115C-34R-1, 31–33 cm, through 54R-CC contain *Sphenolithus heteromorphus* and lack *Helicosphaera ampliaperta* and *S. belemnos,* indicating Zone NN5.

Planktonic Foraminifers

Abundance and Preservation

Specimens were abundant and their preservation good in core catcher samples from Cores 180-1115A-1H, 1115B-1H through 26H, and 1115B-31X; specimens were abundant and their preservation moderate from Samples 180-1115B-27X-CC through 29X-CC, and rare but with good preservation in 30X-CC. Core catchers from Cores 180-1115C-1R through 17R contained abundant specimens with moderate

to good preservation; specimens were rare to few and their abundance moderate to good from Cores 180-1115C-18R-CC to 24R-CC; specimens were common to abundant and their preservation moderate to poor in Samples 180-1115C-31R-CC, 33R-CC through 35R-CC, and 43R-CC through 47R-CC; specimens were few to rare and their preservation moderate to poor in Samples 180-1115C-32R-CC, 37R-CC through 42R-CC, and 49R-CC through 54R-CC.

There were no planktonic foraminifers in the core-catcher samples of Cores 180-1115C-26R through 29R, which yielded shallow-water benthic foraminifers. The sandy sediment of Samples 180-1115C-25R-CC, 30R-CC, and 36R-CC was barren of all foraminifers.

Zonation

The planktonic foraminiferal zonation of Holes 1115A, 1115B, and 1115C is shown in Figure F35 and the species are listed in Table T5. Samples 180-1115A-1H-CC and 180-1115B-1H-CC were assigned to Zone N23 because of the presence of *Beella calida*. Common to abundant specimens of pink *Globigerinoides ruber* in both samples indicate an age no younger than 120 ka. Samples 180-1115B-2H-CC through 16H-CC with *Globorotalia truncatulinoides* lie in Zone N22. Sample 180-1115B-10H-4, 65–67 cm, marks the LO of *Globigerinoides fistulosus* just above the Pliocene/Pleistocene boundary. Zone N21 extends from Sample 180-1115B-17H-CC to Sample 180-1115B-24X-CC, in which is found the first evolutionary appearance of *Globorotalia tosaensis* from its ancestor *G. crassaformis*. Zone N20, in which *G. crassaformis* is present without its descendent, extends through the remainder of Hole 1115B and continues in Hole 1115C to Sample 180-1115C-18R-CC (the sinistral to dextral coiling change in *Pulleniatina* dated at 3.95 Ma is present between 17R-CC and 18R-CC), after which a shallow-water facies lacking planktonic foraminifers is found from Sections 180-1115C-19R-CC through 30R-CC.

The stratigraphic section, interrupted by an unconformity, continues with a middle Miocene (Zone N12) section from Samples 180-1115C-31R-CC through 33R-CC. These samples contain *Globorotalia praemenardii* (with *G. lenguaensis,* which first occurs in Zone N12 in Sample 180-1115C-33R-CC). The presence of the larger foraminifer *Lepidocyclina (Nephrolepidina)* in Sample 180-1115C-34R-CC indicates a middle Miocene age. Sample 180-1115C-41R-CC contains *G. praemenardii,* which ranges from Zone N10 to N12. From Sample 180-1115C-43R-CC to 53R-CC *Globorotalia archaeomenardii, Orbulina* spp., and *Globorotalia peripheroronda* are present, indicating Zone N9 or N10. In Sample 180-1115C-54R-CC, the bottom of the hole, the presence of *Orbulina* spp. indicates an age no older than middle Miocene, Zone N9.

T5. Distribution of planktonic foraminifers, p. 185.

Benthic Foraminifers

Site 1115, at a water depth of ~1150 m, has a surface assemblage of benthic foraminifers dominated by agglutinated species that are not preserved lower in the section, among them *Ammolagena clavata, Reophax* sp., *Rhizammina* sp., *Saccorhiza ramosa,* and *Trochammina* sp. (Sample 180-1115B-1H-1, 0–1 cm). From the seafloor surface through Sample 180-1115B-17H-CC (159.7 mbsf), a Holocene to middle upper Pliocene, upper middle bathyal assemblage (500–1150 m) contains the following characteristic species: *Ceratobulimina pacifica, Cibicidoides*

rugosus, Parrelloides bradyi, Pyrgo murrhina, Sphaeroidina bulloides, and *Triloculina tricarinata*.

From Sample 180-1115B-18H-CC (169.2 mbsf) through 1115C-14R-CC (412.0 mbsf), a middle upper Pliocene to middle Pliocene assemblage is indicative of upper bathyal depths (150–500 m). The characteristic species are: *Anomalinoides colligerus, Heterolepa praecincta, Rectobolivina columellaris, Melonis multicameratus,* and *Siphonina tubulosa/australis*.

From Sample 180-1115C-15R-CC (425.8 mbsf) through 20R-CC (465.9 mbsf), an early Pliocene outer neritic (50–150 m) assemblage is sparsely populated by *Angulogerina* sp. and *Lugdunum hantkenianum*.

From Sample 180-1115C-21R-CC (480.3 mbsf) through 29R-CC (555.3 mbsf) the early Pliocene assemblage is indicative of inner neritic depths (<50 m), with large marine species such as Neoeponides *bradyi, Asterorotalia gaimardii, Elphidium craticulatum,* and *Elphidium* sp. from Sample 180-1115C-21R-CC through 23R-CC; followed by *Ammonia* sp. and *Elphidium* sp., indicating salinity variation from Sample 180-1115C-26R-CC through 29R-CC. Sample 180-1115C-30R-CC was pyritic and barren of all foraminifers.

The stratigraphic section continued downward with middle Miocene strata, indicative of an unconformity between Samples 180-1115C-29R-CC and 31R-CC. From Sample 180-1115C-31R-CC (572.3 mbsf) through 35R-CC (615.0 mbsf) benthic assemblages suggest an outer neritic (50–150 m) environment with larger foraminifers concentrated in Samples 180-1115C-34R-CC and 35R-CC. These include *Amphistegina* spp. and *Lepidocyclina* spp., with *Lepidocyclina (Nephrolepidina) martini* indicative of middle Miocene age (Fig. **F36**).

From Sample 180-1115C-37R-CC (629.0 mbsf) through 53R-CC (790.9 mbsf) the assemblages suggest upper bathyal to upper middle bathyal conditions; *Hoeglundina elegans* is frequently present, *Uvigerina schwageri* is found in Sample 180-1115C-41R-CC, and *Ceratobulimina pacifica, Siphonina* sp., and *Globocassidulina pacifica* are found in Sample 180-1115C-53R-CC.

Sediment Accumulation Rate

We estimated the sedimentation rate based on nannofossil and foraminifer datum events and magnetic chron and subchron boundaries at Site 1115 (Fig. **F37**).

A conglomerate layer is found from Sample 180-1115C-30R-5, 47 cm, to 31R-1, 87 cm (566.5–571.87 mbsf). The very slow sedimentation rate (<5 m/m.y.) from 8.6 to 12.1 Ma is most likely the result of an unconformity at the base of this conglomerate layer (see **"Lithostratigraphy,"** p. 5).

PALEOMAGNETISM

The investigation of magnetic properties at Site 1115 included (1) the measurement of bulk susceptibility of whole core sections, (2) point susceptibility and remanent magnetization of archive half core sections, and (3) susceptibility and its anisotropy and remanent magnetization of discrete samples.

F36. Equatorial section of *Lepidocyclina* (*Nephrolepidina*) *martini*, **p. 102.**

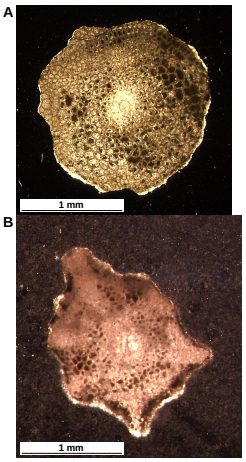

F37. Age-depth relationship at Site 1115, **p. 103.**

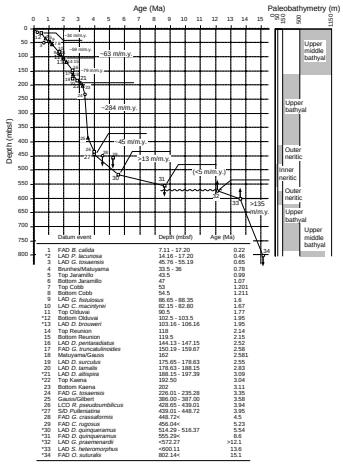

Magnetic Susceptibility

Magnetic susceptibility measurements were made on whole core sections as part of the multisensor track (MST) analysis (see "Physical Properties," p. 47), and on half core sections as part of the archive multisensor track (AMST) analysis. The MST and AMST susceptibilities (uncorrected for volume) ranged between values on the order of 10^{-5} and 10^{-2} SI (Fig. F38A, F38B). In general, susceptibility data from the MST and AMST analyses agreed; differences in magnitude can be attributed to volume differences for the uncorrected data. The apparent constant low values in the AMST data between ~200 and 500 mbsf were caused by technical problems.

The trends of susceptibility and remanent intensity data after AF demagnetization at 20 mT are similar throughout Holes 1115B and 1115C (Fig. F39). The high values below ~580 mbsf and between ~420 and 480 mbsf suggest that the contribution of remanence-carrying ferrimagnetic minerals to the susceptibility and its anisotropy is great. The lower values between ~210 and 420 mbsf, and again between ~480 and 580 mbsf suggest that paramagnetic minerals contribute significantly to the susceptibility. Above ~200 mbsf, both paramagnetic and ferrimagnetic minerals contribute substantially to the susceptibility.

Results of the measurement of susceptibility and its anisotropy (AMS) on discrete samples are shown in Figure F40. The mean magnetic susceptibility, the degree of anisotropy (P_j) and the shape parameter (T) for the susceptibility ellipsoid (Jelinek, 1981), and the inclinations of the maximum (K_{max}) and minimum (K_{min}) axes of the susceptibility ellipsoid are shown vs. depth.

Mean susceptibilities from discrete samples agreed with long-core susceptibilities. Above 200 mbsf, P_j values were lower than 1.02. Between 200 and 600 mbsf, P_j values increased to between 1.02 and 1.07. Below ~650 mbsf (within lithostratigraphic Unit XII; see "Lithostratigraphic Unit XII," p. 24), P_j values increased to a slightly higher range between ~1.04 and 1.08. Above 200 mbsf, T values were scattered between ~–0.5 and 0.5. Between 200 and 600 mbsf, T values were dominantly positive and scattered ~0.5. A slightly greater scattering of T values was observed in lithostratigraphic Units V to X (417–620 mbsf; see "Lithostratigraphy," p. 5), in which silt and sand or larger grain size sediments were abundant; T values may be related to the grain-size variations in these units. Below 650 mbsf (lithostratigraphic Unit XII; see "Lithostratigraphic Unit XII," p. 24), T values were dominantly at or above 0.5, which suggests that an oblate magnetic fabric dominates in lithostratigraphic Unit XII. The oblateness of the fabrics seems to be enhanced by the higher P_j values of this interval. Inclinations of K_{max} and K_{min} axes were scattered above 200 mbsf; however, with increasing depth throughout this interval K_{max} axes shallowed whereas K_{min} axes steepened, so that by ~220 mbsf a clear separation of K_{max} and K_{min} inclinations was evident: K_{max} axes were dominantly very shallow (<20°), while K_{min} axes were dominantly very steep (>70°).

In summary, compaction effects increase through the upper 200 mbsf so that a clear compaction signature is evident from the AMS data below ~200 mbsf.

F38. Susceptibility data from MST and AMST measurements, p. 104.

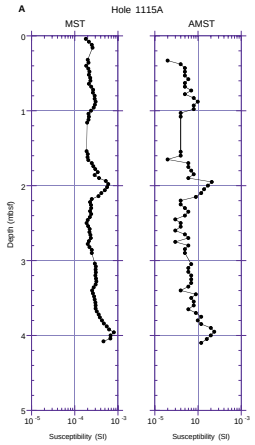

F39. MST susceptibilities and remanent intensities, p. 106.

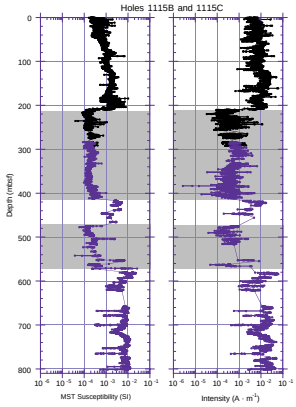

F40. AMS data for discrete samples, p. 107.

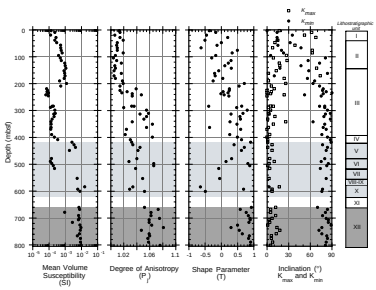

Remanent Magnetization

Measurements of remanent magnetization were made on all but the most disturbed sections from archive half cores and on discrete samples from working half core sections. Results are shown in Figures F41 and F42.

A total of 73 discrete samples were subjected to AF demagnetization experiments to assess the stability of the natural remanent magnetization (NRM). The AF demagnetization results of 23 discrete samples of APC cores from Hole 1115B indicated that the NRMs of these samples consisted of two magnetic components. A soft component, probably drilling-induced, with a steep downward direction was generally removed by demagnetization levels up to 10 mT. After removal of the soft component, many samples yielded a stable component that decayed toward the origin of the vector plot between 15 and 25 mT (Fig. F41A, F41B); this component is referred to as the characteristic remanent magnetization (ChRM). Some samples showed curved demagnetization trajectories on vector plots, which indicated a large contribution of a probably drilling-induced component (Fig. F41C); the ChRM from these samples was not isolated.

Nine samples from XCB cores of Hole 1115B (below 216 mbsf) showed weak remanent intensities ~1 × 10^{-3} A·m^{-1}. All but one sample showed erratic behavior after removal of a drilling-induced component by ~10 mT AF demagnetization (Fig. F41D). One sample showed a soft component with an upward direction, which was removed by 5 mT AF demagnetization, followed by a steeper upward-directed component decaying linearly toward the origin of the vector plot (Fig. F41E).

Among the 41 samples collected from RCB cores of Hole 1115C, a stable magnetic behavior was generally observed in samples from lithostratigraphic Unit V (417–475 mbsf), Unit X (572–619 mbsf), and Unit XII (657–800 mbsf; see "Lithostratigraphy," p. 5). These samples showed relatively high initial intensities above 10^{-2} A·m^{-1}. After removal of a soft component with a shallow to steep downward direction by 10 mT AF demagnetization, samples from Units V and X yielded stable ChRM directions that decayed linearly toward the origin on vector plots (Fig. F41F, F41G). The samples from Unit XII, on the other hand, provided a stable component that did not decay toward the origin of the vector plot (Fig. F41H); this component may represent a remagnetization in the present magnetic field. Samples from the other lithostratigraphic units showed unstable demagnetization behavior after removal of a soft component by 10 mT AF demagnetization.

In Hole 1115A, intensity of remanent magnetization of long cores after AF demagnetization at 20 mT ranged from values on the order of 10^{-3} A·m^{-1} up to values on the order of 10^{-2} A·m^{-1} (Fig. F42A). In Holes 1115B and 1115C, values were on the order of 10^{-3} and 10^{-2} A·m^{-1} throughout the upper 210 m. Low intensities on the order of 10^{-4} A·m^{-1} were found between ~210 and 420 mbsf, and again between ~470 and 520 mbsf (Fig. F42B). Below ~420 mbsf, intensities increased to values on the order of 10^{-2} A·m^{-1}, where they generally persisted to the bottom of the hole.

The polarity of the remanent magnetization after AF demagnetization at 20 mT for Site 1115 was determined from the directions of APC cores and from the inclinations of XCB and RCB cores. Tensor tool data (Table T6) was used to orient directions for Cores 180-1115B-3H through 23H. Declinations corrected for core orientation between ~17

F41. Demagnetization behavior of discrete samples, p. 108.

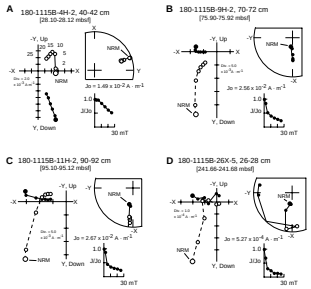

F42. Plots of intensity, declination, and inclination, p. 110.

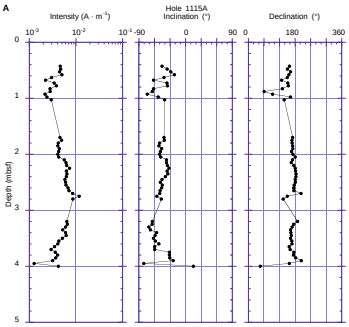

T6. Tensor tool orientation data, p. 187.

and 217 mbsf were consistent with the expected directions and were used in conjunction with the inclinations to interpret polarities. Declinations from XCB and RCB cores were highly scattered, which precluded their use for magnetostratigraphic interpretation. Directions from long cores were corroborated by discrete sample analysis. Downcore variations in remanent intensity, inclination, and declination are shown in Figure F42A and F42B.

Magnetostratigraphy

Figure F43A shows downcore variations in intensity, inclination, declination, and magnetostratigraphic interpretation for Hole 1115B. Figure F43B shows downcore variations in the inclinations for Holes 1115B and 1115C, along with the magnetostratigraphic interpretation. Poor recovery between ~400 and 650 mbsf and high scatter in the data below ~400 mbsf precluded interpretation of the directions in Hole 1115C in terms of the magnetic polarity time scale.

F43. Magnetostratigraphic interpretations, p. 112.

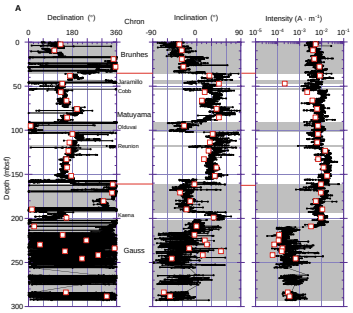

Chron Boundaries

The transition that is found between 33.5 and 36 mbsf represents the Brunhes/Matuyama boundary (0.78 Ma; Berggren et al., 1995). Using estimated sedimentation rates of 34 m/m.y. for the past 0.46 Ma and 59 m/m.y. for the period from 0.46 to 0.78 Ma (see Fig. F37), the Brunhes Chron should span ~34.5 m of section, which is reasonably consistent with the observed span of ~36 m.

The boundary at ~162 mbsf represents the Matuyama/Gauss polarity transition (2.58 Ma; Berggren et al., 1995), which is consistent with the paleontologic data (see "Biostratigraphy," p. 31). Using estimated sedimentation rates of 59 m/m.y. for the period between 0.78 and 1.95 Ma, and 79 m/m.y. for the period between 1.95 and 2.58 Ma (see Fig. F37), the Matuyama Chron should span ~119 m of section, which is reasonably consistent with the observed span of ~126 m.

The Gauss/Gilbert boundary (3.58 Ma; Berggren et al., 1995) occurs at ~386–387 mbsf. Using estimated sedimentation rates of 79 m/m.y. for the period between 2.58 and 3.04 Ma and 284 m/m.y. for the period between 3.04 and 3.58 Ma (see Fig. F37), the Gauss Chron should span ~190 m of section, which is not consistent with the observed span of ~224 m. The estimated sedimentation rate during the early Gauss Chron (between 3.11 and 3.58 Ma) was 393 m/m.y.

Subchrons

The Jaramillo Subchron (C1r.1n; 0.99–1.07 Ma, Berggren et al., 1995) is between ~43.5 and 47 mbsf. Sedimentation rates of ~59 m/m.y. have been estimated for this depth range (see Fig. F37), which suggests that the Jaramillo Subchron should span ~4.7 m of section and is reasonably consistent with the observed span of ~3.5 m.

The Olduvai Subchron (C2n; 1.77–1.95 Ma, Berggren et al., 1995) is between ~90.5 and 102.5–103.5 mbsf. Sedimentation rates of ~63 m/m.y. have been estimated for these depths (see Fig. F37), which suggests that the Olduvai Subchron should span ~11.3 m of section and is consistent with the observed span of ~13 m.

The termination of the Kaena Subchron (C2An.1r; 3.04–3.11 Ma, Berggren et al., 1995) is found at ~192.5 mbsf; the onset of the Kaena Subchron is poorly defined by shallowed inclinations between 202 and 217 mbsf, but is well constrained by the declinations to ~202 mbsf.

The Mammoth Subchron (C2An.2r; 3.22–3.33 Ma, Berggren et al., 1995) does not show up in long-core data; however, data from discrete samples suggest that it may be present between ~320 and 335 mbsf, where core recovery was low. This position is consistent in age with the paleontologic datums above and below, but the high estimated sedimentation rate of ~284 m/m.y. suggests that the Mammoth Subchron should span ~31 m of section, which is not consistent with the 15 m observed. Further study is needed to support this interpretation.

Excursions

Evidence for excursions of the magnetic field is found between 53 and 54.5 mbsf, which probably represents the Cobb Event (C1r.2r.1n; 1.20–1.21 Ma, Berggren et al., 1995). Using the estimated sedimentation rate of ~59 m/m.y. (see Fig. F37), this event is expected to span ~0.6 m, which is not consistent with the observed span of ~1.5 m.

Evidence for the Reunion Event (C2r.2r.2r; 2.14–2.15 Ma, Berggren et al., 1995) is found between ~118 and 119.5 mbsf. Using the estimated sedimentation rate of ~79 m/m.y., this event is expected to span ~0.79 m of section, which is not consistent with the observed span of ~1.5 m.

No evidence for excursions within the Brunhes Chron was observed.

INORGANIC GEOCHEMISTRY

Sixty-three samples were collected during the high-resolution interstitial water (IW) program at Site 1115. Three samples were collected from the only core of Hole 1115A, 29 from Hole 1115B, and 31 from Hole 1115C. Whole-round sections were taken down to Core 180-1115C-54R, the deepest core recovered at this site. Only a few whole rounds in the deeper portion of Hole 1115C yielded insufficient IW to preclude determination of the full suite of constituents that had been analyzed in samples from Site 1109. Thus, a nearly complete data set was generated that enables an excellent comparison to be made with Site 1109.

Results

The IW was analyzed for salinity, pH, alkalinity, major cations (Na^+, K^+, Ca^{2+}, and Mg^{2+}) and anions (Cl^- and SO_4^{2-}), Li^+, Sr^{2+}, SiO_2, and NH_4^+. Results of shipboard inorganic chemical analyses are presented in Table T7. The pH values obtained during the alkalinity determination appear to be reliable for the same reasons as described in the Site 1109 chapter (see "Inorganic Geochemistry," p. 54, in the "Site 1109" chapter and "Inorganic Geochemistry," p. 23, in the "Explanatory Notes" chapter). Profiles of many inorganic constituents (Figs. F44, F45) display a series of depth intervals in which there are substantially different concentration ranges. Large changes in the concentrations of many of the dissolved constituents are found below 400 mbsf.

pH, Alkalinity, Sulfate, and Ammonium

In the upper 400 mbsf of the sediments, pH remains in a narrow range (7.5–8.0). A transitional zone (400–600 mbsf) leads to an increase to near pH 9.0. These values are then maintained to the bottom of Hole 1115C. The titration alkalinity profile displays relatively large varia-

T7. Interstitial water geochemistry, p. 188.

F44. Interstitial water constituents, p. 114.

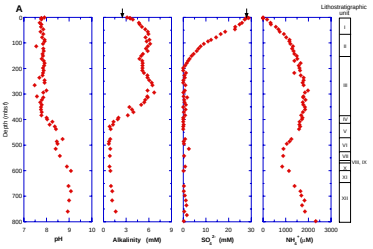

F45. Dissolved SiO_2 in sediments, p. 117.

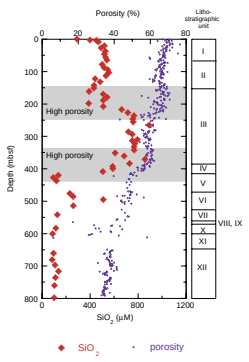

tions, primarily in the upper 400 mbsf (Fig. F44A). Alkalinity reaches a maximum of 6.7 mM (Table T7), which is only approximately half that observed in sediments from Site 1109 (see "Inorganic Geochemistry," p. 54, in the "Site 1109" chapter). Dissolved SO_4^{2-} is strongly depleted downhole and essentially absent from the pore water below a depth of 200 mbsf, other than a very few small excursions at depth. The NH_4^+ profile (Fig. F44A) displays an initial increase that parallels the alkalinity rise in the upper 66 mbsf. Subsequent downhole variations appear decoupled from alkalinity. The NH_4^+ maximum at the bottom of Hole 1115C has no alkalinity counterpart.

Salinity, Sodium, Chloride, Potassium, and Lithium

Salinity varies in the range of 30–38 (Table T7). The minimum is found below the zone of total SO_4^{2-} depletion, whereas the maximum is at the bottom of Hole 1115C. Salinity does not covary strongly with either Na^+ or Cl^-. Additionally, these two IW constituents do not covary throughout the entire sediment column (Fig. F44B). Both constituents display a slightly negative concentration gradient down to 250 mbsf, although the dissolved Cl^- profile displays more variations in this range than does that of Na^+. Concentrations of both constituents increase in the lower 150 m of Hole 1115C. Their profiles are decoupled in the range of 250–600 mbsf.

The K^+ profile (Fig. F44B) shows slight depletion relative to seawater between 100 and 300 mbsf of the sedimentary column, followed by a 150- to 200-m-thick transition zone in which dissolved K^+ is extensively removed from the pore fluids. Below 600 mbsf, the profile is relatively invariant with concentrations near 1 mM, or ~10% of the seawater value.

Dissolved Li^+ (Fig. F44B) exhibits a slightly more variable profile than many other inorganic constituents, although concentrations are generally low (20–55 µM) and do not exceed approximately twice the seawater value. The first significant increase in dissolved Li^+ below 200 mbsf and its maximum (55 M) near 300 mbsf coincides with a large increase in dissolved SiO_2 and the alkalinity maximum, respectively. Other features of the Li^+ profile do not appear to correlate strongly with any single IW constituent.

Calcium, Magnesium, and Strontium

The Ca^{2+} profile reveals a 50% depletion relative to seawater by the depth where SO_4^{2-} becomes fully removed, followed by a return to near seawater values by 350 mbsf (Fig. F44C). Below 400 mbsf, Ca^{2+} displays a sharp increase to a broad maximum of 120–130 mM below 600 mbsf. No significant variation is observed further downhole. The Mg^{2+} profile is slightly more variable in the upper 400 mbsf, with a number of smooth fluctuations found within the predominantly nannofossil-rich sediments of lithostratigraphic Units I–III (see "Lithostratigraphy," p. 5). Below this depth, however, dissolved Ca^{2+} and Mg^{2+} exhibit a near antithetical correlation.

The depth ranges in which the Sr^{2+} profile displays major features (Fig. F44C) appear to correspond more closely to those of Mg^{2+} than those of Ca^+. Variations in the Sr^{2+} profile, however, are more marked than those of either Ca^{2+} or Mg^{2+}. Two Sr^{2+} maxima exist. The first is relatively narrow and is found at 66 mbsf in lithostratigraphic Unit II,

whereas the second is broad and extends between 486 and 542 mbsf in sediments of lithostratigraphic Units VI and VII (see "Lithostratigraphy," p. 5). This deep-seated broad Sr^{2+} maximum is situated slightly below where the Ca^{2+} and Mg^{2+} profiles cross over, unlike at Site 1109 where these features coincided.

Silica

As commonly observed in deep-sea sediments, the dissolved SiO_2 profile (Fig. F45) displays greater complexity than those of other pore-water constituents. This is manifested in various excursions in concentration downhole. These, nonetheless, fall mostly within three broadly defined concentration ranges. In the upper 200 mbsf, dissolved SiO_2 increases sharply immediately below the mudline then remains between 400 and 500 µM. Higher concentrations and larger variations are present between 210 and 390 mbsf, an interval punctuated by two local maxima reaching near 900 µM. From 390 to 420 mbsf, dissolved SiO_2 concentrations decrease sharply and remain well below 200 µM in the deeper part of the hole (>500 mbsf).

Discussion

Changes in the chemistry of interstitial fluids at Site 1115 result from many of the same diagenetic reactions that were observed to mediate the pore-water composition at Site 1109. However, significant differences in the IW constituent profiles exist between the two sites and attest to the presence of sedimentary reactions here that do not occur at Site 1109. Coring at Site 1115 also penetrated a forearc sediment sequence (lithostratigraphic Units X–XII; see "Lithostratigraphy," p. 5) that was not reached at Site 1109. Hence, the lowermost 240 m of the profiles presented here provides insight into processes occurring below the late Miocene unconformity at the top of the forearc sequence (between lithostratigraphic Units IX and X; see "Lithostratigraphy," p. 5).

The concentrations of IW constituents in the upper 300 mbsf result primarily from the oxidation of organic matter mediated by microbial activity and the concomitant early diagenesis of biogenic carbonates. Within the latter are included the dissolution of aragonite, recrystallization of calcite, dolomite precipitation, and to a very minor extent the formation of ankerite (see "Site 1115 Thin Sections," p. 89, and "Lithostratigraphy," p. 5). Other important processes in the sediment column are the alteration of volcanic matter, formation of authigenic clay and zeolite minerals, and precipitation of pyrite, as well as transformations of pre-existing detrital minerals.

A general reaction was previously given describing the bacterially mediated oxidation of organic matter (e.g., Claypool and Kaplan, 1974; see "Inorganic Geochemistry," p. 54, in the "Site 1109" chapter). This process leads to strong depletion of SO_4^{2-} within the first 200 mbsf and increases in both alkalinity and NH_4^+ concentrations (Fig. F44A). A slight decrease in pH was observed over the first 50 mbsf (Table T7), as expected from the degradation of organic matter. Yet the pH remains higher than typical Pacific seawater at depths of ~1000 m (Millero and Sohn, 1992). The relatively invariant pH in the upper section of the sediments is also considerably higher than values observed in sediments undergoing extensive rates of degradation of organic matter (e.g., Eberli

et al., 1997). Therefore, either a lower rate of microbial oxidation of organic matter is present here, or sufficient detrital matter containing Fe exists to buffer the pH to higher values (Ristvet, 1978; Mackenzie et al., 1981). The increased alkalinity in the shallower sediments (~100 mbsf) promotes dissolution and recrystallization of biogenic carbonates (e.g., Morse and Mackenzie, 1990).

Sediments in the upper 100 mbsf contain significant amounts of biogenic aragonite in addition to calcite (see **"Site 1115 Thin Sections,"** p. 89, and **"Lithostratigraphy,"** p. 5). The dissolution of this metastable phase and the recrystallization of calcite are reflected in the dissolved Ca^{2+}, Mg^{2+}, and Sr^{2+} profiles and in changes in the Ca/Mg ratio (Fig. **F44C**). The release of dissolved Sr^{2+} (e.g., Baker, 1986) produces a well-defined maximum of 338 µM at 66 mbsf (Fig. **F44C**). The disappearance of aragonite below this depth (until well into Hole 1115C) is manifested in a return to lower dissolved Sr^{2+} further downhole. Recrystallization of calcite is present between ~20 and 150 mbsf as evidenced by close to 50% depletion of Ca^{2+} relative to seawater at the bottom of this interval (Table **T7**). The decreasing concentration of dissolved Mg^{2+} between ~100 and 240 mbsf, a subminimum in alkalinity between 160 and 210 mbsf, and a slightly increasing Ca/Mg ratio, as well as the identification of dolomite in samples subjected to XRD analysis (see **"Site 1115 Thin Sections,"** p. 89, and **"Lithostratigraphy,"** p. 5), are all consistent with dolomite precipitation over this interval. Because dolomite was identified by XRD down to ~300 mbsf (see **"Lithostratigraphy,"** p. 5), dolomitization continues, although probably on a more limited basis at least down to this depth. The Ca/Mg ratio variations in this depth interval support this inference. It is plausible that the lower alkalinity maxima observed here relative to Site 1109 reflect consumption of HCO_3^- during dolomitization, although the greatest extent of dolomite precipitation is found near 160 mbsf, consistent with where the alkalinity subminimum is observed. Ankerite, an Fe-Mg-Mn-enriched calcium carbonate mineral, was tentatively identified by XRD as a minor mineral constituent in samples from 240 mbsf, providing further evidence of calcium carbonate precipitation reactions.

Calcium carbonate mineral reactions are also important in sediments deep within Hole 1115C. These are evidenced by a broad Sr^{2+} maximum between 480 and 540 mbsf. Here aragonite provides a source of this element in the form of gastropod shells from the inner neritic environment of lithostratigraphic Units VI through the lagoonal setting of lithostratigraphic Unit VIII (see **"Lithostratigraphy,"** p. 5). The dissolved Sr^{2+} maximum is found over a broader interval and has a much lower concentration than in the corresponding units at Site 1109 (see Fig. **F70C,** p. 164, and **"Inorganic Geochemistry,"** p. 54, both in the "Site 1109" chapter). Diffusion has likely been more extensive at this site because sediments bounding the dissolved Sr^{2+} maximum at Site 1109 were much more clay rich, less porous, and underlain by dolerite, which acts as an effective barrier to fluid flow. Other calcium carbonate reactions deep in Hole 1115C likely include calcite cementation of the sediments, as evidenced by a substantial increase in pH below 500 mbsf and the presence of calcareous sandstone and limestone in lithostratigraphic Unit VIII (see **"Lithostratigraphic Unit VIII,"** p. 18). The latter coincides with the onset of pH values near 9.0. Maintenance of a high pH downhole is also consistent with the presence of calcite cements.

Increases in the Ca/Mg ratio between 250 and 400 mbsf, where dissolved Mg^{2+} concentrations actually increase slightly, probably reflect a

release of Ca^{2+} during weathering of volcaniclastic sands and ash layers. This process exerts greater control over the concentrations of these constituents than dolomitization reactions, which are present only to a minimal extent below ~250 mbsf. Indeed, increases in dissolved Ca^{2+} over this interval are accompanied by substantial increases in dissolved Sr^{2+} and Li^+, as well as very localized SiO_2 maxima (Figs. **F44B, F44C, F45**), all of which are also likely derived from alteration of volcanic matter. Visual core descriptions and results of XRD analyses support this inference. Abundance and thickness of volcaniclastic sand layers are greatest between 250 and 400 mbsf, as is the presence of plagioclase as a major constituent of the sediments (see Fig. **F3**). The lower dissolved Li^+ concentrations between 500 and 600 mbsf may simply reflect a diffusive profile with sources of this constituent located above (e.g., 300–400 mbsf) and below (e.g., 750 mbsf) this zone. Alternatively, a sink for dissolved Li^+ may exist near 600 mbsf at the boundary between lithostratigraphic Units X and XI (see **"Lithostratigraphic Unit X,"** p. 20, and **"Lithostratigraphic Unit XI,"** p. 22), possibly clay minerals and zeolites (e.g., De Carlo, 1992). The submaximum in dissolved Li^+ deep within forearc sediments of lithostratigraphic Unit XII (see **"Lithostratigraphic Unit XII,"** p. 24) also indicates a source of this element deep downhole. This requirement is satisfied possibly by the abundant plagioclase observed in this portion of the hole.

Examination of the dissolved K^+ profile (Fig. **F44B**) reveals a steadily decreasing concentration below 100 mbsf. Because the illite observed in this depth range is believed to be detrital, it is unlikely an effective sink for K^+. Perhaps the profile simply reflects diffusion with respect to the much steeper removal of this constituent below ~300 mbsf. Froelich et al. (1991) attributed linear negative K^+ gradients in sediments to an absence of sedimentary reactions and control by low temperature uptake of this constituent into basement. Although this is clearly not the case here, the nearly linear gradient in the upper 300 mbsf reflects the absence of reactions involving K^+ in that section of the sediment column. The absence or very low abundance of K-feldspar within the volcaniclastic sands and ashes of lithostratigraphic Units II and III, which could act as a source, is also consistent with the observed profile. This contrasts with Site 1109, where a significant source of dissolved K^+ existed near 400 mbsf (see Fig. **F70B,** p. 163, and **"Inorganic Geochemistry,"** p. 54, both in the "Site 1109" chapter). Formation of chlorite or smectite does not occur in the upper half of the sediment column, as confirmed by results of XRD analyses (see **"Lithostratigraphy,"** p. 5) and cannot contribute to the decrease in dissolved Mg^{2+} described above. It is only below at least 450 mbsf that Mg^{2+} begins to be removed substantially from the pore water. The XRD data indicate the appearance of clay minerals that require Mg^{2+} to form (e.g., chlorite and smectite) below 450 mbsf. However, based only on qualitative XRD results, these minerals are present more often as minor rather than as major constituents. It is also possible that zeolites, which become quite abundant near 600 mbsf, constitute another sink for dissolved Mg^{2+} (see **"Site 1115 Thin Sections,"** p. 89, and **"Lithostratigraphy,"** p. 5).

As observed at Site 1109, large changes are present in the pore-water constituent profiles in sediments that were deposited in neritic environments relative to those deposited at bathyal depths. At Site 1109, these changes occurred primarily below 550 mbsf (see **"Lithostratigraphic Unit VII,"** p. 22, in the "Site 1109" chapter) and were marked, for

example, by a large increase in dissolved Ca^{2+}. A similar trend is found below ~450 mbsf in lithostratigraphic Unit V of Hole 1115C.

At this site, the shapes of the Ca^{2+}, Mg^{2+}, and Ca/Mg ratio profiles between 400 and 600 mbsf are not influenced extensively by calcium carbonate mineral reactions. Rather, they are typical of sediment/pore-water systems in which substantial alteration of basement rock is found. These profiles are consistent with observations previously made at many other ODP sites where alteration of volcanic matter or Layer II basalt was invoked (e.g., Gieskes and Lawrence, 1981; Gieskes, 1983; Torres et al., 1995). Alteration of volcanic matter may also account indirectly for increases in dissolved Cl^- (Fig. **F44A**) observed further downhole. Because Cl^- is not normally involved in diagenetic reactions other than halite diagenesis, its concentration increase must occur through hydration of ash as well as the formation of hydrous clay and zeolite minerals, which simply increase the pore-water salinity (Martin et al., 1995). Both types of minerals are observed deep downhole at this site and the covariance of the Na^+ and Cl^- profiles in lithostratigraphic Unit XII (see **"Lithostratigraphic Unit XII,"** p. 24) is consistent with the occurrence of such a process. The smaller increases in dissolved Cl^- between 300 and 450 mbsf may also derive from this process, although the near invariance or slight depletion of dissolved Na^+ require its removal, ostensibly through formation of authigenic feldspars or other phases rich in Na (e.g., Gieskes and Lawrence, 1981).

Profiles of dissolved Li^+ and SiO_2 (Figs. **F44B, F45**) display variations that suggest the composition of the pore fluids is mediated by alteration of volcanic matter. Early dissolution of biogenic silica (e.g., diatoms and radiolaria) may also contribute to the observed pore-water SiO_2 concentration in the uppermost few meters of Holes 1115A and 1115B. This source of dissolved SiO_2, however, becomes progressively less important downhole as the alteration of volcanic glass contained in abundant ash layers in lithostratigraphic Units I and II potentially contributes most of the dissolved SiO_2 (see Figs. **F29, F45,** and **"Lithostratigraphy,"** p. 5). The relative invariance of dissolved Li^+ in the upper 220 mbsf, an interval in which both volcanic ash and volcaniclastic sands are present, is consistent with either only limited alteration of the most soluble glass in the ash (which contains low abundances of trace elements), or with the volcanic matter below 220 mbsf having a solid phase composition distinct from that above. Because relatively wide fluctuations in dissolved SiO_2 concentrations below 220 mbsf correspond roughly to the broad dissolved Li^+ maximum here, it is also reasonable to assume that the source of elevated dissolved SiO_2 in sediments of lithostratigraphic Units III and IV is a combination of terrigenous and volcaniclastic matter. Magnetic susceptibility exhibits a sharp drop near 220 mbsf (see **"Magnetic Susceptibility,"** p. 35). Although further work is needed to elucidate the reason for these changes, compositional differences in sediments above and below this depth appear quite likely.

It is known that rates and stratigraphic occurrences of silica diagenesis in sediments are controlled by a combination of burial time, pressure, temperature, and sediment composition (Torres et al., 1995, and references therein). Reactions leading to the formation of low-permeability horizons during the alteration of volcaniclastic material are also important. Thus, discerning which of these processes controls silica diagenesis is not always simple. For example, a depth relationship was reported by De Carlo (1992) for silica conversions in pelagic to hemipe-

lagic sediments from Sites 762 and 763 on the Exmouth Plateau, Indian Ocean. The relationship existed in spite of the fact that otherwise equivalent lithostratigraphic units were widely separated in depth and volcanic matter was largely absent from these two sites. Thus, burial depth and presumably temperature controlled the observed reaction sequence at these sites. A somewhat analogous yet potentially different situation exists at Sites 1109 and 1115, where equivalent lithostratigraphic units are present at different depths in the sediment column, and where dissolved SiO_2 profiles are remarkably similar in terms of depths at which major transitions occur (see **"Inorganic Geochemistry,"** p. 54, and **"Lithostratigraphy,"** p. 7, both in the "Site 1109" chapter). The sharp decrease in dissolved SiO_2 from >800 µM to <200 µM in the deeper portions of Holes 1109C and 1115C is found near 500 mbsf at both sites. This final transition was observed to be between 500 and 600 mbsf at Sites 762 and 763 (De Carlo, 1992). The Shipboard Scientific Party (1976) reported an equivalent transition near 600 mbsf at Site 317 on the Manihiki Plateau in the Pacific Ocean. Abundant examples exist, however, where dissolved SiO_2 profiles and their transitions are found at much shallower depths, such as in areas where basaltic basement is present at sufficiently shallow depths to exert a stronger influence on the overlying sediments (e.g., Gieskes and Lawrence, 1981; Gieskes, 1983; Eberli et al., 1997). At sites containing either volcanic matter disseminated in the sediments or where sediments overlie doleritic sills, a silicification front was identified that is associated with reactions involving increases in Ca^{2+} and decreases in Mg^{2+} and K^+ in interstitial waters. More elevated temperatures are also known to enhance such reactions (e.g., Sites 474, 482; Gieskes, 1983).

The drop in dissolved SiO_2 to concentrations of 100–200 µM is found near the boundary between lithostratigraphic Units VI and VII, the marine sand/brackish silt transition (see **"Lithostratigraphic Unit VI,"** p. 15, and **"Lithostratigraphic Unit VII,"** p. 17), here and at Site 1109. At Site 1109, this transition corresponds to a sharp decrease in porosity (Fig. **F71,** p. 165, **"Inorganic Geochemistry,"** p. 54, **"Lithostratigraphy,"** p. 7, and **"Physical Properties,"** p. 61, in the "Site 1109" chapter). Although the covariance with porosity is less distinct here (Fig. **F45**) than at Site 1109, it remains probable that the transition to low dissolved SiO_2 represents a silicification front at both sites, as invoked by Gieskes (1983) for various Deep Sea Drilling Project sites.

Because Sites 1109 and 1115 have similar temperature gradients (31°C·km^{-1} and 28°C·km^{-1}, respectively) and contain abundant volcanic matter in the sediment column, the observed dissolved SiO_2 profiles likely reflect a combination of temperature of burial effects and the influence of the alteration of volcanic matter.

Summary

The chemical composition of the IW is mediated by a series of sedimentary diagenesis reactions. These include the alteration of volcanic ash layers, volcaniclastic sand layers, and volcanic minerals dispersed throughout the sediments, calcium carbonate dissolution and recrystallization reactions associated with the microbial oxidation of organic matter, as well as other inorganically mediated calcium carbonate mineral reactions and silicification reactions including authigenic clay, zeolite, and quartz formation. Dolomite formation, which was not observed at Site 1109, is important here. The inferences based upon

variations in the chemical composition of the IW are supported here by results of XRD analysis, lithostratigraphic observations, and, to a lesser extent, by changes in the physical properties of the sediment in a manner similar to what was observed at Site 1109.

ORGANIC GEOCHEMISTRY

At Site 1115, the shipboard organic geochemistry consisted of determinations of total organic carbon, inorganic carbon, total carbon, total nitrogen, and total sulfur, in addition to the routine hydrocarbon gas safety monitoring procedure. The analytical techniques used are outlined in "Organic Geochemistry," p. 25, in the "Explanatory Notes" chapter.

Volatile Hydrocarbons

Headspace methane concentrations for Site 1115 displayed a profile with two distinct highs (Fig. F46). Very low methane concentrations (~2–4 ppmv) were found between 0 and 210 mbsf. Below this depth, methane levels increased rapidly to ~1200 ppmv and generally remained between 1000 and 3200 ppmv to 448 mbsf. From 448 mbsf, the methane concentration gradually dropped to 2–3 ppmv at ~515 mbsf (Fig. F46), only to rise again to >15,000 ppmv by 584 mbsf; they remained generally between 20,000 and 45,000 ppmv until the bottom of the hole (798 mbsf). Ethane (C_2) was the only other hydrocarbon consistently detected. Increased C_2 concentrations coincided with the two regions of elevated methane concentration, but remained low (<10 ppmv) throughout the hole (Table T8; Fig. F46). For this reason, the C_1/C_2 ratio remained high (>1000) throughout the Hole (Fig. F46).

The increase in methane below 210 mbsf coincided with the disappearance of sulfate in the pore water (see Fig. F44A), indicating that the methane in the upper interval of high concentration is bacterially derived. The origin of methane in the lower interval is less certain and could be either biogenic, as suggested by the corresponding increase in NH_4^+ at 600 mbsf (see Fig. F44A), or thermogenic in origin.

F46. C_1, C_2, and C_1/C_2 hydrocarbon profiles, p. 118.

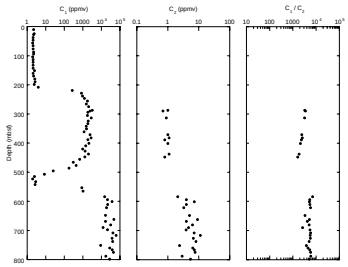

T8. Headspace gas in sediments, p. 189.

$CaCO_3$, Sulfur, Organic Carbon, and Nitrogen

Organic carbon and sulfur contents at Site 1115 were both found to be low, averaging 0.34 and 0.35 wt%, respectively. The peaks in both carbon (3.84 wt%) and sulfur (6.52 wt%) at 563 mbsf correspond to an organic-rich claystone that is probably partially pyritized (see "Lithostratigraphic Unit VIII," p. 18). The few available C/N ratios show that the organic carbon has a mixed marine and terrigenous source with periods of predominantly terrigenous organic material (Table T9; Fig. F47). The $CaCO_3$ concentrations are shown in Table T9 and Figure F47.

T9. Calcium carbonate, carbon, nitrogen, and sulfur contents, p. 191.

F47. $CaCO_3$, organic carbon, total sulfur, and C/N profiles, p. 119.

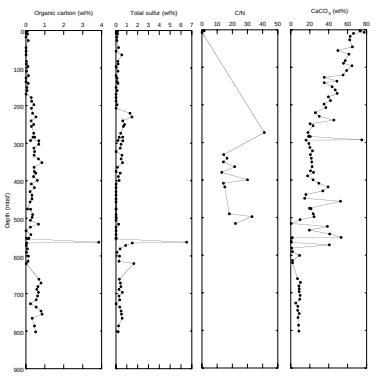

MICROBIOLOGY

Samples for microbiological analysis were obtained from Holes 1115A (APC), 1115B (APC/XCB), and 1115C (RCB). Forty-four samples were prepared for direct microscopic examination aboard ship. Twelve whole-round samples were taken for further shore-based analysis to measure potential bacterial activities and culturable microorganisms. Samples

obtained from the bottom of Hole 1115C represent the deepest samples obtained to date from deep-sea sediments for both microscopy (Section 180-1115C-54R-7, 801 mbsf) and potential activity/culturability experiments (Section 180-1115C-54R-4, 798 mbsf). (Note that deeper samples were subsequently recovered at Site 1118.)

Bacteria were present in all samples examined (Table T10; Fig. F48); their numbers decreased rapidly with increasing depth. Total bacterial numbers were 2.83×10^8 cells/cm^3 in the mudline sample (Sample 180-1115A-1H-1, 0–1 cm). Total organic carbon in the uppermost sample obtained from Hole 1115A (2.82 mbsf) was 0.05% (see Table T9). Thus the numbers of bacteria present in surficial sediment at Site 1115 are nearly the same as those at other sites with similar overlying water depths and near-surface organic carbon concentrations (see Table T10, p. 125, in the "Site 1108" chapter). Dividing and divided cells follow a similar trend to total bacterial numbers, although no cell involved in division was observed in the deepest sample, 801 mbsf.

Total bacterial numbers in sediments from Site 1115 conform to the general model for bacterial depth distributions in deep-sea sediments (Parkes et al., 1994). Bacteria were present in the deepest sample analyzed, 801 mbsf, at 3.51×10^5 cells/cm^3. Although this value is three orders of magnitude lower than near-surface bacterial populations in deep-sea sediments, it still represents a substantial bacterial community at considerable depth. In spite of the absence of dividing or recently divided cells, the continued presence of a bacterial community over 800 mbsf, into indurated sandstones, is of fundamental significance. The persistence of microbial life in indurated sedimentary rock (with a biostratigraphic age of ~15 Ma; see "Biostratigraphy," p. 31) adds to a steadily growing body of evidence for an extensive biosphere in deep-sea sediments (e.g., Parkes et al., 1994) and even into basalts (Furnes et al., 1996; Giovannoni et al., 1996). The current limit of the deep subseafloor biosphere remains unknown.

The activity of the deep subsurface microbial populations is also evident in geochemical data from Site 1115. Pore-water sulfate is fully depleted by ~200 mbsf (see "Inorganic Geochemistry," p. 38). In contrast, headspace methane concentrations remain low in the uppermost ~200 mbsf (in the range 2–4 ppmv between 0 and 200 mbsf), increase rapidly to ~1200 ppmv by 246 mbsf, and remain high downcore, although there was a distinct minimum at ~515 mbsf, which may indicate two separate production zones. The C_1/C_2 ratios remain high (>1000) throughout the hole, indicative of a biogenic source (see Fig. F46). A similar profile is also evident in pore-water ammonia concentrations, with a distinct minimum at ~520–580 mbsf, which again reinforces the notion of continuing action of bacterial processes downhole. In situ temperature increases with depth, which may result in greater organic matter bioavailability. This may in turn be reflected in increases in the concentration of important metabolic intermediates such as acetate (Wellsbury et al., 1997). The temperature gradient at Site 1115 is ~28°C·km^{-1} below a seafloor at ~4°C (see "In Situ Temperature Measurements," p. 58), which suggests a temperature of ~22°–25°C around 650–750 mbsf. Methane concentrations are high at this depth (e.g., ~62,000 ppmv at 716 mbsf). Whether deep methane production at Site 1115 can be attributed to acetoclastic methanogenesis will be investigated further.

T10. Bacterial populations and dividing and divided cells, p. 193.

F48. Bacterial populations and dividing and divided cells, p. 120.

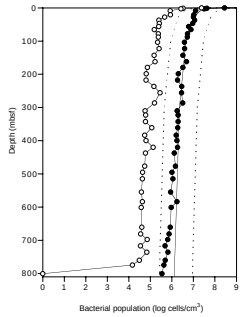

PHYSICAL PROPERTIES

Introduction

Physical properties evaluation at Site 1115 included nondestructive measurements of bulk density, bulk magnetic susceptibility, natural gamma ray, and *P*-wave velocity on unsplit cores using the MST. Discrete measurements of longitudinal and transverse *P*-wave velocities and index properties were collected on split cores. Depending on the level of sediment induration, thermal conductivity was measured from either unconsolidated whole cores or discrete rock slices. Measurements of compressive strength and undrained shear strength were taken until the level of consolidation became too high.

Density and Porosity

Bulk densities at Site 1115 were derived from both gamma-ray attenuation porosity evaluator (GRAPE) measurements conducted on unsplit cores and discrete mass and volume measurements. Composite profiles of these independently-derived bulk densities indicate a similar trend in the two data sets (Fig. **F49**). The GRAPE bulk densities exceed the index properties values above 226 mbsf (APC cores). This discrepancy was also observed at Site 1109 (see **"Density and Porosity,"** p. 62, in the "Site 1109" chapter), and no obvious explanation has been found. The GRAPE bulk densities agree reasonably well with the index properties measurements between 226 and 290 mbsf (XCB cores), and are generally less than index properties values below 290 mbsf (RCB cores). For RCB cores, GRAPE underestimation of bulk density may be related to small core diameters. Corrections were attempted at a previous site (see **"Density and Porosity,"** p. 62, in the "Site 1109" chapter), but could not fully account for the discrepancy. Because of these discrepancies and the large scatter in the GRAPE data, our discussion will focus primarily on the discrete bulk density measurements. GRAPE data from the MST measurements can be found on the accompanying LDEO CD-ROM, and the discrete density data are compiled in Table **T11.**

F49. Bulk density, **p. 121.**

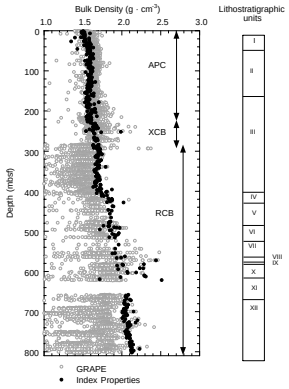

T11. Index properties in cores, **p. 194.**

Bulk density increases rapidly from 1.50 to 1.60 g·cm^{-3} in the upper 60 m (Fig. **F49**), which contain the nannofossil ooze of lithostratigraphic Unit I and the upper part of the nannofossil-rich silty clay of lithostratigraphic Unit II. Below 60 mbsf, bulk densities decrease slightly with depth down to 200 mbsf, with no significant variation observed at the boundary (~150 mbsf) between lithostratigraphic Unit II and lithostratigraphic Unit III, which is a calcareous silty clay. Between 200 and 410 mbsf, bulk densities increase to 1.70 g·cm^{-3} and then remain relatively constant to slightly decreasing. Exceptions to the general trend are observed in GRAPE values and in one index property sample at 251 mbsf. High-density spikes are observed in the logging data at 246, 248, and 256 mbsf. These spikes are associated with elevated photoelectric effect (PEFL) values, which suggest increased calcium carbonate content (see **"Downhole Measurements,"** p. 52). However, measured calcium carbonate content was similar to surrounding sediments (see **"Organic Geochemistry,"** p. 45), and no unusual lithology was noted in this core (see **"Lithostratigraphy,"** p. 5).

At ~410 mbsf, the bulk densities jump to ~1.80 g·cm^{-3}. This discontinuity is located slightly above the boundary between lithostratigraphic Unit IV (calcareous sandy silty claystone) and Unit V (silty sandstone).

Below 410 mbsf, bulk densities generally increase steadily to 1.90 g·cm^{-3} at 550 mbsf. This interval contains the siltstones and sandstones of lithostratigraphic Units V, VI, and VII. Large scatter is present between 560 and 650 mbsf, which probably results from the highly variable sediments of lithostratigraphic Units VIII, IX, X, and XI. Densities range from 1.70 to 2.50 g·cm^{-3}, the latter of which is the highest density measured at Site 1115. Below 650 mbsf, bulk densities steadily increase from 2.10 to 2.15 g·cm^{-3} at the base of the hole.

A profile of the grain densities with depth indicate discontinuities at ~230 and ~440 mbsf (Fig. **F50**). Grain densities average ~2.65 g·cm^{-3} between the seafloor and 230 mbsf, where grain densities suddenly decrease to 2.60 g·cm^{-3}. Between 230 and 440 mbsf, grain densities increase to values of ~2.65 to 2.70 g·cm^{-3} within the calcareous silty claystones of Unit IV (Fig. **F50**). At 440 mbsf, grain densities are sharply offset to <2.60 g·cm^{-3} and then increase to 2.70–2.75 g·cm^{-3} at the base of Hole 1115 (Fig. **F50**). Large scatter in grain densities is observed between 560 and 610 mbsf. This latter interval corresponds to lithostratigraphic Units V through XII, but exceptionally high grain densities of up to 2.80 g·cm^{-3} are found in the conglomerates and sandstones of lithostratigraphic Units IX and X (see **"Lithostratigraphy,"** p. 5). High grain densities may reflect the presence of igneous clasts within the conglomerates. No geologically realistic reason has been found for outlier values of 2.95–3.00 g·cm^{-3} in Units IV and XII, leaving experimental or instrumental error as the most likely explanations.

In general, porosity profiles reflect a combination of loading history and lithostratigraphic effects such as variability in sediment strength, degree of pore filling by cementation, or permeability differences that affect dewatering rates. Several of these factors are observed at Site 1115. Typically, seafloor porosities of marine oozes are high, as previously measured at Site 1109 (~80%; see **"Density and Porosity,"** p. 62, in the "Site 1109" chapter). For homogeneous sediments that are not overpressured, porosity loss follows an exponential relationship (e.g., Terzaghi, 1925; Athy, 1930). In contrast, the porosities from Site 1115 show unusually low values (65%–70%) at the seafloor, and decrease only slightly within the uppermost ~140 m (Fig. **F51**). This profile may reflect surficial erosion, as indicated by the >120 ka age for Core 180-1118-1H (see **"Biostratigraphy,"** p. 31).

Distinct zones of relatively high porosity are found between 140 and 240 mbsf and between ~320 and 420 mbsf. From 200 to 450 mbsf, a high sedimentation rate of ~284 m/m.y. has been estimated (see **"Biostratigraphy,"** p. 31). This sedimentation rate may contribute to undercompaction and anomalously high porosities within the lower interval (300–420 mbsf). Above 200 mbsf, sedimentation rates are lower (~63 m/m.y.) and would not be as likely to result in undercompaction.

The lower boundaries (~240 and 420 mbsf) of the two high-porosity intervals are near discontinuities in the grain density profile (~230 and 440 mbsf), suggesting a mineralogic control on porosity. The IW silica data indicate elevated values between ~210 and 420 mbsf (see **"Inorganic Geochemistry,"** p. 38). These data suggest that the decrease in pore space below 420 mbsf may be related to cementation of sediment with silica, which would increase average grain density and decrease pore space.

Porosities are extremely scattered between 560 and 620 mbsf. Low porosities probably reflect low-porosity igneous clasts within the conglomerates of Units IX and X. At 572 mbsf, an unconformity is present

F50. Grain density, **p. 122.**

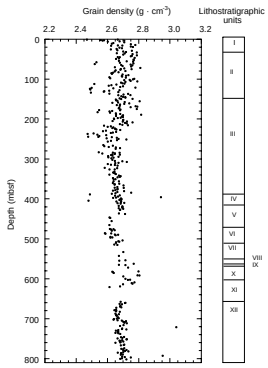

F51. Porosity, **p. 123.**

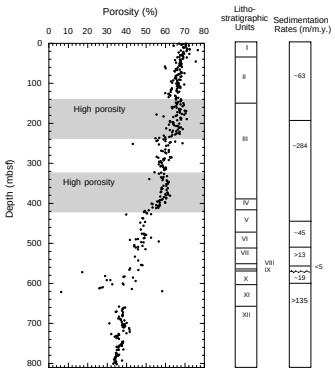

(see "Biostratigraphy," p. 31). If the amount eroded were greater than the present overburden, a jump to lower porosities would be expected at the unconformity. Because the porosity profile is not significantly offset across this boundary (Fig. F51), it is reasonable to assume that erosion did not exceed 572 m of thickness, the depth of the uncomformity.

Compressional Wave Velocity

Compressional wave velocity was measured on whole cores using the MST *P*-wave logger (PWL). On split cores, the PWS1 probe was used to measure longitudinal (z) velocities and the PWS2 and PWS3 probes were used to measure transverse (y and x, respectively) velocities, with the split core remaining in the core liner. When the degree of sediment induration was sufficient, or hard rock samples were recovered, the PWS3 probe was used to measure both the longitudinal and transverse velocities. The PWL yielded poor quality results, and thus this discussion will be limited to PWS velocity data. From Cores 180-1115A-1H to 180-1115B-7H, velocity measurements were taken in the z and y directions. Insufficient sediment induration precluded measurement in the x direction. From Cores 180-1115B-8H to 11H, the x, y, and z velocities were routinely measured. From Cores 180-1115B-12H to 180-1115C-1R, because of the degree of sediment induration, only the x velocity was measured. From Core 180-1115C-2R to the bottom of the hole, the level of induration was sufficient for ~10-cm³ cubes to be cut from the cores, thereby allowing for velocity to be measured in the transverse and longitudinal directions. The PWL data are presented in Table T12.

From the seafloor to 405 mbsf, velocities increase gradually from ~1550 to 1850 m·s^{-1} (Fig. F52). This depth range includes lithostratigraphic Units I, II, III, and IV (see "Lithostratigraphy," p. 5). A single spike in the velocity at 293 mbsf corresponds to a thin dolomite-rich layer (see "Lithostratigraphy," p. 5). Within lithostratigraphic Units IV, V, and VI (405–505 mbsf), velocities average ~1850 m·s^{-1}. From 505 to 620 mbsf, velocities show an increase in scatter, with some velocities exceeding 3000 m·s^{-1}, and three values exceeding 4500 m·s^{-1}. These depths correspond to the variable lithologies of Units VII through X. From 660 mbsf to the base of Hole 1115C (lithostratigraphic Units XI and XII), velocities gradually increase from 2350 to 2600 m·s^{-1}, with outliers occasionally exceeding 4000 m·s^{-1}.

A comparison between transverse and longitudinal velocities indicates that velocities are isotropic above 520 mbsf (Fig. F53). Below this point there is a fair degree of scatter, which reduces below 660 mbsf. The predominance of positive anisotropies below 660 mbsf coincides with lithostratigraphic Unit XI, which consists of sandstone, packstone, siltstone, and silty claystone (see "Lithostratigraphic Unit XI," p. 22). Here, the transverse velocity is almost always greater than the longitudinal velocity.

Thermal Conductivity

Thermal conductivity measurements at Site 1115 show an overall increase with depth, ranging from ~0.95 W·m^{-1}·°C^{-1} near the seafloor to ~1.15 W·m^{-1}·°C^{-1} at the base of Hole 1115C (Fig. F54). Measurements could not be taken between 240 and 280 mbsf, where sediments were

T12. Longitudinal and transverse velocities for cores, p. 203.

F52. *P*-wave velocities, p. 124.

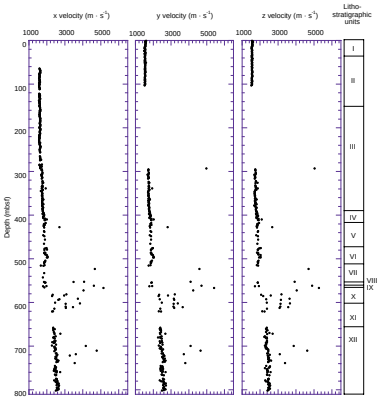

F53. Longitudinal vs. average transverse velocity and *P*-wave anisotropy, p. 125.

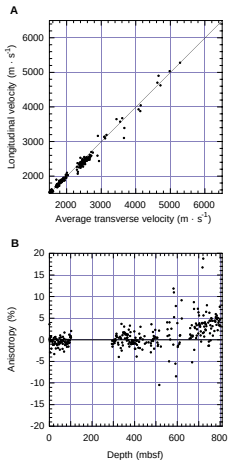

F54. Thermal conductivity, p. 126.

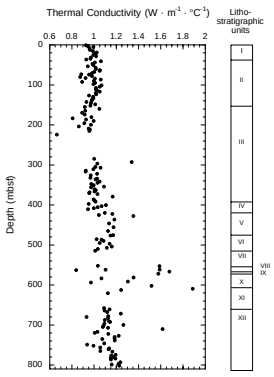

too indurated for needle-probe insertion and too soft for half-space measurements. A full compilation of the data is presented in Table T13.

Some intervals indicate slight deviation from the downhole increase with depth. Thermal conductivity decreases slightly below 120 mbsf, which correlates well with the top of a zone of high porosity (see above). Conversely, sediments that are thermally more conductive (e.g., siltstones and sandstones of Units V and VI) are found between 420 and ~510 mbsf, where lower porosities were observed (Fig. F54). Large scatter is observed between 550 and 620 mbsf (Units VIII–XI; see "Lithostratigraphic Unit VIII," p. 18, "Lithostratigraphic Unit IX," p. 19, "Lithostratigraphic Unit X," p. 20, and "Lithostratigraphic Unit XI," p. 22), which is also consistent with the porosity data.

T13. Thermal conductivity values in cores, p. 210.

Shear and Compressive Strength

Split cores from Holes 1115B and 1115C were subjected to undrained shear strength and unconfined compressive strength tests using the motorized miniature vane-shear device and the pocket penetrometer, respectively. Below 240 mbsf, strength parameters could not be measured as a result of incipient induration. The data are presented in Figure F55 and Table T14.

Undrained shear strength (S_u) was measured in the uppermost ~60 mbsf of the sedimentary succession drilled (i.e., within the nannofossil oozes and clays of lithostratigraphic Unit I). The data show an increase with depth, rising from ~5kPa at the seafloor to around 80 kPa at 60 mbsf (Fig. F55). Unconfined compressive strength (2 S_u) increases along a similar trend as the undrained shear strength, starting from near zero strength at the seafloor (Fig. F55). At ~200 mbsf, values between 180 and 220 kPa are reached. The state of sediment consolidation can be estimated by comparing the range of strengths measured relative to normally consolidated sediment, expressed as the ratio of undrained strength (S_u) to effective overburden stress (P_0'). Normally consolidated sediments show S_u/P_0' values of 0.2 (e.g., Mesri, 1975), as shown by the dashed line in Figure F55. It can be seen that the data from Site 1115 plot slightly below this line, suggesting slight underconsolidation.

F55. Shear and compressive strength data, p. 127.

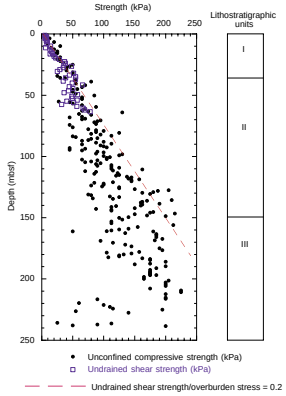

T14. Compressive and vane shear strength, p. 219.

Magnetic Susceptibility

To evaluate the nature and origin of the magnetic mineralogy for the recovered Site 1115 sediment, the magnetic susceptibility, natural gamma ray (NGR), and remanent intensity were compared (Fig. F56). All magnetic susceptibility data can be found with the MST measurement data set (in ASCII format) on the accompanying LDEO CD-ROM. For the entire section, there exists a direct correlation between the susceptibility and the remanent intensity. From this we can infer that, in general, the mineralogy controlling the magnetic susceptibility is the same as that controlling the remanent magnetic intensity. Further, the correlation between NGR variations and the magnetic susceptibility suggests that the clays and sands containing radioactive material also are rich in ferromagnesium minerals.

A more detailed comparison between the lithology and grain-size distribution with the susceptibility indicates that there is no clear relationship between either grain size or the main lithostratigraphic boundaries. Nevertheless, the magnetic susceptibility as a function of depth has a number of clear trends. In particular, there is a first-order

F56. Magnetic susceptibility, magnetic intensity, and NGR, p. 128.

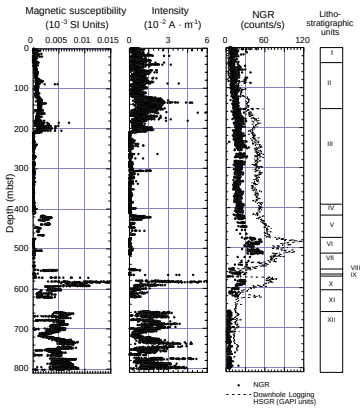

difference between the high-amplitude susceptibility variations within the upper part of the section (50–220 mbsf) and the low-amplitude variations within the middle part of the section (220–420 mbsf). The transition occurs within lithostratigraphic Unit III, which is characterized by abundant volcaniclastic sands. In contrast, lithostratigraphic Unit II is dominated by ashes. Likewise, grain sizes between 25 and 140 mbsf are associated with high-frequency, fine-grained distal turbidites whereas the section between 140 and 380 mbsf comprises high-frequency, proximal turbidites (see **"Lithostratigraphy,"** p. 5). Again, no simple relationship exists between grain-size distribution and the trends in the susceptibility.

Second-order trends are represented by the relatively high amplitude susceptibility variations of the shallow-marine, lagoonal, and fluvial deposits of lithostratigraphic Units VII, VIII, and IX, and the outer neritic and upper bathyal calcareous sandstones and siltstones of the forearc lithostratigraphic Units X, XI, and XII. Presumably, the extreme anoxic environment within the brackish lagoons and swamps were conducive to formation of iron sulfides and clays (e.g., pyrite and smectite; see **"Lithostratigraphy,"** p. 5).

Natural Gamma Ray

The NGR emissions were recorded for all cores at Site 1115, as part of the continuous MST measurements. Because K, U, and Th are the principal sources of NGR and often preferentially bind to clay particles, an increasing NGR count typically correlates to an increasing clay/shale content. In contrast, sand-prone and calcium carbonate units are usually characterized by low NGR counts. However, this usual relationship has been confounded by the presence of radiogenic sands and clays within the basin, which are being produced from the erosion or alteration of volcaniclastic, igneous, and metamorphic terranes. Composite NGR data from Site 1115 are presented graphically in Figure **F56,** and all NGR data can be found with the MST measurement data set (in ASCII format) on the accompanying LDEO CD-ROM.

The NGR data are approximately constant between the seafloor and 100 mbsf, and correlate with the nannofossil ooze of lithostratigraphic Unit I and the upper part of lithostratigraphic Unit II (see **"Lithostratigraphic Unit I,"** p. 6, and **"Lithostratigraphic Unit II,"** p. 8). Between 100 and 180 mbsf, the NGR count gradually increases from 10 to 20 counts/s, after which the count remains fairly constant to slightly decreasing until ~400 mbsf. This second interval corresponds to lithostratigraphic Units II and III. These units are characterized by clays containing ash layers and clays with volcaniclastic sands, respectively. From 400 to 470 mbsf the NGR count increases gradually to 30 counts/s within the silty sandstone of lithostratigraphic Unit IV. There is an abrupt increase in NGR count to an average of 45 counts/s within Unit V, comprising sandy siltstone and silty sandstone, before tailing off to ~5 counts/s at 660 mbsf. Throughout lithostratigraphic Unit XII, NGR count remains scattered tightly below 6 counts/s. The correlation of high NGR count with sandstone is not typical, and thus may be indicative of provenance and again is symptomatic of radiogenic sands within the basin. It is important to note that the discontinuities observed in the NGR (180 and 400 mbsf) are similar to those observed in magnetic susceptibility (220 and 410 mbsf), and in porosity.

Given only the shipboard analyses, the general NGR trends are difficult to explain in terms of either grain size or lithostratigraphic varia-

tions. For example, in the interval 200–400 mbsf, both relatively thick clays and sands (e.g., at 197–207 and 417–426 mbsf, respectively) have an identical NGR count of 20 counts/s. Individual spikes superposed on the general trend increase the NGR count by 10–15 counts/s and tend to be correlated with volcaniclastic sands. In contrast, the NGR maxima between 480 and 520 mbsf are associated with the relatively "clean" neritic sands and carbonaceous siltstones of lithostratigraphic Units VI and VII (see "Lithostratigraphic Unit VI," p. 15, and "Lithostratigraphic Unit VII," p. 17).

Hole-to-Hole Correlation

Magnetic susceptibility and NGR were used to correlate between Holes 1115A, 1115B, and 1115C (Figs. F57, F58). Interhole correlation is based on recognizing characteristic features in the data sets. Magnetic susceptibility and GRAPE density proved difficult in correlating between Holes 1115B and 1115C because of (1) a major data gap within the overlap zone, and (2) the lack of distinguishing features outside of the data gap. Figure F57 shows a magnetic susceptibility peak at 2.0 mbsf in both Holes 1115A and 1115B. A second peak, correlating with an ash layer, is present at 3.9–4.1 mbsf in Hole 1115A and 3.75–4.1 mbsf in Hole 1115B. Within the lower part of the section, an offset of 15–20 cm is suggested, whereas there is minimal offset in the upper section between the two holes. The ~20-cm offset in the upper part of the section is consistent with the lithostratigraphy. With respect to Holes 1115B and 1115C, Figure F58 shows correlation between two minima (shown by dashed lines) and correlation between a series of small NGR peaks, numbered 1 to 6 for Hole 1115B and 1' to 6' for Hole 1115C, superposed onto a relatively long wavelength low between 287.5 and 289.5 mbsf. The correlation suggests that an offset of 0.3–0.7 m exists between Holes 1115B and 1115C.

F57. Magnetic susceptibility correlation between Holes 1115A and 1115B, p. 129.

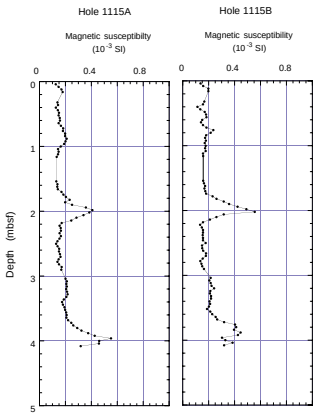

F58. Magnetic susceptibility correlation between Holes 1115B and 1115C, p. 130.

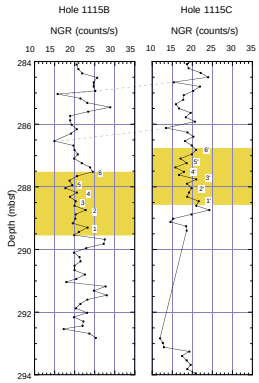

DOWNHOLE MEASUREMENTS

Operations

Four logging strings were run in Hole 1115C: one triple combo that logged from a total depth of 784 mbsf to above mudline, one FMS-sonic run that logged from total depth to the bottom of the pipe, an ultrasonic borehole imager string that failed downhole and did not record any useful data, and a VSP run (Table T15). The VSP data and operations are described in the section, "Vertical Seismic Profile and Depth Conversion," p. 59, and this section concentrates on the other runs.

For the first run, the pipe was raised to 99 mbsf, and the triple combo with the dual induction tool (see Table T7, p. 74, and Fig. F15, p. 66, both in the "Explanatory Notes" chapter) was lowered downhole. Natural gamma ray logging (HNGS) data were monitored during the descent in the pipe to locate the mudline, where the string was stopped for 3 min to provide a depth reference for the temperature-logging tool (TLT) temperature log. Upon reaching open hole, HNGS and dual induction tool (DIT) data were logged during the descent to near total depth at 784 mbsf (Table T15). An upward log was then recorded at 300 m/hr. The pipe was raised to 79 mbsf, and the tool string was stopped at the mudline for a few minutes both to run calibrations and to give the TLT

T15. Summary of logging operations, p. 224.

data a depth reference, after which logging continued up to 38 m above seafloor.

The caliper log from the lithodensity tool (Fig. F59) revealed a narrow interval at 567 mbsf where the borehole diameter was 13 cm (5 in) and smaller than drill-bit size (25.1 cm [9 in]). Log quality is degraded in areas of enlarged diameter and rapidly changing hole diameter (see "Downhole Measurements," p. 34, in the "Explanatory Notes" chapter). In Hole 1115C, the caliper from the triple combo run reached maximum extension between 618 and 624 mbsf and intermittently between 508 and 566 mbsf (Fig. F59).

For the second run the pipe was lowered again to 99 mbsf, and the FMS-sonic string (see Table T7, p. 74, and Fig. F15, p. 66, both in the "Explanatory Notes" chapter) was lowered downhole. The string reached near total depth at 787 mbsf (Table T15), and a first pass was recorded up at 300 m/hr. The real-time FMS images seemed to indicate an irregular tool motion, and it was thought that this could be caused by poor synchronization of the heave compensator. The pass was therefore aborted at 726 mbsf, the tool brought back down to total depth, and the heave compensator stopped and restarted for a second pass. In fact the image quality of this second pass was similar to that of the first pass, and the log was recorded up to 152.4 mbsf. The tool was then lowered to total depth again for a third pass to increase the borehole coverage of the images. The imaging log ended at the bottom of the pipe, which was raised to 79 mbsf (Table T15) where the pads were closed, but NGR continued to be recorded up to 42 mbsf.

The ultrasonic borehole imager string was then sent downhole, but it could detect neither hole fluid sonic velocity while going down in the pipe nor borehole wall reflections upon reaching open hole. The log was then aborted and the tool string brought back to the rig floor.

Depth Shifts

The mudline wireline depth (Table T15), which defines the depth shift from mbrf to mbsf, was located by its associated gamma-ray decay for the triple combo run (Fig. F60). The depth shift for the two FMS-sonic passes was derived by correlating the NGR with that of the triple combo run within the 534–578 mbsf interval, which was chosen for its large characteristic variations (Fig. F61). It appears that differential cable stretching can result in depth mismatch up to 0.5 m in a few places (such as at 555 mbsf; Fig. F61).

Lithologic Analysis

The interpretation, based mainly on NGR, the relationship between the neutron (APLC) and density porosity (DPHI), and the PEFL (see "Downhole Measurements," p. 34, in the "Explanatory Notes" chapter), and the results of core analysis (see "Lithostratigraphy," p. 5), defines nine logging units (Fig. F62).

Log Unit L1 (79–153 mbsf)

The neutron porosity is larger than the density porosity, which indicates a significant clay content. The logs show little indication of coarser grained beds.

F59. Hole 1115C composite log, p. 131.

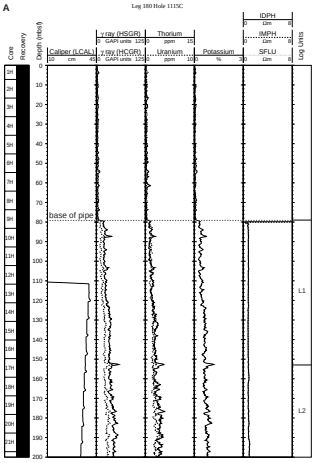

F60. Hole 1115C total volume gamma ray after depth shifts, p. 139.

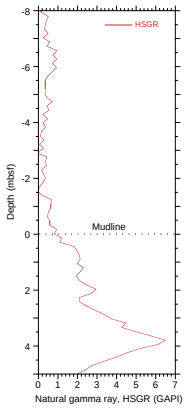

F61. Hole 1115C total volume gamma ray and FMS-sonic string, p. 140.

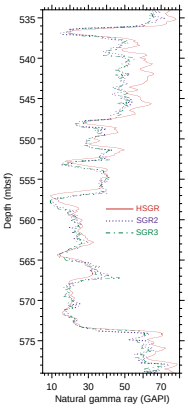

Log Unit L2 (153–413 mbsf)

The clay content is still large, but there are many short intervals where the two porosity logs converge, indicating thin "clean" beds. In two such beds at 246 and 248 mbsf, high PEFL and high density suggest high calcium carbonate content, which is confirmed by high calcium carbonate in core samples (see **"Organic Geochemistry,"** p. 45). A third thin bed at 292 mbsf exhibits very high density and PEFL of about 4 barns/e–, which suggests dolomite. The presence of dolomite is confirmed by XRD analysis (see **"Lithostratigraphy,"** p. 5). High calcium carbonate content is indicated by chemical analysis (see **"Organic Geochemistry,"** p. 45). The thin bed at 292 mbsf corresponds to a high sonic velocity of 5.2 km·s^{-1} measured on core samples (see **"Physical Properties,"** p. 47) but not observed on the sonic log, and to a hole diameter decrease. It is also located at the depth where it became necessary to abandon XCB coring for RCB coring.

Log Unit L3 (413–474 mbsf)

A PEFL increase indicates higher calcium carbonate content than in log Unit L2, but the unit is generally not clean as shown by the porosity divergence. However, several coarser grained intervals exist where the porosity curves converge. Bulk density also increases slightly at the boundary between log Units L2 and L3.

Log Unit L4 (474–506 mbsf)

This unit does not wash out and shows slightly elevated PEFL because of calcium carbonate content. The relationship between neutron and density porosities is variable and suggests a thin-bedded variable lithology that includes sands, clays, and mixtures of both. Uranium content is the highest of any unit, indicating reducing conditions at the time of deposition.

Log Unit L5 (506–535 mbsf)

Like log Unit L4, this unit has a high uranium content (a consistent 5 ppm), which indicates a reducing environment, but it shows a series of washouts that affect the porosity measurements. Where the data quality is good, the convergence of neutron and density porosities, coupled with low PEFL, indicate a primarily sandy formation. The consistent total gamma-ray character suggests that the washed out intervals are similarly sandy.

Log Unit L6 (535–565 mbsf)

This unit shows a series of washouts, some correlating with gamma-ray lows. Only one small section from 553 to 557 mbsf yields good porosity data. The difference between the neutron and density porosities suggests that it is a clay. It has a moderate gamma-ray magnitude. The gamma-ray lows are up to 2 m thick and are unusual in that they have low resistivity and low sonic velocity. Thin streaks of lignite were observed in the core (see **"Lithostratigraphy,"** p. 5); one can speculate that these gamma-ray lows are large beds of ligneous coal or peat. The upper part of this unit shows an increase in uranium, which is likely to indicate increasingly reducing conditions upsection. The washed-out nature of the upper section, combined with generally increasing total

F62. Hole 1115C log units and correlations, **p. 141.**

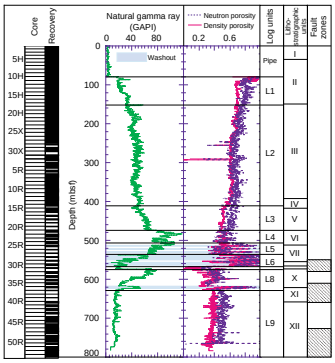

gamma-ray magnitude, suggests a predominantly sandy formation. It is noteworthy also that the Th/K ratio is ~4 ppm/%, a value commonly observed in sands at Site 1109 (see "Downhole Measurements," p. 69, in the "Site 1109" chapter).

Log Unit L7 (565–573.5 mbsf)

The FMS image clearly shows this unit to be a conglomerate with resistive cobbles up to a few centimeters in size. The high bulk density and low natural gamma-ray magnitude suggests that the clasts are intermediate or mafic igneous rocks, and the response of the logs bears similarity to the dolerite conglomerate observed in Hole 1109D (see "Downhole Measurements," p. 69, in the "Site 1109" chapter). In this 2-m interval, a large increase in porosity, along with a swollen formation evidenced by the caliper, suggest that the matrix has changed from a coarser grained matrix to predominantly clay in this interval. A conglomerate with apparently basaltic clasts and predominantly sandy matrix was observed in the cores at this depth (see "Lithostratigraphy," p. 5).

Log Unit L8 (573.5–628.5 mbsf)

There are two similar sequences within this unit, the lower boundary of which is most easily recognized by an increase in bulk density. The lower sequence begins with a few meters containing thin streaks that are resistive and have a high PEFL, suggesting that they are calcium carbonate dominated. Above this, improved convergence between neutron and density porosities, decreasing PEFL, and increasing NGR magnitude indicate that sand content increases upward. The top of the first sequence at 619 mbsf is almost pure sand. The second sequence is much thicker, with a more homogeneous massive carbonate at the bottom. Again, the formation grades upward into a thick radioactive sand. It is interesting to note that in these sands, the Th/K ratio is about 2 ppm/%, which is lower than that of any other sands observed during this leg. The presence of potassium minerals, possibly muscovite or K-feldspar, is therefore suggested.

Log Unit L9 (628.5–784 mbsf)

This unit appears to be rich in clay, but also has significant calcium carbonate content inferred from the moderately high PEFL. The relatively low total NGR may result from this calcium carbonate content. Several short intervals (<10 cm to 4 m) are found where density and neutron porosities converge, suggesting a "clean" lithology. Some of the thinner instances show a slight PEFL increase, indicating a possible calcium carbonate dominated bed rather than sand or silt, which appears more commonly.

Borehole Geometry, Magnetic Field, and FMS Dynamics

The accelerometer data of the FMS show that the hole deviation remains below a half degree (Fig. F63). They also show acceleration magnitudes (Fig. F64) that deviate by 0.2 $m \cdot s^{-2}$ from the average, which is twice the amount of a good quality run (such as the lower run in Hole 1109D; see "Downhole Measurements," p. 69, in the "Site 1109"

F63. Hole 1115C deviation, p. 142.

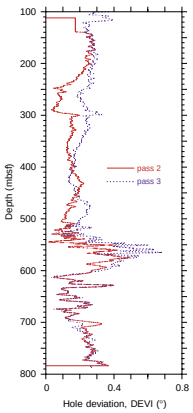

F64. FMS tool string acceleration in Hole 1115C, p. 143.

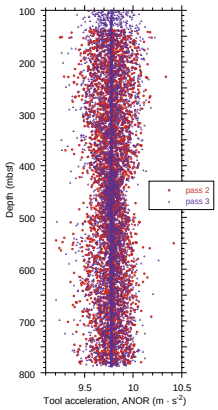

chapter). This translates into irregular tool movements and lower quality raw images, as observed on those displayed during logging.

The FMS caliper data reveal three washout intervals where the natural tool rotation slows down, at 120–290, 500–565, and 590–670 mbsf (Fig. F65). The steady tool orientations cluster around the north-south and east-west directions, suggesting an oriented hole ellipticity. To further investigate this trend, the difference between the two caliper measurement (C1 and C2) and the orientation of the largest of the two diameters are displayed in Figure F66. The orientations are displayed only if the caliper difference is above a threshold of either 2 or 5 cm.

Between 120 and 290 mbsf, washouts are probably caused by the circulation that is maintained when the drill bit progression halts during core retrieval, because the spacing between the washouts corresponds to the core length of ~10 m. Because both caliper readings are above drill-bit size, these elongations correspond to a preferential orientation of the washouts. The small elongations in the 135–250 mbsf interval strike northwest, and their orientation becomes erratic in the 230–290 mbsf interval.

The thick washed-out intervals between 500 and 565 mbsf (Fig. F67) are sufficiently large so that one or even both of the caliper measurements are saturated. The orientation of the elongation generally trends north-south, but with a significant deviation. Further detailed analysis will need to separate measurements where both calipers are saturated and the orientation is, therefore, meaningless, from those where only one caliper is saturated and the orientation is meaningful.

The thinner elongations observed between 590 and 675 mbsf (Fig. F68) are present in intervals where the smallest caliper reads close to drill-bit size (25 cm [9⅞ in]). One of these elongations, seen at 595 mbsf, must be restricted in azimuth because it is almost missed by the second pass. It also prevents rotation during the third pass. The thicker elongation at 618–625 mbsf also locks the tool rotations. In all cases the elongations are oriented north-south. These elongations, therefore, satisfy most of the breakout criteria (see "Borehole Geometry," p. 39, in the "Explanatory Notes" chapter). They could be related to structural directions (faulting or bedding directions), or to a north-south minimum horizontal principal stress direction (i.e., to a north-south active extension). The main goal of the failed ultrasonic borehole imager logging run was to further investigate the shape of these elongations.

The magnetometer measurements yield an inclination around –30° (Fig. F69A). The scatter at the bottom of the hole might partly be caused by poorer tool centralization in the washouts. Alternatively, it may correspond to a real change because it correlates with both the L8/L9 log unit boundary and an intensity increase (Fig. F69B).

FMS Images

The two FMS images acquired from Hole 1115C are rotated by as much as 45° with respect to each other for about one-fifth of the two passes (Fig. F65), which provides improved coverage of the borehole in these intervals. The FMS processing steps for this site included speed correction, depth shifting to seafloor (Table T15), and static and dynamic normalization using a 1-m moving window. A smaller cable confidence factor of 4, instead of the more commonly used value of 5, was applied during speed correction to allow for the large amount of tool sticking that occurred during the two passes. (The cable confidence factor is used in the design of relative weights in a Kalman filter, which

F65. Hole 1115C geometry, p. 144.

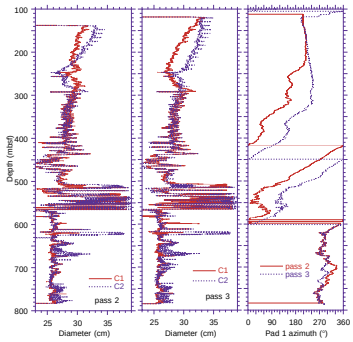

F66. Hole 1115C ellipticity, p. 145.

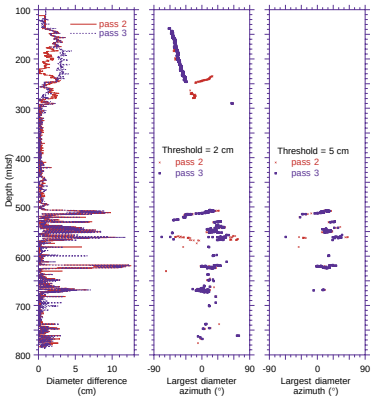

F67. Hole 1115C geometry, 500–570 mbsf, p. 146.

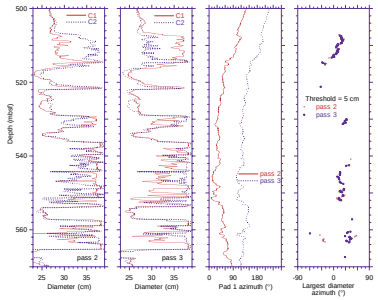

F68. Hole 1115C geometry, 575–675 mbsf, p. 147.

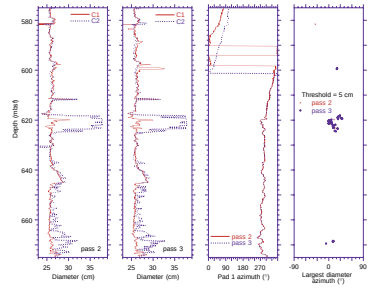

is applied to find the best estimates of tool speed and depth that are consistent with cable depth and the three-axis magnetometer-inclinometer logging tool (GPIT) z-axis accelerometer data.) Tool sticking resulted in often large, variable vertical depth shifts between the two passes after speed correction, and thus, the data require additional post-cruise processing.

Hole 1115C is characterized by generally uniform, flat-lying (<5°) clayey beds with thin (5–10 cm) resistive sandy or calcium carbonate–rich layers overlying more thinly layered beds that correlate to the late Miocene forearc sequence (see **"Lithostratigraphy,"** p. 5, and **"Biostratigraphy,"** p. 31). Many of the log units defined on the basis of the triple combo logs are not very distinctive with respect to each other in the FMS images; therefore, several of the units are grouped together in the discussion below.

Log Units L1 and L2 (79–153 mbsf and 153–413 mbsf, Respectively)

These units are characterized by uniformly low resistivity with minor occurrences of thin (<5 cm) more resistive layers that correspond to calcareous silty clays and volcanic ash layers observed in core samples (Fig. **F70;** see **"Lithostratigraphy,"** p. 5). An increase in frequency of presence of thicker (5–10 cm), resistive beds is found near the top of log Unit L2, ~153 mbsf, and continues downward throughout log Unit L2. The resistive beds commonly have sharp boundaries against the surrounding, more clayey material.

Log Units L3 and L4 (413–474 mbsf and 474–506 mbsf, Respectively)

Large-scale resistivity varies within log Units L3 and L4 and increases with depth. Few resistive beds are present, and those that do occur show a consistent thickness of ~10 cm. The unit displays a grainy texture in the FMS images (Fig. **F71**) that is commonly observed within calcareous units at this site, as well as in Hole 1109D (see **"Downhole Measurements,"** p. 69, in the "Site 1109" chapter). Bedforms are deformed to nonexistent within this interval, which may be caused by bioturbation (see **"Lithostratigraphy,"** p. 5). Thin, resistive layering is more frequent toward the base of log Unit L4, suggesting less bioturbation.

Log Units L5 and L6 (506–535 mbsf and 535–565 mbsf, Respectively)

The FMS image quality within log Units L5 and L6 was degraded by poor pad contact with the borehole because of numerous washouts as shown in the caliper log (Fig. **F59A**). The few well-imaged intervals appear similar to the clayey units above, contain thin resistive sandy or calcium carbonate–rich layers, and possess a grainy texture characteristic of calcium carbonate–rich sediments in this area.

Log Units L7 and L8 (565–573.5 mbsf and 573.5–628.5 mbsf, Respectively)

The top 2 m of log Unit L7 are composed of coarse-grained, low-resistivity material overlying highly resistive, wavy layers at 565.5 mbsf. The

F69. Hole 1115C magnetic field, **p. 148.**

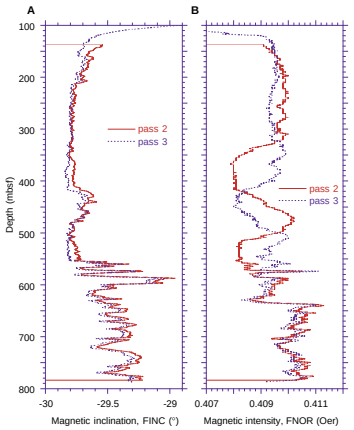

F70. Dynamically normalized FMS images of log unit L2, **p. 149.**

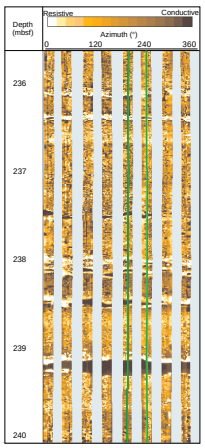

F71. Dynamically normalized FMS images of log unit L4, **p. 150.**

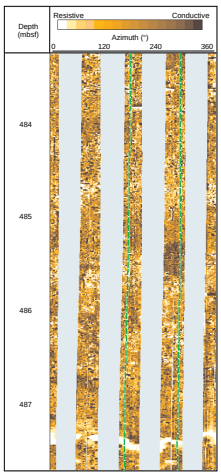

resistive layers are interbedded with conglomeratic material composed of a moderately resistive matrix (Fig. F72). Unit L8 consists of north-northwestward–dipping (5°–10°), thinly layered (<0.5 cm) beds, the top of which are interpreted to approximately correlate with the late Miocene forearc sequence at 573.5 mbsf (see "Depositional History," p. 27, and "Biostratigraphy," p. 31). Beds within log Unit L8 occasionally show cross lamination. At 605 mbsf, layering abruptly terminates, and the sediments appear structureless toward the base of Unit L8.

Log Unit L9 (628.5–784 mbsf)

The top of log Unit L9 is cut by steep (~70°), south-southwest–dipping fractures between 626.5 and 631 mbsf (Fig. F73), and corresponds to a zone of low core recovery (Cores 180-1115C-36R through 39R). Below 631 mbsf, the unit appears structureless and only occasional resistive beds show continuity from pad to pad. However, flat-lying beds are better defined toward the base of log Unit L9, particularly where bright, resistive beds are clearly imaged across all four (or eight) FMS pads. Thin, near-vertical, low-resistivity lines commonly are present in the images within log Unit L9 and appear to be artificial gouges in the formation caused by the logging tools during previous passes or may represent material (e.g., mud, pebbles) that was dragged along by the FMS pads (Fig. F74).

Temperature Data

The temperature profiles within the pipe and in open hole are shown in Figure F75. The temperature at the bottom of the hole (785 mbsf) reaches 12°C, but this is not representative of in situ temperatures. No evidence for influx of warm fluids can be seen in the profile. Mudline temperature was measured to be 4.3°C. This value is lower than those measured during the Adara temperature tool (Adara) and Davis-Villinger temperature probe (DVTP) runs (see "In Situ Temperature Measurements," p. 58), which were suspected of being erroneously high.

IN SITU TEMPERATURE MEASUREMENTS

In situ thermal measurements were successfully conducted within Hole 1115B using the Adara on Cores 180-1115B-3H, 5H, 7H, and 9H at 26.2, 45.2, 64.2, and 83.2 mbsf, respectively (Fig. F76). An additional temperature measurement was obtained before Core 180-1115B-25X using the DVTP at a probe-tip depth of 226.9 mbsf (Fig. F77).

Equilibrium formation temperatures were estimated using the TFIT program for Adara runs, and the CONEFIT program for the DVTP run (see "In Situ Temperature Measurements," p. 40, in the "Explanatory Notes" chapter). The estimates of equilibrium temperature used the thermal conductivity determined by core measurements (see "Thermal Conductivity," p. 49) rounded to the nearest 0.1 $W \cdot m^{-1} \cdot °C^{-1}$.

The mudline temperature in Hole 1115B is equivocal. The lowest temperatures (~4.6°C) were observed briefly in the water column rather than during the interval where the tool was held at mudline (~5.2°C to 5.5°C; Fig. F76). This occurred during all the Adara runs. A possibility is that mudline temperature is anomalously warm, either because of flow out of the borehole or very recent bottom-water temperature fluctuations. The alternate possibility is that the tool was being consistently

F72. Statically and dynamically normalized FMS images, log unit L7, p. 151.

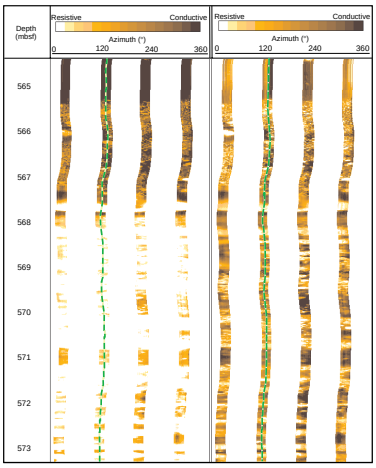

F73. Dynamically normalized FMS image and tadpole plot, log unit L9, p. 152.

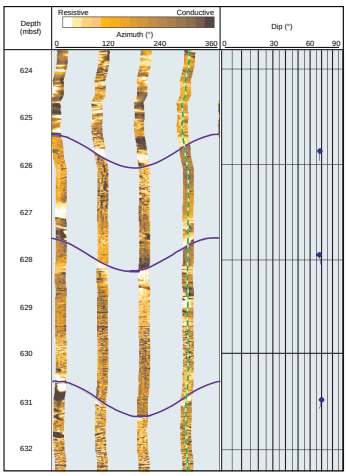

F74. Dynamically normalized FMS image of low resistivity, log unit L9, p. 153.

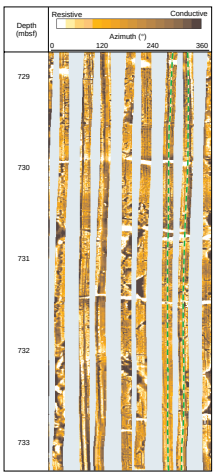

held slightly below mudline. The lowest temperature observed during the runs (4.6°C) is shown on the depth profile, but it is likely that this is an overestimate, because the tool would not have had time to fully equilibrate.

If the mudline temperature is excluded on the assumption that it is either inaccurate or nonrepresentative, a linear regression results in an estimated thermal gradient of 0.028°C·m^{-1} (28°C·km^{-1}; Fig. **F78**). Core measurements suggest an average thermal conductivity of 1.0 W·m^{-1}·°C^{-1} above 170 mbsf (see **"Thermal Conductivity,"** p. 49), yielding a heat flow of 28 mW·m^{-2} (± 5%, for rounding of the thermal conductivity estimates).

VERTICAL SEISMIC PROFILE AND DEPTH CONVERSION

A VSP experiment was conducted during the logging run at Site 1115. The goals of the VSP experiment were to give accurate depth estimations of reflectors identified in the multichannel seismic (MCS) data, thereby allowing correlation of lithostratigraphic units, and to provide parameters with which to improve velocity processing of existing MCS data. A 300-in^3 air gun was used to generate a source signal, which was received in the hole by the WST. The source signal was also recorded on a hydrophone close to the air gun (see **"Vertical Seismic Profiling,"** p. 42, in the "Explanatory Notes" chapter).

As part of the preparation for recording the VSP, the end of the drill pipe was positioned at 100 mbsf. A restriction in the hole prevented the WST from being lowered past 554.0 mbsf. The WST was raised to 552.2 mbsf, at which point the clamping arm was engaged, pushing the instrument against the wall of the hole. A total of twelve stations were occupied. Clamping intervals were variable (Table **T16**), largely because of poor hole conditions at the first four stations, or a better location was found on the caliper log from the triple combo run (see **"Downhole Measurements,"** p. 52). A recurring (1.2–1.5 s) signal, with a peak at ~30 Hz, was a problem at all stations, and attempts to limit it largely governed the location of subsequent stations. High noise levels eventually caused the abandonment of the VSP. Shots that did not have a clear first arrival and showed high noise levels were flagged. At each station, the air gun was triggered a number of times. Each good shot was stacked, with firing continuing until the stack contained seven shots. Movement of the WST after it had been clamped against the side of the hole was minimal, or masked by external noise.

The recurring 30-Hz signal had a similar amplitude and power spectrum to the air gun source signal, and was received on both the geophone in the hole and the hydrophone close to the sea surface, even when the air gun was not fired. The noise was not seen on the WST signal when the instrument was returned to the bottom of the hole and positioned on the restriction at 554.0 mbsf, possibly because of better clamping conditions at that location. Identification of a source originating from the *JOIDES Resolution* was unsuccessful. Reorienting the ship relative to the prevailing currents and wind direction provided a minimal reduction in the amplitude of the noise. Although the signal was of a similar frequency to that of the ship's main propellers (judging from the revolutions per minute), no changes in operation had taken place since the last VSP experiment that could explain the new signal.

F75. Temperature profile within and above 1115C, **p. 154.**

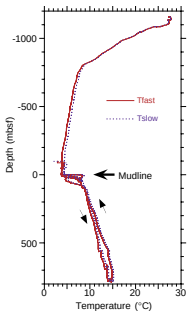

F76. Temperature as a function of time for Adara temperature tool runs, **p. 155.**

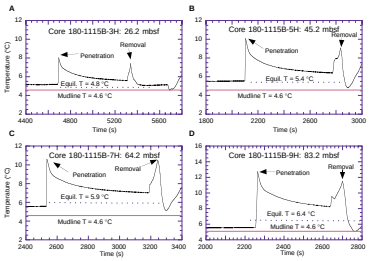

F77. Temperature as a function of time for DVTP temperature run, **p. 156.**

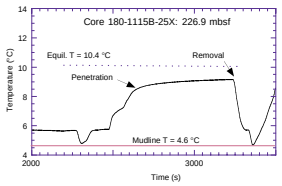

F78. Temperatures as a function of depth and best-fit linear regression, **p. 157.**

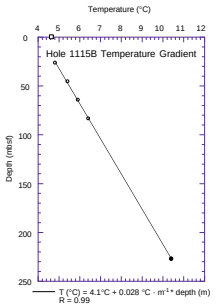

T16. VSP experiment time data, **p. 225.**

Interval velocities were calculated for stations at 552.2, 532.1, 505.0, and 490.1 mbsf (Table **T16;** Fig. **F79**). The results are variable, but fitting a straight line by linear regression gives an interval velocity of 2044 m·s^{-1} (Fig. **F80**). Physical properties (see **"Physical Properties,"** p. 47) and logging measurements (see **"Downhole Measurements,"** p. 52) of velocities in the VSP interval vary from 1757 to 4702 m·s^{-1}. The high degree of variability comes mainly from lithostratigraphic Unit VI, characterized by frequent calcium carbonate–rich horizons that locally elevate the *P*-wave velocity. Interval velocities determined from the VSP experiment may have averaged out the effect of these high-velocity layers.

To convert between seismic traveltime and depth below seafloor, we examined the velocity information available from laboratory measurements and sonic logs to develop a model of the variation of velocity with depth. In this model, the more densely sampled velocities (DTCO; see **"Downhole Measurements,"** p. 52) measured downhole were used preferentially to values determined from laboratory measurements. Exceptions were from 0 to 152.41 mbsf and 779.9 to 802.5 mbsf, where log sonic velocities were absent. Because of an offset between the laboratory velocities measured using the PWS3 transducer and those of the PWS1 and PWS2 transducers (see **"Compressional Wave Velocity,"** p. 49), the consistently 40 m·s^{-1} higher PWS3 (transverse) measurement was used. Where velocities measured using the PWS3 transducer were absent, the vertical velocity measured using the PWS1 transducer was substituted with a + 40 m·s^{-1} offset. The resultant velocity-depth function (Fig. **F80**) was passed through a 2-m Gaussian filter and resampled to 1 m before being used to convert from depth to two-way traveltime (TWT). To confirm the viability of the depth conversion, it was compared with VSP check-shot information. The *P*-wave transit time to the WST geophone at depth (Table **T16**) was properly corrected for the geometry of the experiment (see **"Vertical Seismic Profiling,"** p. 42, in the "Explanatory Notes" chapter) to give a direct and absolute tie between TWT and depth. Comparing this to the MCS data correlates horizons in TWT to depth. The VSP is limited to depths from 490.1 to 552.2 mbsf; therefore, this comparison was made only over a short depth interval. Table **T17** shows that the difference between the VSP depth and that calculated for an equivalent time from the velocity-depth function ranges from 2.72 to 7.53 m, with an average of 4.86 m. We infer that depth conversions using our velocity-depth relationship are accurate to ~5 m above 552.2 mbsf.

A synthetic seismic trace was generated using velocity and density data from Site 1115. Density data were compiled from downhole logging measurements (RHOM) and laboratory index properties measurements. Similar to the compilation of velocity measurements, in situ logging measurements were preferred to laboratory measurements, except where they were absent or of poor quality (0–100 mbsf and 776 mbsf to the bottom of the hole; Fig. **F81**). Additionally, RHOM densities <1.7 g·cm^{-3} were removed from the data set below 500 mbsf. A number of synthetic seismic traces were computed following the application of different filtering parameters to the velocity and density data. The synthetic trace that best matched the data was generated by applying a 0.5-m median filter (to remove spikes), and an Akima spline (to resample the data to 1 m) to both data sets. An Akima spline was used in preference to a simple linear extrapolation because of the variation in measurement interval between the laboratory (meter scale) and downhole (centimeter scale) measurements. A reflection coefficient

F79. Depth vs. transit time for Site 1115 VSP, **p. 158.**

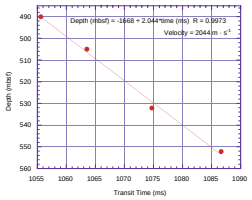

F80. Velocity vs. depth function for Site 1115, **p. 159.**

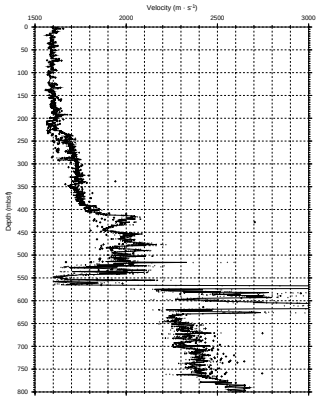

T17. Comparison of VSP data with depth estimates, **p. 226.**

F81. Density vs. depth function for Site 1115, **p. 160.**

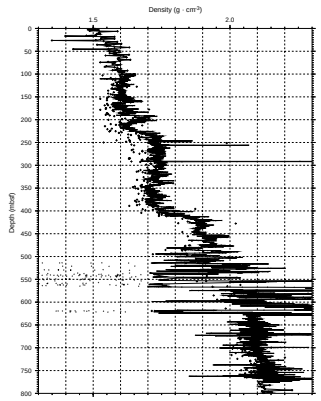

was subsequently calculated from the two data sets. Using the relationship derived above, the reflection coefficient was converted from depth to time (Fig. **F82**). A source signal, comprising the first 500 ms of the direct wave from the migrated MCS coinciding with Site 1109, was convolved with the reflection coefficient to give the synthetic seismic trace. Using the depth-time function derived above, both the synthetic trace and a number of migrated MCS traces close to the site were converted to depth (Fig. **F82**).

There are obvious problems with the correlations between the synthetic seismic data and the MCS data (Fig. **F82**). For example, a prominent doublet seen in the MCS data between 270 and 300 mbsf is not reproduced in the synthetic data and may be of the wrong polarity. Given that we have shown above that our conversion between time and depth is accurate, this indicates that the problem is with the parameters used to generate the synthetic seismic trace. Further work on this problem will include adjusting the filtering parameters of the velocity and density data, as well as experimenting with the source signal.

Figure **F83** shows the correlation between the MCS data in time, the depth converted MCS traces, and the lithostratigraphy column (see **"Lithostratigraphy,"** p. 5). Lines are drawn at 30-m intervals connecting the depth-converted MCS data and the lithostratigraphy column to the MCS data in time. The top of lithostratigraphic Unit X, which corresponds to what is interpreted as the top of the Miocene forearc sequence, is estimated to be at 2.21 s TWT and corresponds to the brightest reflector on top of the forearc sequence.

F82. MCS data, seismic trace, and reflection coefficient, **p. 161.**

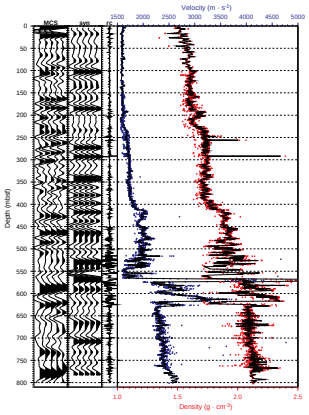

F83. MCS Line EW9510-1366 cut at Site 1115, **p. 162.**

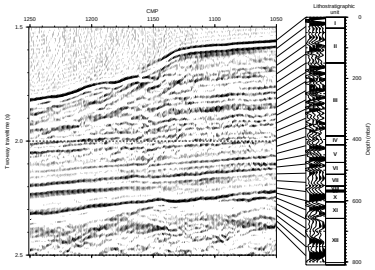

REFERENCES

Athy, L.F., 1930. Density, porosity, and compaction of sedimentary rocks. *AAPG Bull.,* 14:1–24.

Baker, P.A., 1986. Pore-water chemistry of carbonate-rich sediments, Lord Howe Rise, Southwest Pacific Ocean. *In* Kennett, J.P., von der Borch, C.C., et al., *Init. Repts. DSDP,* 90: Washington (U.S. Govt. Printing Office), 1249–1256.

Berggren, W.A., Kent, D.V., Swisher, C.C., III, and Aubry, M.-P., 1995. A revised Cenozoic geochronology and chronostratigraphy. *In* Berggren, W.A., Kent, D.V., Aubry, M.-P., and Hardenbol, J. (Eds.), *Geochronology, Time Scales and Global Stratigraphic Correlation*. Spec. Publ.—Soc. Econ. Paleontol. Mineral. (Soc. Sediment. Geol.), 54:129–212.

Carey, S., and Sigurdsson, H., 1980. The Roseau ash: deep-sea tephra deposits from a major eruption on Dominica, Lesser Antilles arc. *J. Volcanol. Geotherm. Res.,* 7:67–86.

Claypool, G.E., and Kaplan, I.R., 1974. The origin and distribution of methane in marine sediments. *In* Kaplan, I.R. (Ed.), *Natural Gases in Marine Sediments:* New York (Plenum), 99–139.

Davies, H.L., Symonds, P.A., and Ripper, I.D., 1984. Structure and evolution of the southern Solomon Sea region. *BMR J. Aust. Geol. Geophys.,* 9:49–68.

De Carlo, E.H., 1992. Geochemistry of pore water and sediments recovered from the Exmouth Plateau. *In* von Rad, U., Haq, B.U., et al., *Proc. ODP, Sci. Results,* 122: College Station, TX (Ocean Drilling Program), 295–308.

Eberli, G.P., Swart, P.K., Malone, M.J., et al., 1997. *Proc. ODP, Init. Repts.,* 166: College Station, TX (Ocean Drilling Program).

Fisher, R.V., and Schmincke, H.-U., 1984. *Pyroclastic Rocks*: Berlin (Springer-Verlag).

Froelich, P.N., Mortlock, R.A., Mefferd, M., and Powers, J., 1991. Interstitial-water chemistry: abyssal South Atlantic and East Georgia Basins, Islas Orcadas and Meteor Rises. *In* Ciesielski, P.F., Kristoffersen, Y., et al., *Proc. ODP, Sci. Results,* 114: College Station, TX (Ocean Drilling Program), 719–731.

Furnes, H., Thorseth, I.H., Tumyr, O., Torsvik, T., and Fisk, M.R., 1996. Microbial activity in the alteration of glass from pillow lavas from Hole 896A. *In* Alt, J.C., Kinoshita, H., Stokking, L.B., and Michael, P.J. (Eds.), *Proc. ODP, Sci. Results,* 148: College Station, TX (Ocean Drilling Program), 191–206.

Gieskes, J.M., 1983. The chemistry of interstitial waters of deep-sea sediments: interpretation of deep-sea drilling data. *In* Riley, J.P., and Chester, R. (Eds.), *Chemical Oceanography* (Vol. 8): London (Academic), 221–269.

Gieskes, J.M., and Lawrence, J.R., 1981. Alteration of volcanic matter in deep-sea sediments: evidence from the chemical composition of interstitial waters from deep sea drilling cores. *Geochim. Cosmochim. Acta,* 45:1687–1703.

Giovannoni, S.J., Fisk, M.R., Mullins, T.D., and Furnes, H., 1996. Genetic evidence for endolithic microbial life colonizing basaltic glass/seawater interfaces. *In* Alt, J.C., Kinoshita, H., Stokking, L.B., and Michael, P.J. (Eds.), *Proc. ODP, Sci. Results,* 148: College Station, TX (Ocean Drilling Program), 207–214.

Jelinek, V., 1981. Characterization of the magnetic fabric of rocks. *Tectonophysics,* 79:63–67.

Johnson, R.W., Mackenzie, D.E., and Smith, I.E.M., 1978. Volcanic rock associations at volcanic plate boundaries: re-appraisal of the concept using case histories from Papua New Guinea. *Tectonophysics,* 46:197–216.

Lock, J., Davies, H.L., Tiffin, D.L., Murakami, F., and Kisomoto, K., 1987. The Trobriand subduction system in the western Solomon Sea. *Geo-Mar. Lett.,* 7:129–134.

Mackenzie, F.T., Ristvet, B.L., Thorsenson, D.C., Lerman, A., and Leeper, R.H., 1981. Reverse weathering and chemical mass balance in a coastal environment. *In* Reeder, R.J. (Ed.), *Carbonates: Mineralogy and Chemistry:* Chelsea (Mineral Soc. Am.), 97–144.

Martin, J.B., Kastner, M., and Egeberg, P.K., 1995. Origins of saline fluids at convergent margins. *In* Taylor, B., and Natland, J. (Eds.), *Active Margins and Marginal Basins of the Western Pacific*. Geophys. Monogr., Am. Geophys. Union, 88:219–239.

Mesri, G., 1975. Discussion of new design procedures for stability of soft clays. *J. Geotech. Div., Am. Soc. Civ. Eng.,* 101-GT4:409–412.

Millero, F.J., and Sohn, M.L., 1992. *Chemical Oceanography:* Boca Raton (CRC Press).

Morse, J.W., and Mackenzie, F.T. 1990. *Geochemistry of Sedimentary Carbonates:* New York (Elsevier).

Parkes, R.J., Cragg, B.A., Bale, S.J., Getliff, J.M., Goodman, K., Rochelle, P.A., Fry, J.C., Weightman, A.J., and Harvey, S.M., 1994. A deep bacterial biosphere in Pacific Ocean sediments. *Nature,* 371:410–413.

Ristvet, B., 1978. Reverse weathering reactions within recent nearshore marine sediments, Kaneohe Bay, Oahu. Test Directorate Field Command, Kirtland AFB, New Mexico.

Shipboard Scientific Party, 1976. Site 317. *In* Schlanger, S.O., Jackson, E.D., et al., *Init. Repts. DSDP:* 33, Washington, (U.S. Govt. Printing Office), 161–300.

Smith, I.E.M., 1976. Peralkaline rhyolites from the D'Entrecasteaux Islands, Papua New Guinea. *In* Johnson, R.W. (Ed.), *Volcanism in Australasia:* Amsterdam (Elsevier), 275–285.

Smith, I.E.M., and Milsom, J.S., 1984. Late Cenozoic volcanism and extension in eastern Papua. *In* Kokelaar, B.P., and Howells, M.F. (Eds.), *Marginal Basin Geology.* Geol. Soc. Spec. Publ. London, 16:163–171.

Stolz, A.J., Davies, G.R., Crawford, A.J., and Smith, I.E.M., 1993. Sr, Nd and Pb isotopic compositions of calc-alkaline and peralkaline silicic volcanics from the D'Entrecasteaux Islands, Papua New Guinea, and their tectonic significance. *Mineral. Petrol.,* 47:103–126.

Terzaghi, K., 1925. *Erdbaumechanik auf bodenphysikalischer Grundlage:* Leipzig (Deuticke).

Torres, M.E., Marsaglia, K.M., Martin, J.B., and Murray, R.W., 1995. Sediment diagenesis in Western Pacific Basins. *In* Taylor, B., and Natland, J. (Eds.), *Active Margins and Marginal Basins of the Western Pacific*. Geophys. Monogr., Am. Geophys. Union, 88:241–258.

Wellsbury, P., Goodman, K., Barth, T., Cragg, B.A., Barnes, S.P., and Parkes, R.J., 1997. Deep marine biosphere fueled by increasing organic matter availability during burial and heating. *Nature,* 388:573–576.

Figure F1. Lithologic units recovered. **A.** Hole 1115B. For key to symbols, see Fig. F2, p. 52, in the "Explanatory Notes" chapter. (Continued on next page.)

A

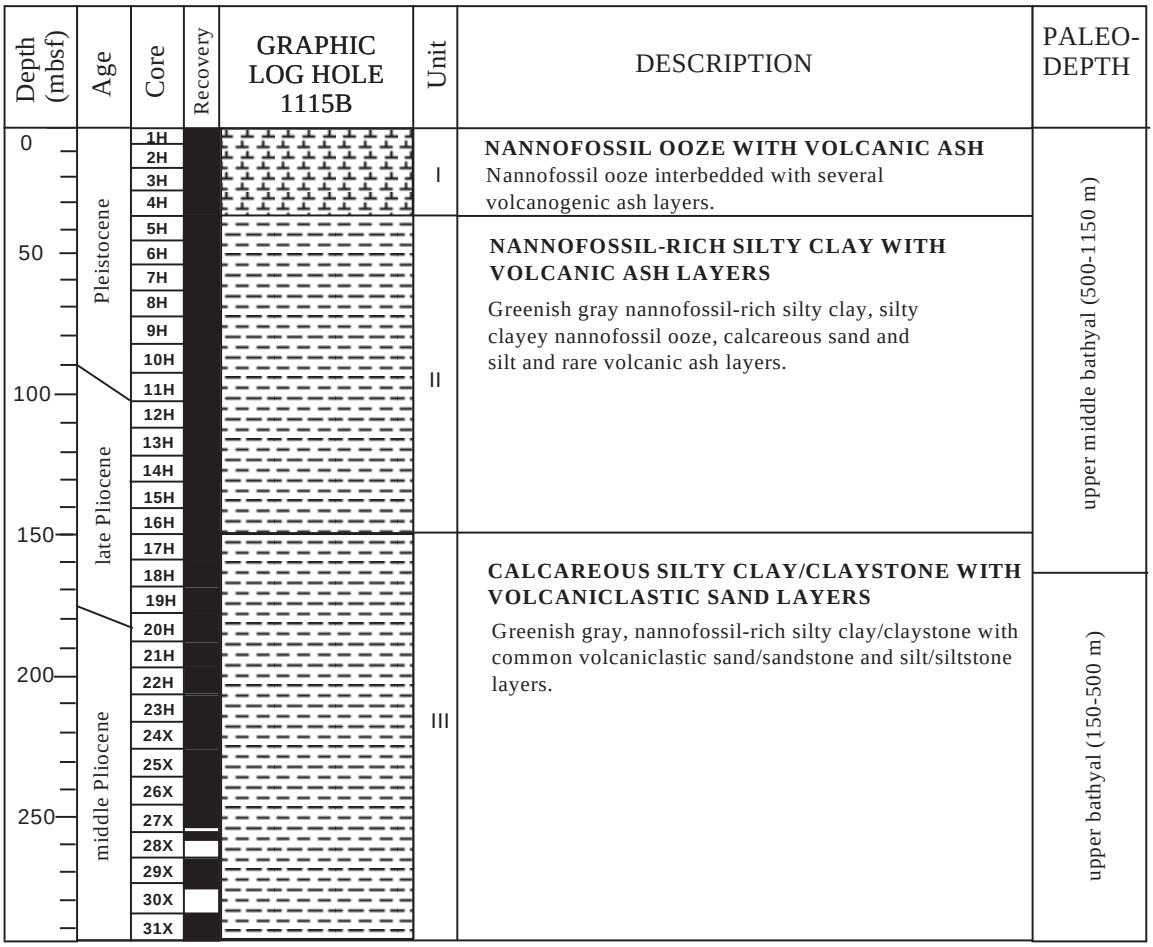

Figure F1 (continued). B. Hole 1115C.

B

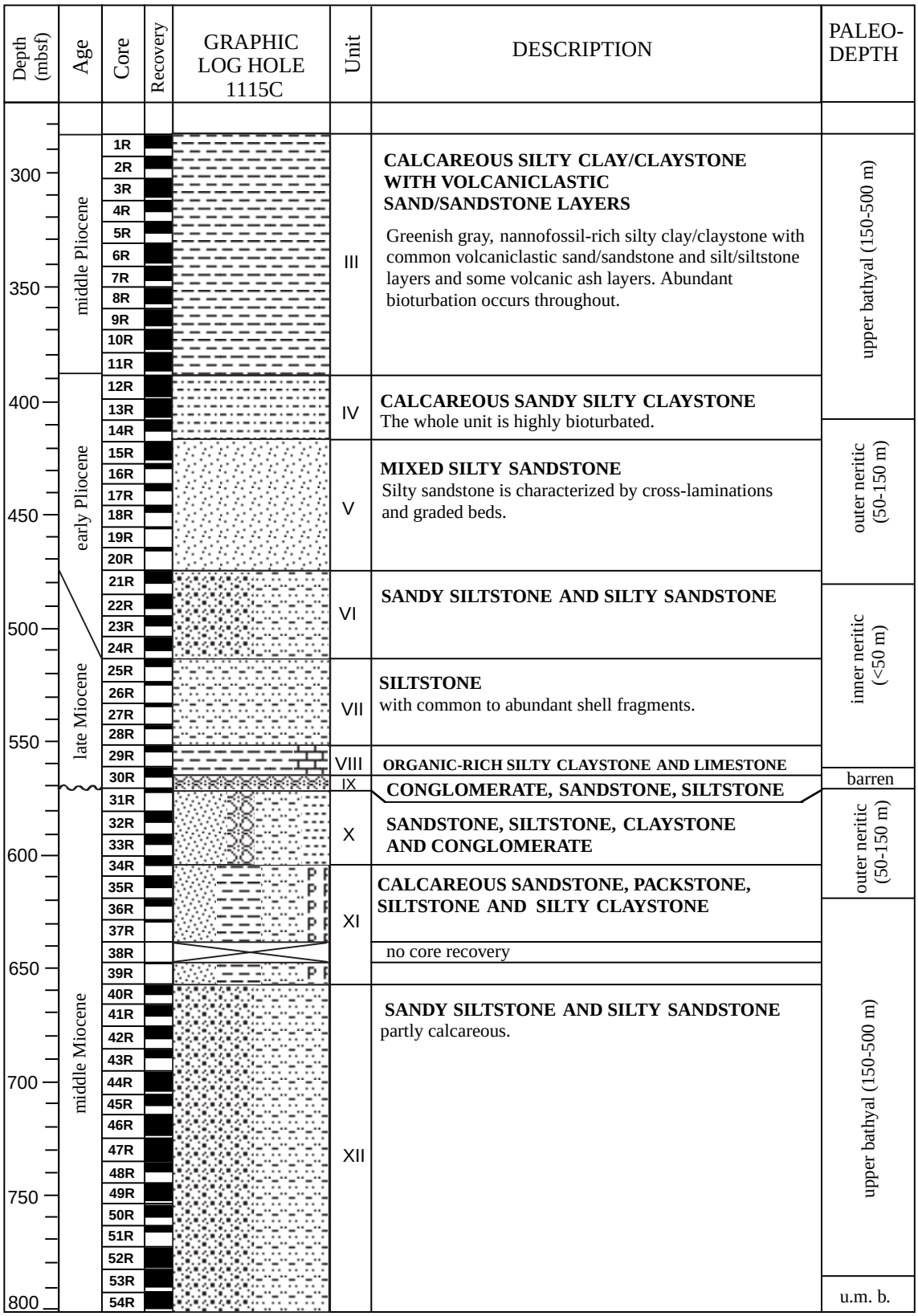

u.m. b. = upper middle bathyal

Figure F2. Grain-size trend (generalized from the barrel sheets) for the units recovered. **A.** Hole 1115B. For key to symbols, see Fig. F2, p. 52, in the "Explanatory Notes" chapter. (Continued on next page.)

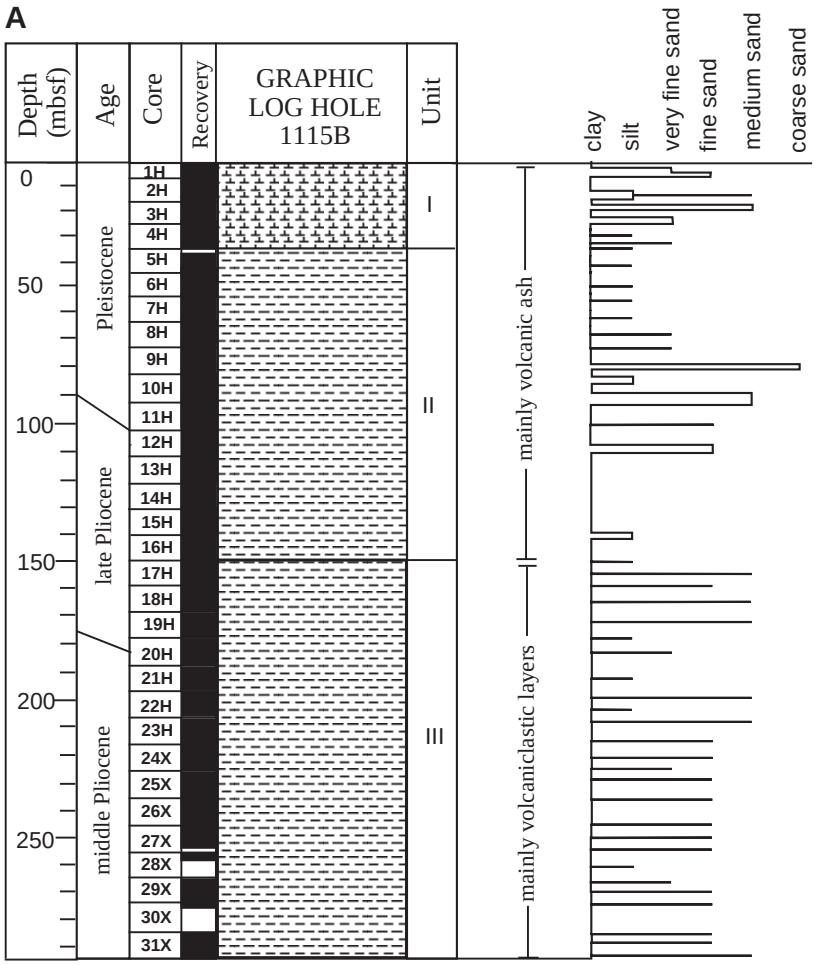

Figure F2 (continued). B. Hole 1115C. Note that anomalies may result in areas of low core recovery.

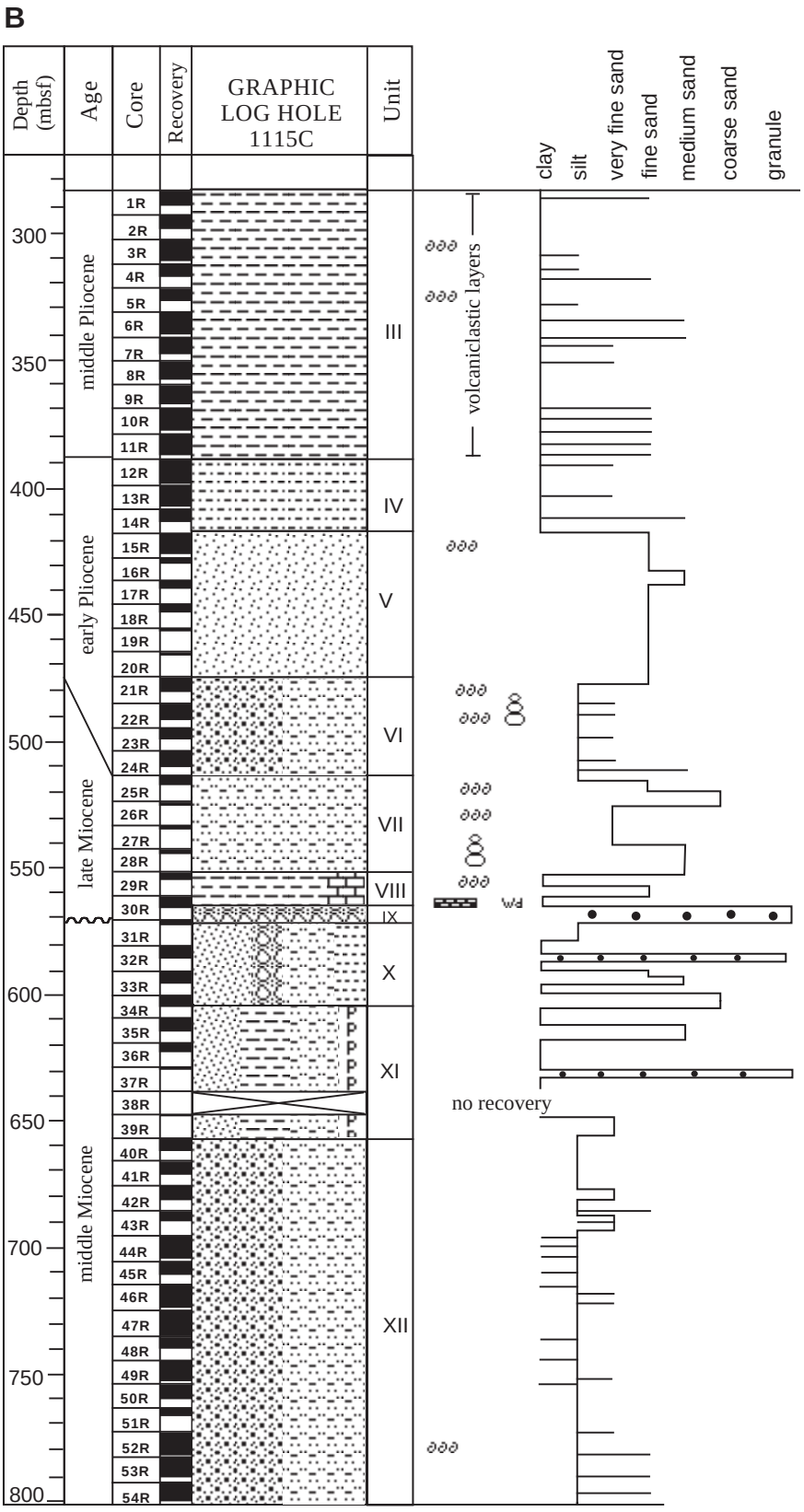

Figure F3. Interbedded nannofossil ooze with volcanic ash layers that exhibit basal contacts and a gradational upper part. Unit I (interval 180-1115A-1H-4, 85–110 cm).

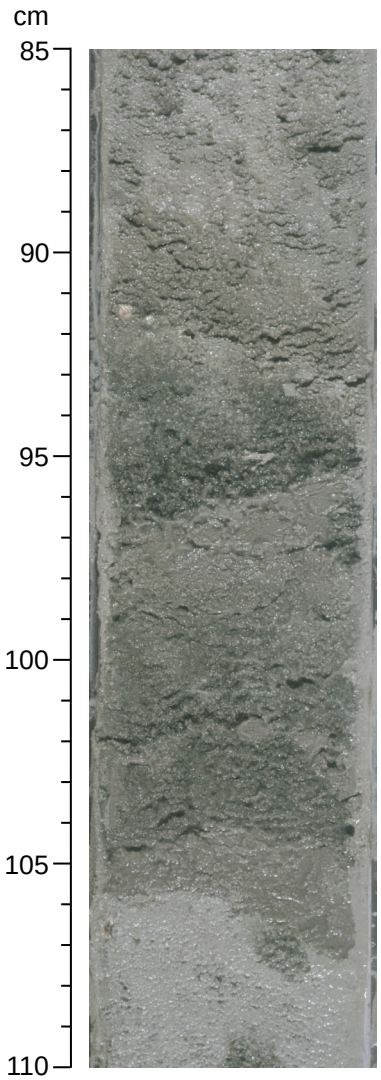

Figure F4. Pyroclastic and epiclastic volcanogenic layers. The lower layer (58–62.5 cm) is mostly composed of volcanic glass suggesting it is a volcanic ash, whereas the overlying layer is rich also in glass, but contains a considerable amount of ferromagnesian minerals. The contact between the two layers is sharp to diffuse. Unit II (interval 180-1115B-10H-4, 48–66 cm).

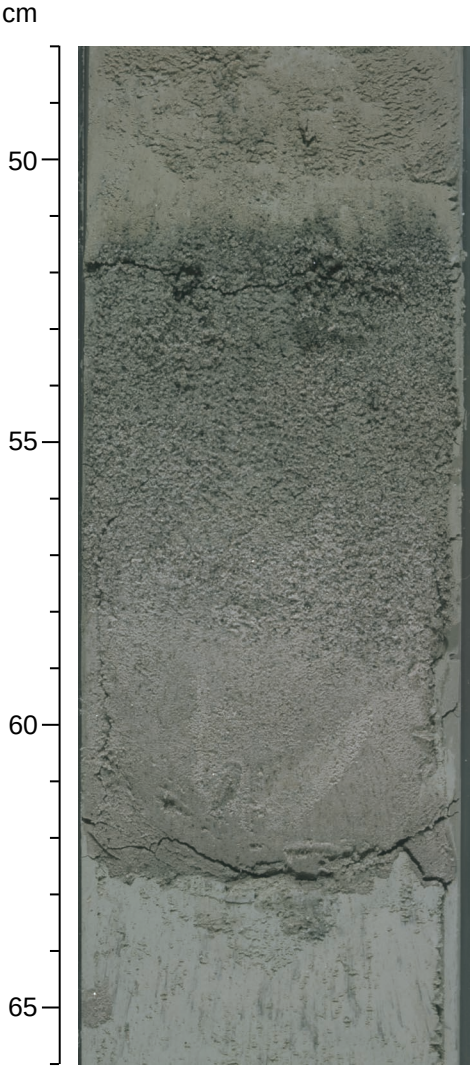

Figure F5. Digital photomicrograph (crossed nicols) of a silty claystone with common unaltered detrital grains of plagioclase, biotite, hornblende, and planktonic foraminifers. Note the zoned plagioclase (lower left) (interval 180-1115C-10R-1, 5–7 cm).

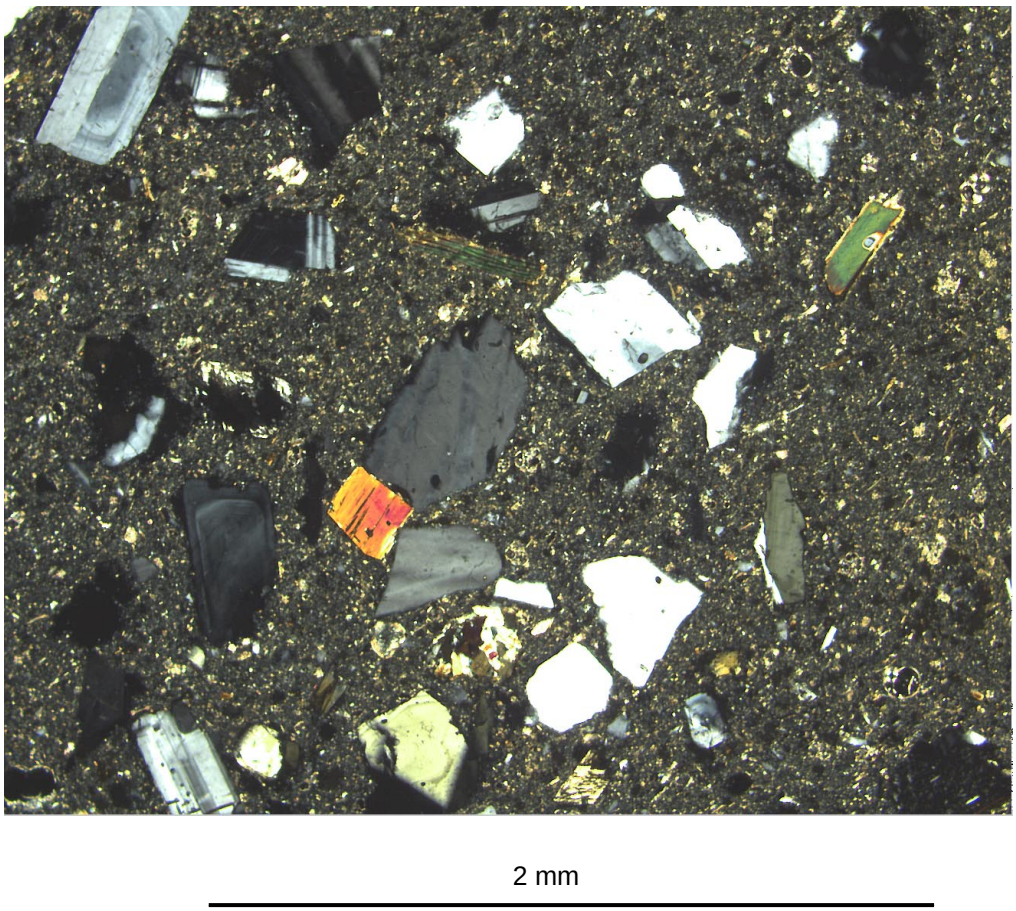

Figure F6. Sharp-based, normally graded volcaniclastic sand layer. The lower part is rich in dark minerals, whereas the upper part is rich in colorless glass. Compare with Figure **F4,** p. 69 (interval 180-1115B-17H-3, 75–95 cm).

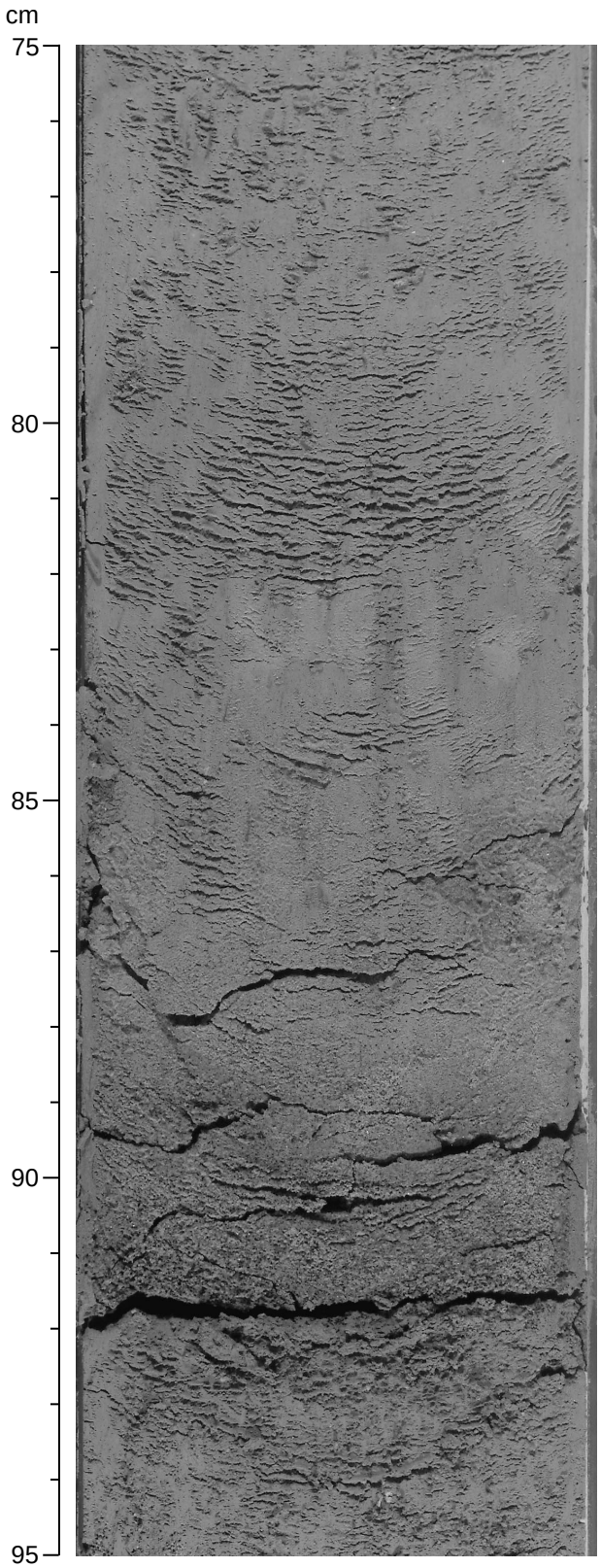

Figure F7. Digital photomicrograph (crossed nicols) of a sandy silty claystone containing subrounded basalt and acidic volcanic rock fragments, unaltered detrital sand-size grains of angular plagioclase, hornblende, and planktonic foraminifers tests. Note the multiple twinned and zoned plagioclase grains (interval 180-1115C-12R-4, 144–148 cm).

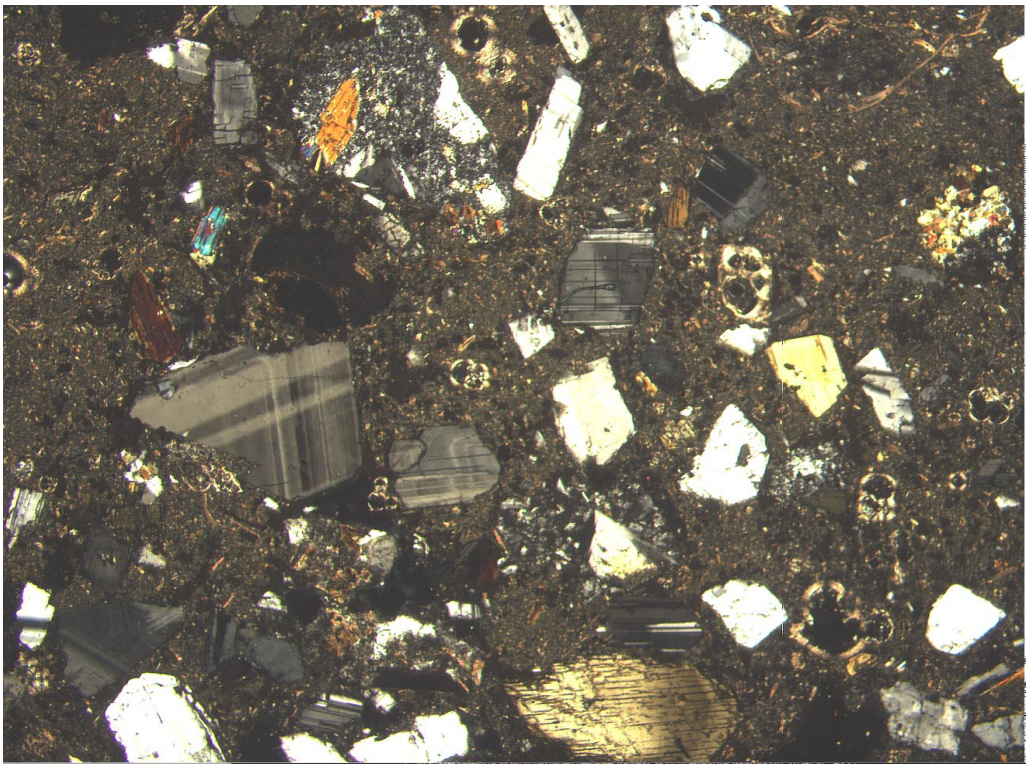

Figure F8. Digital photomicrograph (plane-polarized light) of a pumaceous rock containing phenocrysts of hornblende within a glassy groundmass. The rock is a granule-size clast within a sandy silty claystone (interval 180-1115C-12R-5, 50–53 cm).

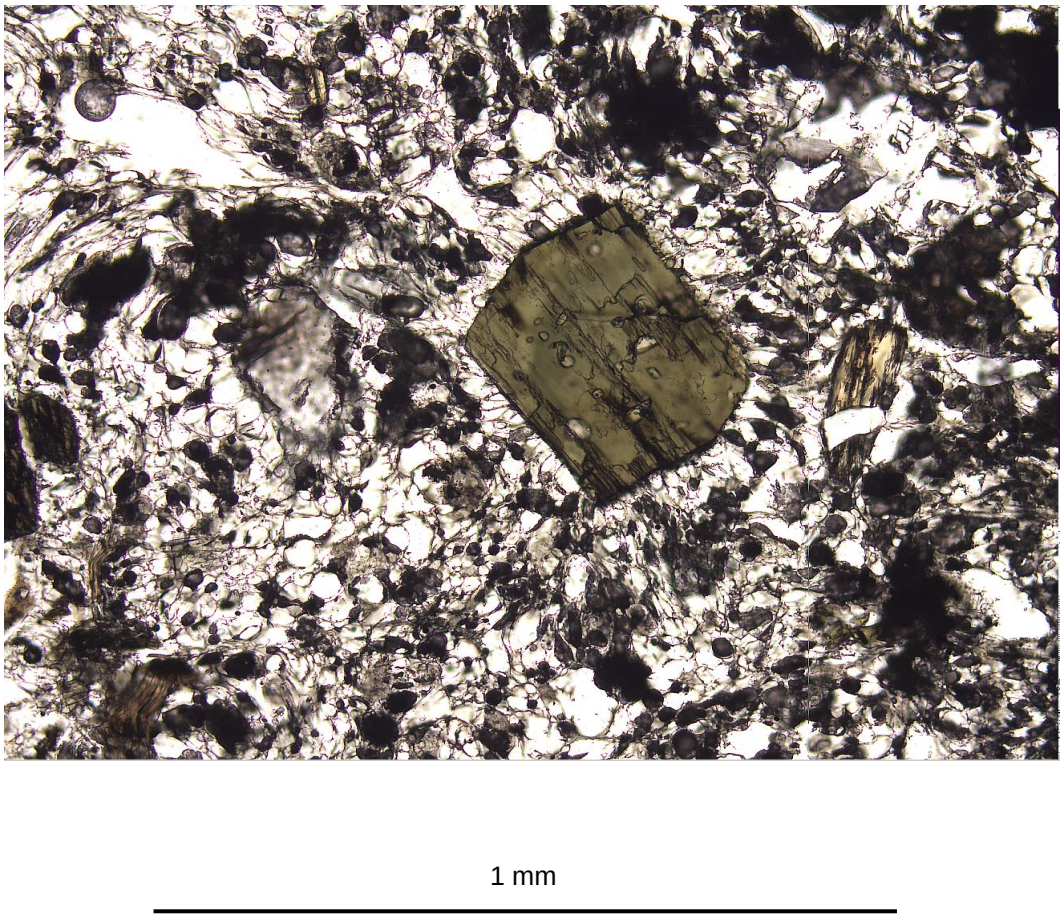

Figure F9. Cross-bedded, fine-grained sandstone with a single set of ripple-laminated sand at 37 cm (interval 180-1115C-18R-1, 20–50 cm).

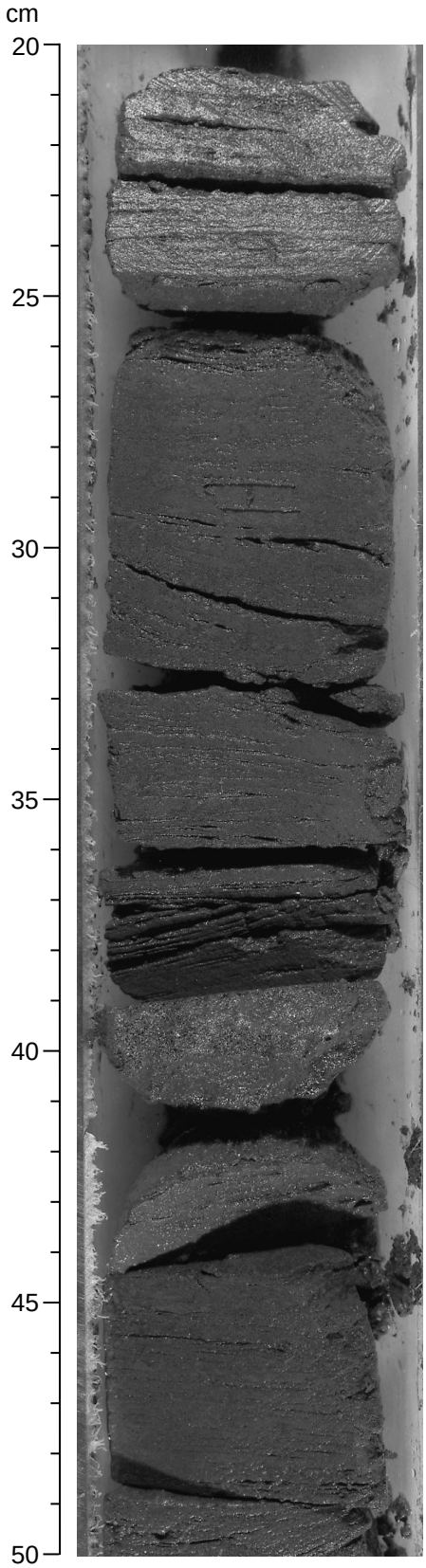

Figure F10. Structureless, coarse- to medium-grained sandstone. These sandstones are rich in foraminifers and shell fragments (interval 180-1115C-15R-3, 50–70 cm).

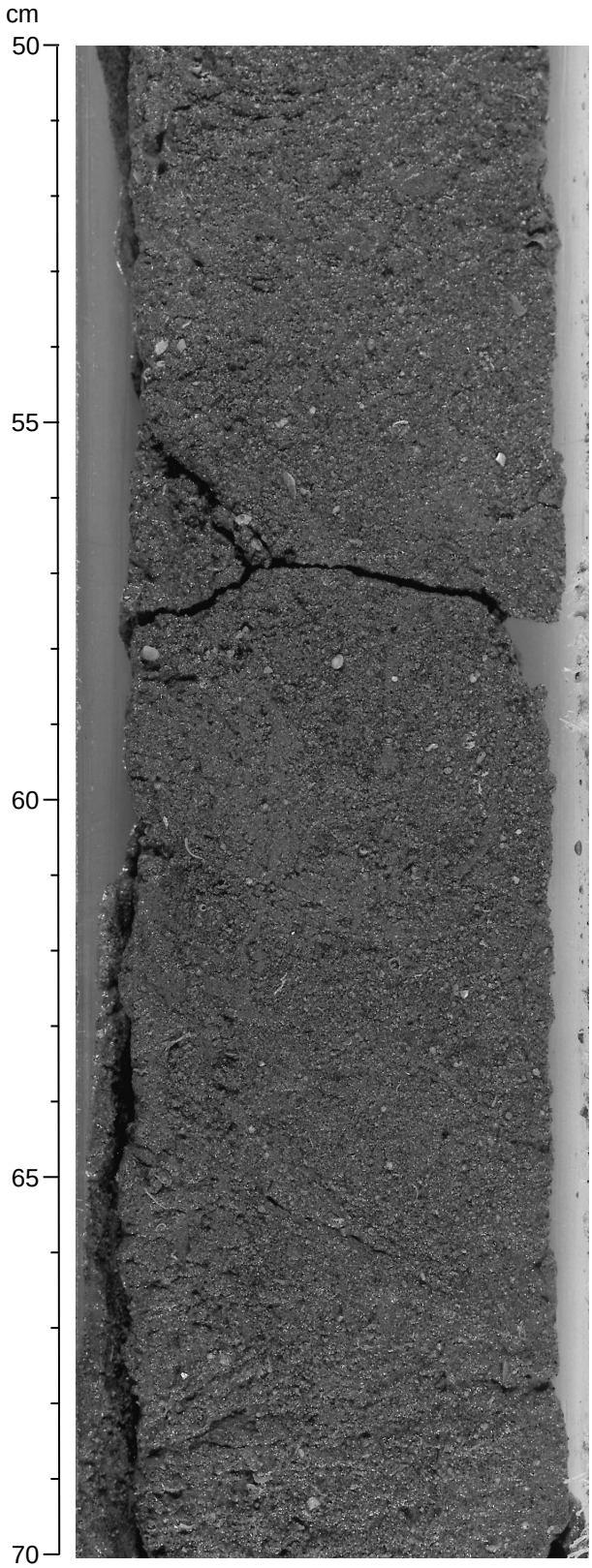

Figure F11. Digital photomicrograph (crossed nicols) of a mixed coarse-grained sandstone containing fragments of planktonic and rare benthic foraminifer tests, subrounded grains of basalt and andesite with phenocrysts of plagioclase and rare hornblende, polycrystalline quartz (center), subangular plagioclase, and biotite in a micritic cement (interval 180-1115C-15R-3, 79–83 cm).

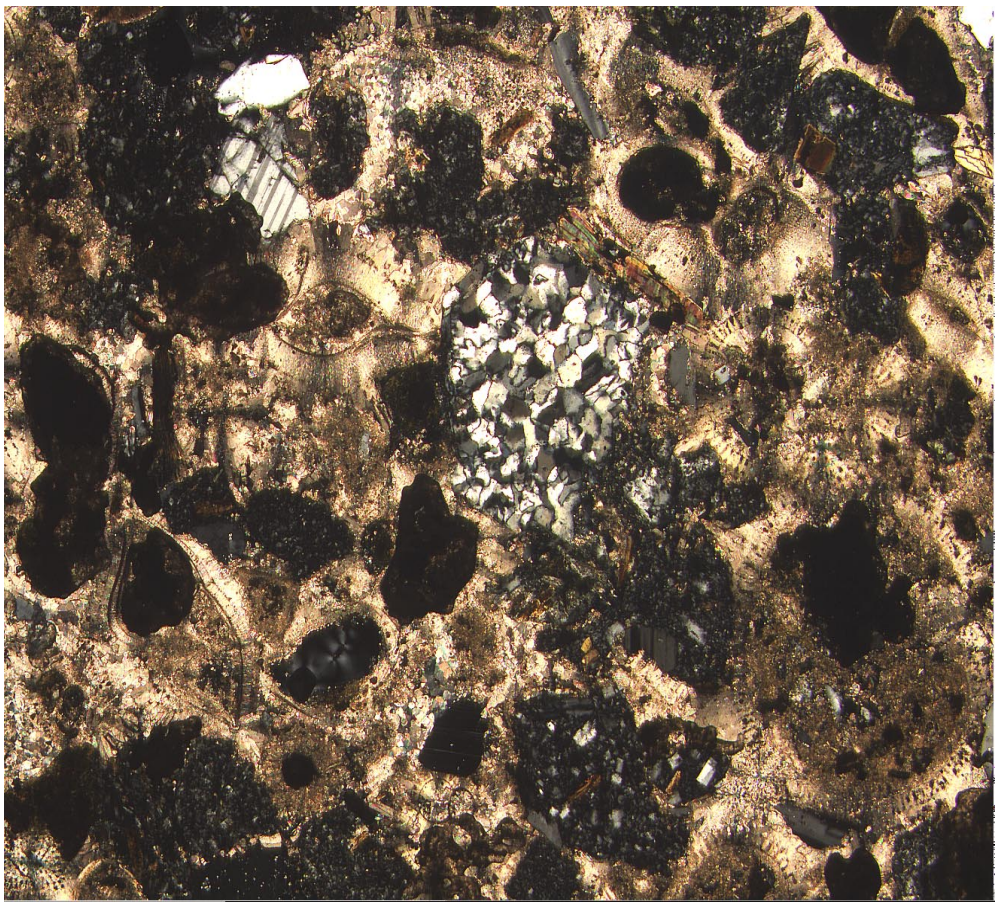

Figure F12. Digital photomicrograph (crossed nicols) of a sandy siltstone containing detrital grains of plagioclase, hornblende, biotite, and fragments of planktonic and benthic foraminifers. Rare subrounded grains of basalt with plagioclase and rare hornblende phenocrysts (interval 180-1115C-23R-1, 93–94 cm).

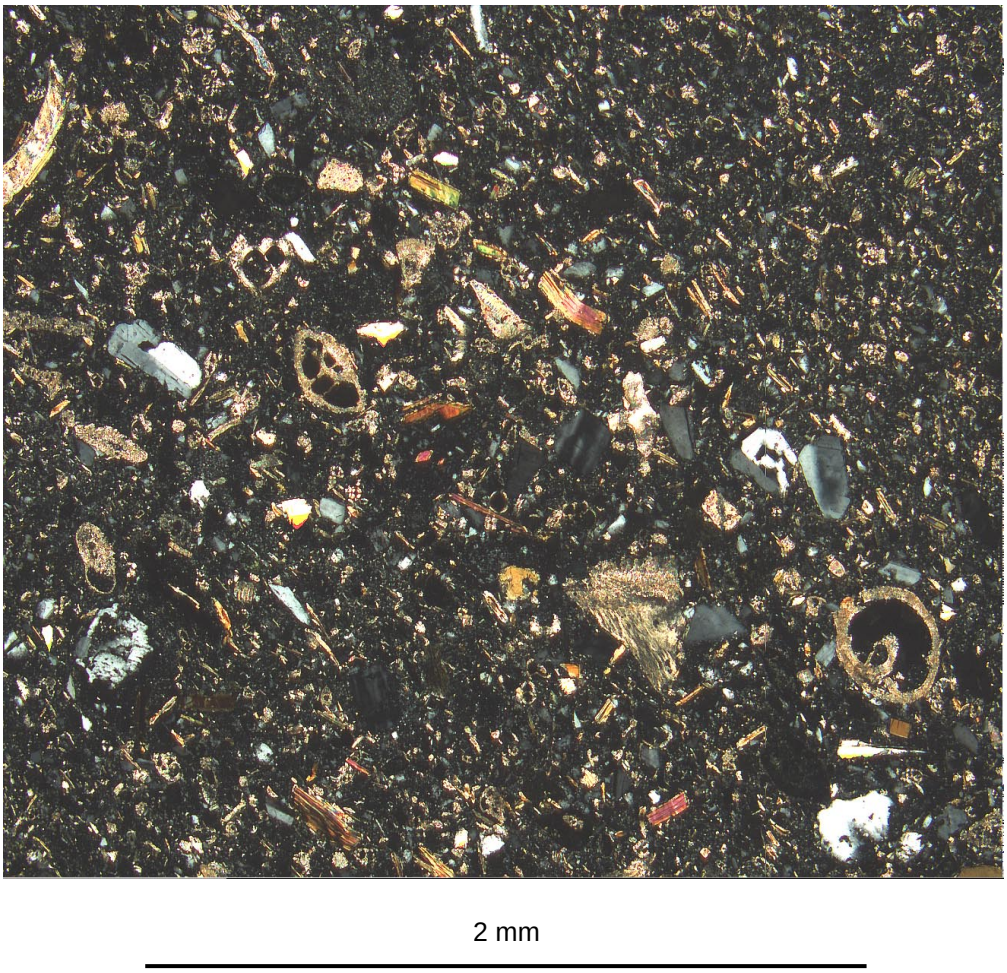

Figure F13. Intensely bioturbated foraminifer- and shell-fragment–rich silty sandstones. These sandstones also contain rare to common fragments of organic matter (e.g., at 89 cm) (interval 180-1115C-23R-1, 86–110 cm).

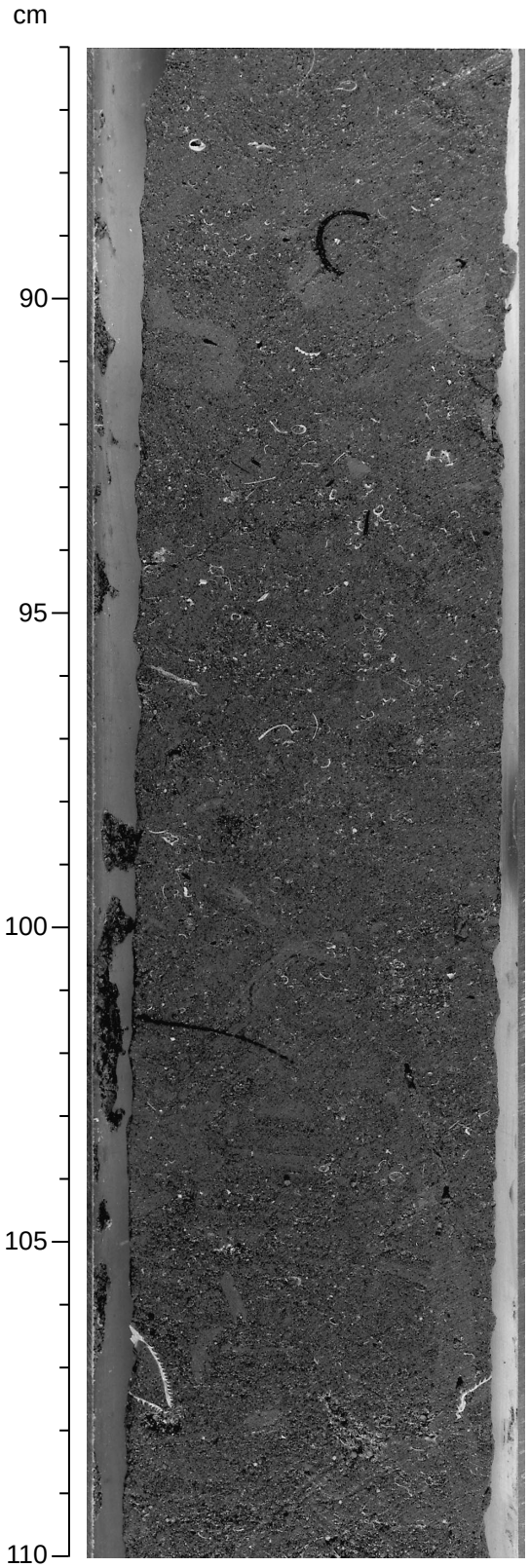

Figure F14. Calcareous sandstone with abundant shells and shell fragments (interval 180-1115C-28R-1, 60–80 cm).

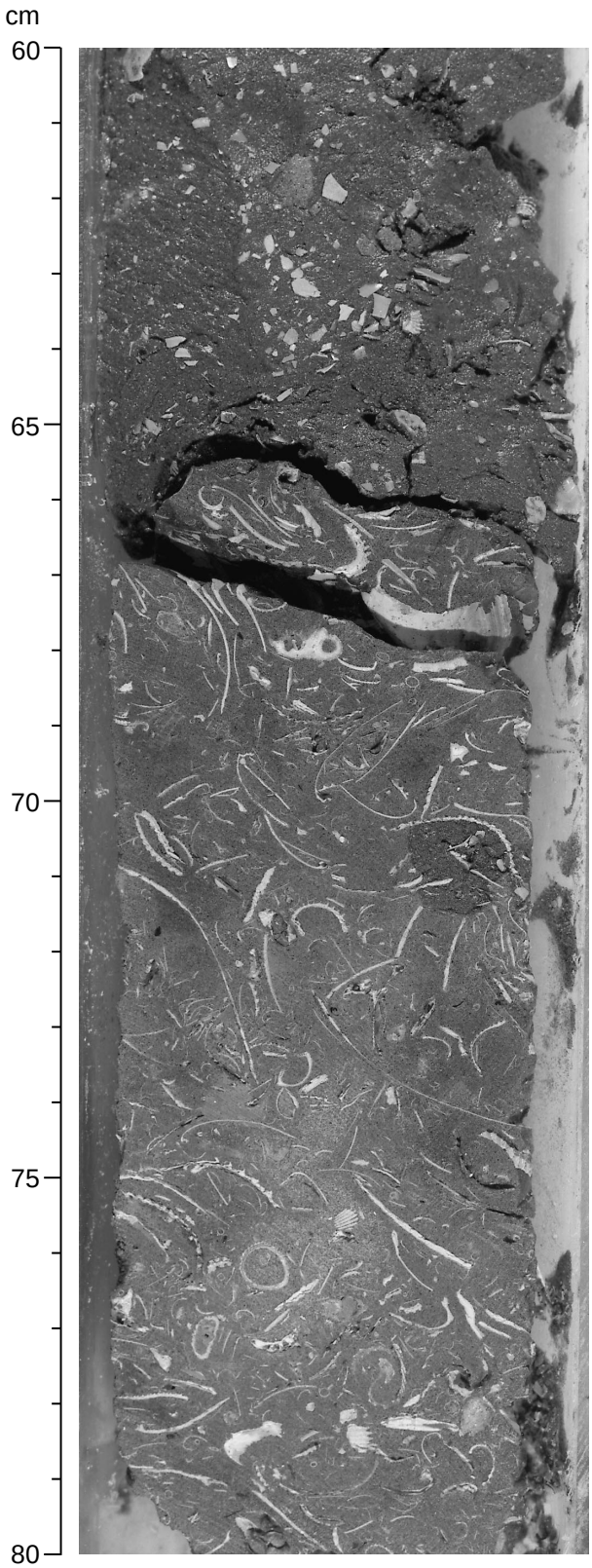

Figure F15. Digital photomicrograph (crossed nicols) of a coarse-grained sandstone with a micritic cement containing angular to subangular detrital grains of plagioclase, quartz, biotite, hornblende, and subrounded plagioclase phyric basalt fragments (interval 180-1115C-26R-1, 8–9 cm).

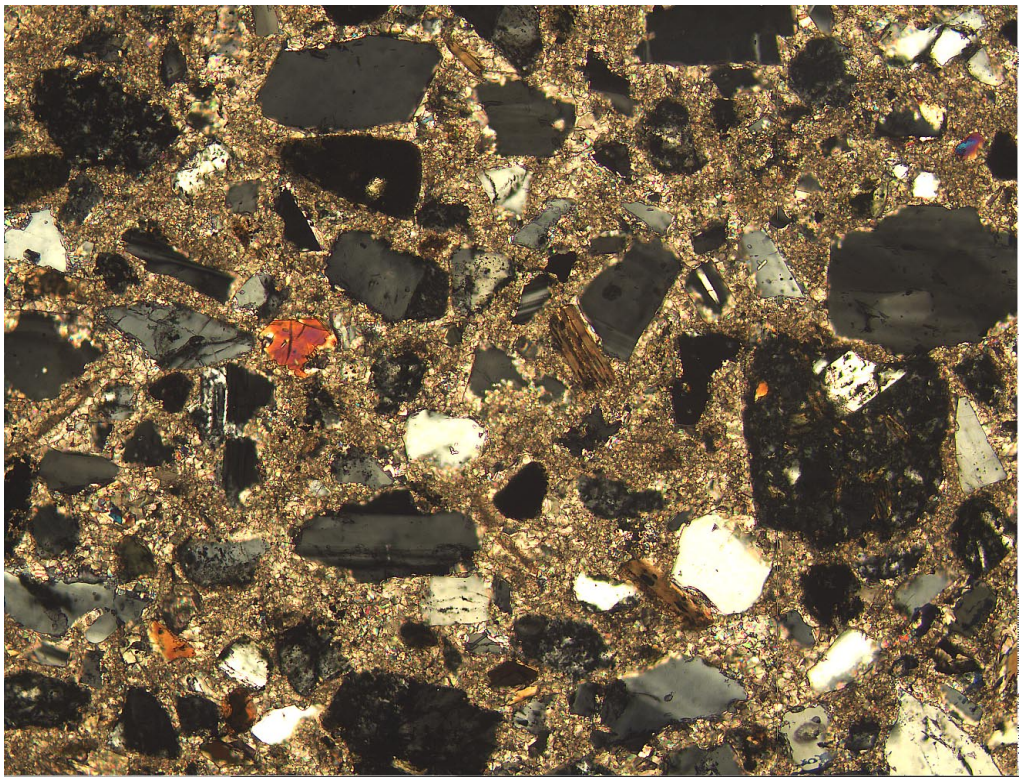

Figure F16. Silty sandy claystone with thin interbeds of organic-rich clayey siltstone (interval 180-1115C-30R-3, 2–18 cm).

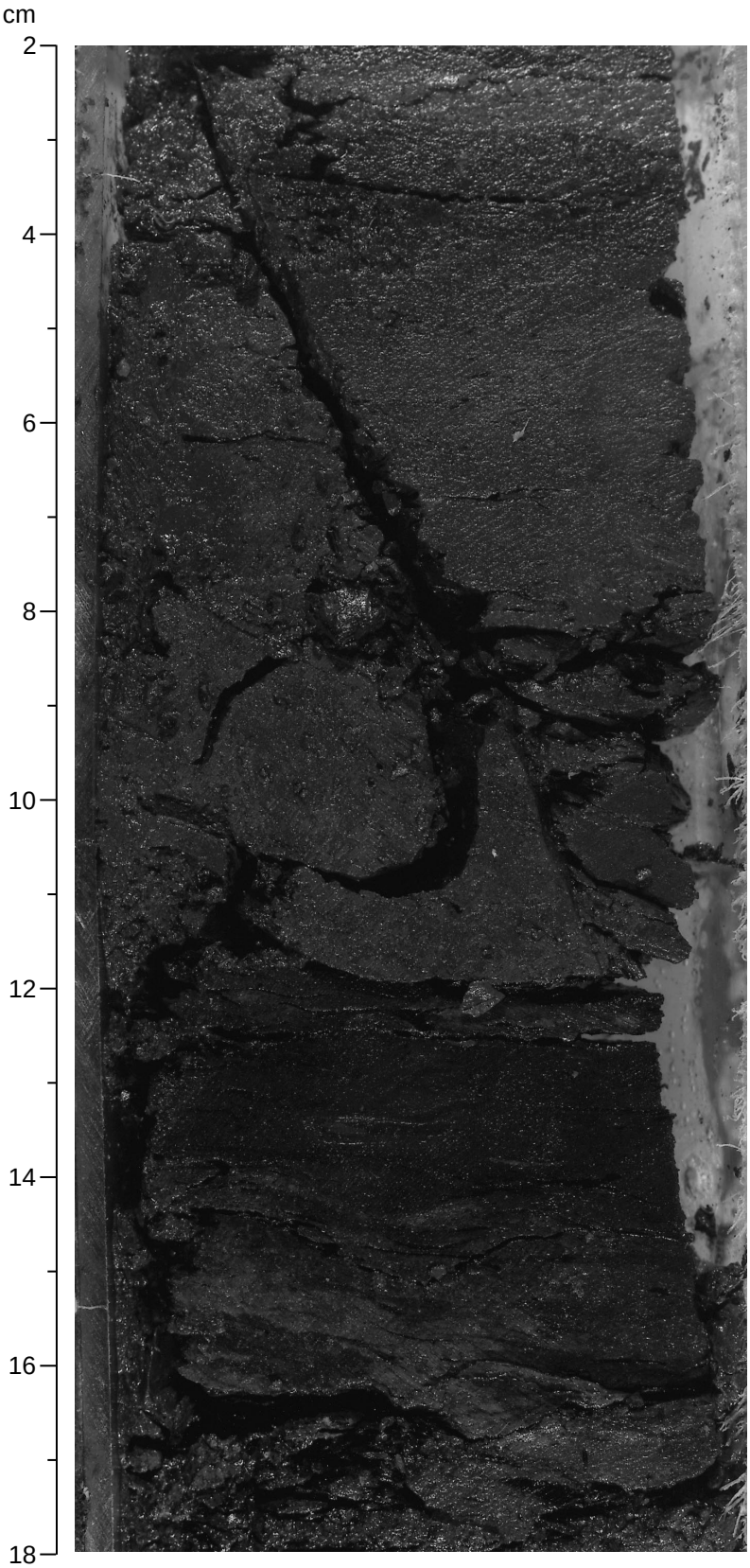

Figure F17. Digital photomicrograph (crossed nicols) of a medium-grained sandstone with a sparry calcite cement containing subrounded to rounded fragments of plagioclase phyric basalt, subangular detrital grains of plagioclase, hornblende, clinopyroxene, biotite, and rare quartz (interval 180-1115C-29R-1, 72–73 cm).

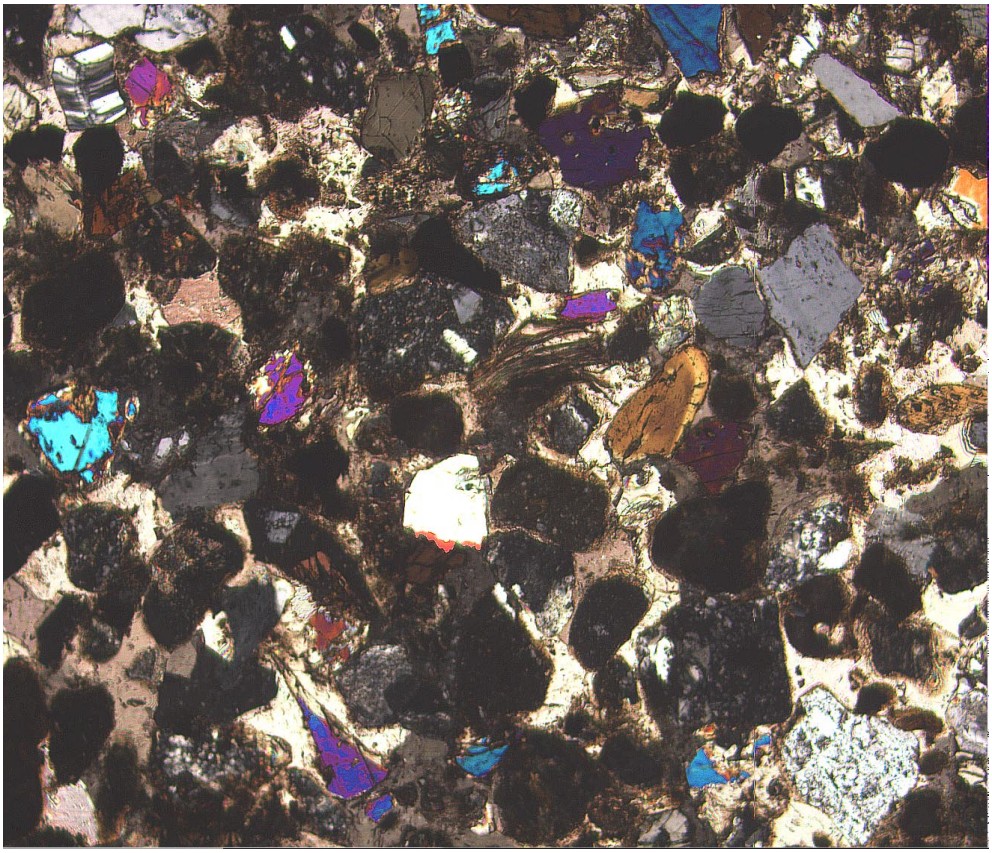

Figure F18. Pebble and granule matrix-supported conglomerate. The very well rounded clasts are composed of variable rocks (basalt, siltstone, and sandstone; interval 180-1115C-30R-5, 48–61 cm).

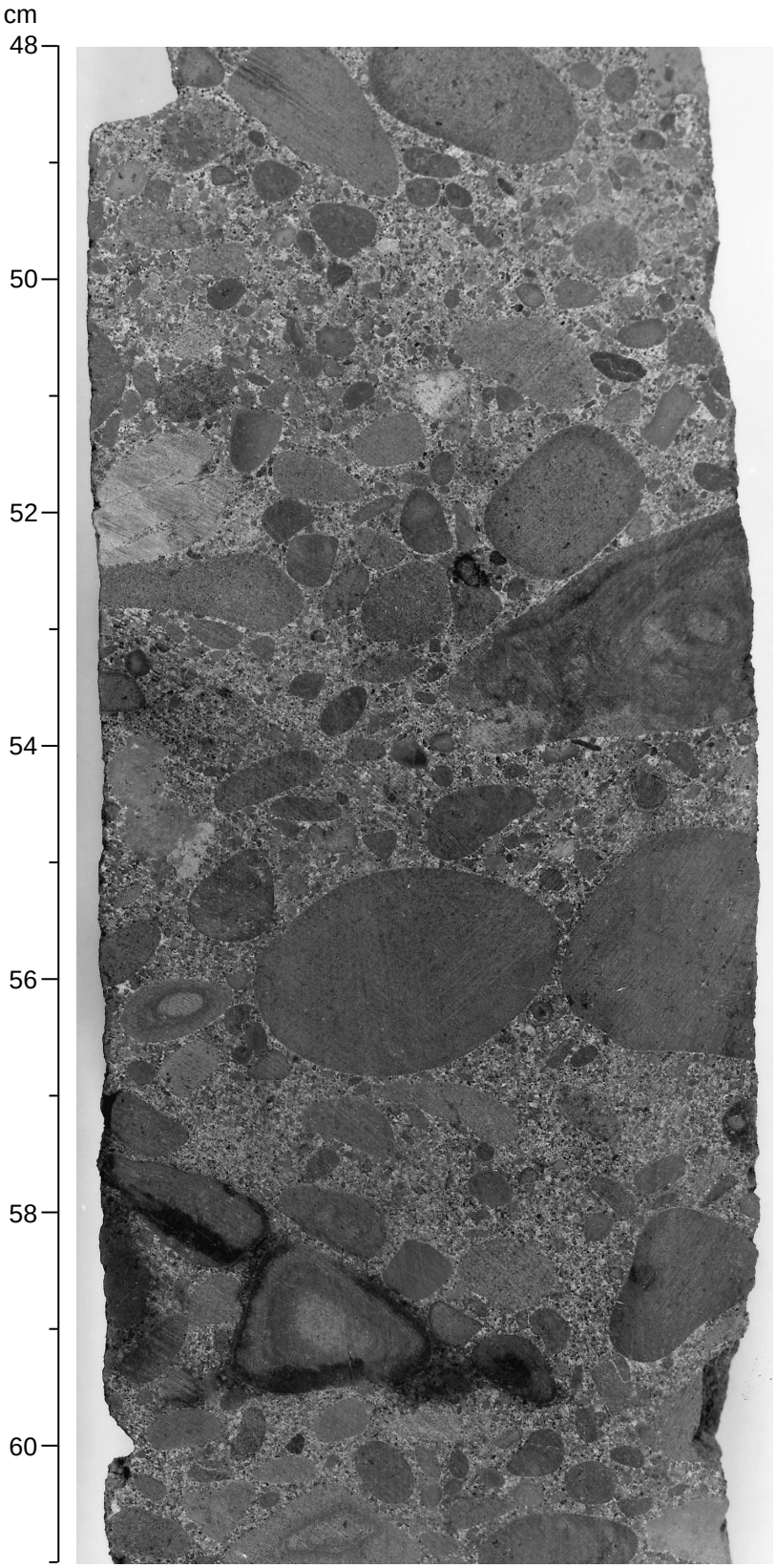

Figure F19. Digital photomicrograph (crossed nicols) of a coarse-grained sandstone containing subrounded to rounded porphyritic basalt, andesite, acidic volcanics, and subangular detrital grains of plagioclase, hornblende, clinopyroxene, and rare quartz in a sparry calcite cement (interval 180-1115C-30R-CC, 16–19 cm).

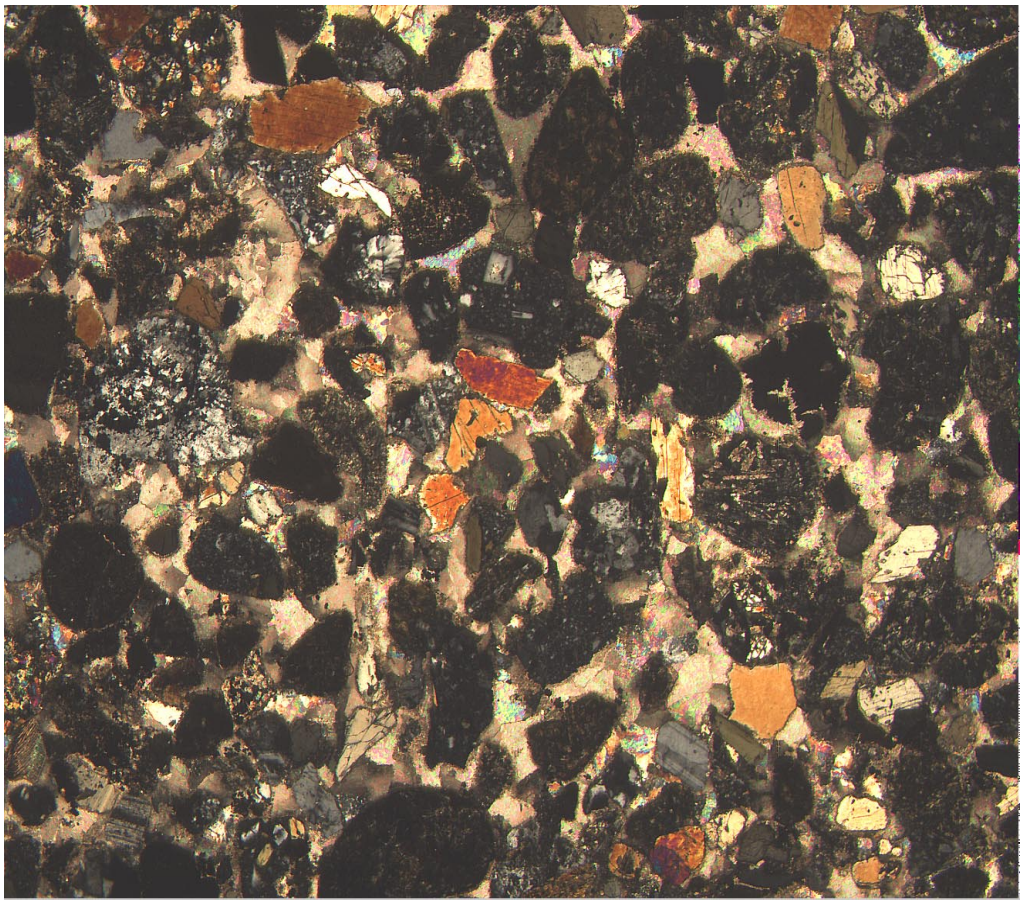

Figure F20. Poorly sorted, medium- to coarse-grained sandstone with abundant rounded mud clasts in the upper part. Some of these beds are characterized by inverse-to-normal grading (interval 180-1115C-32R-3, 54–68 cm).

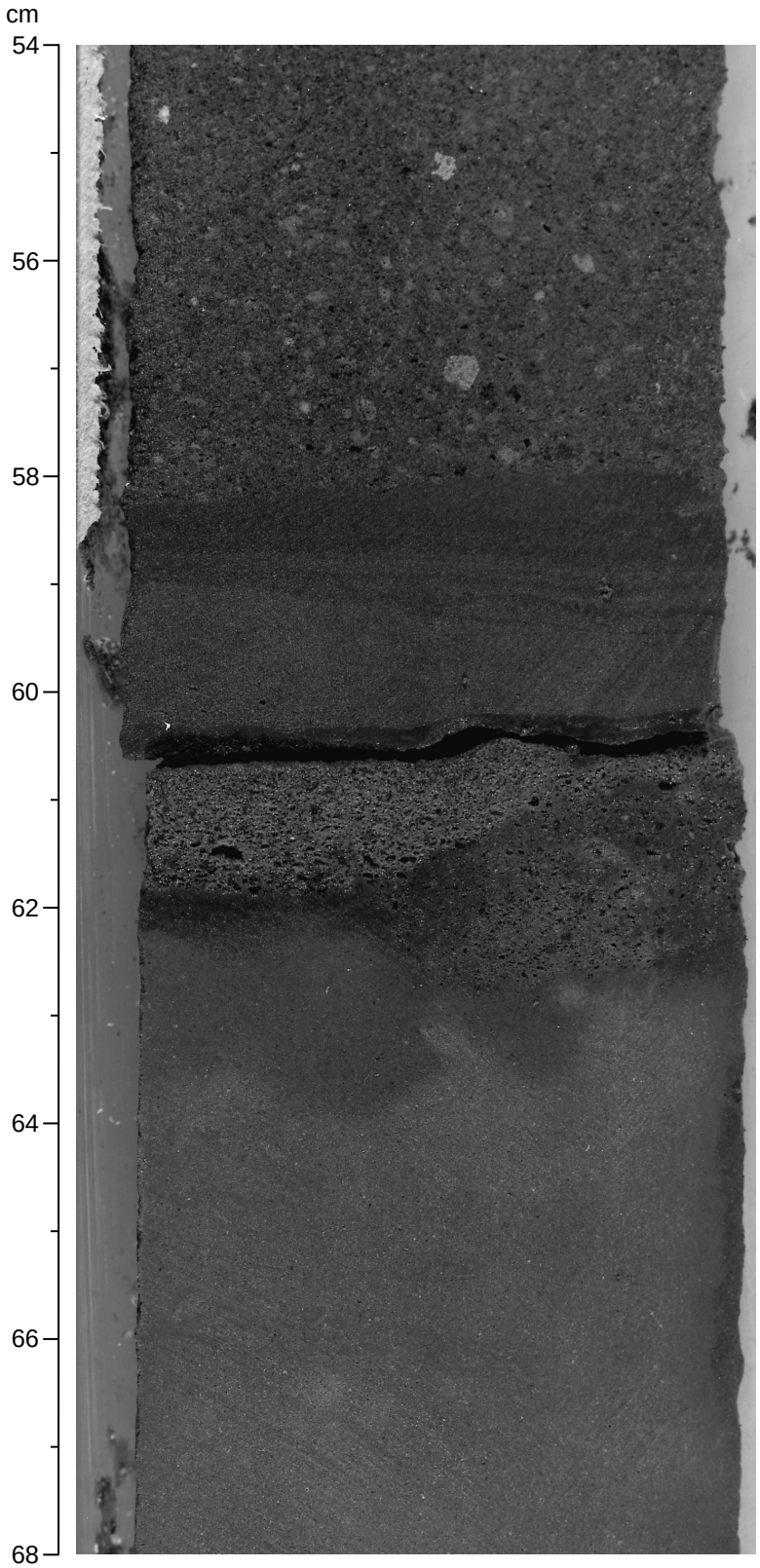

Figure F21. Digital photomicrograph (crossed nicols) of a coarse-grained sandstone containing abundant detrital grains of clinopyroxene, rare plagioclase, and subrounded basaltic rock fragments (interval 180-1115C-32R-1, 138–140 cm).

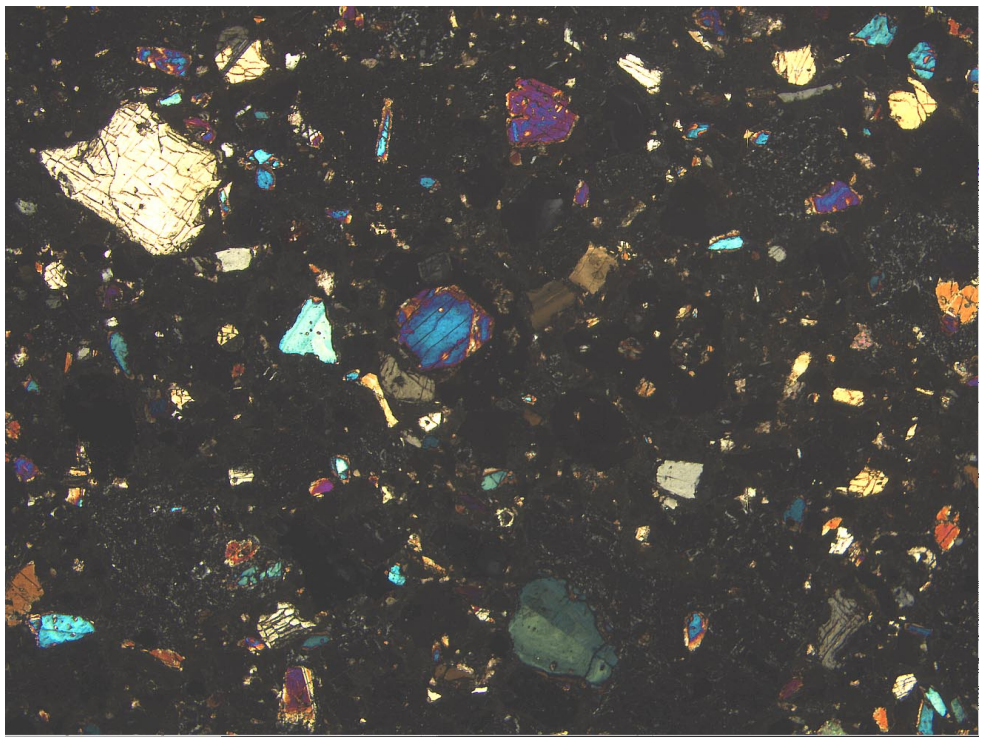

Figure F22. Irregular shell-rich sandstone (light color) and poorly sorted, fine-grained sandstone. These irregular structures may have been formed as a result of dewatering and fluid escape, sediment injection, slumping, or other soft-sediment deformation phenomena (interval 180-1115C-34R-3, 10–45 cm).

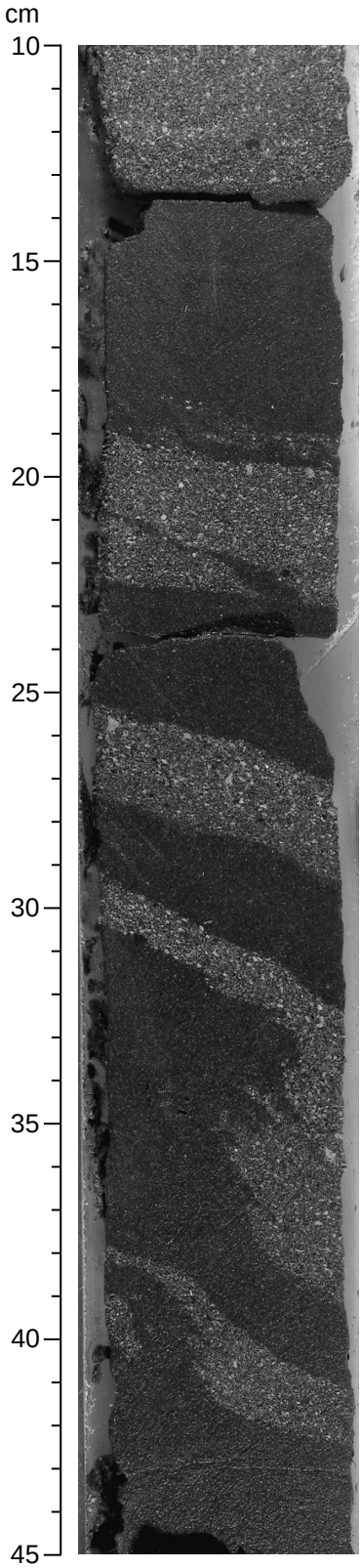

Figure F23. Sharp-based calcium carbonate sandstone/pebbly packstone sharply overlying noncarbonate silty claystone that has thin laminae of siltstone. In other parts of this unit the packstones contain well-rounded pebbles of siltstone and claystone (interval 180-1115C-35R-1, 90–115 cm).

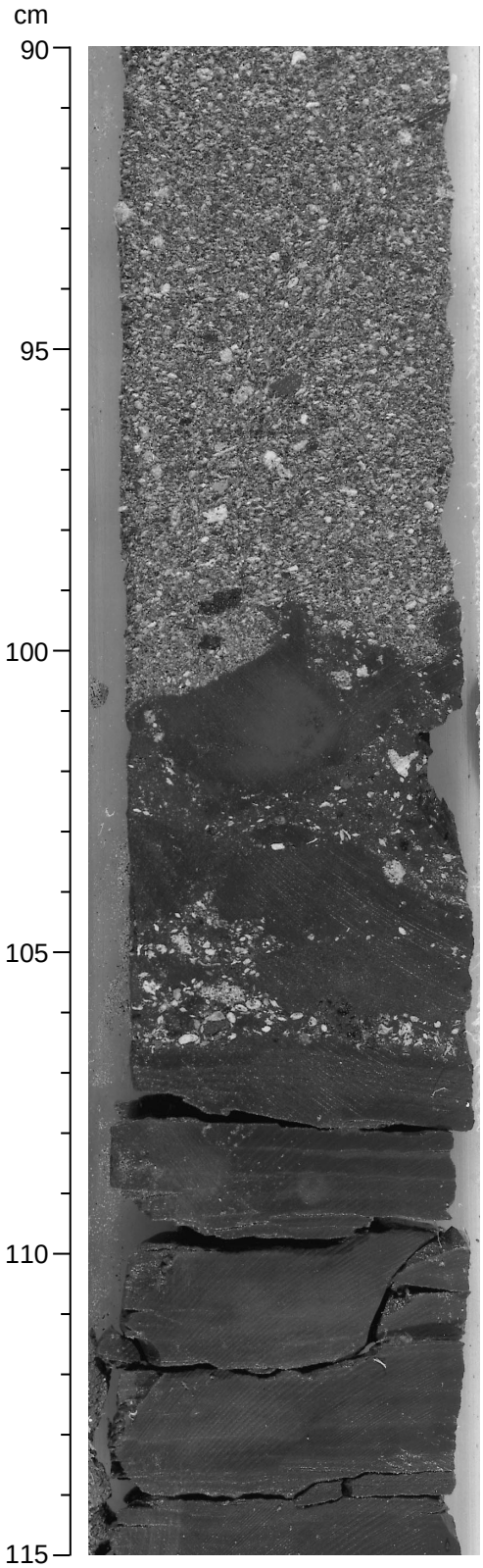

Figure F24. Digital photomicrograph (crossed nicols) of a mixed coarse-grained sandstone with abundant large benthic and rare smaller planktonic foraminifers tests, coral fragments, red algae, and subrounded fragments of basalt and andesite. Rare detrital grains of clinopyroxene and feldspar (interval 180-1115C-35R-1, 85–88 cm).

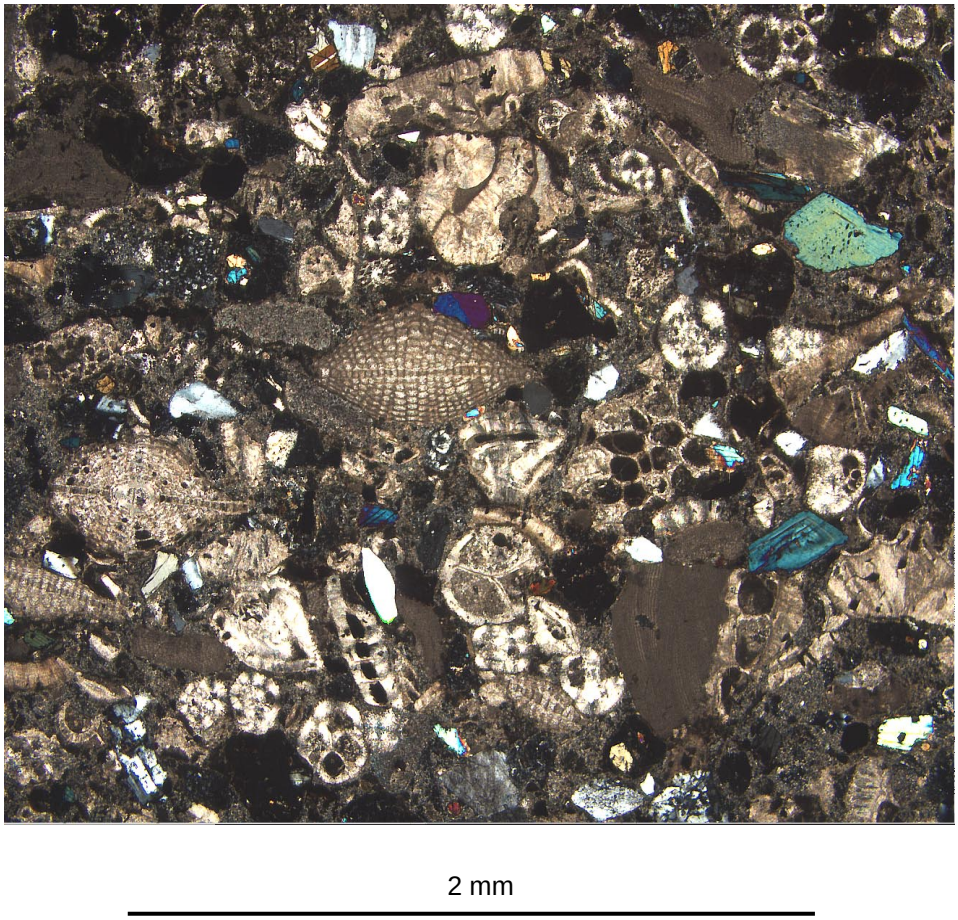

Figure F25. Digital photomicrograph (plane-polarized light) of a silty claystone with very thin silt- and clay-rich laminae. Contains abundant subangular detrital grains of feldspar, clinopyroxene, and rare quartz (interval 180-1115C-36R-1, 25–27 cm).

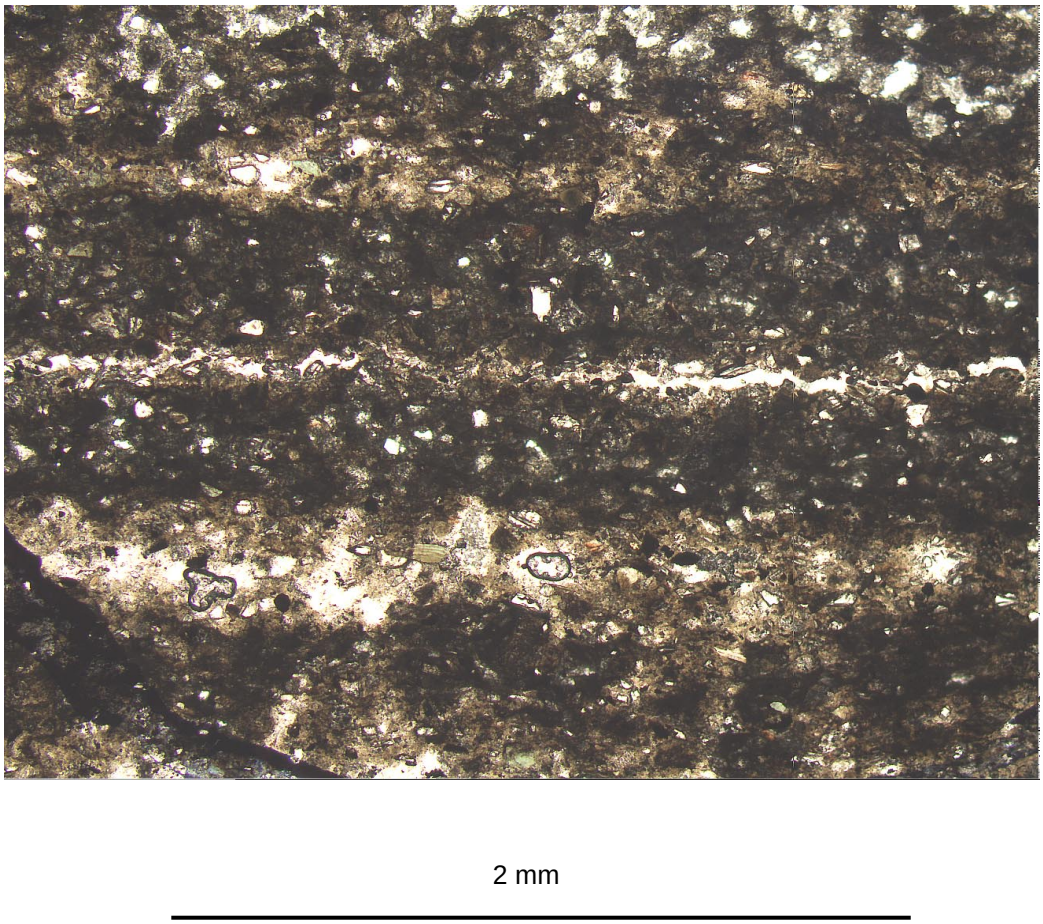

Figure F26. Sandy siltstone with abundant bioturbation and planar lamination (interval 180-1115C-41R-1, 20–42 cm).

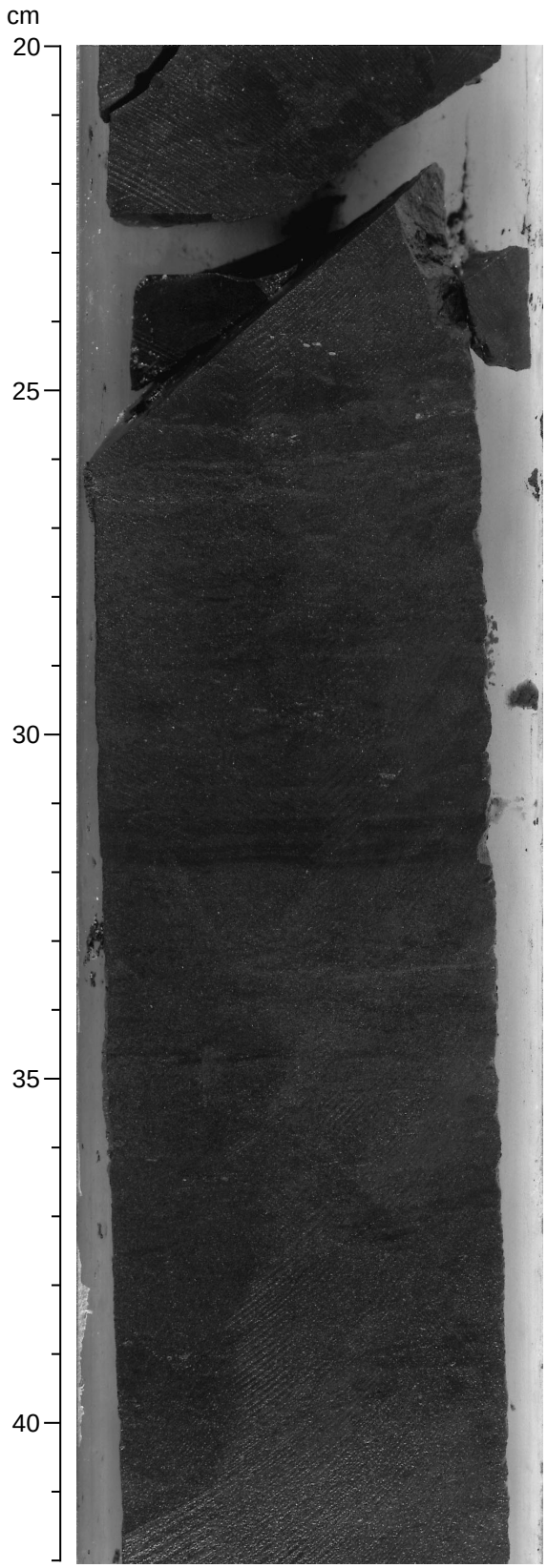

Figure F27. Digital photomicrograph (crossed nicols) of a siltstone with detrital grains of abundant biotite, feldspar, clinopyroxene, rare quartz, planktonic foraminifers, and subrounded basaltic rock fragments (interval 180-1115C-40R-2, 105–107 cm).

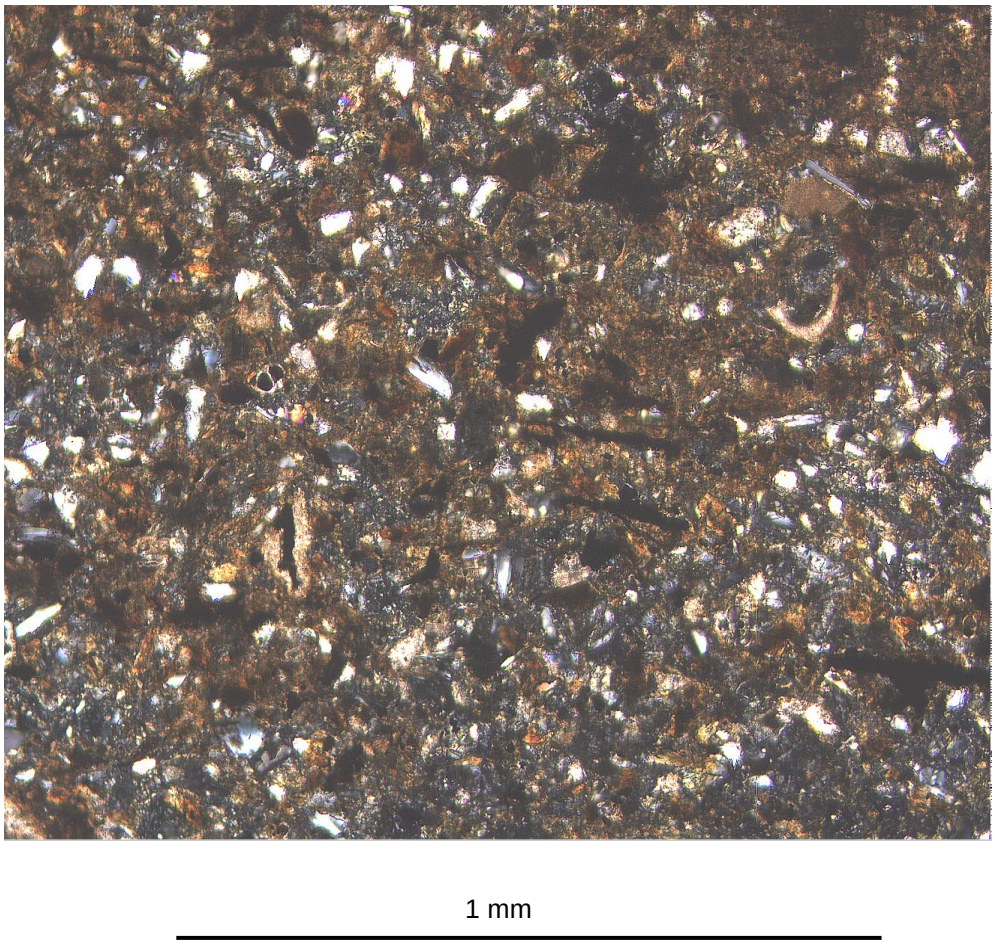

Figure F28. Medium-bedded, very fine grained sandstone with sharp upper and lower contacts and little or no bioturbation. Unit XII (interval 180-1115C-47R-1, 63–97 cm).

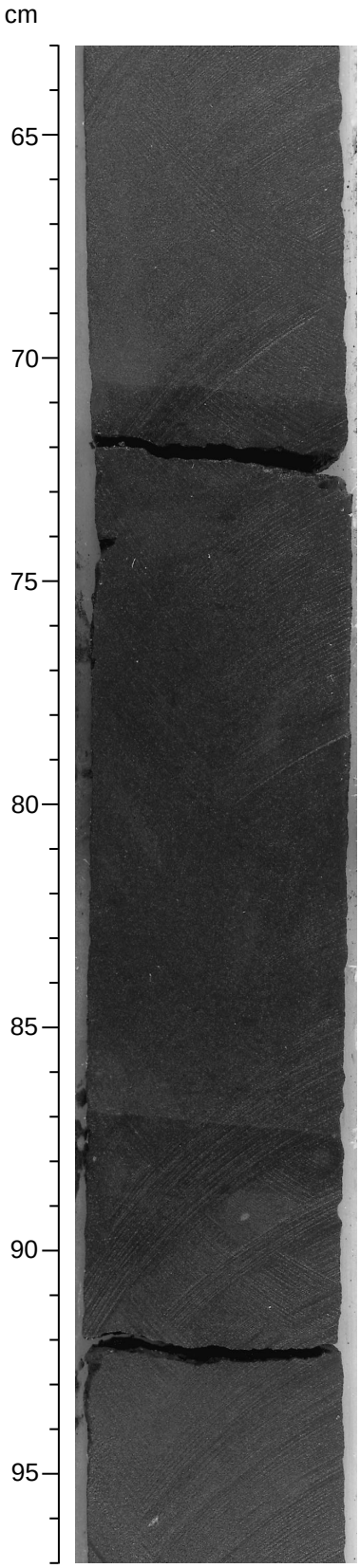

Figure F29. Number of volcanogenic ash layers (black) and total volcanogenic ash thickness per core (cm; shaded) at Site 1115. Note that the variation may not be representative of the actual recovery within intervals of low recovery. For example, the apparent absence of volcanogenic ash layers around 259 mbsf (Core 180-1115B-28X) may be an artifact of relatively poor core recovery (23.1%).

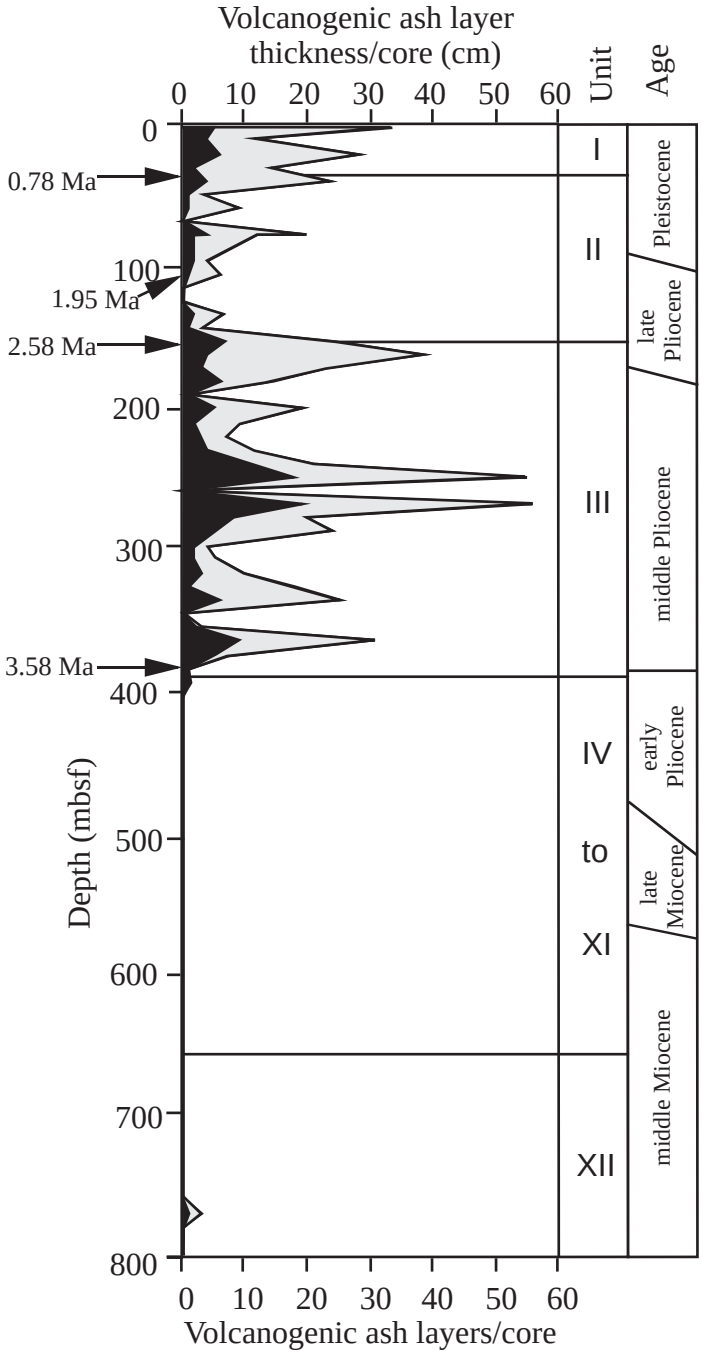

Figure F30. Summary of the main structural features observed at Site 1115. For key to symbols, see Fig. F2, p. 52, in the "Explanatory Notes" chapter. **A.** Hole 1115B. **B.** Hole 1115C.

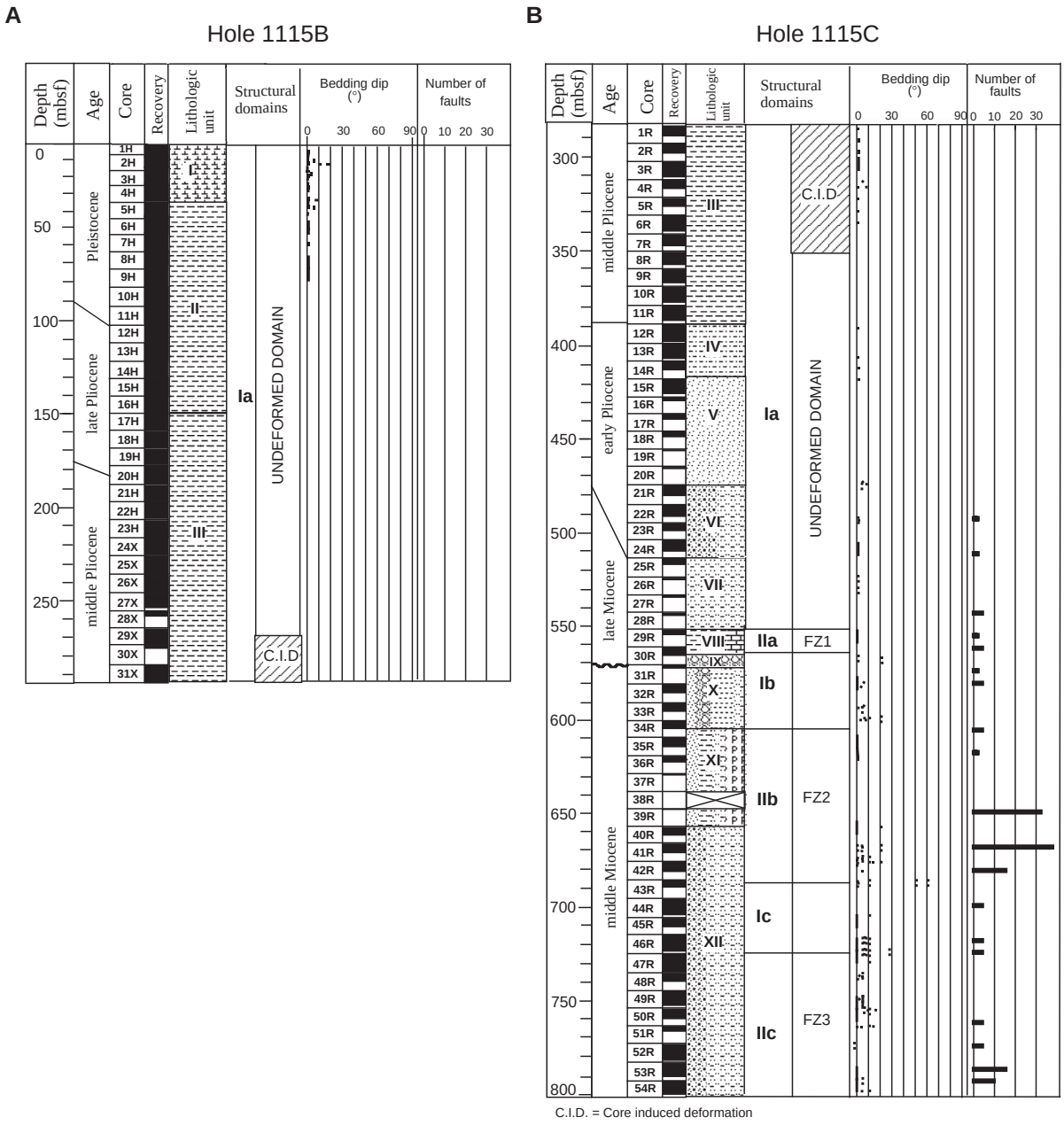

Figure F31. (A) Bedding and (B) fault dips measured in Holes 1115B and 1115C. N = number of measurements.

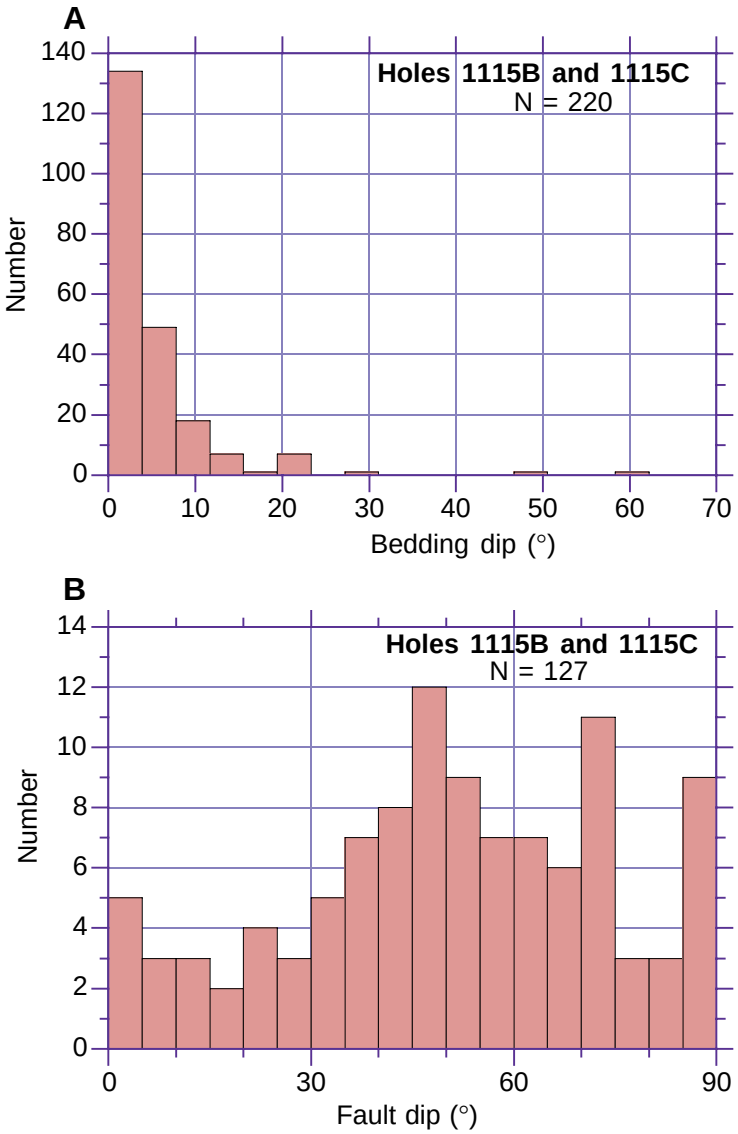

Figure F32. Structural measurements of Fault Zone 2 (FZ2). Histograms of (**A**) bedding dips, (**B**) fault dips, and (C) plot of slickenside plunge vs. fault dip. SS = strike slip; DS = dip slip; N = number of measurements.

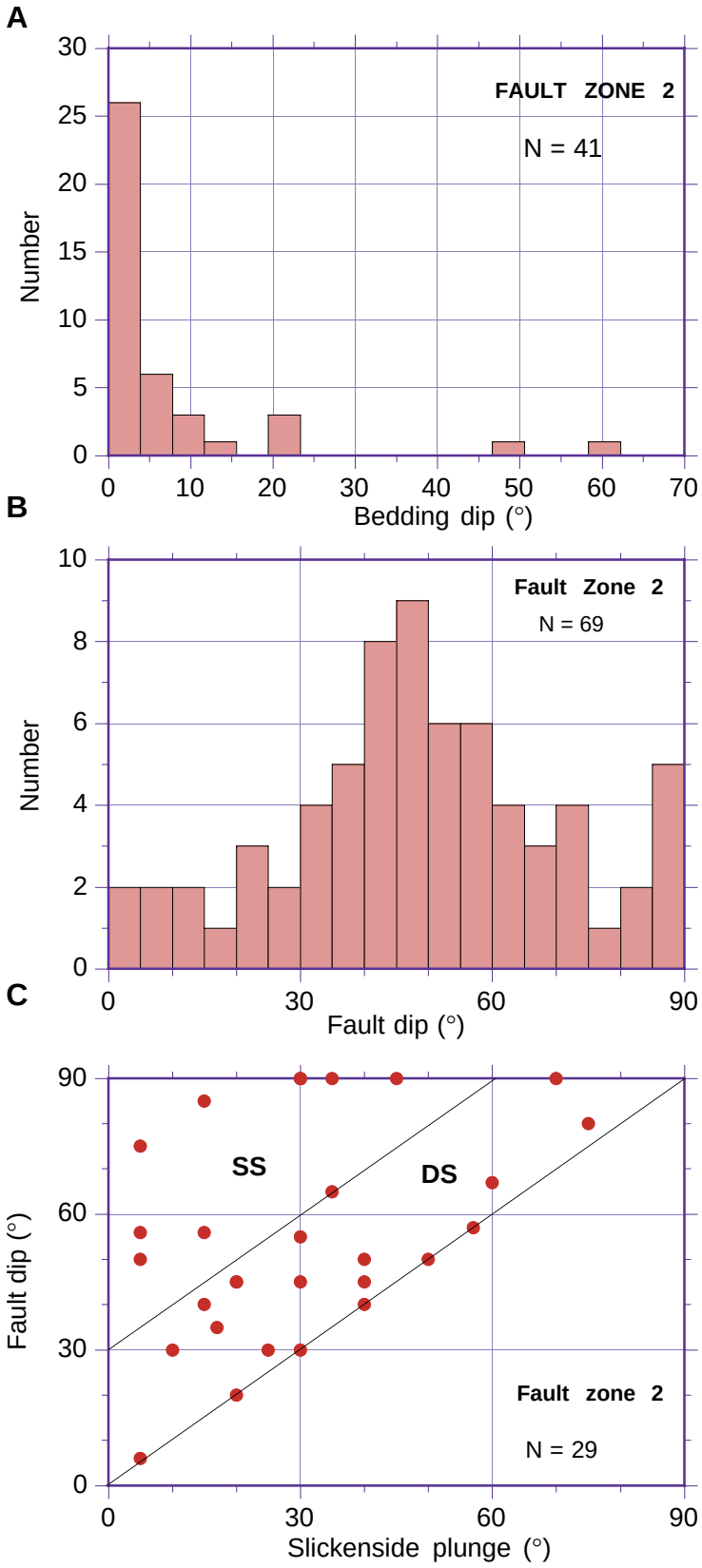

Figure F33. Bedding dips measured in Fault Zone 3 (FZ3). N = number of measurements.

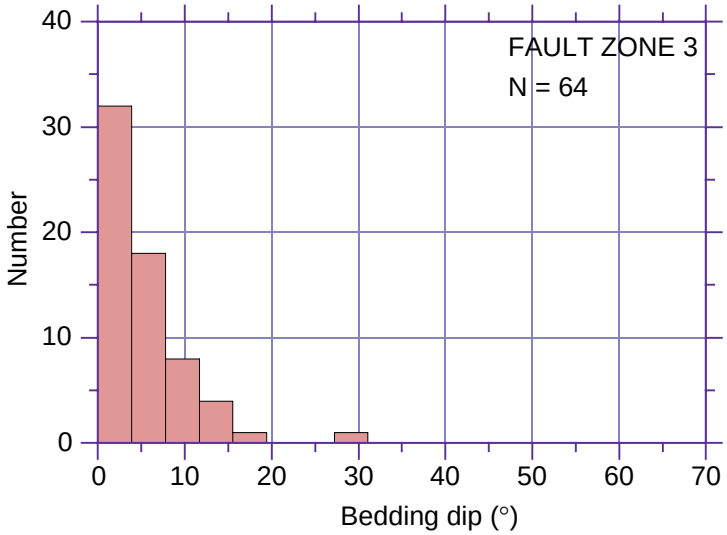

Figure F34. A. Total bedding dip measurements in the synrift series. **B.** The forearc sequence. N = number of measurements.

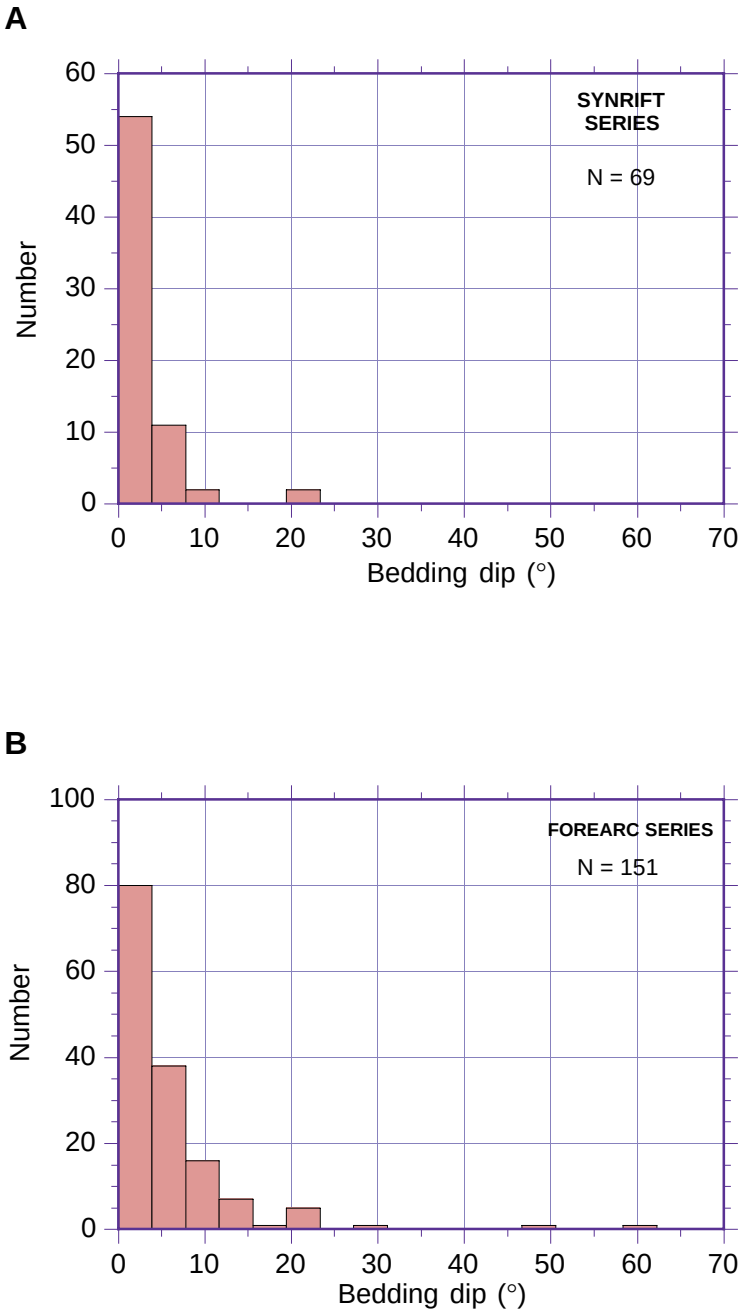

Figure F35. Biostratigraphic units and ages. **A.** Holes 1115A and 1115B. Dashed lines indicate that the true zonal boundary may lie above or below the indicated level. (Continued on next page.)

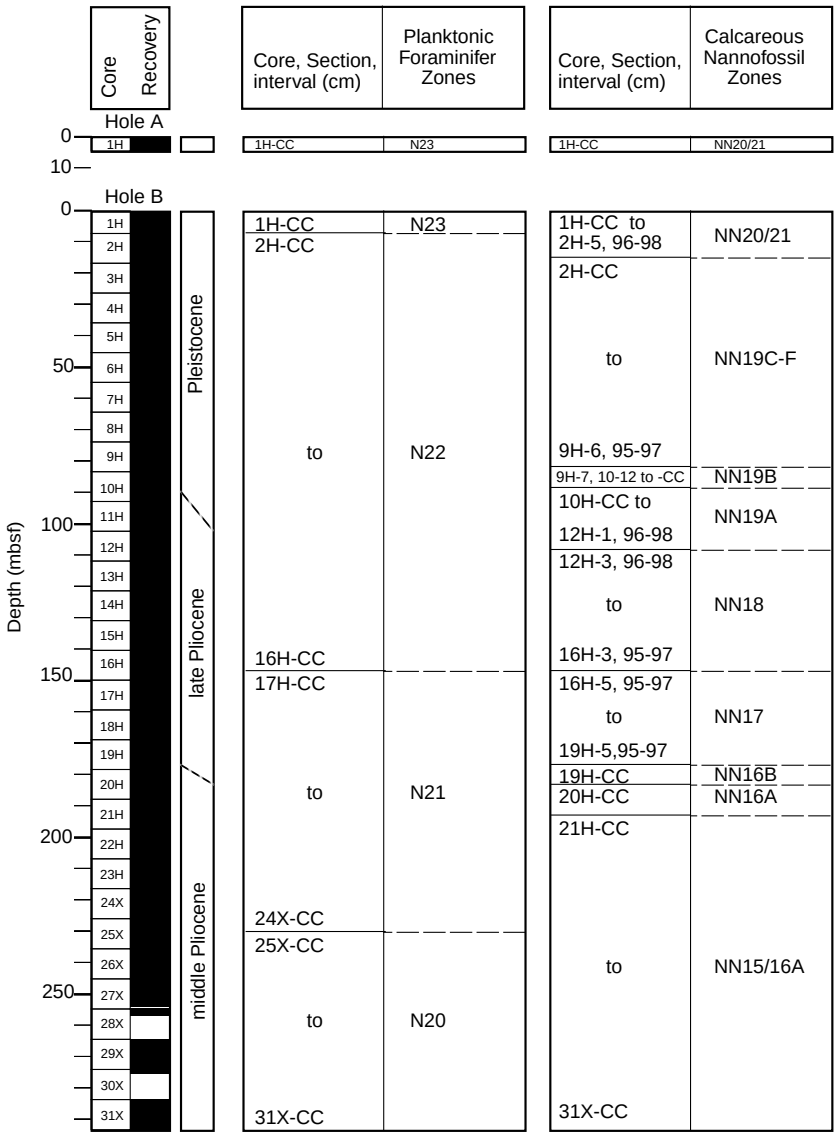

Figure F35 (continued). B. Hole 1115C.

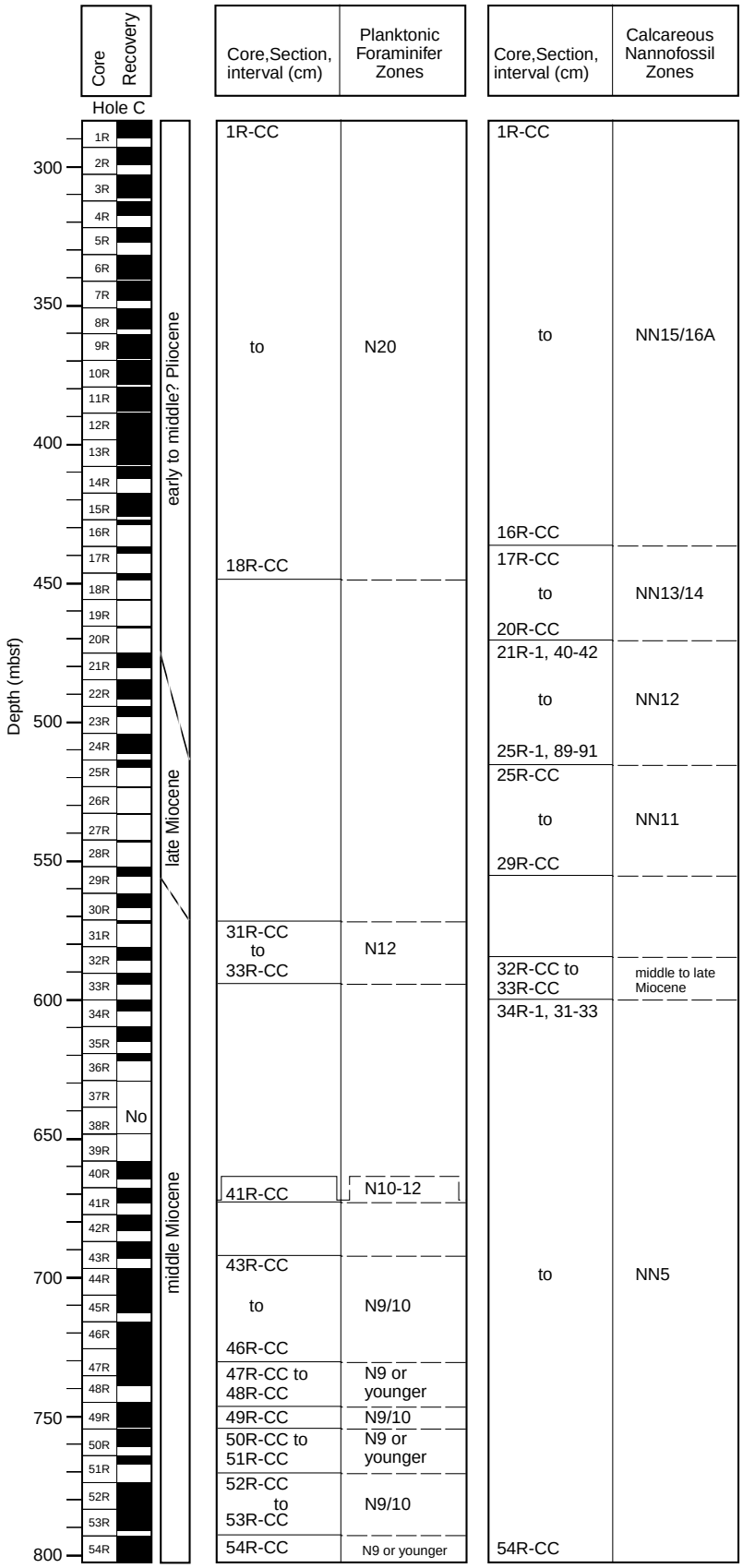

Figure F36. A. Equatorial section of *Lepidocyclina* (*Nephrolepidina*) *martini,* lenticular form, from middle Miocene (Sample 180-1115C-34R-CC). **B.** Equatorial section of *Lepidocyclina* (*Nephrolepidina*) *martini,* stellate form, from middle Miocene (Sample 180-1115C-34R-CC).

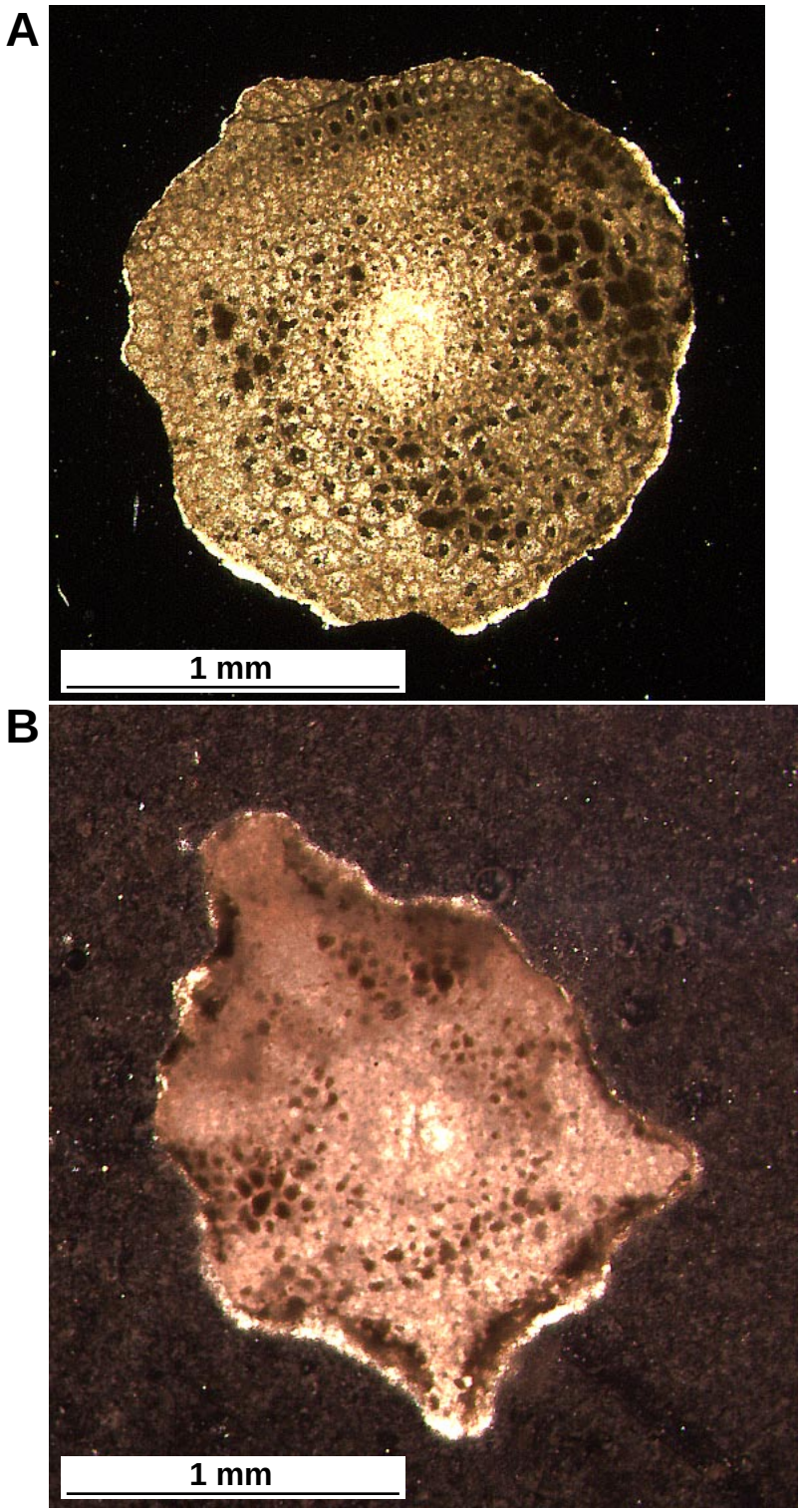

Figure F37. Age-depth relationship at Site 1115 based on nannofossil (square) and planktonic foraminiferal (circle) datum events and magnetic chron and subchron boundaries (triangle), and paleobathymetry (right column), based on benthic foraminifers. Sediment accumulation rates are estimated in m/m.y. The numbers plotted near symbols correspond to numbers in the left column of the datum table.

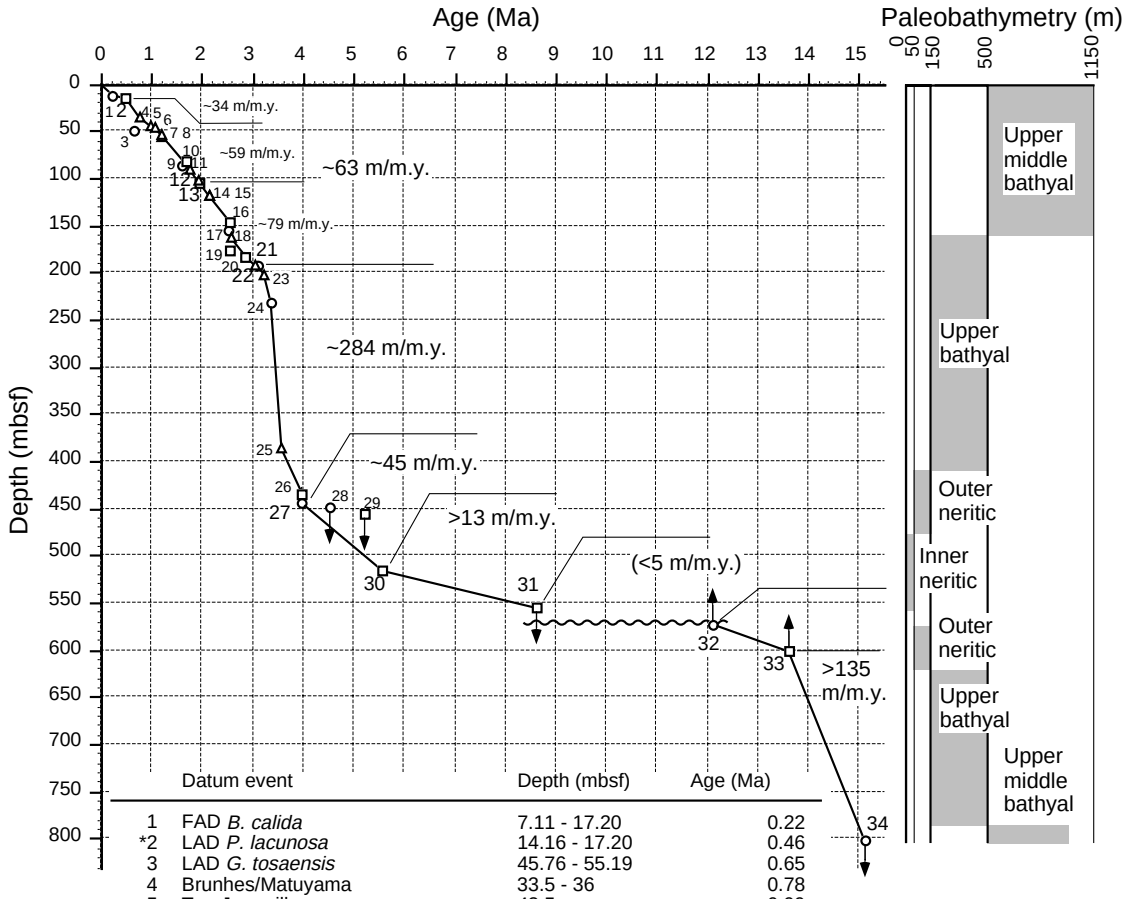

	Datum event	Depth (mbsf)	Age (Ma)
1	FAD *B. calida*	7.11 - 17.20	0.22
*2	LAD *P. lacunosa*	14.16 - 17.20	0.46
3	LAD *G. tosaensis*	45.76 - 55.19	0.65
4	Brunhes/Matuyama	33.5 - 36	0.78
5	Top Jaramillo	43.5	0.99
6	Bottom Jaramillo	47	1.07
7	Top Cobb	53	1.201
8	Bottom Cobb	54.5	1.211
9	LAD *G. fistulosus*	86.65 - 88.35	1.6
10	LAD *C. macintyrei*	82.15 - 82.80	1.67
11	Top Olduvai	90.5	1.77
*12	Bottom Olduvai	102.5 - 103.5	1.95
*13	LAD *D. brouweri*	103.16 - 106.16	1.95
14	Top Reunion	118	2.14
15	Bottom Reunion	119.5	2.15
16	LAD *D. pentaradiatus*	144.13 - 147.15	2.52
17	FAD *G. truncatulinoides*	150.19 - 159.67	2.58
18	Matuyama/Gauss	162	2.581
19	LAD *D. surculus*	175.65 - 178.63	2.55
20	LAD *D. tamalis*	178.63 - 188.15	2.83
*21	LAD *D. altispira*	188.15 - 197.39	3.09
*22	Top Kaena	192.50	3.04
23	Bottom Kaena	202	3.11
24	FAD *G. tosaensis*	226.01 - 235.28	3.35
25	Gauss/Gilbert	386.00 - 387.00	3.58
26	LCO *R. pseudoumbilicus*	428.65 - 439.01	3.94
*27	S/D *Pulleniatina*	439.01 - 448.72	3.95
28	FAD *G. crassaformis*	448.72<	4.5
29	FAD *C. rugosus*	456.04<	5.23
*30	LAD *D. quinqueramus*	514.29 - 516.37	5.54
*31	FAD *D. quinqueramus*	555.29<	8.6
*32	LAD *G. praemenardii*	<572.27	>12.1
*33	LAD *S. heteromorphus*	<600.11	13.6
*34	FAD *O. suturalis*	802.14<	15.1

* Datum used in sedimentation rate calculation

Figure F38. Susceptibility data (uncorrected for volume) from MST and AMST measurements. **A.** Hole 1115A. (Continued on next page.)

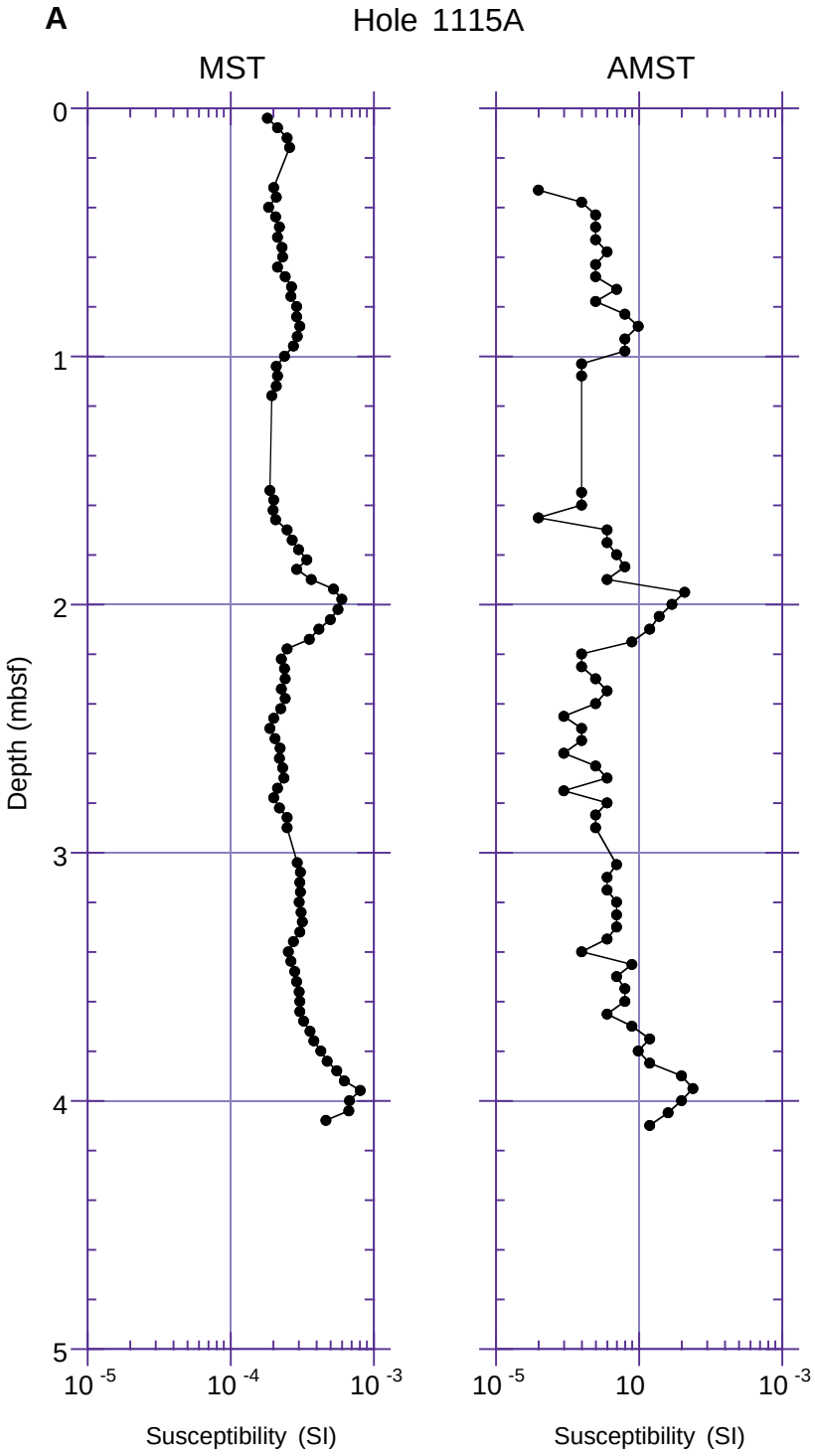

Figure F38 (continued). B. Holes 1115B and 1115C.

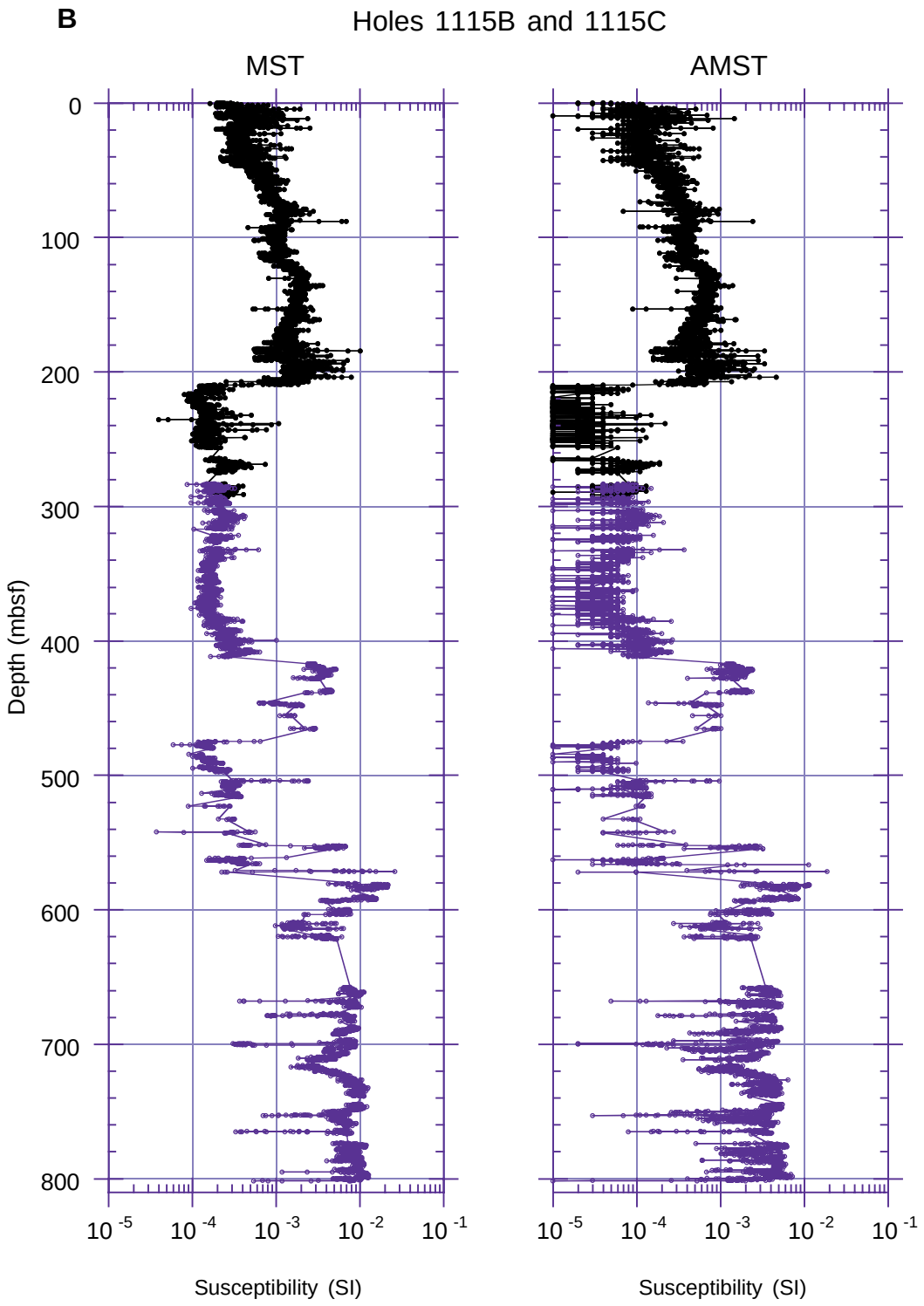

Figure F39. Comparison of MST susceptibilities and remanent intensities after AF demagnetization at 20 mT for Holes 1115B and 1115C. Shaded intervals show where low susceptibility and intensity values dominate.

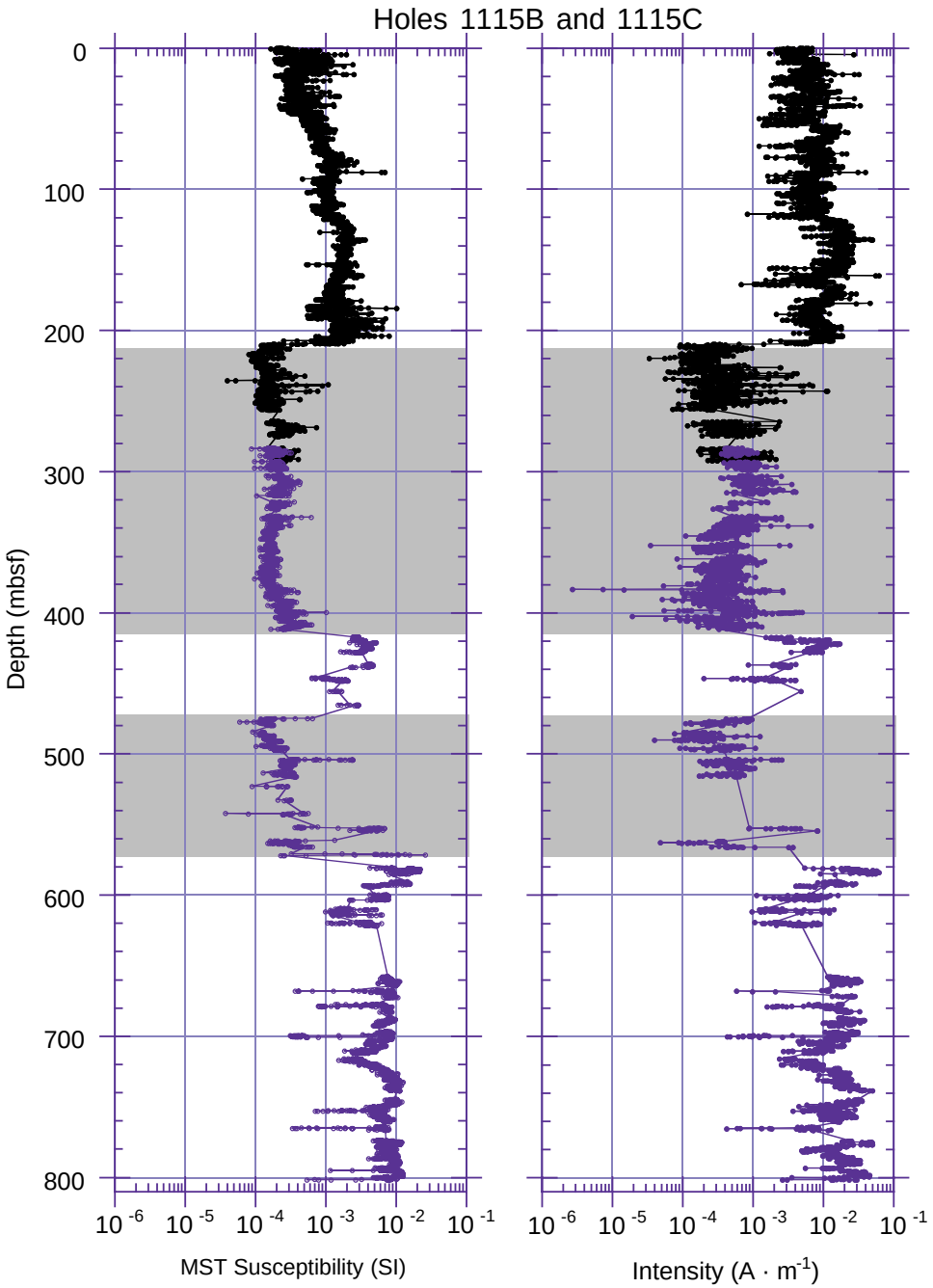

Figure F40. Magnetic susceptibility and its anisotropy (AMS) data for discrete samples from Holes 1115B and 1115C. Degree of anisotropy (P_j) and the shape parameter (T) calculated according to Jelinek (1981). Lighter shading: interval in which variation in T values may be related to grain-size variations of lithostratigraphic Units V through X. Darker shading: interval in which oblate magnetic fabrics coincide with lithostratigraphic Unit XII. For descriptions of lithostratigraphic units, see **"Lithostratigraphy,"** p. 5.

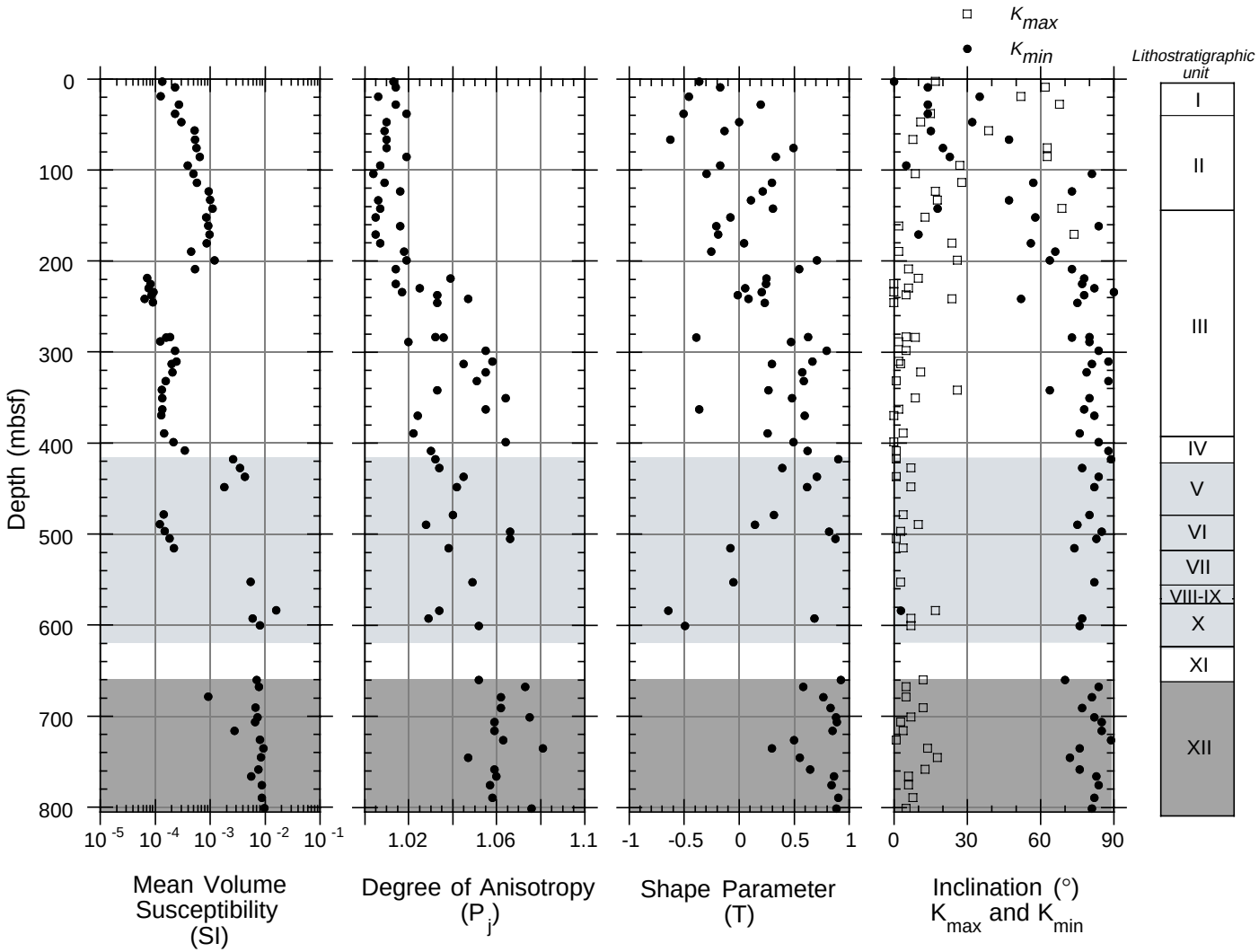

Figure F41. Demagnetization behavior of discrete samples from working halves of core sections. Vector plots: horizontal component = solid circles, vertical component = open circles. Stereonet plots: lower hemisphere = solid circles, upper hemisphere = open circles. NRM = natural remanent magnetization; Div. = Division; Jo = NRM intensity. **A.** Sample 180-1115B-4H-2, 40–42 cm (28.10–28.12 mbsf). **B.** Sample 180-1115B-9H-2, 70–72 cm (75.90–75.92 mbsf). **C.** Sample 180-1115B-11H-2, 90–92 cm (95.10–95.12 mbsf). **D.** Sample 180-1115B-26X-5, 26–28 cm (241.66–241.68 mbsf). (Continued on next page.)

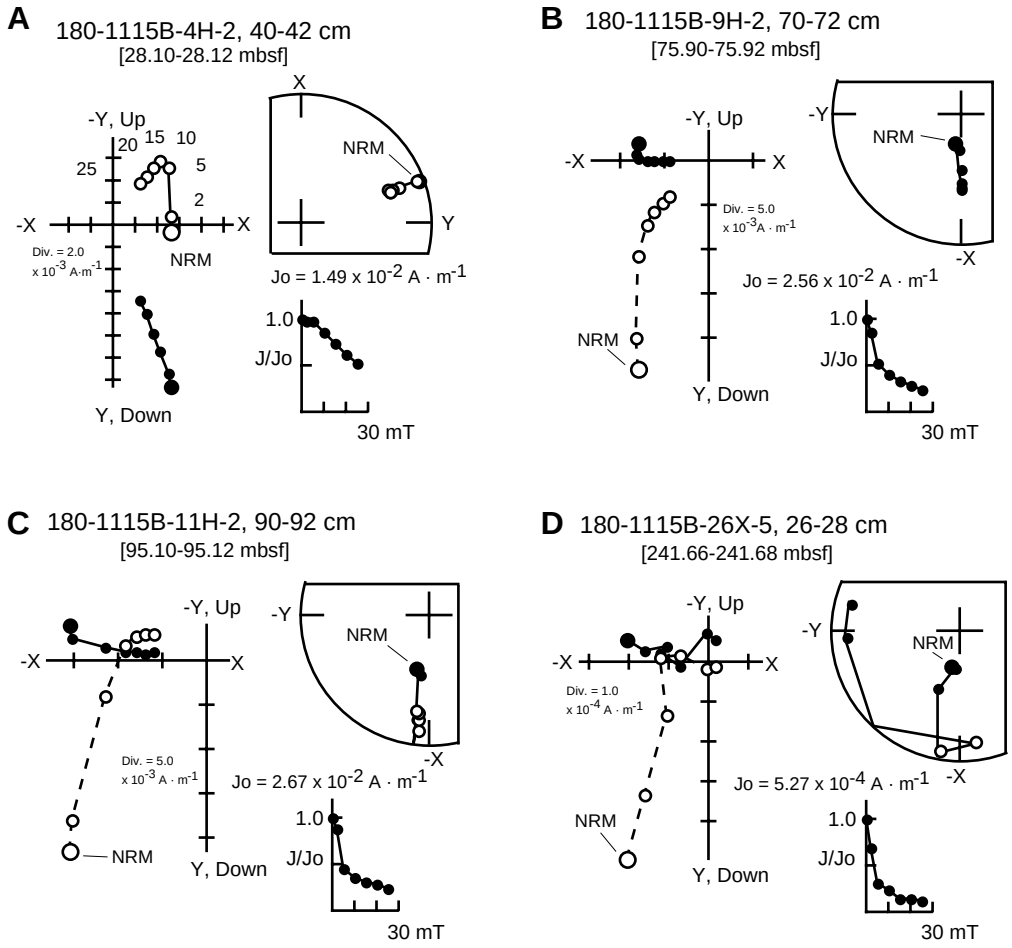

Figure F41 (continued). **E.** Sample 180-1115B-31X-1, 50–52 cm (284.00–284.02 mbsf). **F.** Sample 180-1115C-16R-1, 52–54 cm (427.42–427.44 mbsf). **G.** Sample 180-1115C-32R-3, 78–80 cm (583.79–583.81 mbsf). **H.** Sample 180-1115C-42R-2, 98–100 cm (678.87–678.89 mbsf).

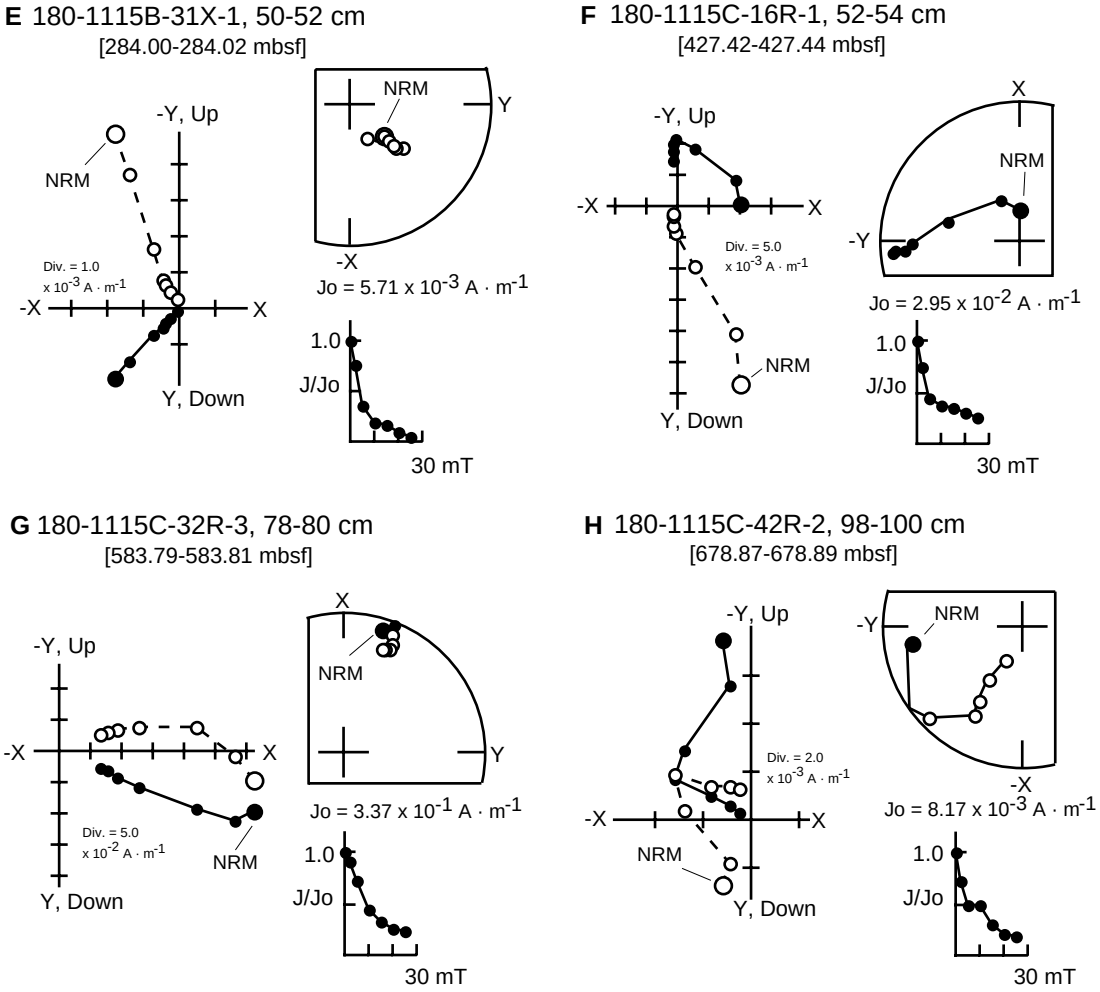

Figure F42. Downhole plots of intensity, declination, and inclination. **A.** Hole 1115A. (Continued on next page.)

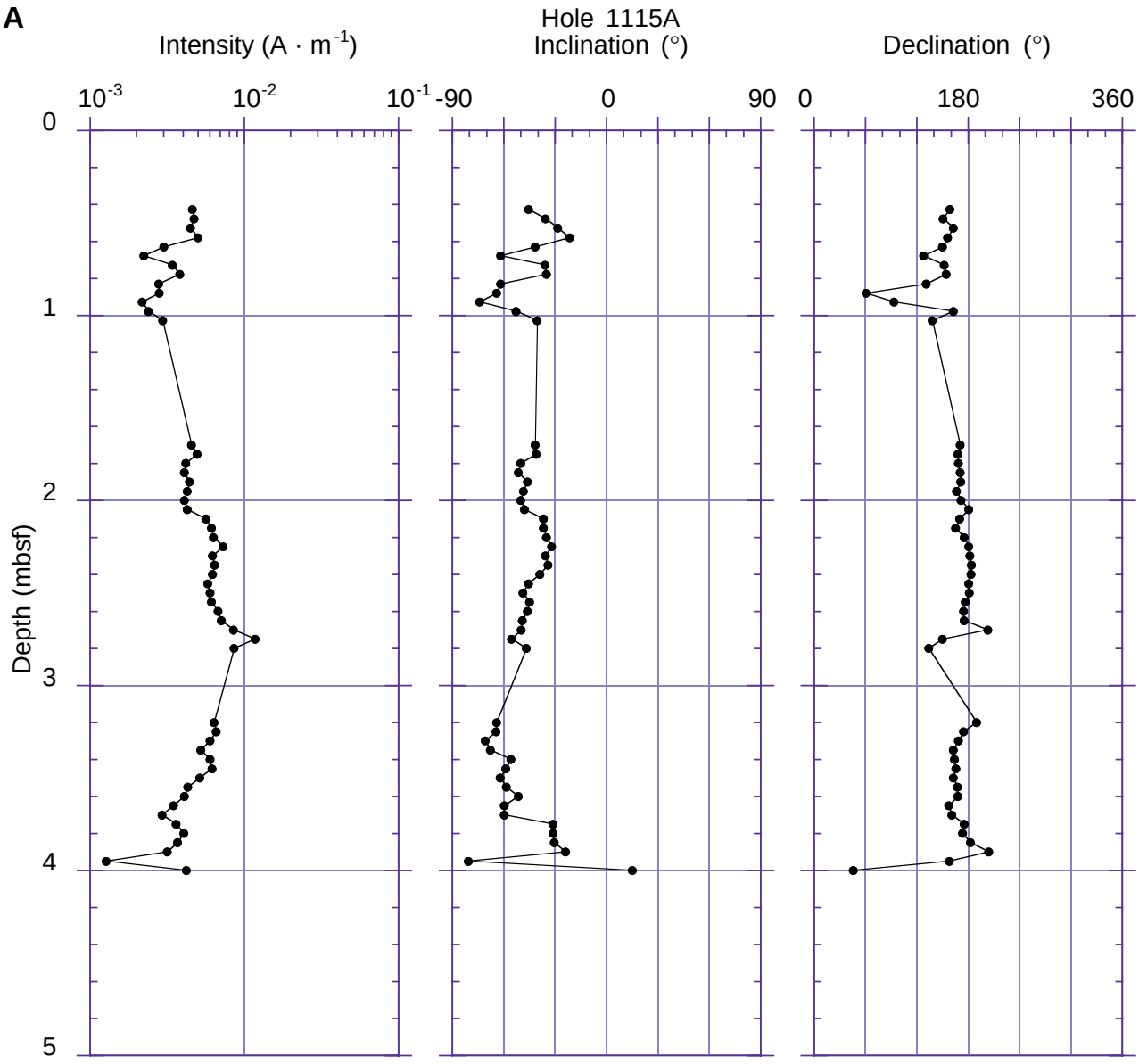

Figure F42 (continued). B. Holes 1115B and 1115C. Data from long cores after AF demagnetization at 20 mT shown as solid circles (Hole 1115A) or black dots (Holes 1115B and 1115C); data from discrete samples after AF demagnetization at 25 mT shown as open squares.

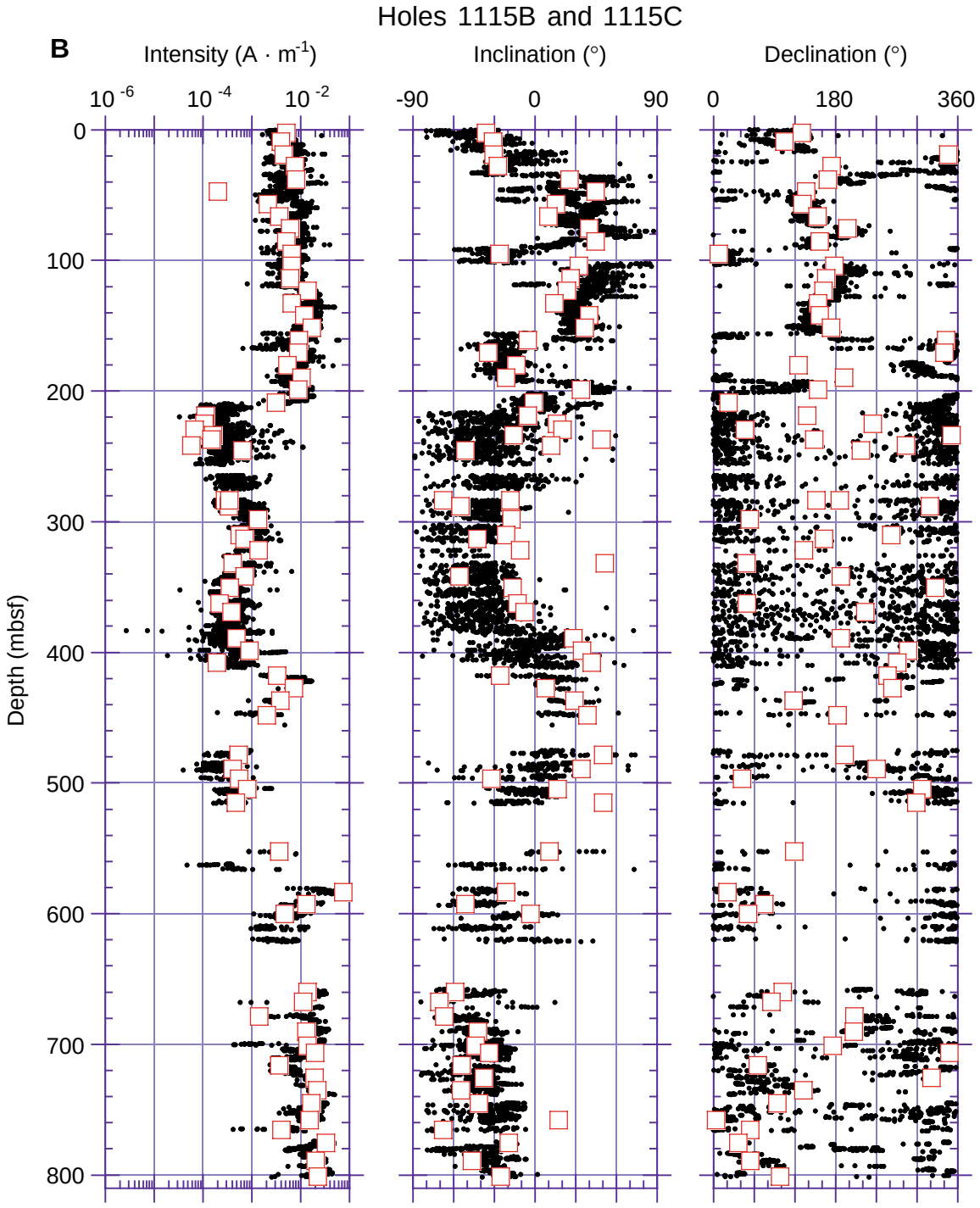

Figure F43. Magnetostratigraphic interpretations. **A.** Upper 300 m of Hole 1115B. (Continued on next page.)

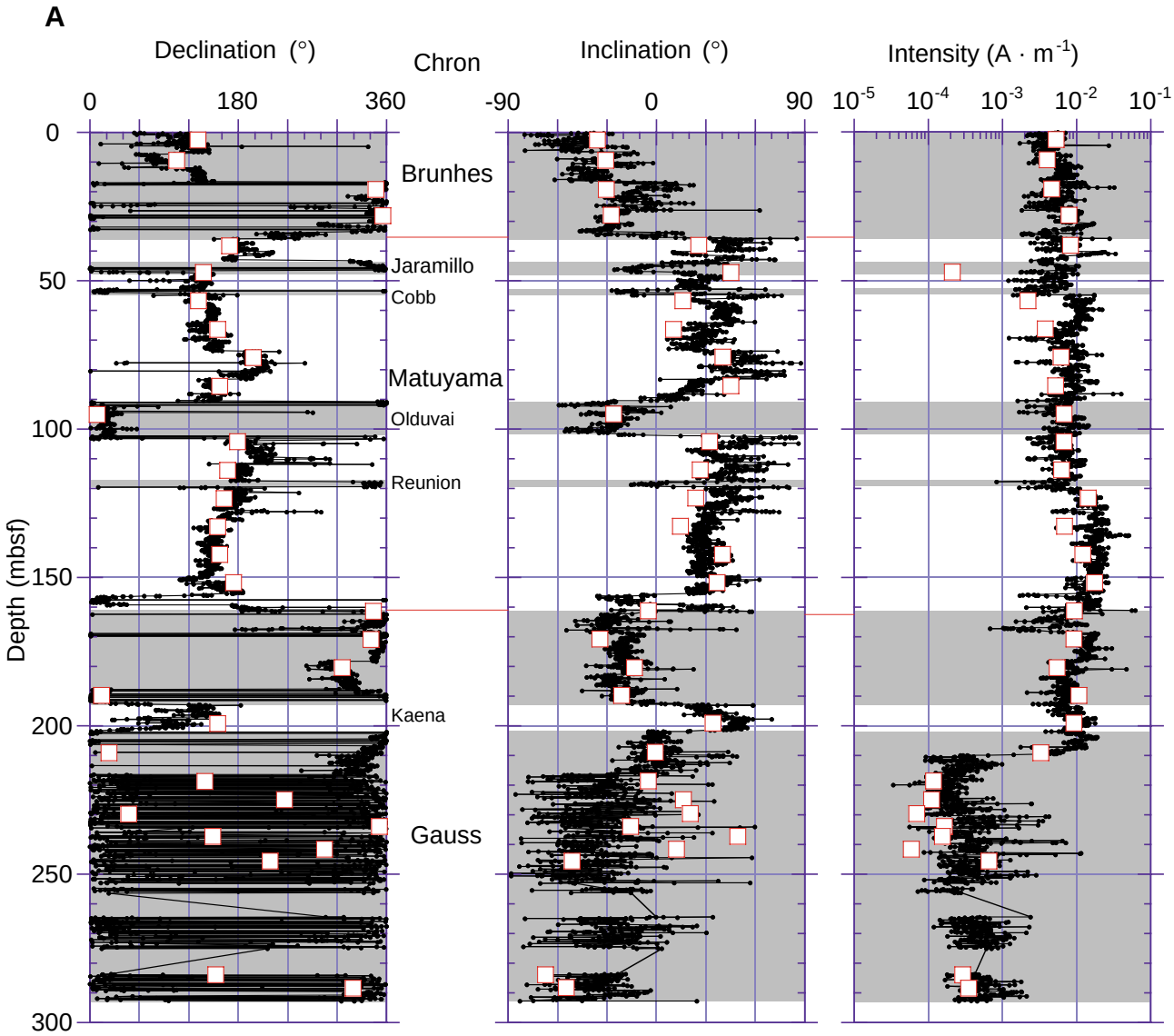

Figure F43 (continued). B. Holes 1115B and 1115C. Polarity: normal = black or gray shading; reversed = white; undetermined = diagonal lines. Chrons: C1n = Brunhes (0.0–0.78 Ma); C1r = upper part of the Matuyama (0.78–1.77 Ma); Jaramillo (0.99–1.07 Ma); Cobb (1.20–1.21 Ma); C2n = Olduvai (1.77–1.95 Ma); Reunion (2.14–2.15 Ma); C2r = lower part of the Matuyama (1.95–2.58 Ma); C2An.1n = upper part of the Gauss (2.58–3.04 Ma); C2An.1r = Kaena (3.04–3.11 Ma); C2An = lower part of the Gauss (3.11–3.58 Ma); C2An.2r = Mammoth (3.22–3.33 Ma); C2Ar = upper part of the Gilbert (3.58–4.18 Ma).

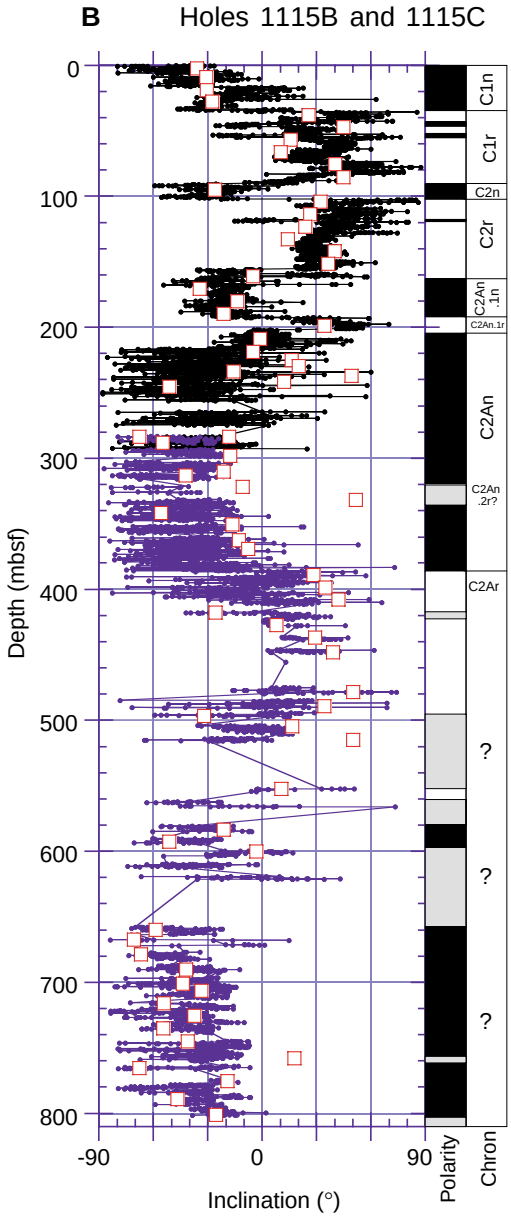

Figure F44. Interstitial water constituents at Site 1115. Seawater values indicated by arrows at the top of profiles are taken from Millero and Sohn (1992). **A.** pH, alkalinity, SO_4^{2-}, and NH_4^+. (Continued on next two pages.)

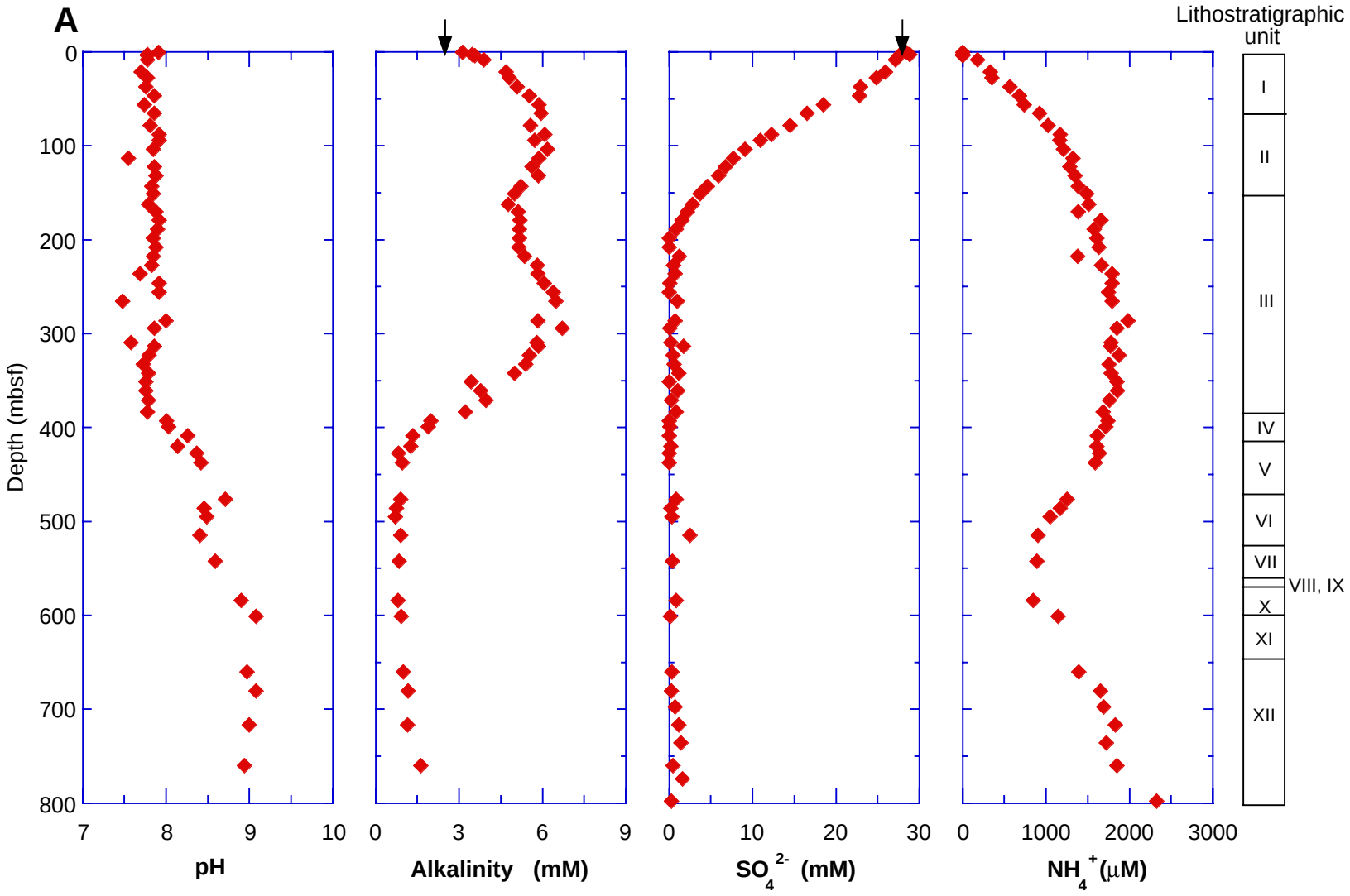

Figure F44 (continued). B. Na^+, Cl^-, K^+, and Li^+. I.C. = chloride by ion chromatography.

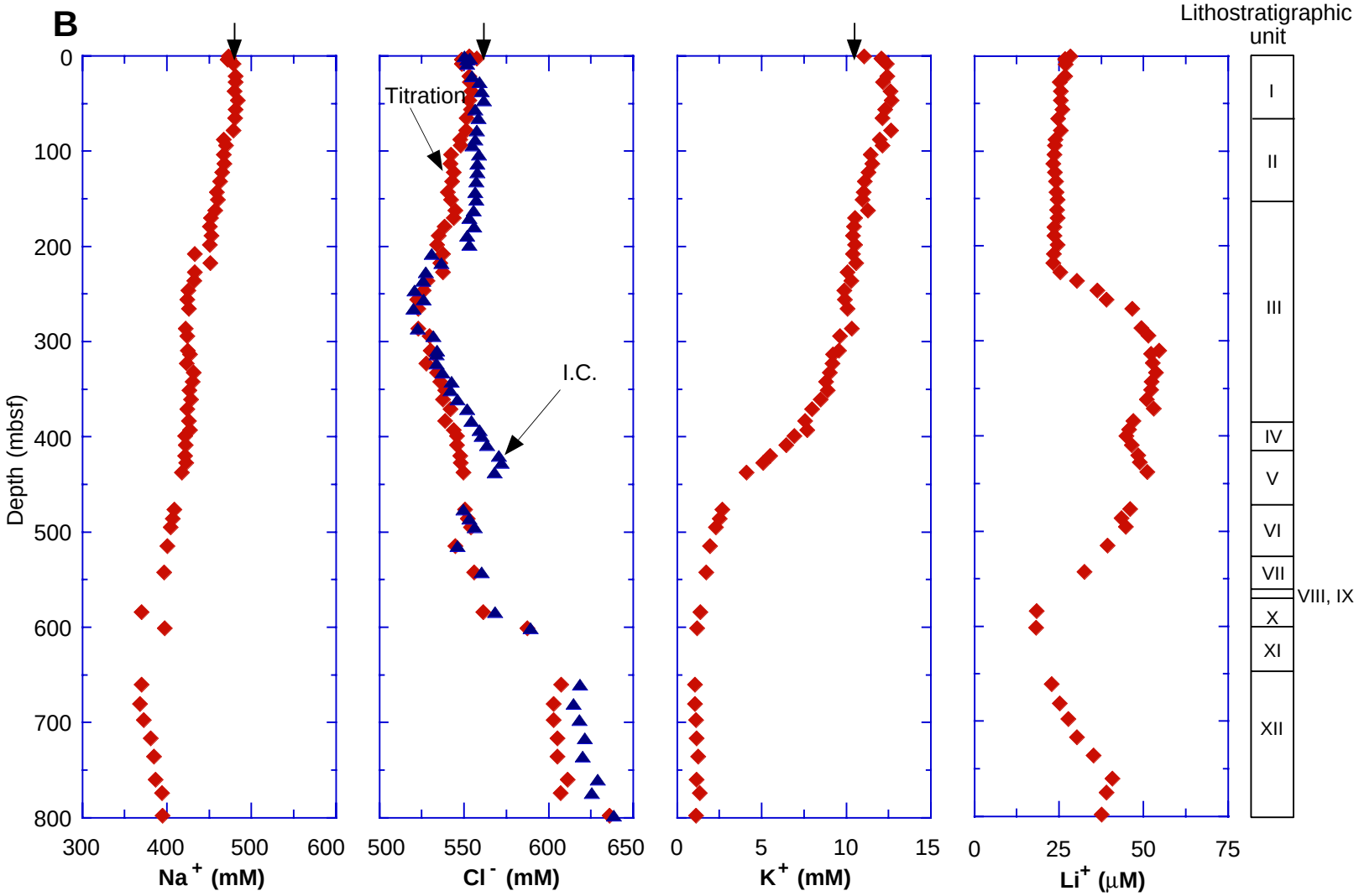

Figure F44 (continued). C. Ca^{2+}, Mg^{2+}, Sr^{2+}, and Ca/Mg.

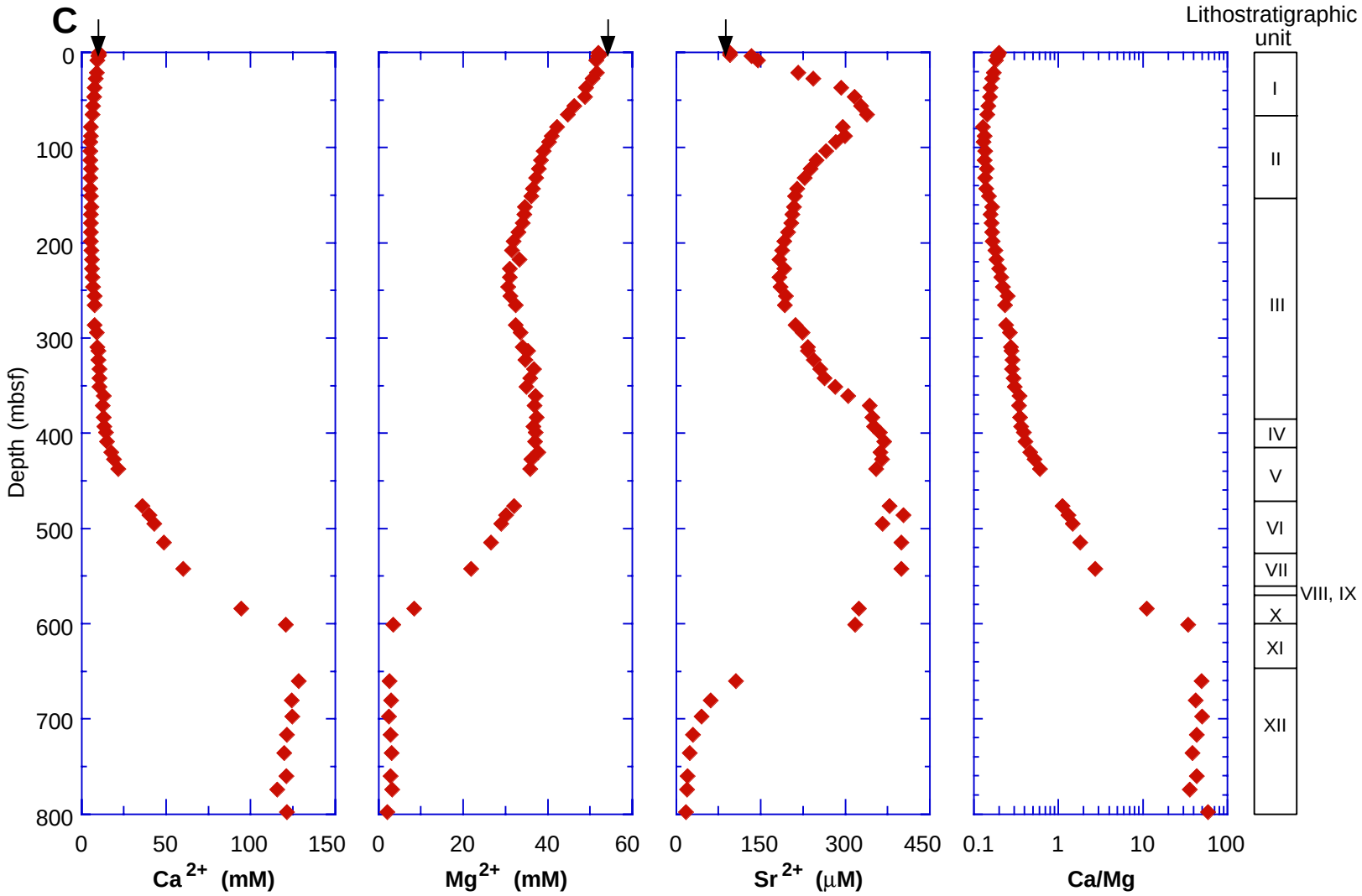

Figure F45. Dissolved SiO_2 in sediments of Site 1115 superposed on sediment porosity. An antithetic correlation exists between these parameters in the upper 100 mbsf because of early diagenesis of easily solubilized solid phases containing silica. Below 220 mbsf, porosity and dissolved SiO_2 covary.

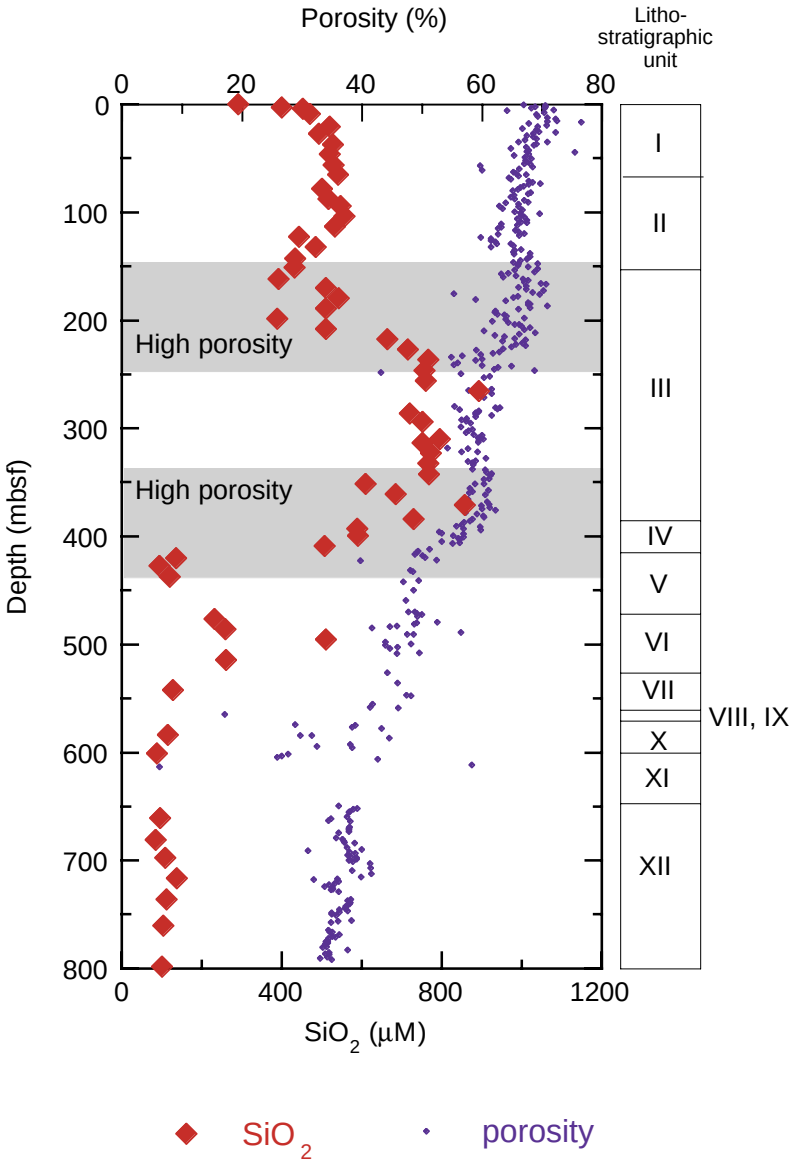

Figure F46. C_1, C_2, and C_1/C_2 hydrocarbon profiles, Site 1115.

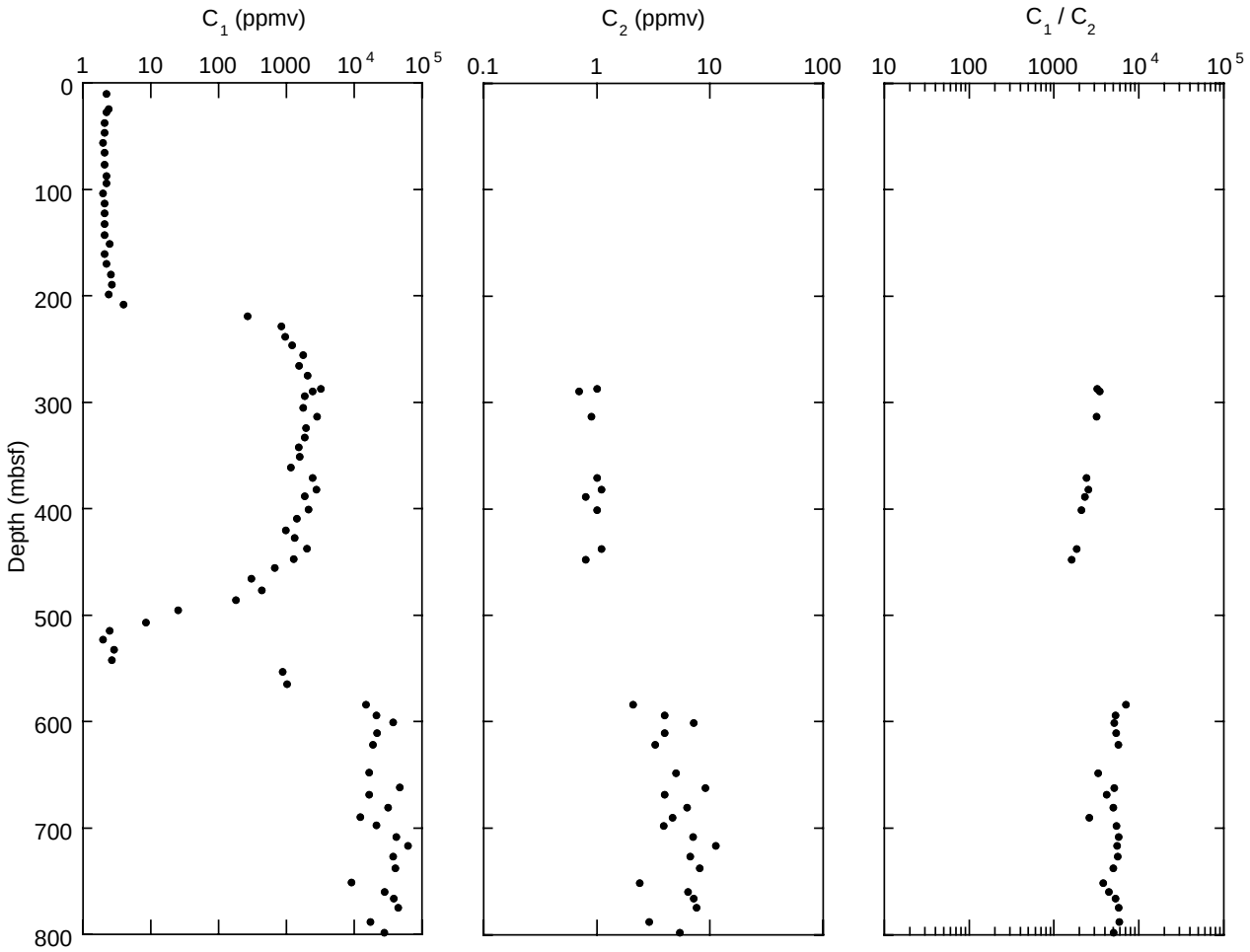

Figure F47. Organic carbon, total sulfur, C/N ratio, and $CaCO_3$ profiles, Site 1115.

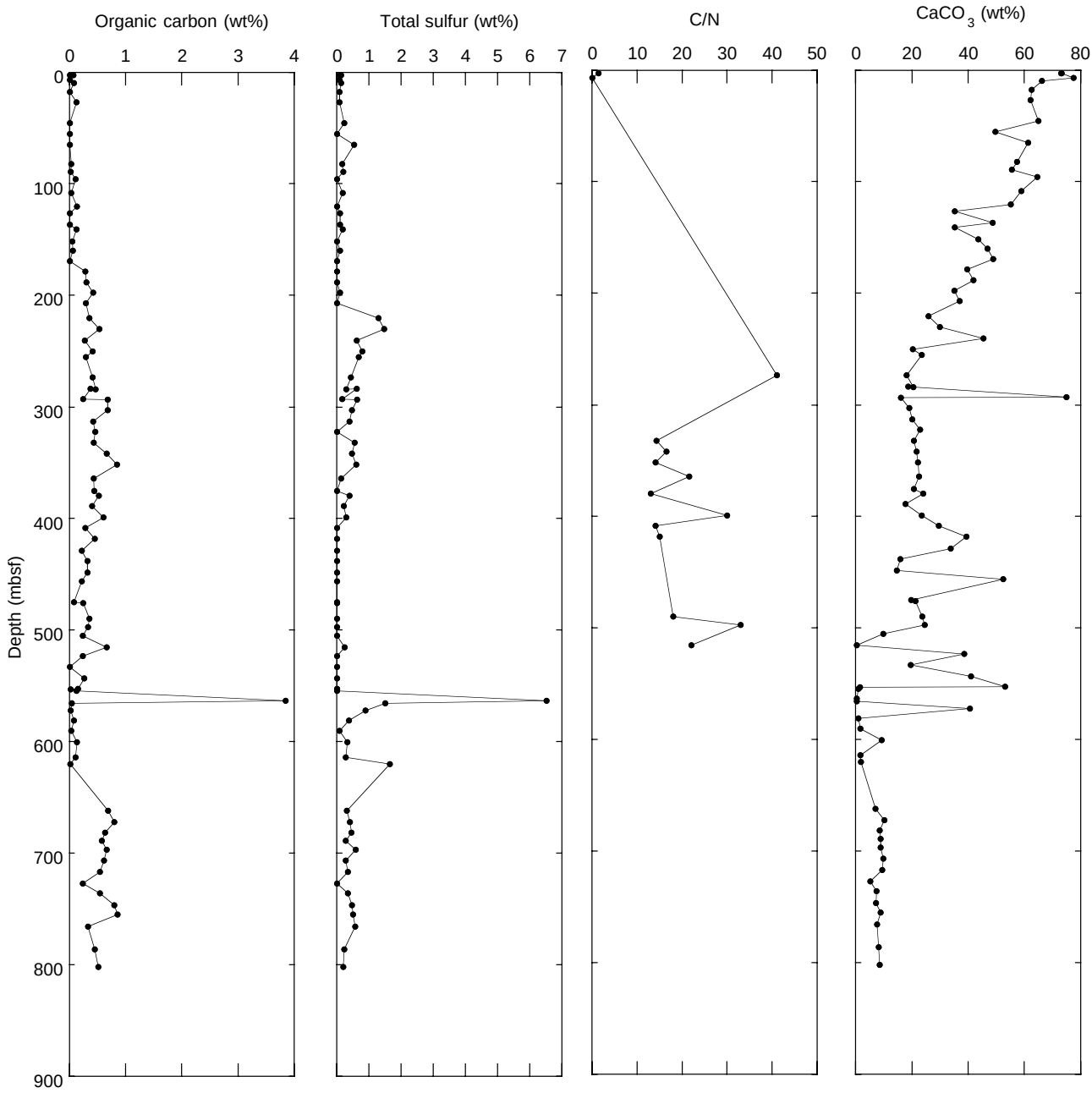

Figure F48. Depth distributions of total bacterial populations (solid circles) and dividing and divided cells (open circles) in sediment samples from Site 1115. The solid curve represents a general regression line of bacterial numbers vs. depth in deep-sea sediments (Parkes et al., 1994), with 95% upper and lower prediction limits shown by dashed curves.

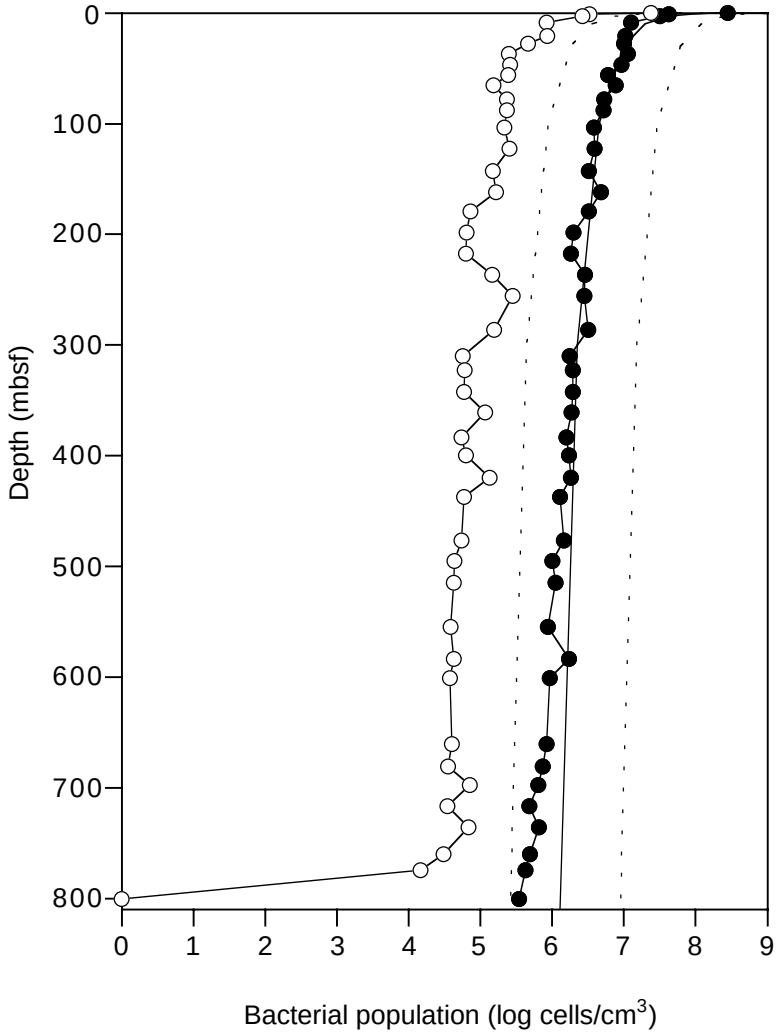

Figure F49. Site 1115 bulk density derived from GRAPE (open circles) and index properties (solid circles) measurements. The depth-range of the various coring techniques is superposed.

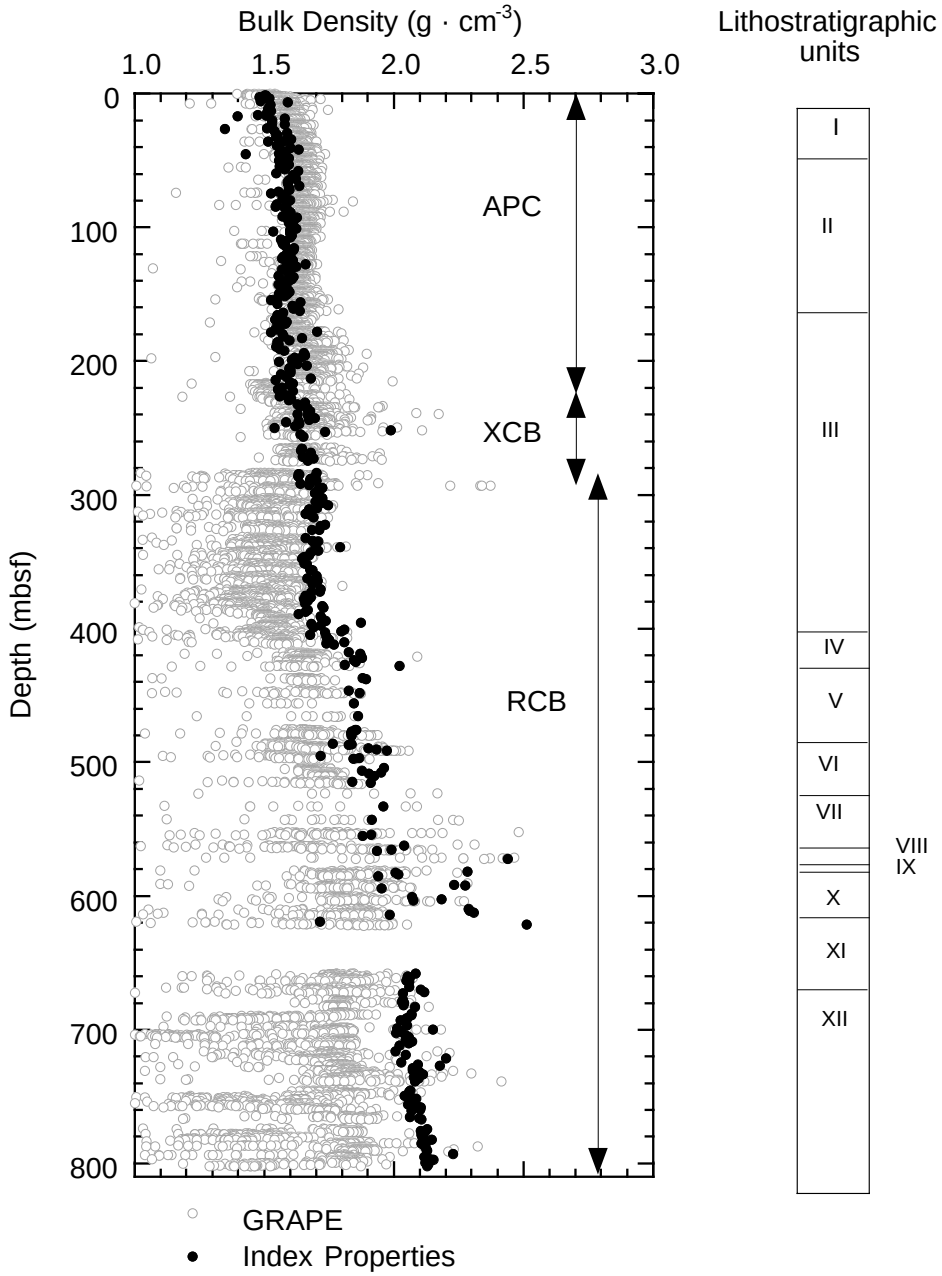

Figure F50. Site 1115 grain density derived from MAD index properties measurements.

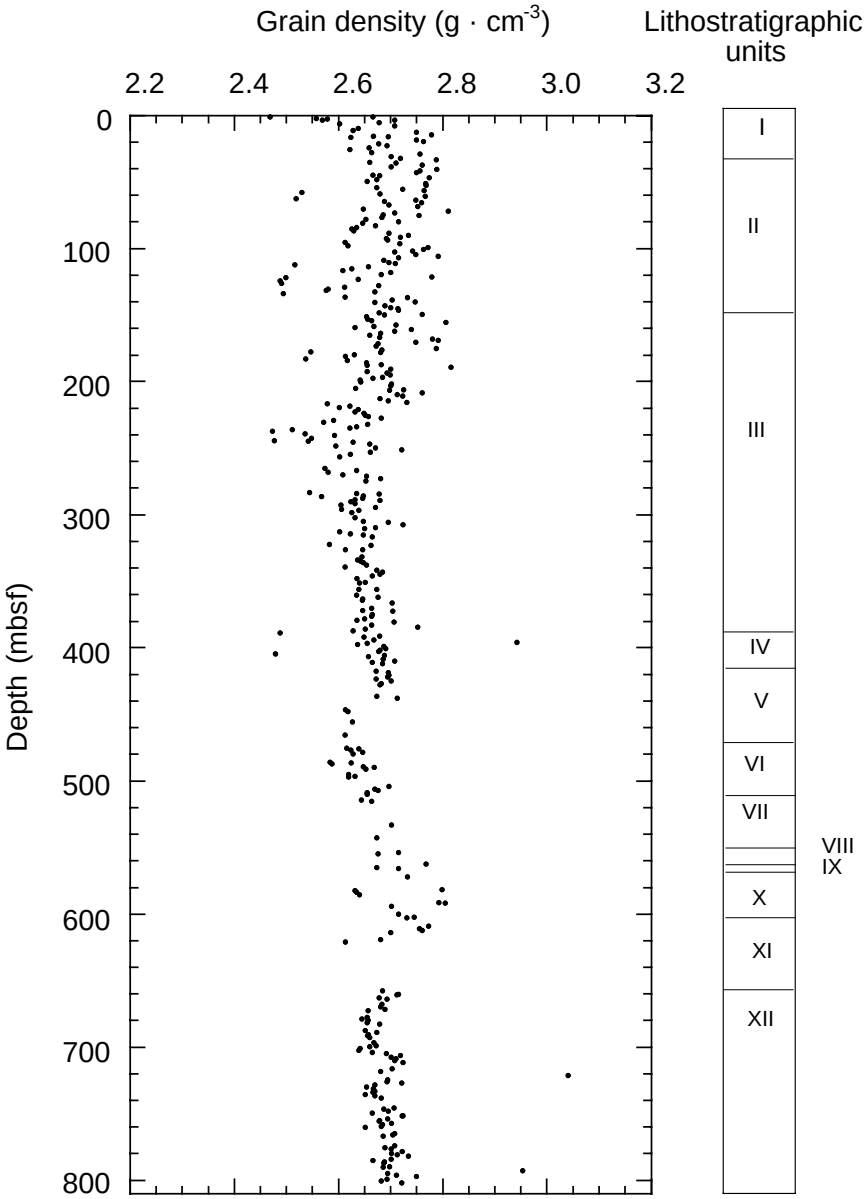

Figure F51. Site 1115 porosity. Highlighted zones reflect the regions of relatively high porosity.

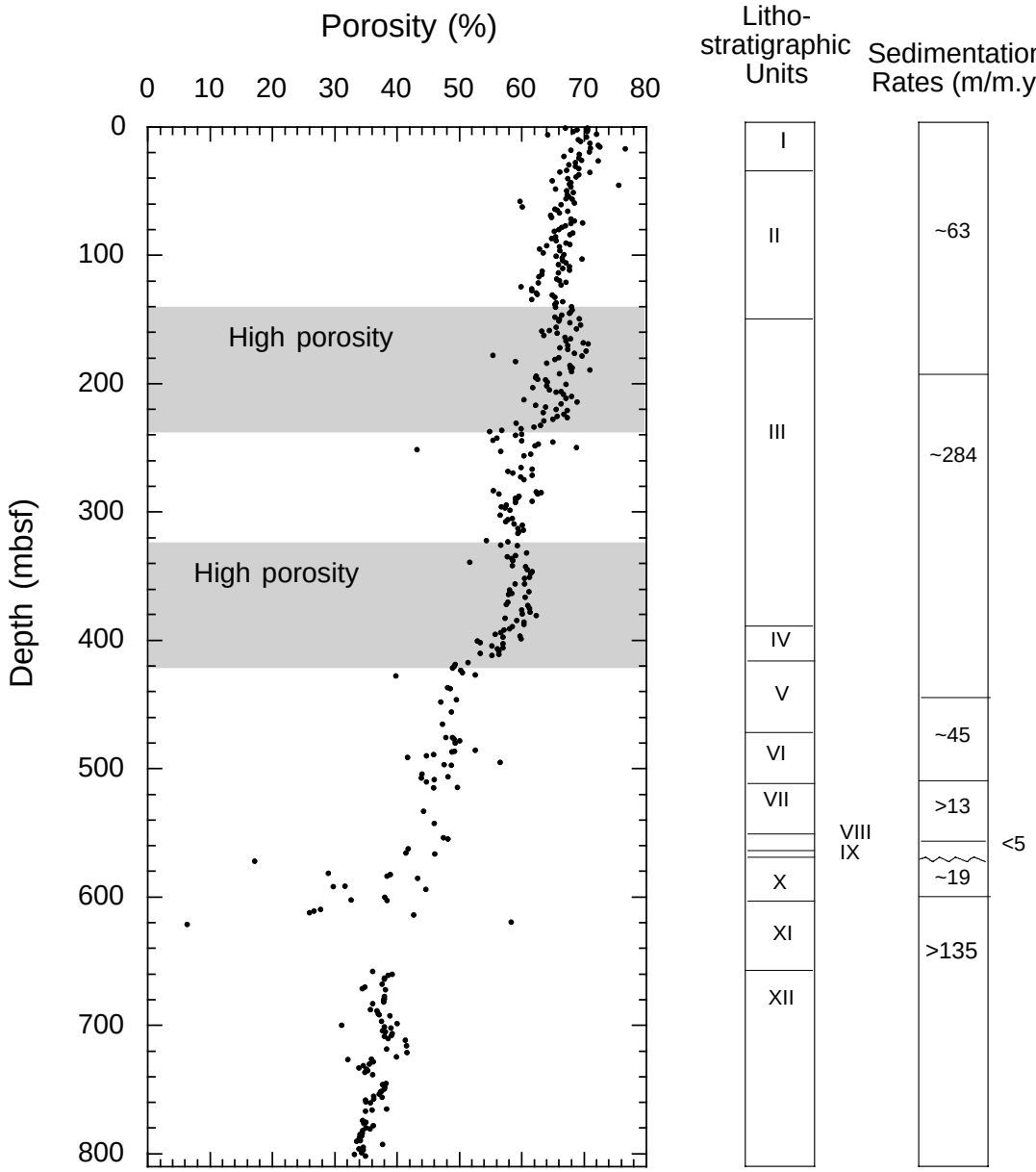

Figure F52. Site 1115 *P*-wave transverse (x, y) and longitudinal (z) velocities.

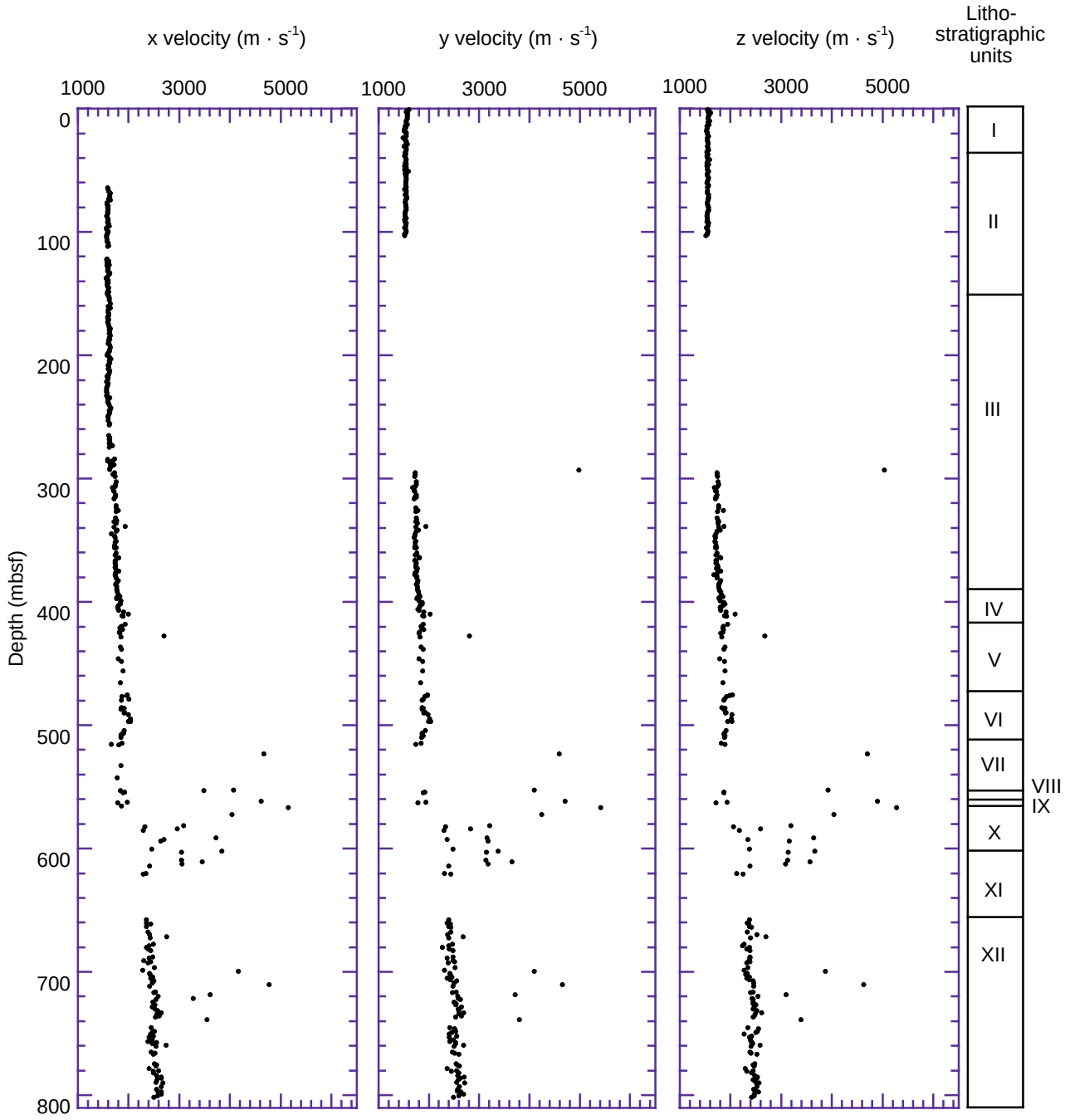

Figure F53. Longitudinal velocity vs. average transverse velocity and *P*-wave anisotropy (see **"Paleomagnetism,"** p. 21, in the "Explanatory Notes" chapter for method used). A positive anisotropy indicates that the transverse is greater than the longitudinal velocity.

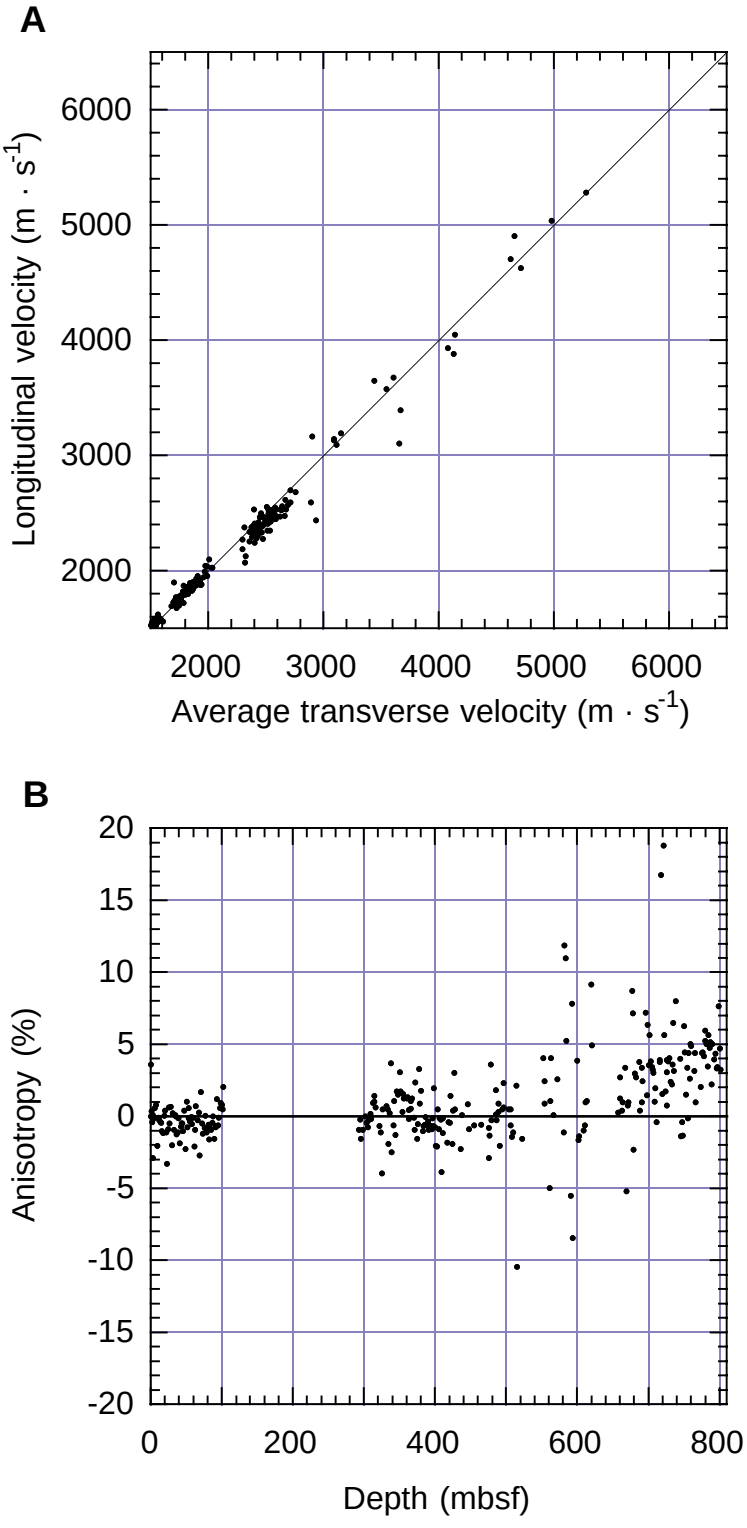

Figure F54. Site 1115 thermal conductivity values.

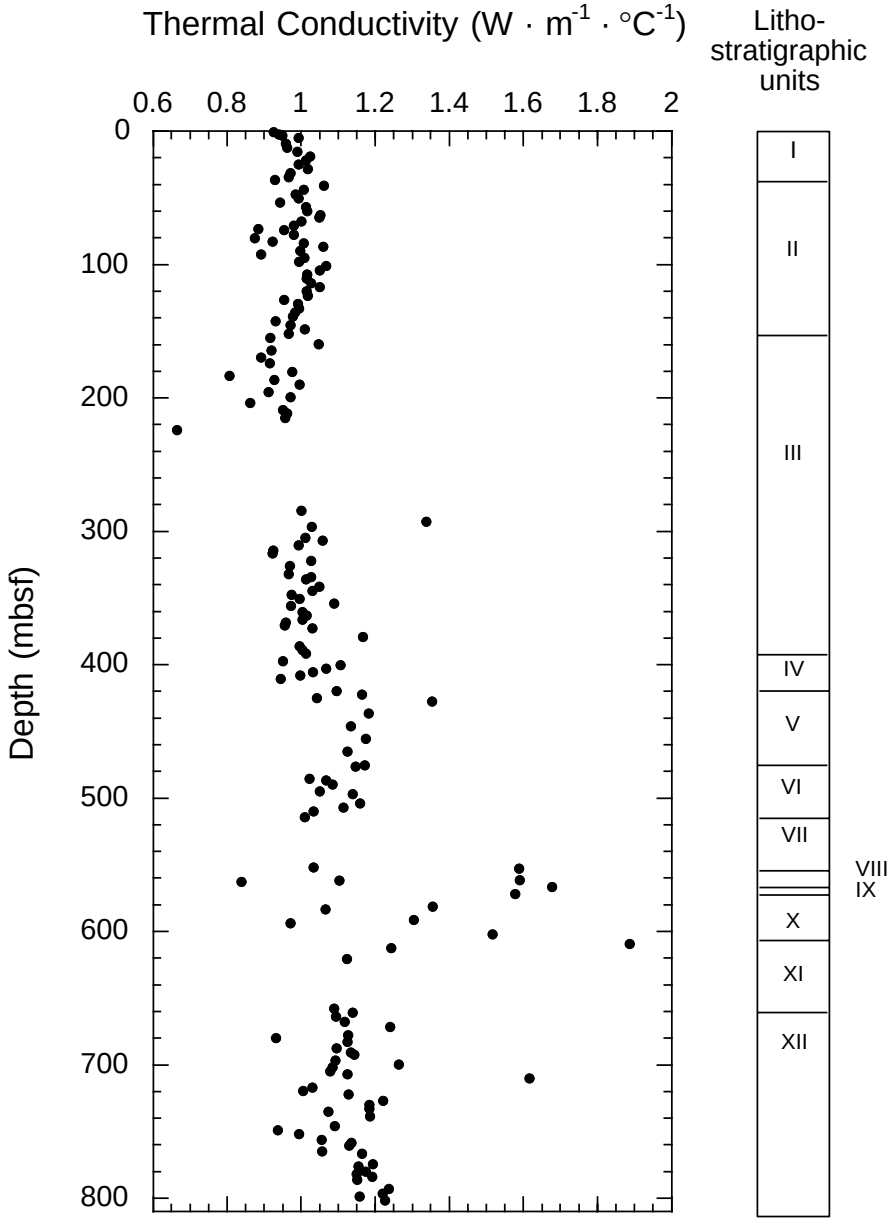

Figure F55. Site 1115 shear and compressive strength data.

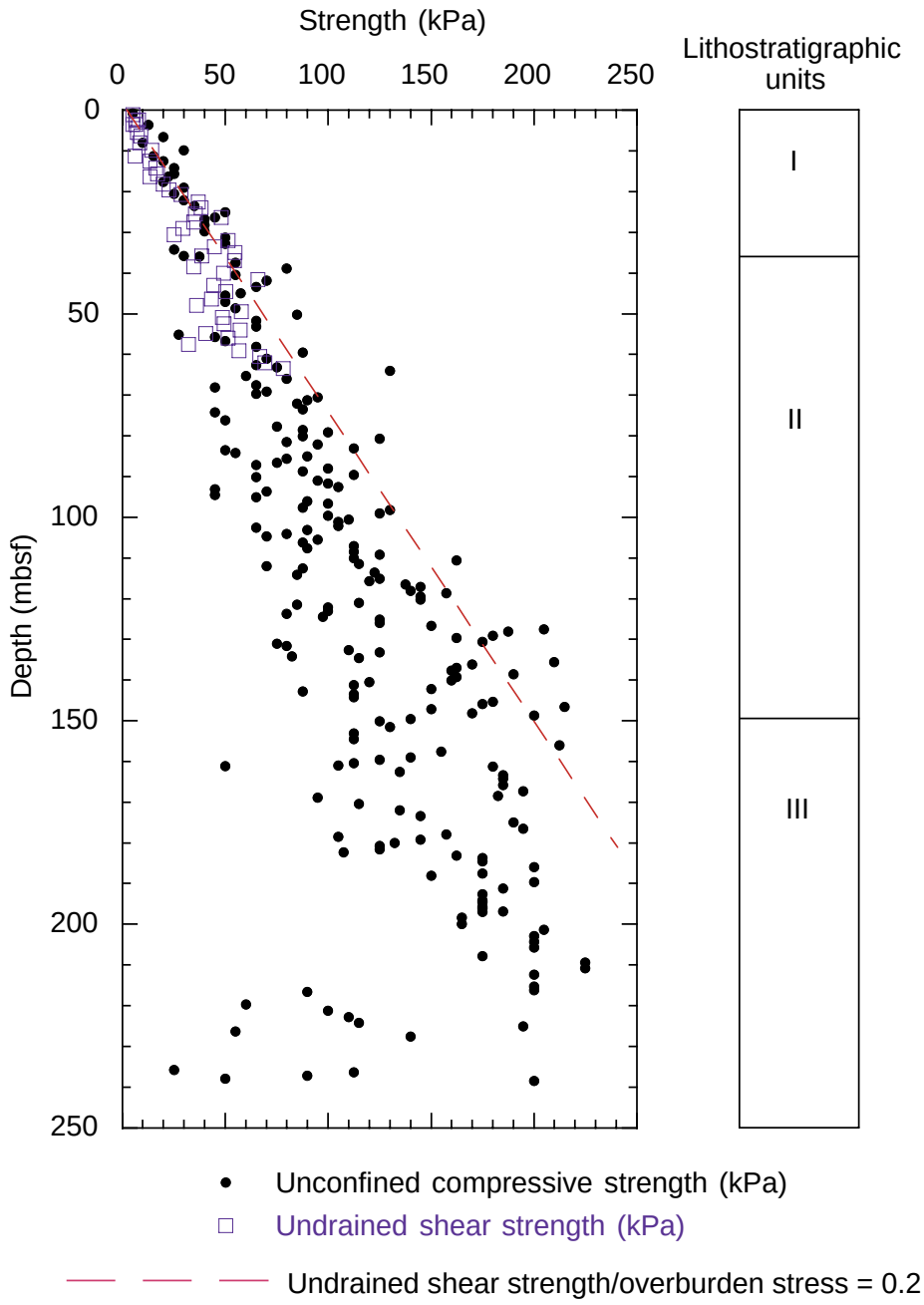

Figure F56. Site 1115 magnetic susceptibility from MST, magnetic intensity, and NGR profiles from physical properties. Downhole logging (HSGR) data are also shown to indicate trends in areas of poor core recovery.

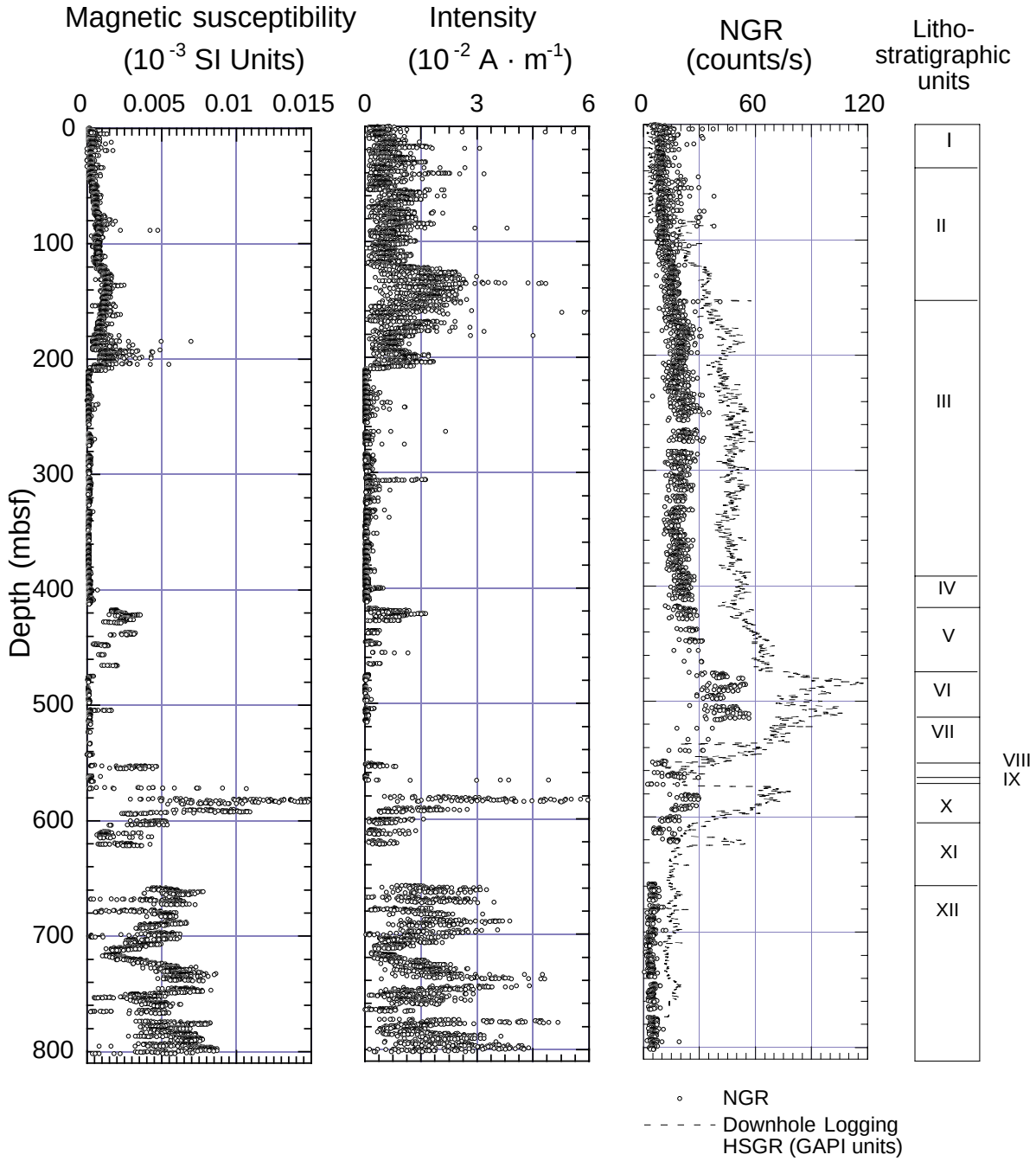

Figure F57. Correlation between Holes 1115A and 1115B using distinctive features in the magnetic susceptibility between 0 and 5 mbsf.

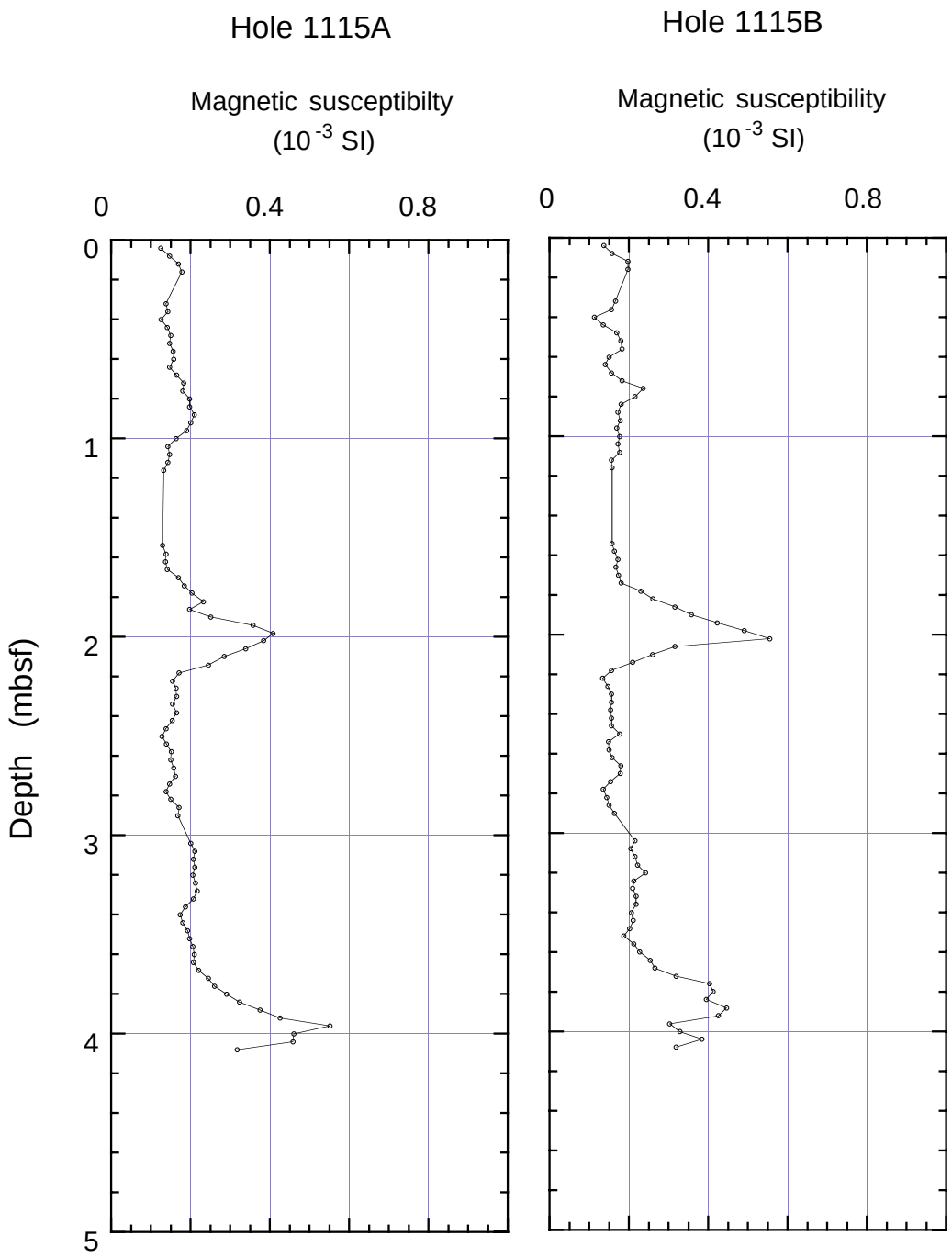

Figure F58. Correlation between Holes 1115B and 1115C using distinctive NGR features between 284.0 and 289.5 mbsf. The highlighted zone identifies the NGR peaks used for the interhole correlation.

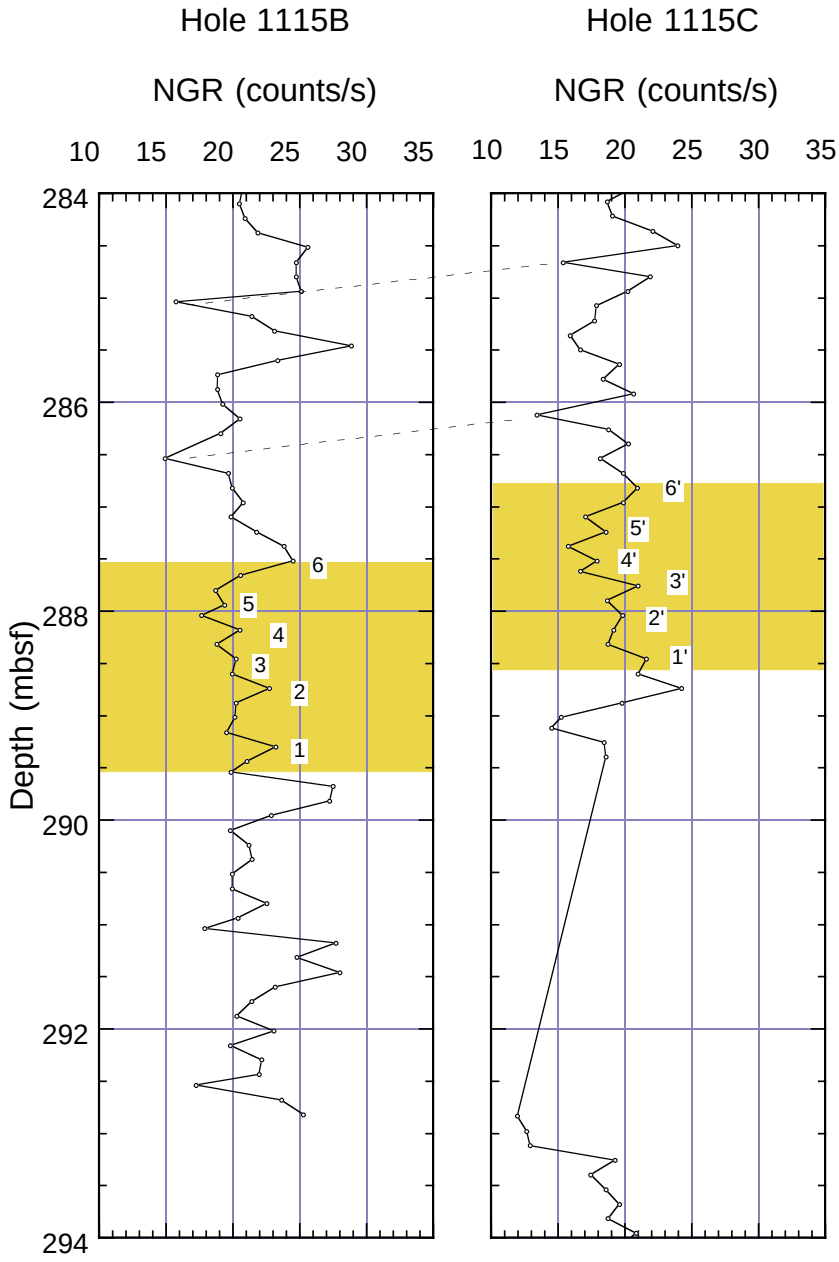

Figure F59. Hole 1115C composite log from 0 to 800 mbsf. **A.** Left to right: (1) core number and recovery intervals from Holes 1115B and 1115C; (2) caliper measurements from the triple combo run (LCAL); (3) total natural gamma ray (HSGR) and total natural gamma ray minus uranium contribution (HCGR); (4) thorium and uranium content; (5) potassium content; (6) resistivity from the DIT tool, consisting of deep induction (IDPH), medium induction (IMPH), and shallow spherically focused current (SFLU); and (7) log units. (Continued on next seven pages.) Composite log from 0 to 200 mbsf. To compare other logs at equivalent depth, see Figure **F59B,** p. 135.

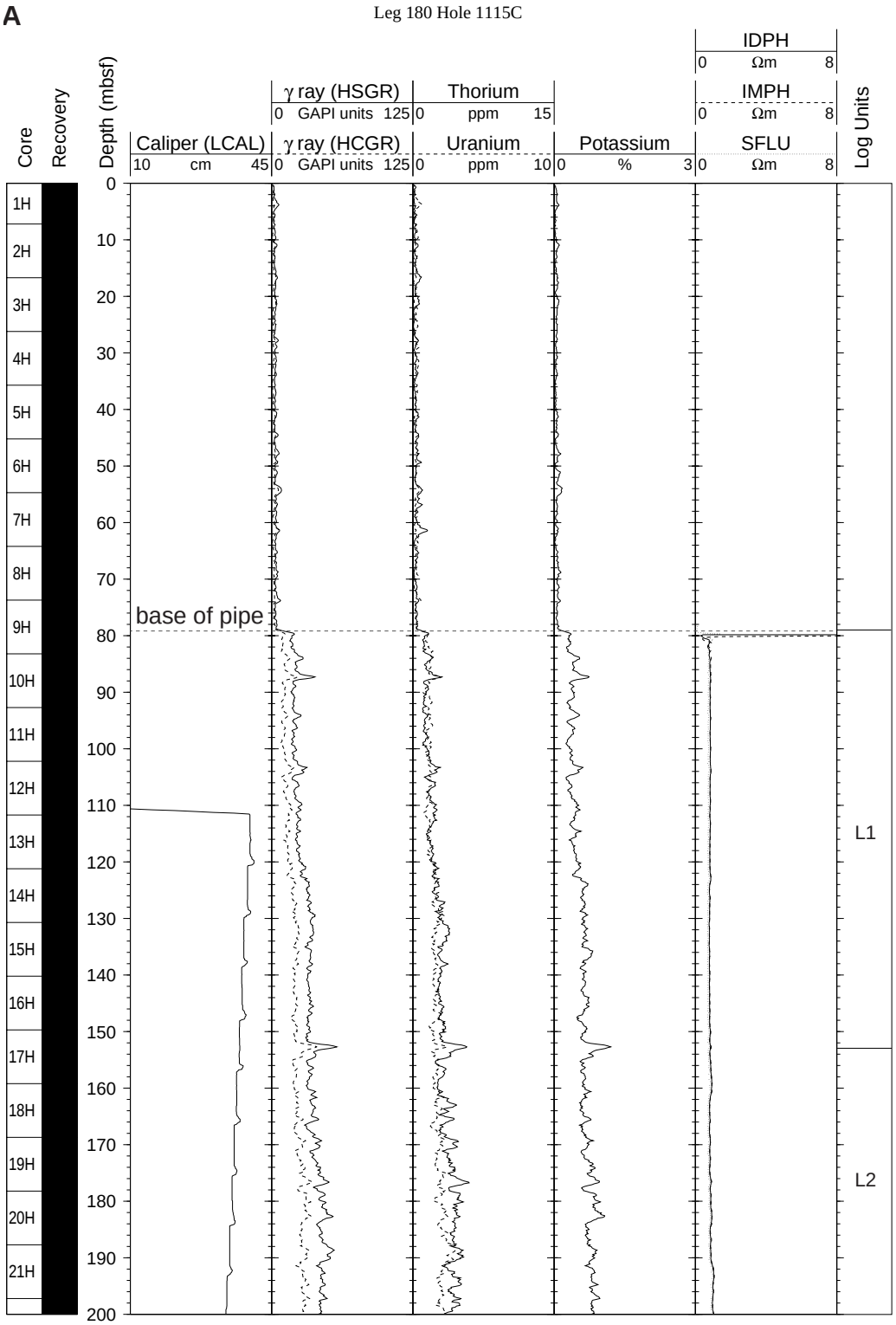

Figure F59 (continued). Composite log from 200 to 400 mbsf. To compare other logs at equivalent depth, see Figure **F59B,** p. 136.

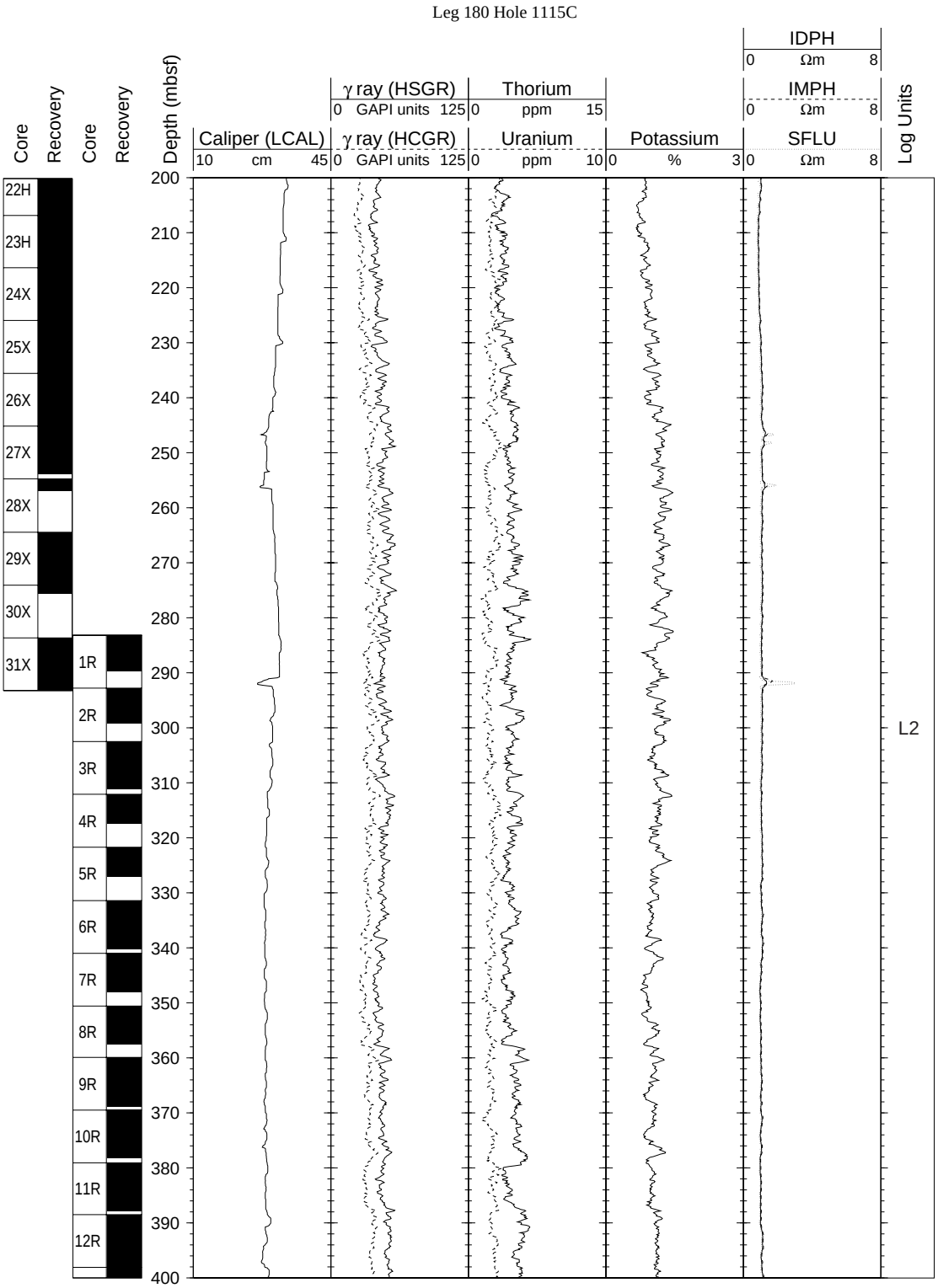

Figure F59 (continued). Composite log from 400 to 600 mbsf. To compare other logs at equivalent depth, see Figure **F59B,** p. 137.

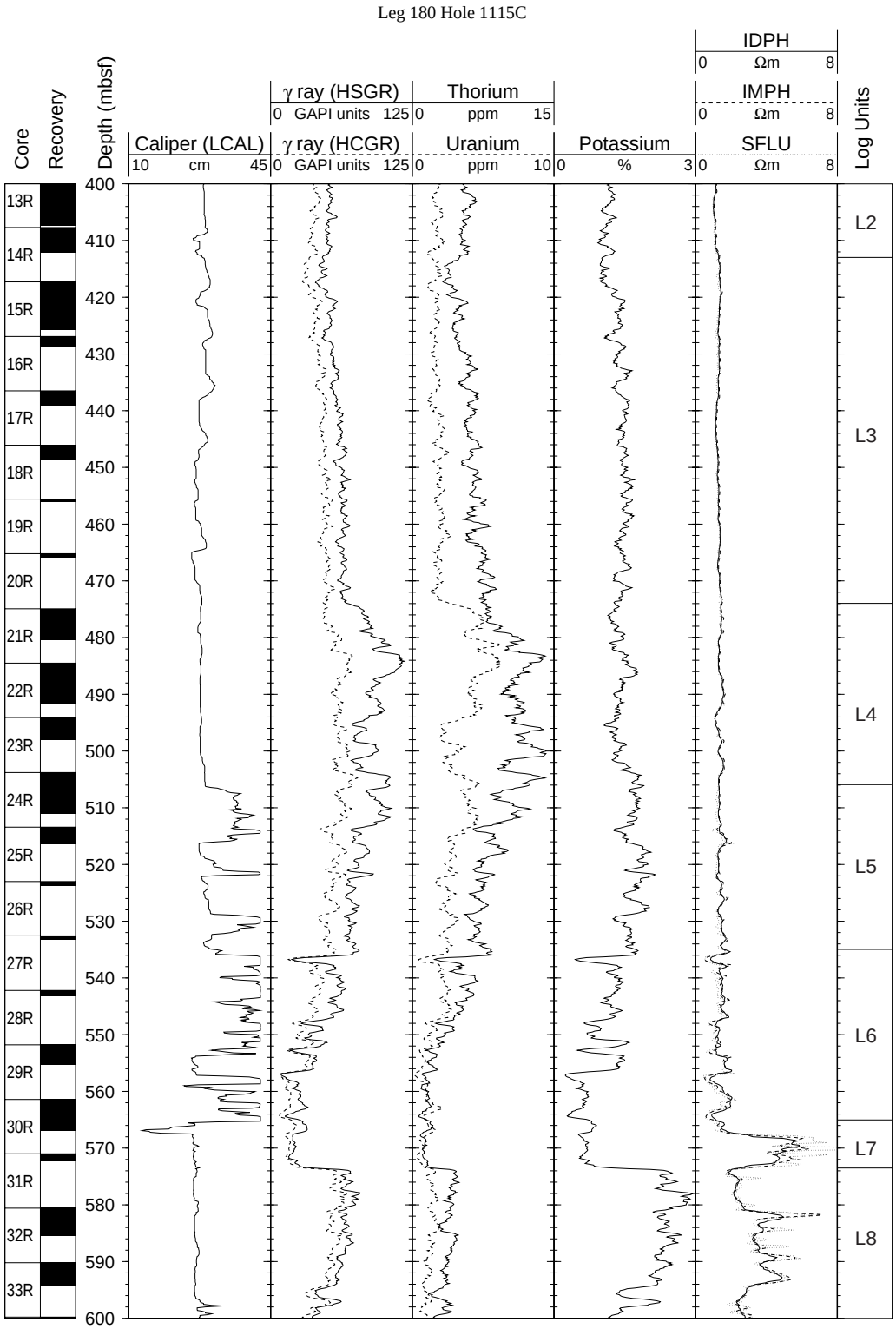

Figure F59 (continued). Composite log from 600 to 800 mbsf. To compare other logs at equivalent depth, see Figure **F59B,** p. 138.

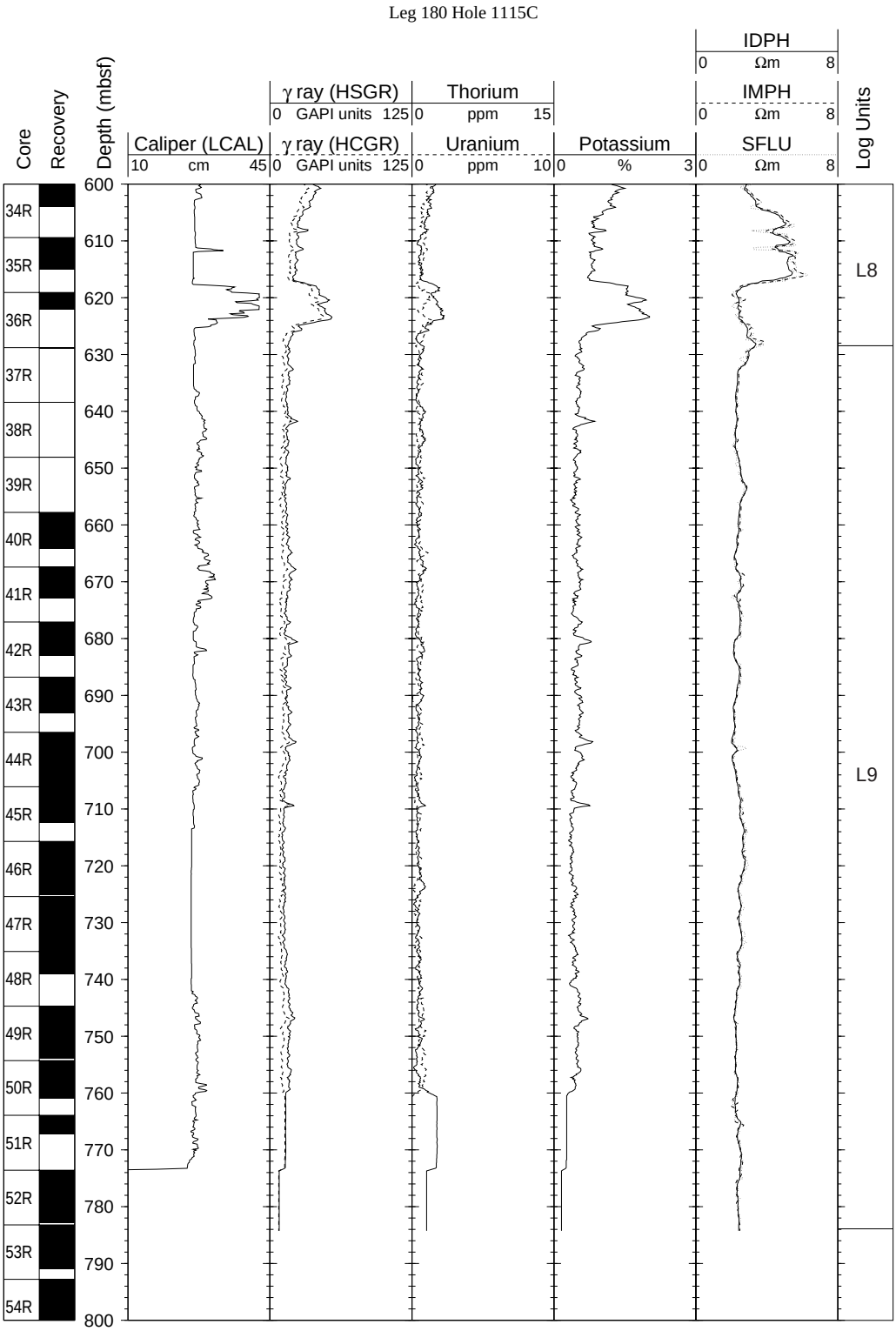

Figure F59 (continued). B. Left to right: (1) core number and recovery intervals from Holes 1115B and 1115C; (2) bulk density (RHOM) from the lithodensity sonde (HLDS) and from measurements on cores; (3) photoelectric effect (PEFL); (4) density porosity (DPHI), porosity from measurements on cores, and neutron porosity (APLC); (5) neutrons capture rate (SIGF); (6) sonic velocity from z-axis measurements on cores and from array sonic tool (DTCO); and (7) log units. Composite log from 0 to 200 mbsf. To compare other logs at equivalent depth, see Figure **F59A,** p. 131.

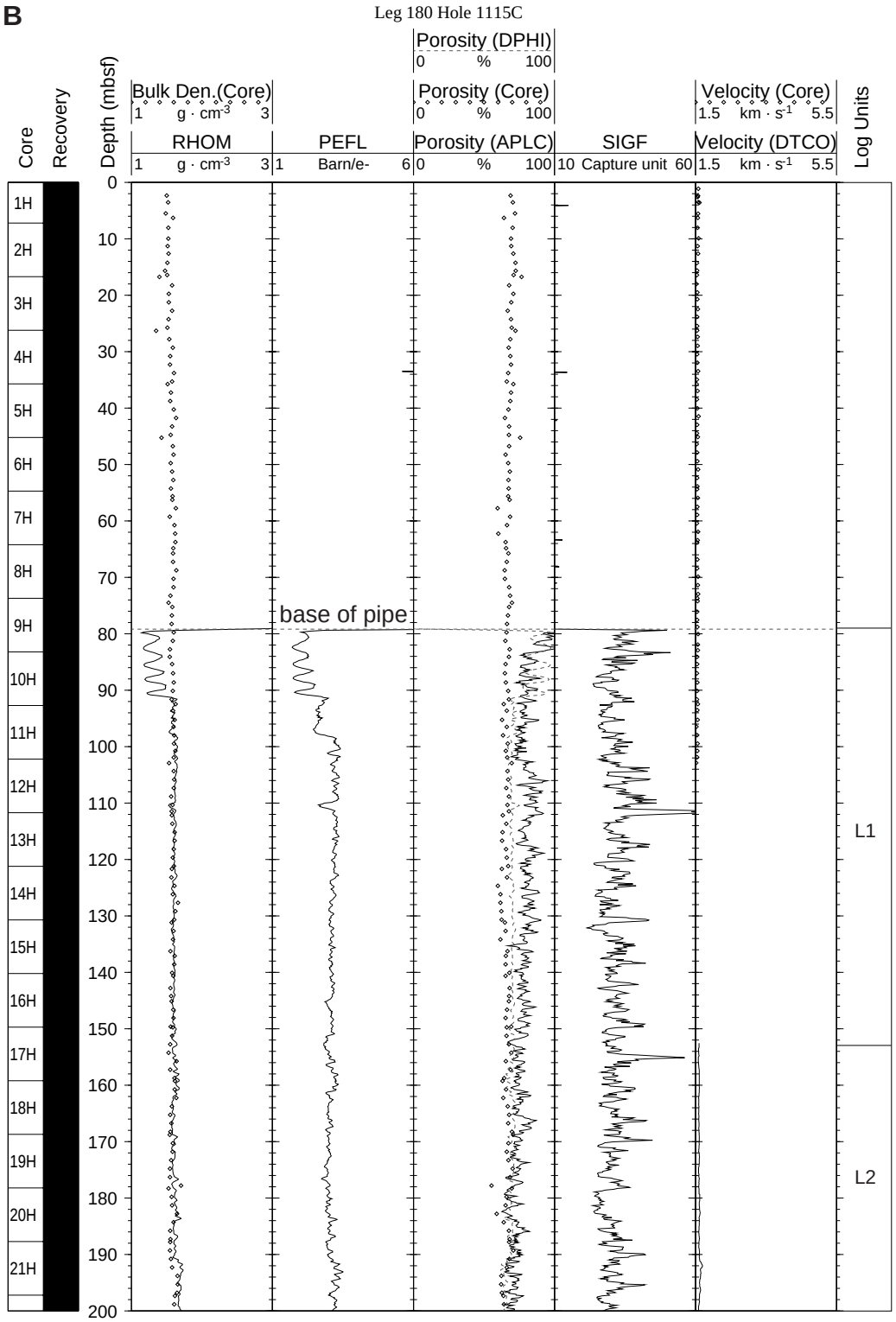

Figure F59 (continued). Composite log from 200 to 400 mbsf. To compare other logs at equivalent depth, see Figure **F59A,** p. 132.

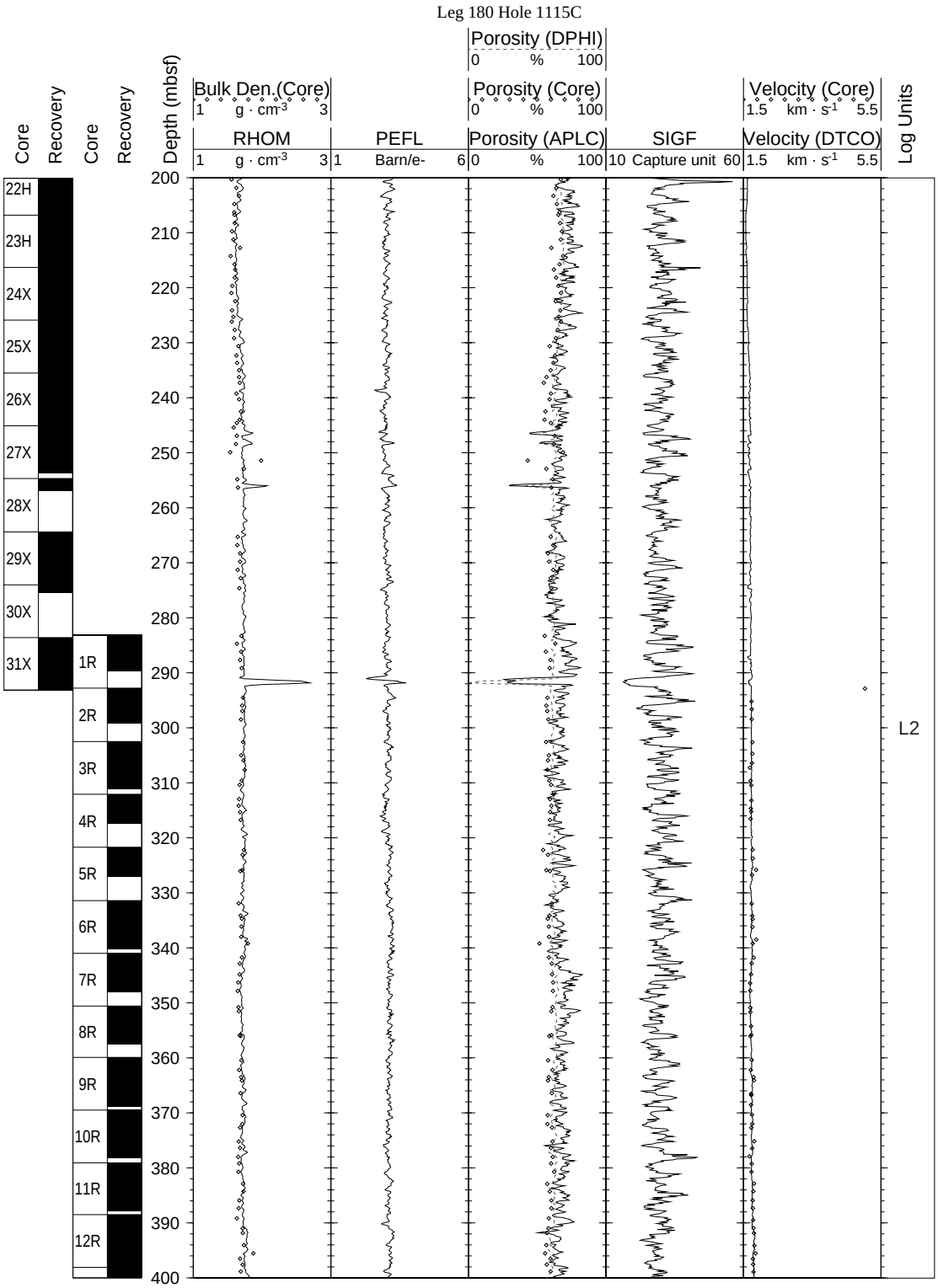

Figure F59 (continued). Composite log from 400 to 600 mbsf. To compare other logs at equivalent depth, see Figure **F59A,** p. 133.

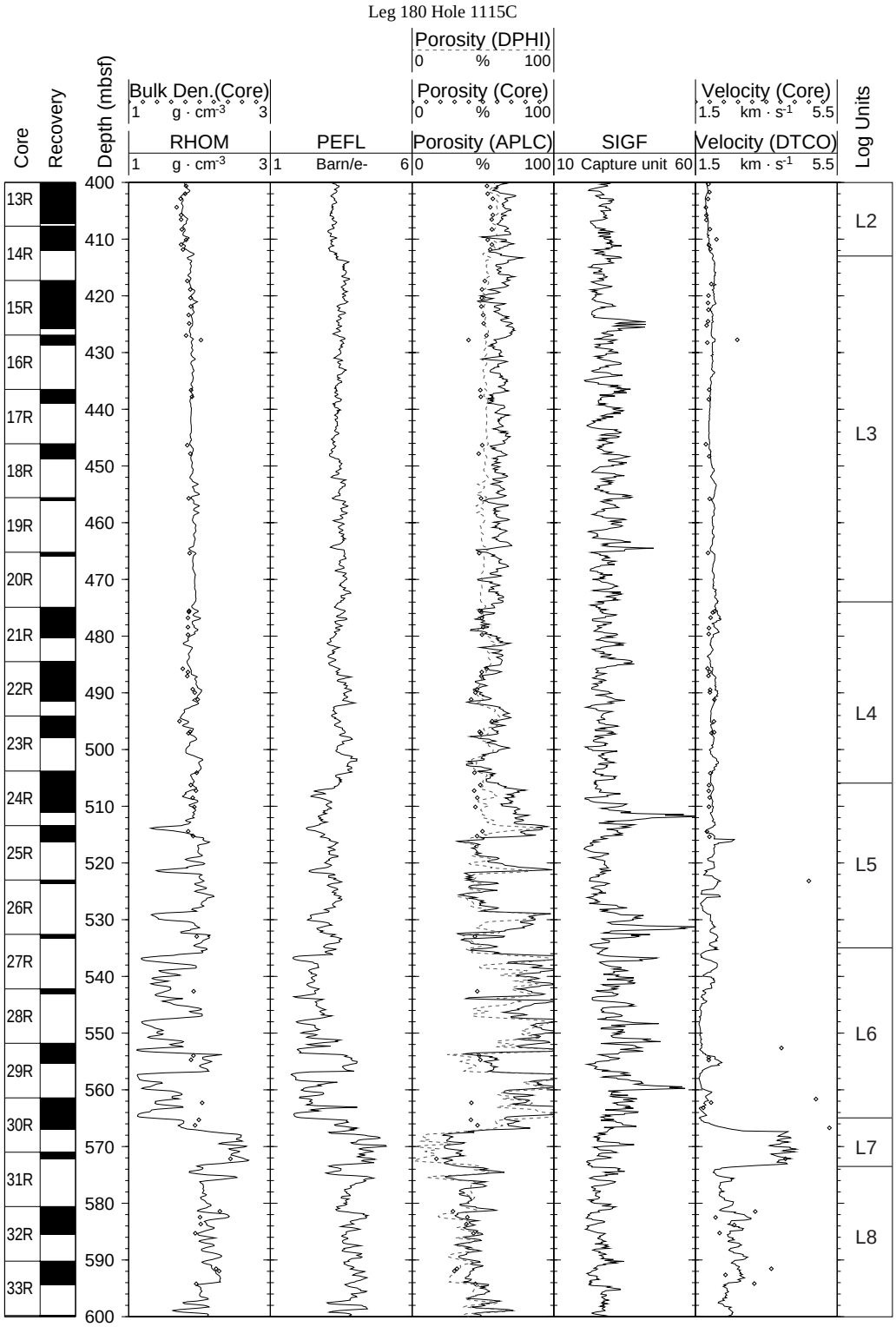

Figure F59 (continued). Composite log from 600 to 800 mbsf. To compare other logs at equivalent depth, see Figure **F59A,** p. 134.

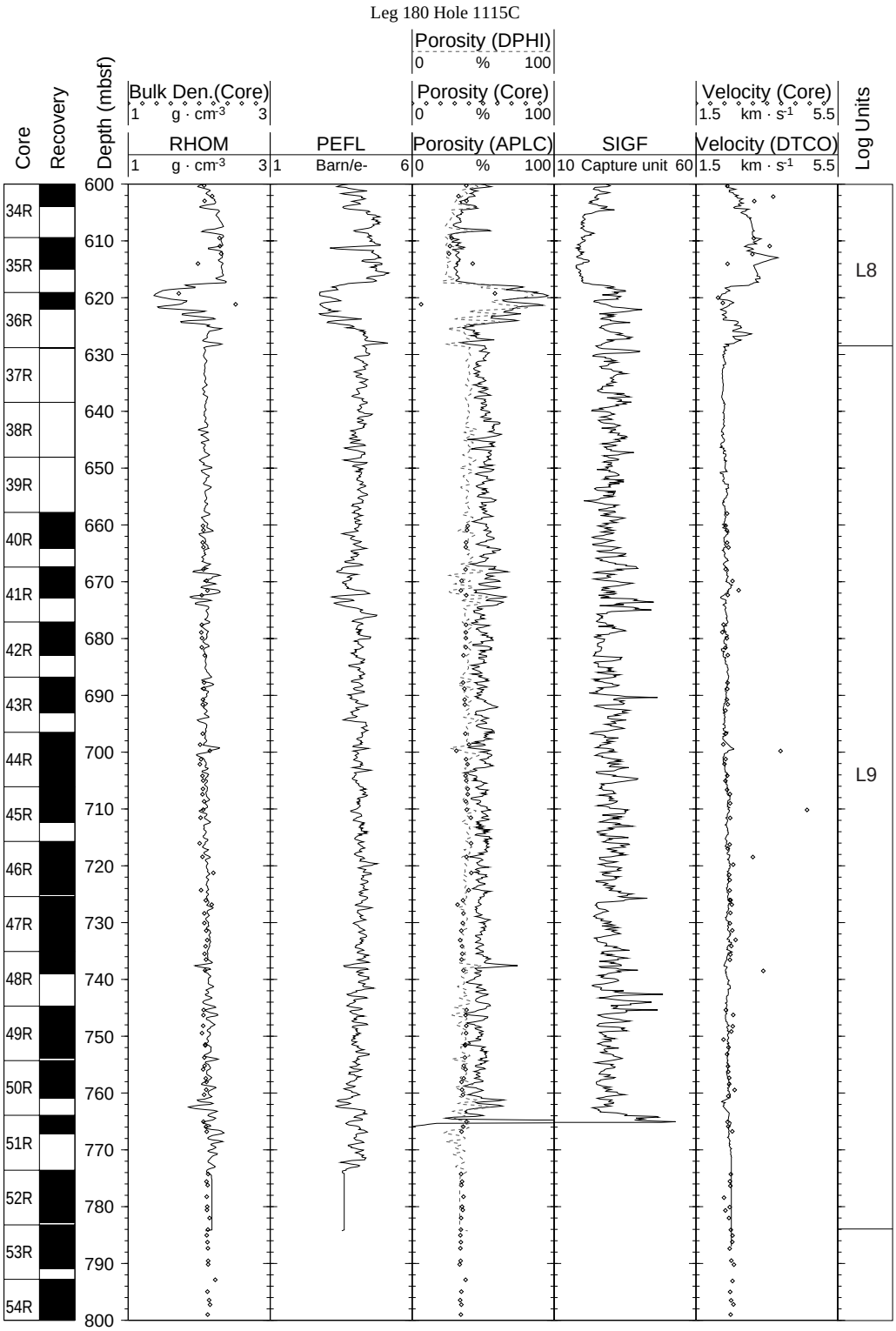

Figure F60. Hole 1115C total volume gamma ray (HSGR) from triple combo at the mudline after depth shifts as given in Table T15, p. 224.

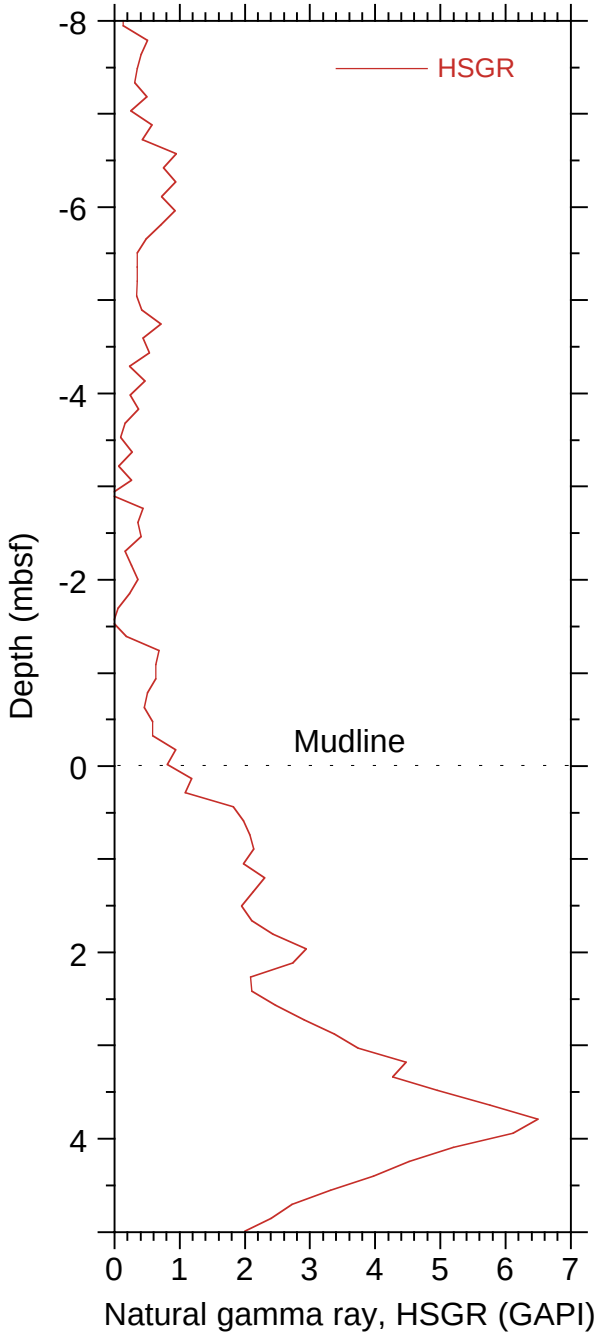

Figure F61. Hole 1115C total volume gamma ray from triple combo (HSGR) and FMS-sonic string passes 2 (SGR2) and 3 (SGR3) after depth shifts as given in Table T15, p. 224.

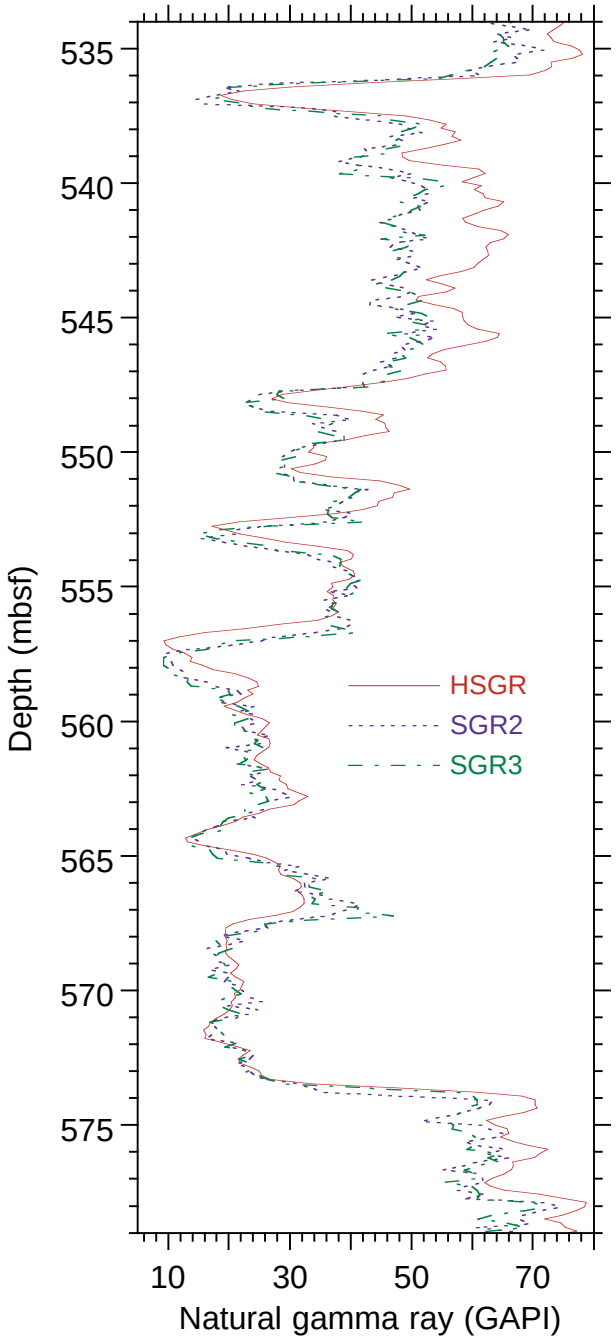

Figure F62. Lithologic units derived from logging response at Hole 1115C and core analysis from Holes 1115B and 1115C. Left to right: core recovery for Holes 1115B and 1115C, natural gamma ray (HSGR), density (DPHI) and neutron (APLC) porosity, units defined by the logging response, lithostratigraphic units defined in **"Lithostratigraphy,"** p. 5, and fault zones defined in **"Structural Geology,"** p. 29. Shaded areas show areas of maximum caliper extension where quality of some logs may be compromised (see **"Structural Measurements,"** p. 16, in the "Explanatory Notes" chapter).

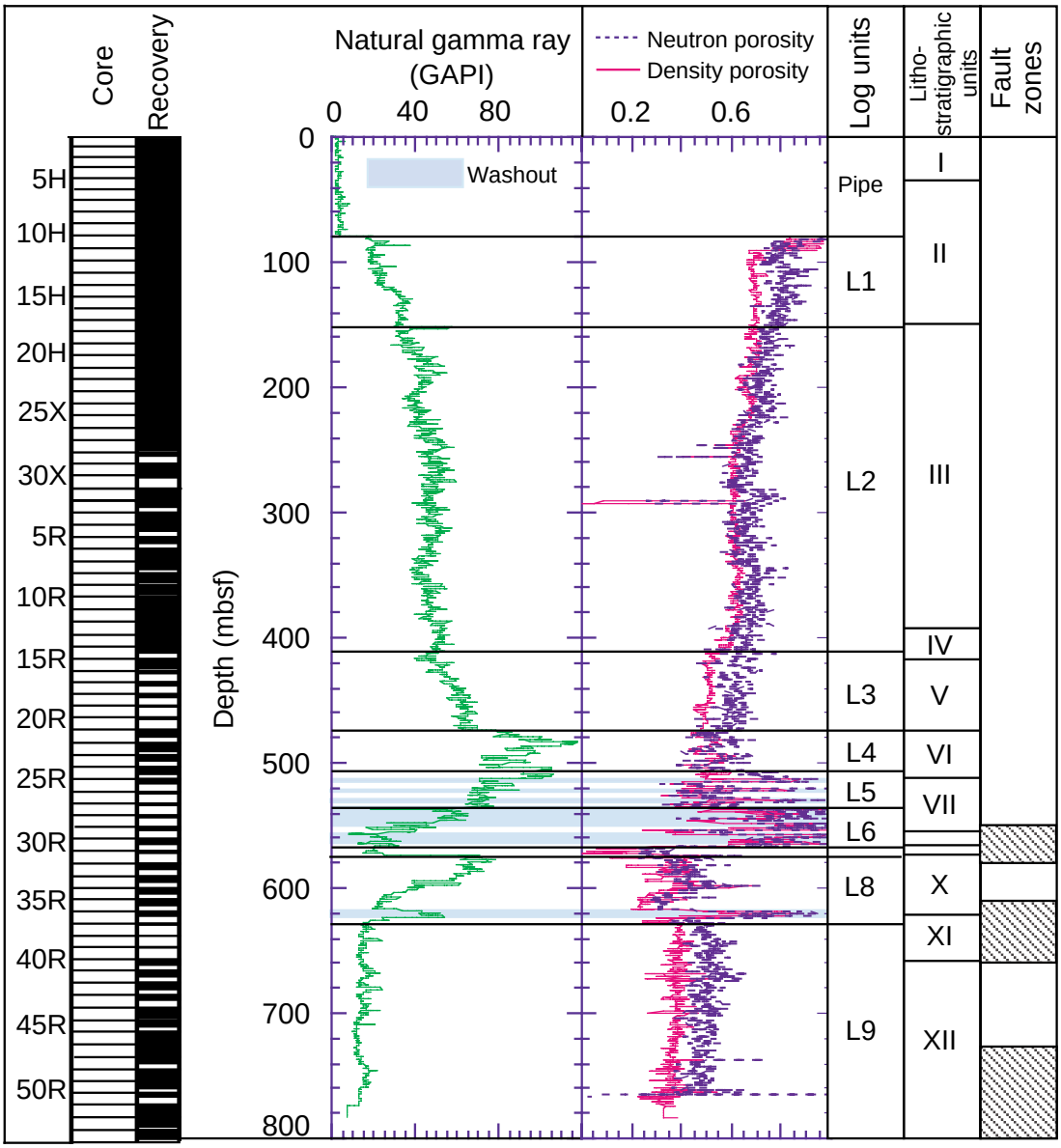

Figure F63. Hole 1115C deviation.

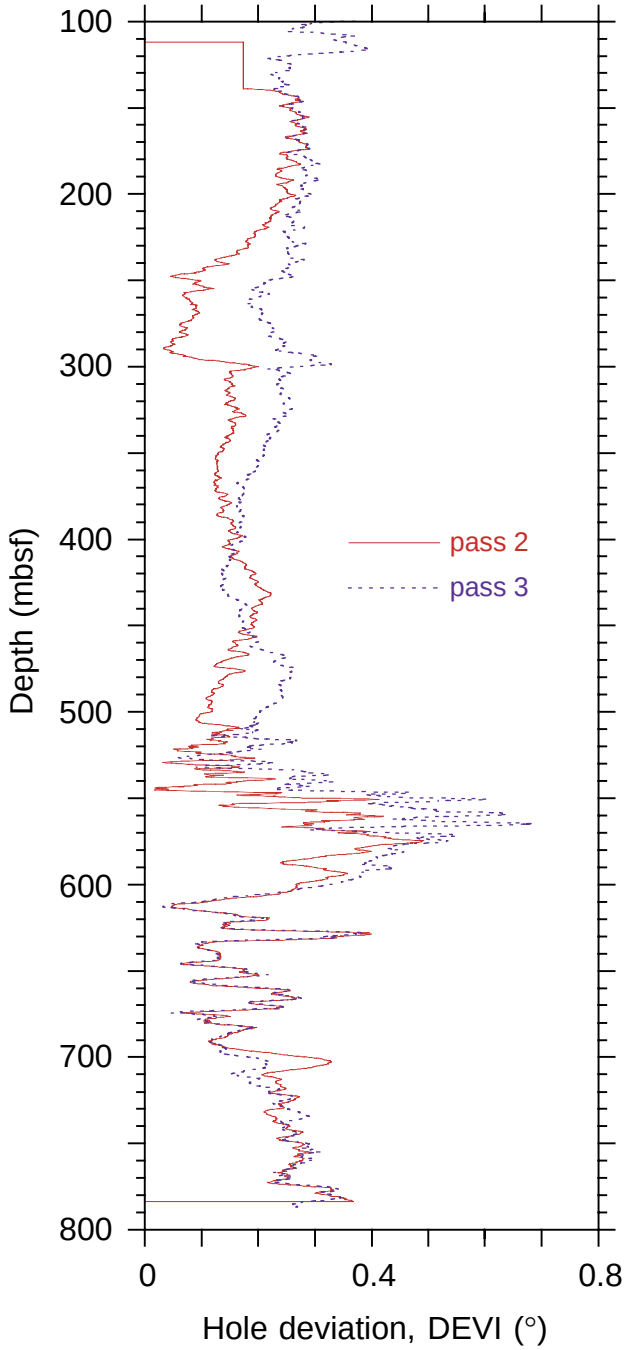

Figure F64. FMS tool string acceleration in Hole 1115C.

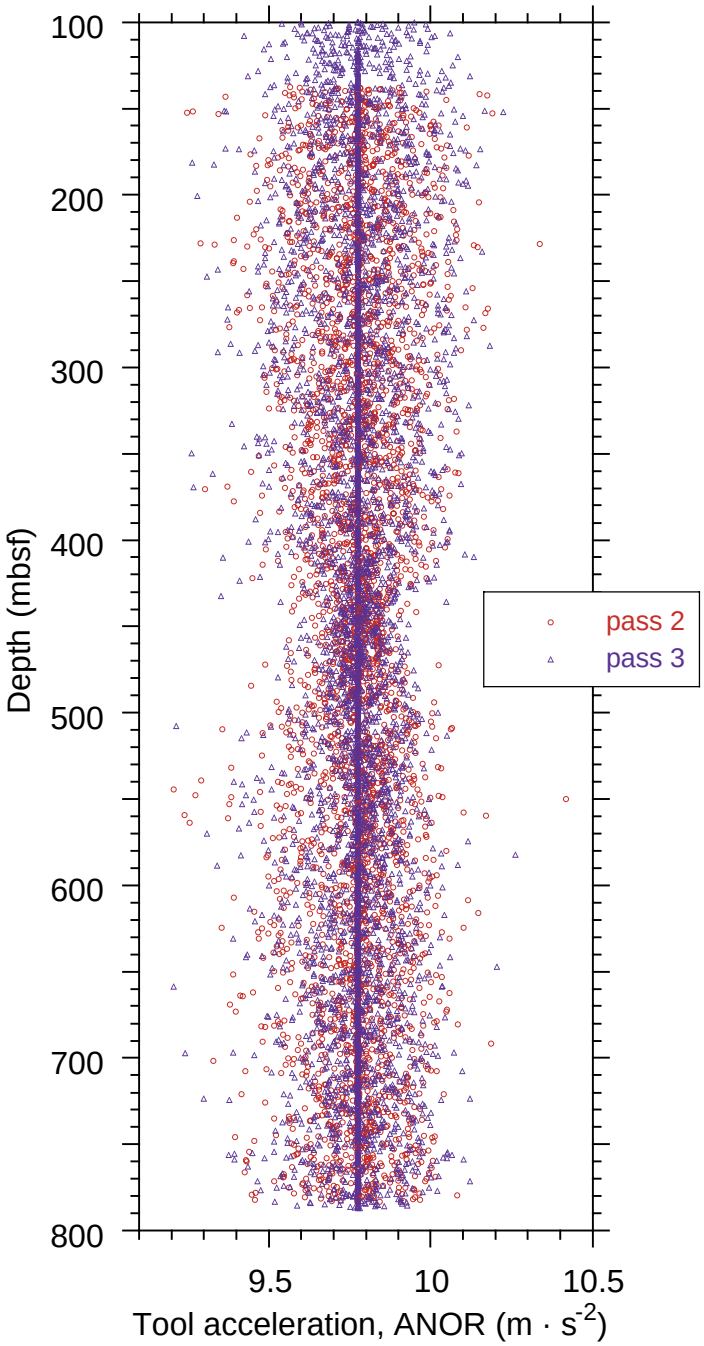

Figure F65. Hole 1115C geometry. Left to right: FMS (C1 and C2) caliper data from pass 2 and pass 3 and FMS Pad 1 azimuth (P1AZ) with respect to geographic north.

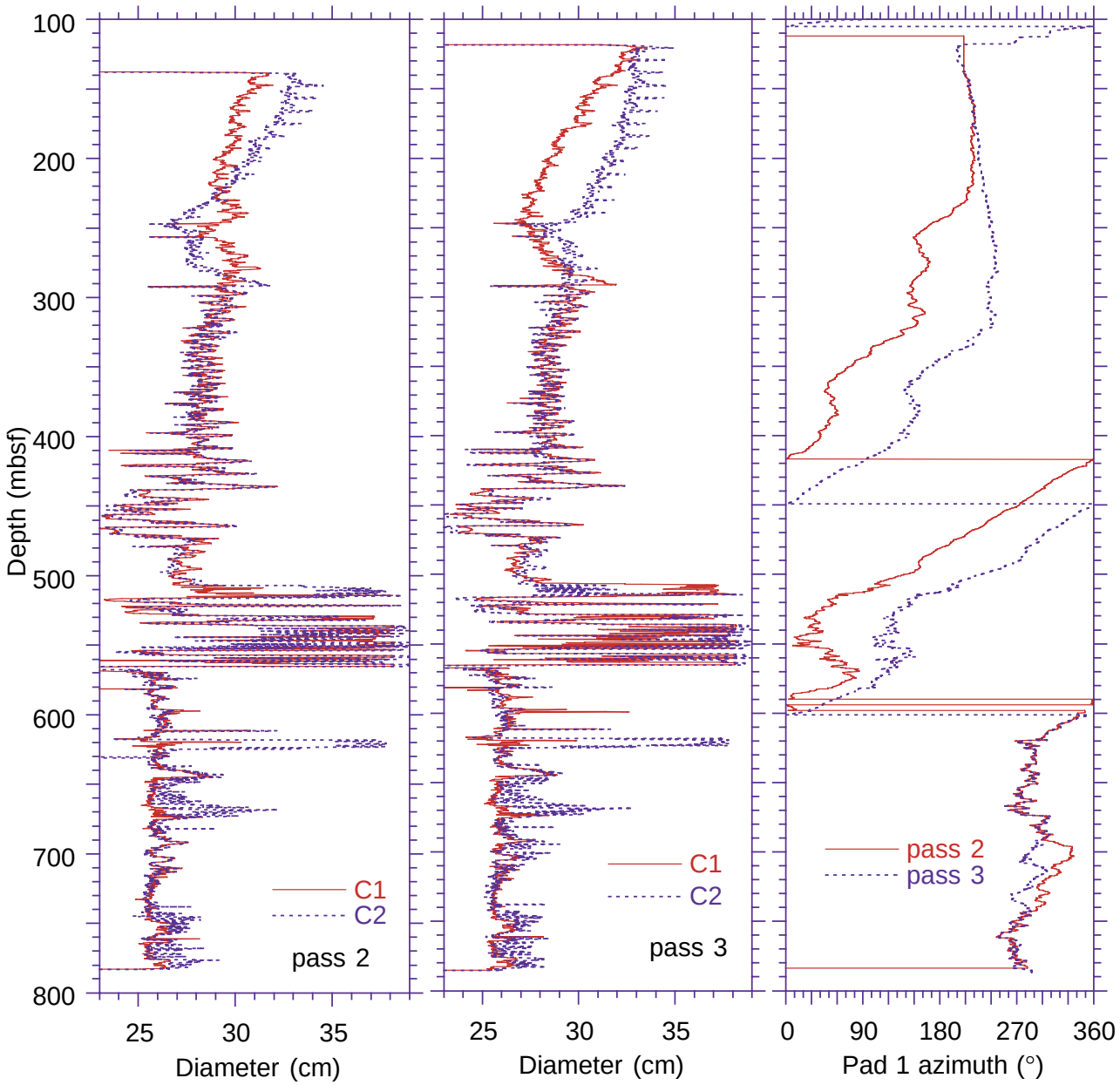

Figure F66. Hole 1115C ellipticity. Left to right: absolute value of the difference between the two caliper measurements (C1–C2), for passes 2 and 3, azimuth of the greatest diameter when the caliper difference is above 2 and 5 cm.

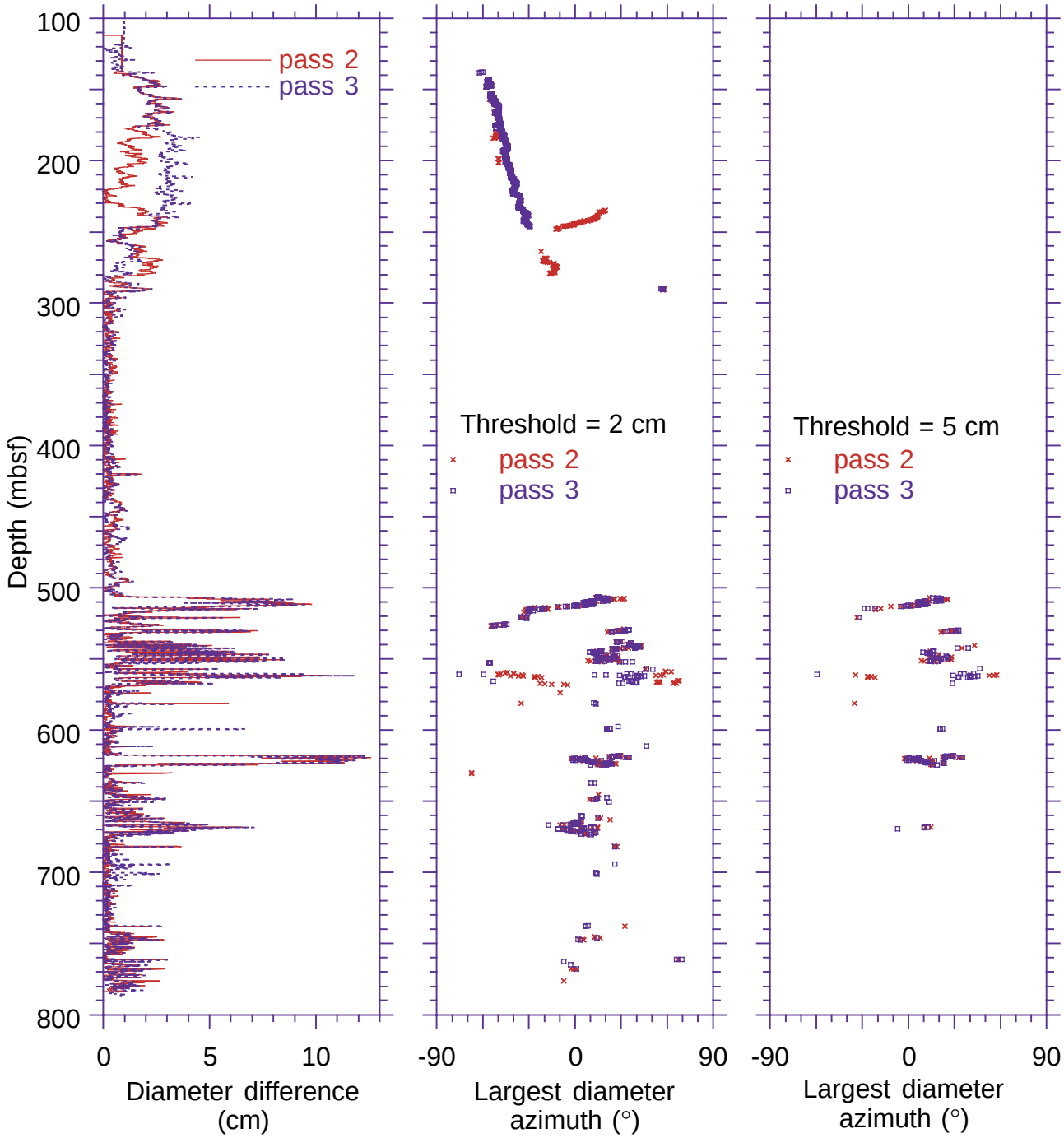

Figure F67. Hole 1115C geometry between 500 and 570 mbsf. Left to right: FMS (C1 and C2) caliper data from pass 2 and pass 3 and FMS Pad 1 azimuth (P1AZ) with respect to geographic north, and azimuth of the greatest diameter when the caliper difference is above 5 cm.

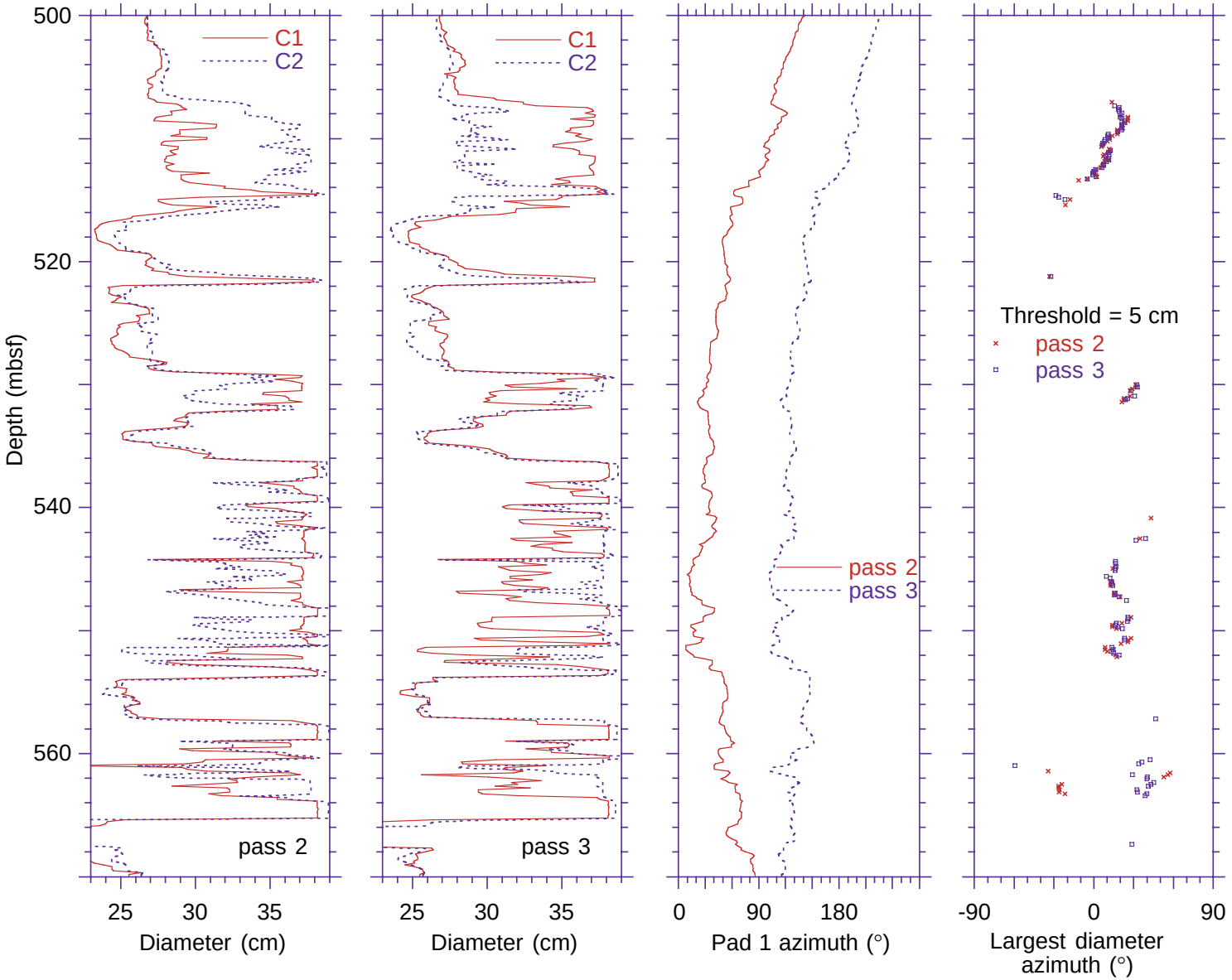

Figure F68. Hole 1115C geometry between 575 and 675 mbsf.

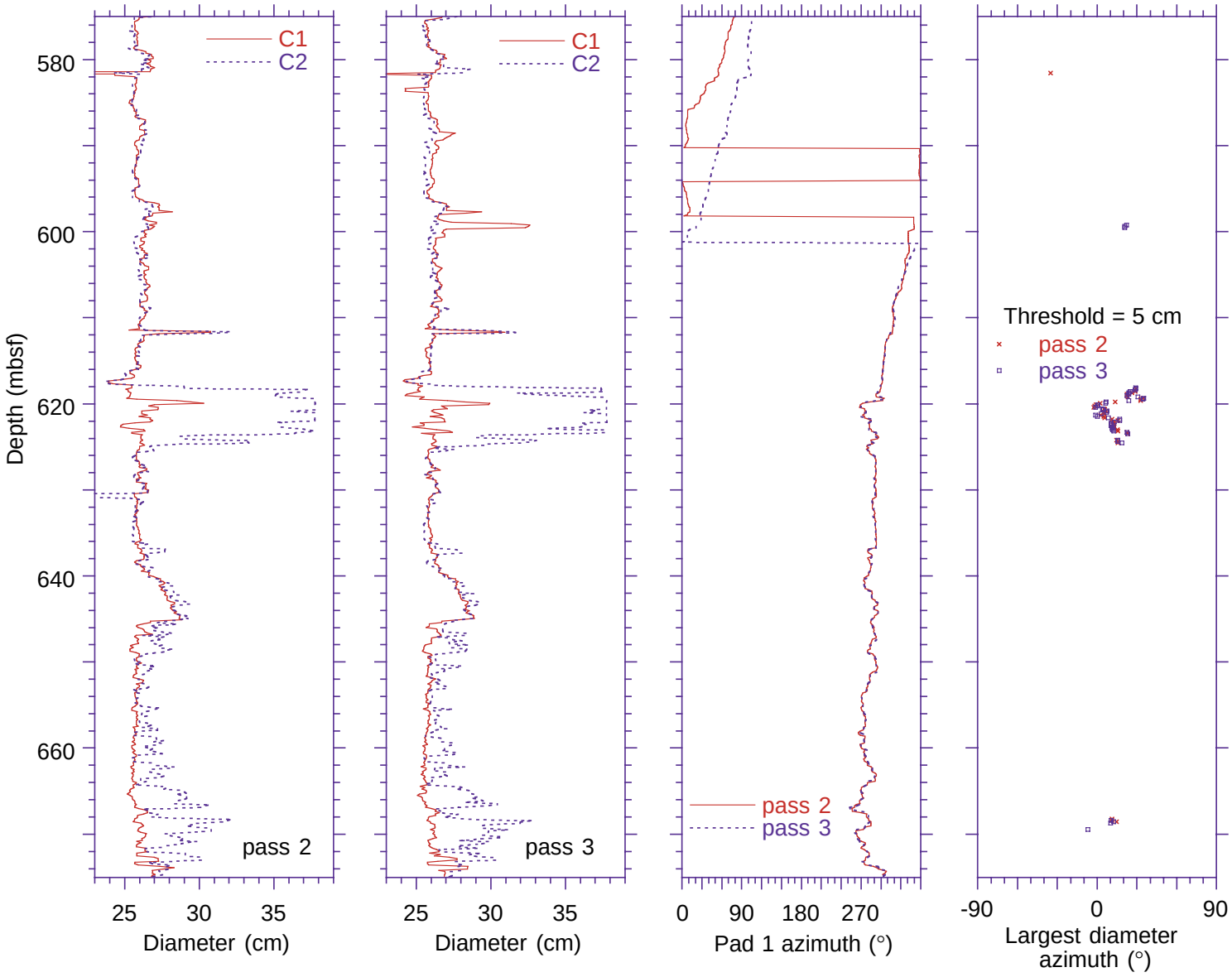

Figure F69. Hole 1115C magnetic field. **A.** Inclination (FINC). **B.** Intensity (FNOR).

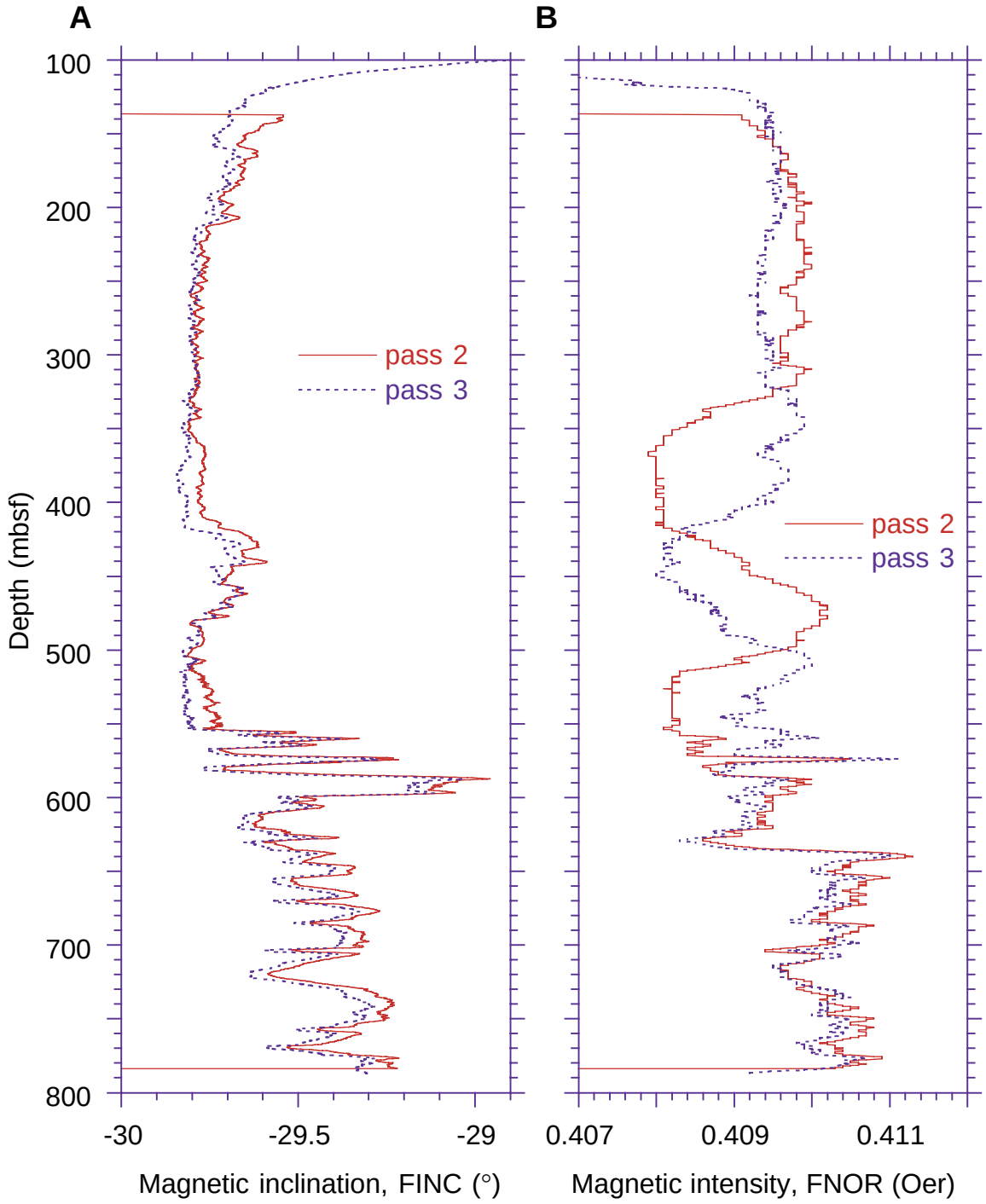

Figure F70. Hole 1115C dynamically normalized FMS images from log Unit L2 show flat lying, resistive, sandy or calcium carbonate–rich layers within a more conductive, clayey matrix. The green (vertical) lines mark the Pad 1 azimuth trace of each FMS pass. The FMS image is oriented from 0° to 360° from geographic north. Vertical scale = 1:20.

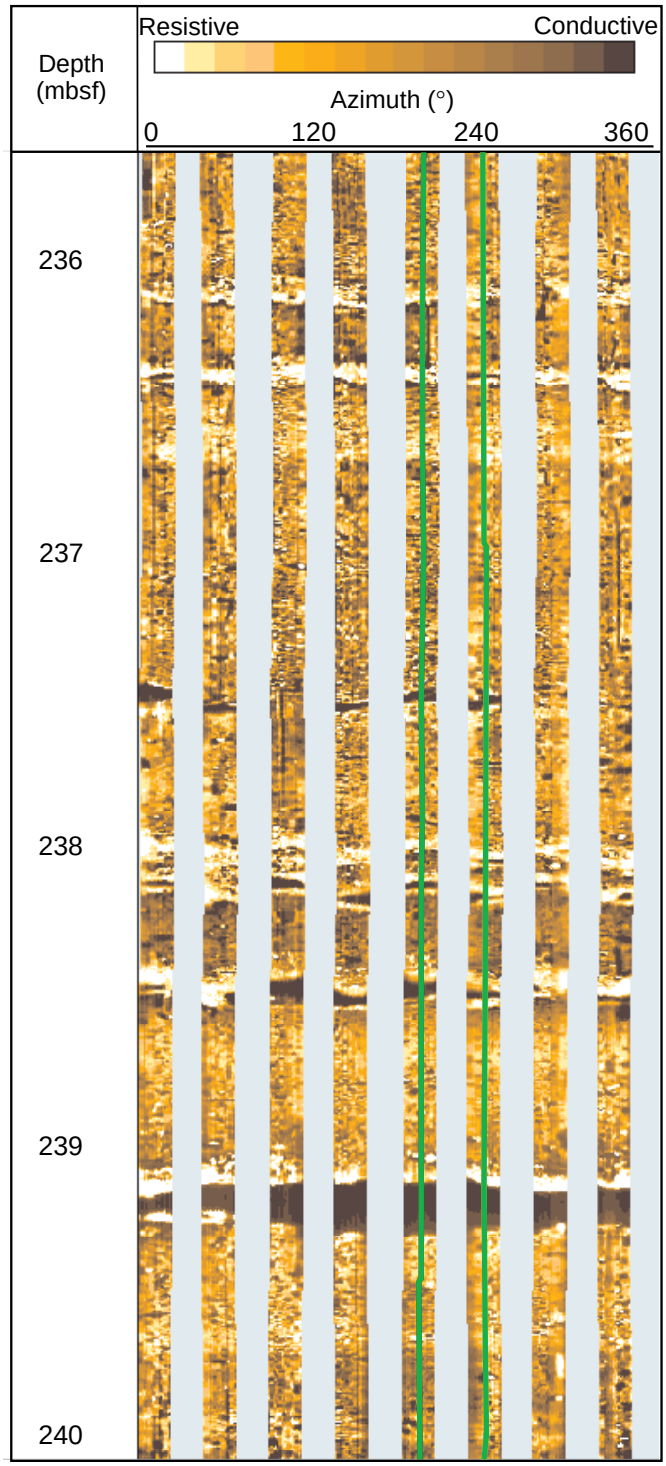

Figure F71. Hole 1115C dynamically normalized FMS images show the structureless, grainy character of log Unit L4. The thin (~10 cm) resistive layer near 487 mbsf displays a fair degree of continuity between pads, indicating that disruption is not complete. Vertical scale = 1:20.

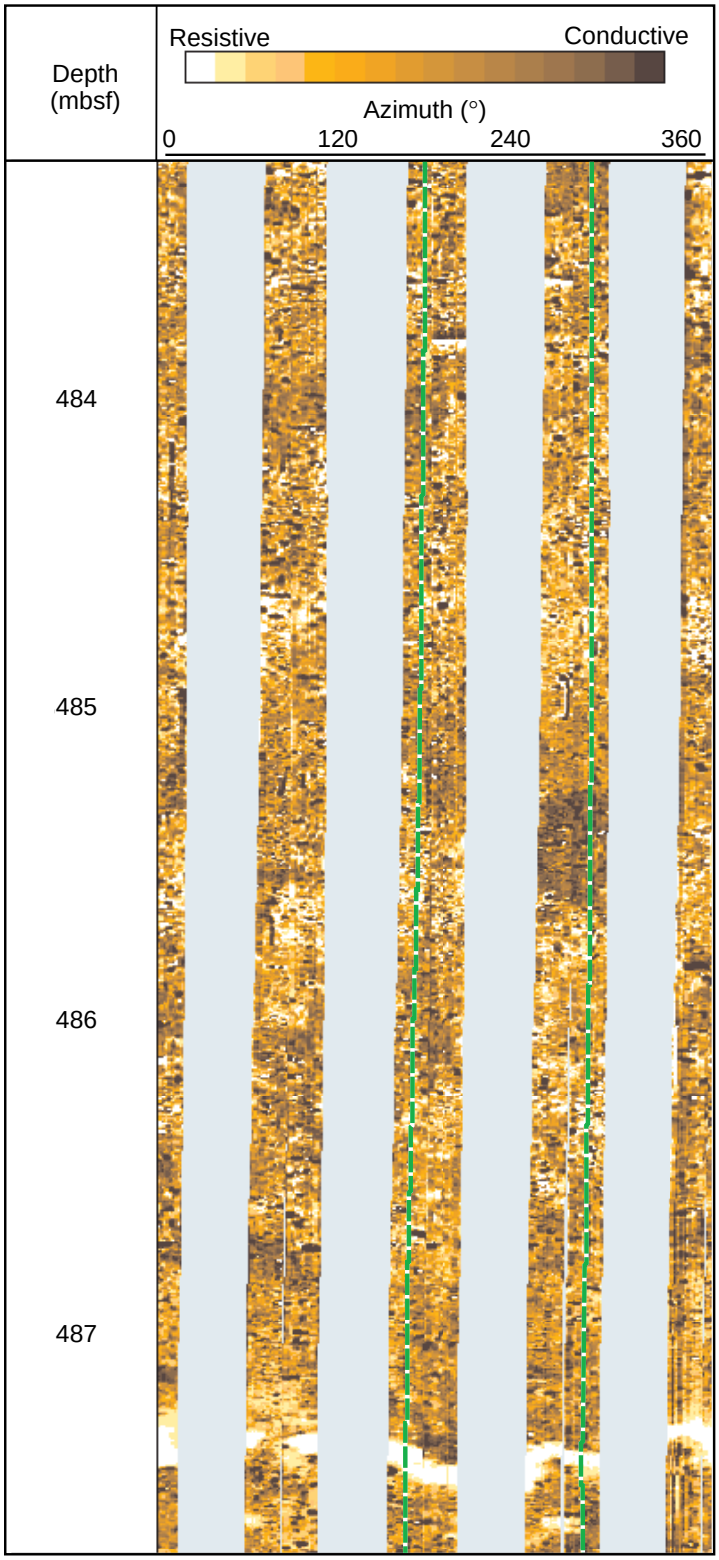

Figure F72. Hole 1115C statically (left) and dynamically (right) normalized FMS images of log Unit L7. The large increase in resistivity at 567.5 mbsf indicates a change from clayey to sandy or calcium carbonate–rich material. Vertical scale = 1:40.

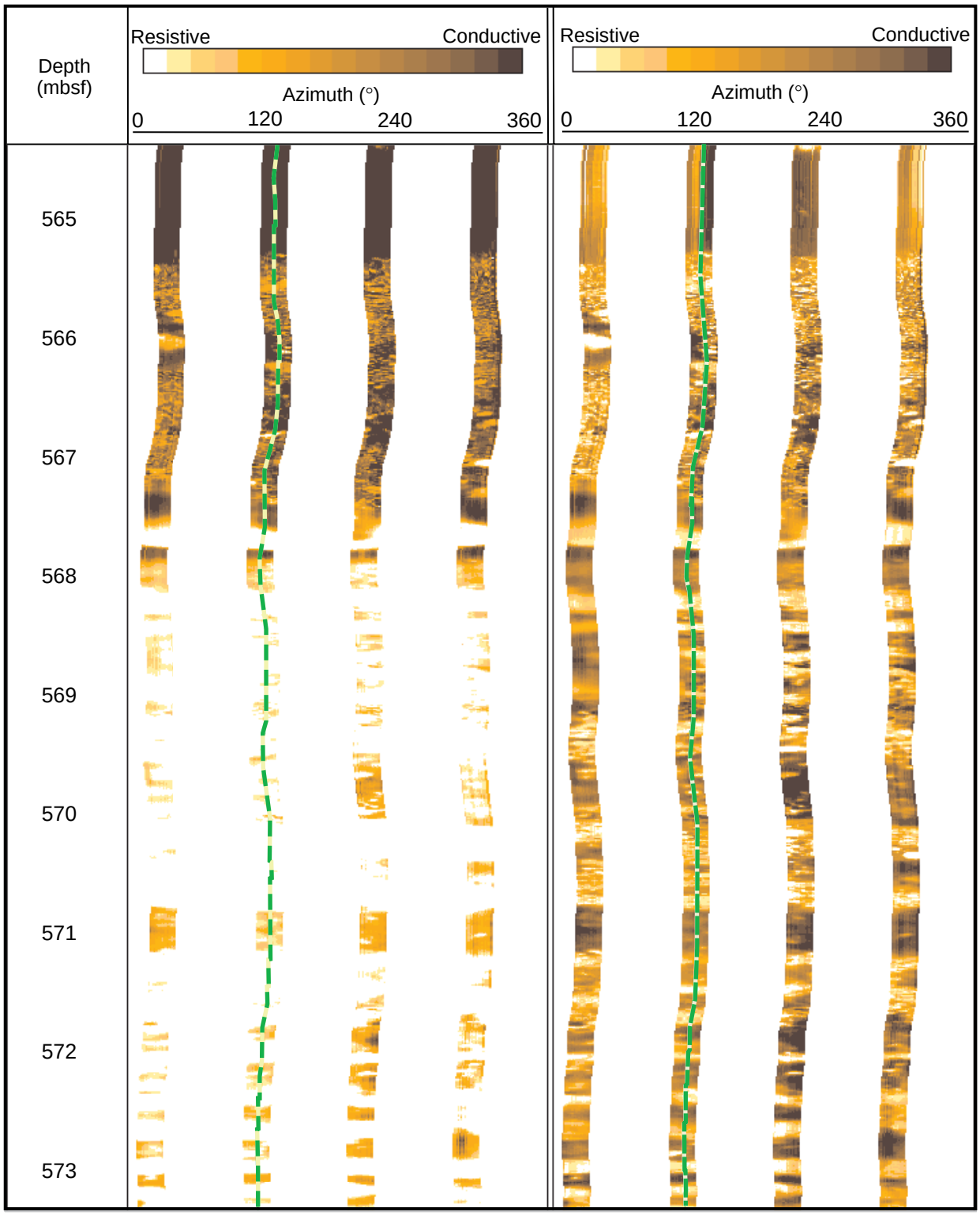

Figure F73. Hole 1115C dynamically normalized FMS image and tadpole plot of the fractured interval at the top of log Unit L9. This fracturing probably contributed to the poor core recovery within the interval between Cores 180-1115C-36R and 39R (620–658 mbsf). The fractures dip ~70° to the south. Vertical scale = 1:40.

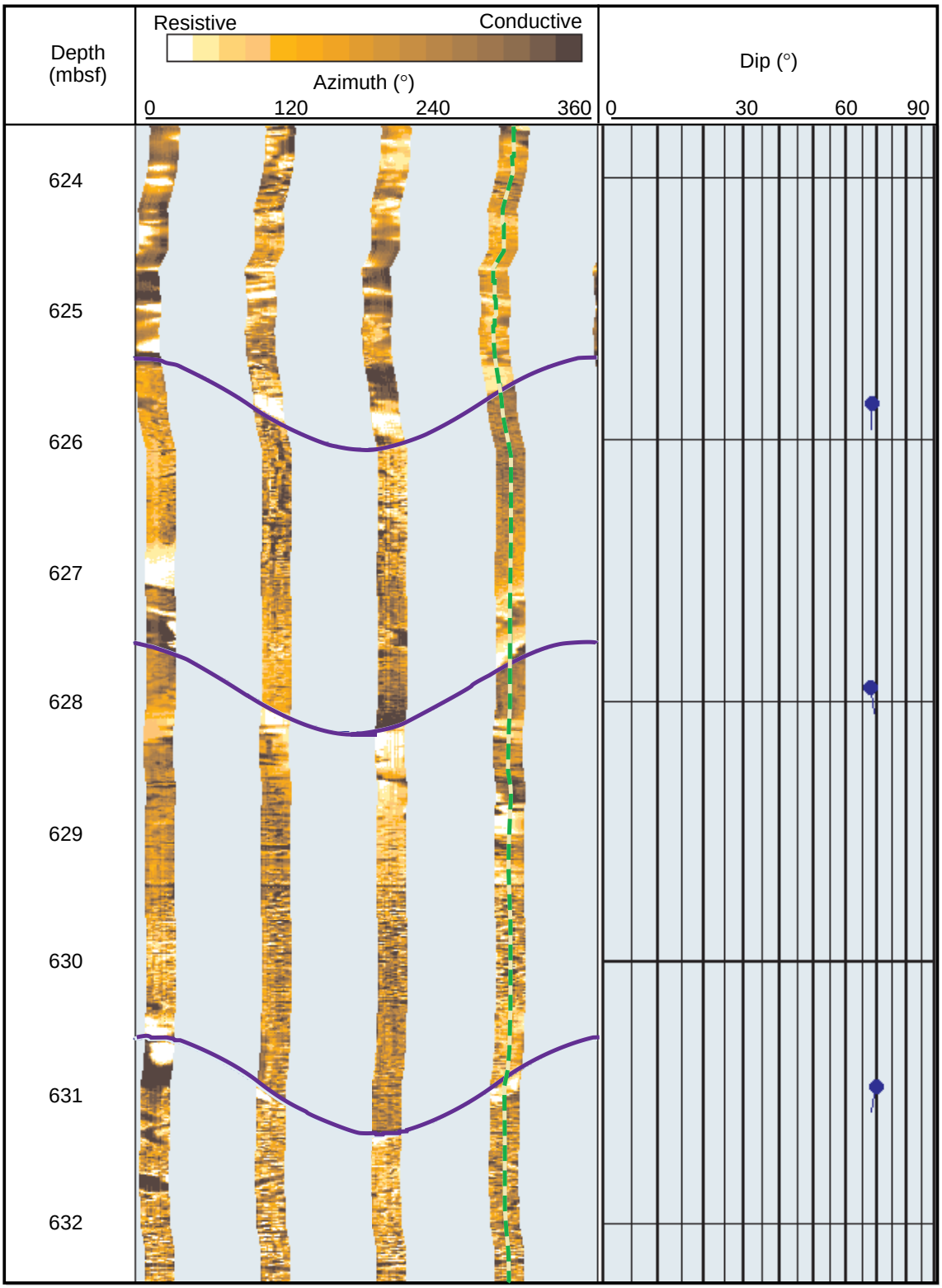

Figure F74. Hole 1115C dynamically normalized FMS image of the near vertical lines of low resistivity that follow the FMS pads through the lower portion of log Unit L9. The lines appear to be artificial and caused by either tool scraping from previous logging passes or the FMS pads dragging the more resistive material along the borehole. Vertical scale = 1:20.

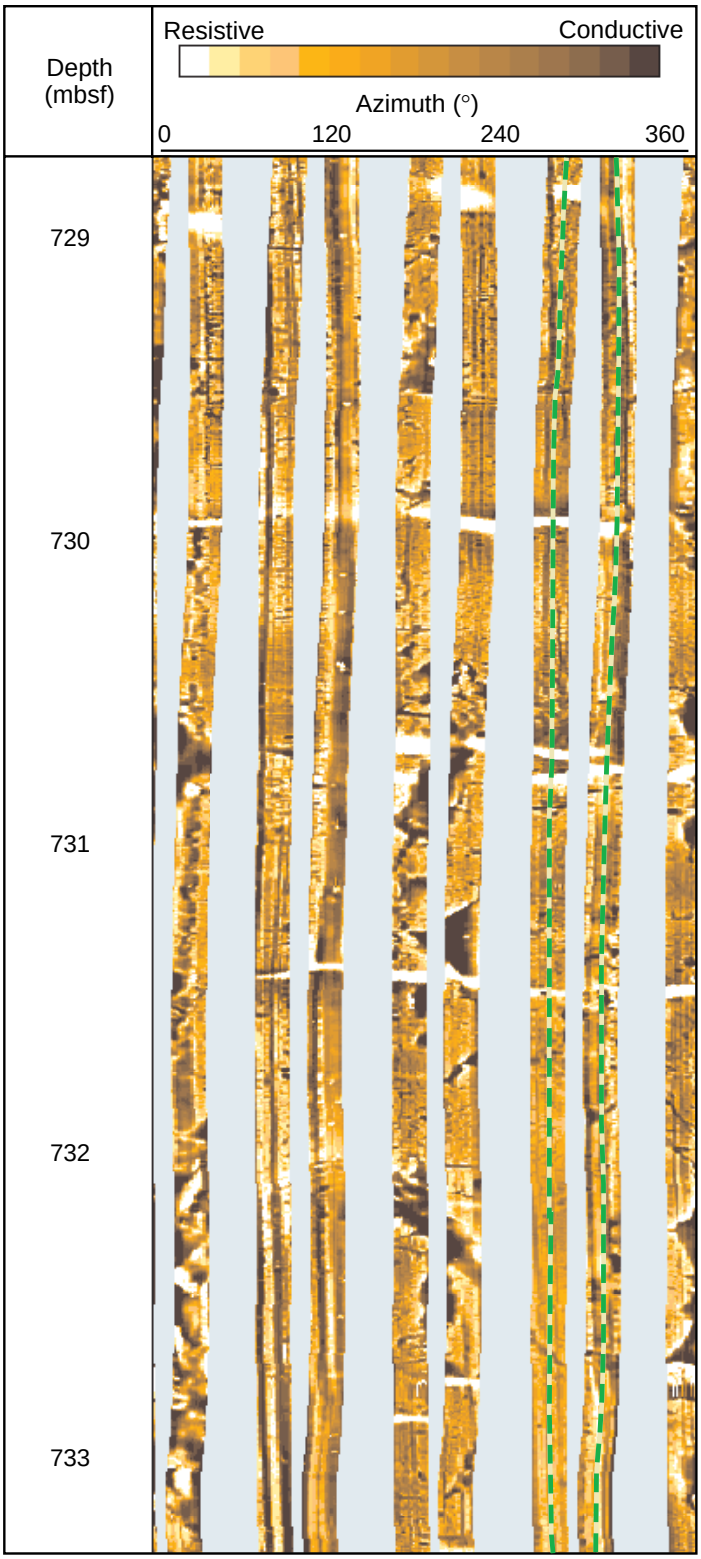

Figure F75. Temperature profile within and above Hole 1115C. T_{fast} and T_{slow} refer to the fast and slow thermistors, respectively. The log started on the way down 100 m above seafloor and continued until the tool reached the rig floor.

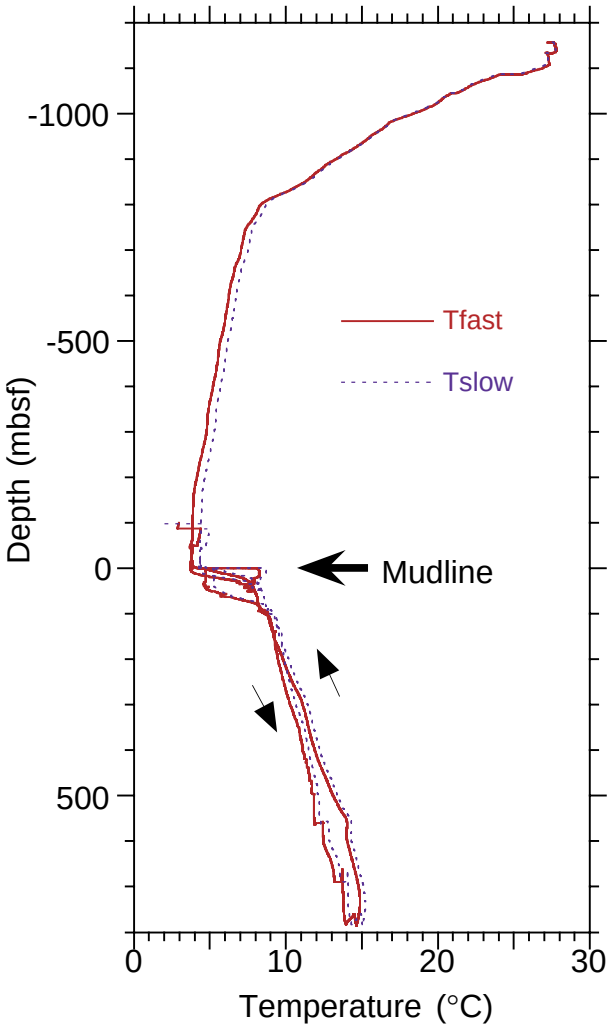

Figure F76. Temperature as a function of time for the Adara temperature tool runs at **A.** 26.2 mbsf; **B.** 45.2 mbsf; **C.** 64.2 mbsf; and **D.** 83.2 mbsf. Estimated mudline temperature is marked by a solid line, whereas extrapolated equilibrium temperatures are marked by a dashed line.

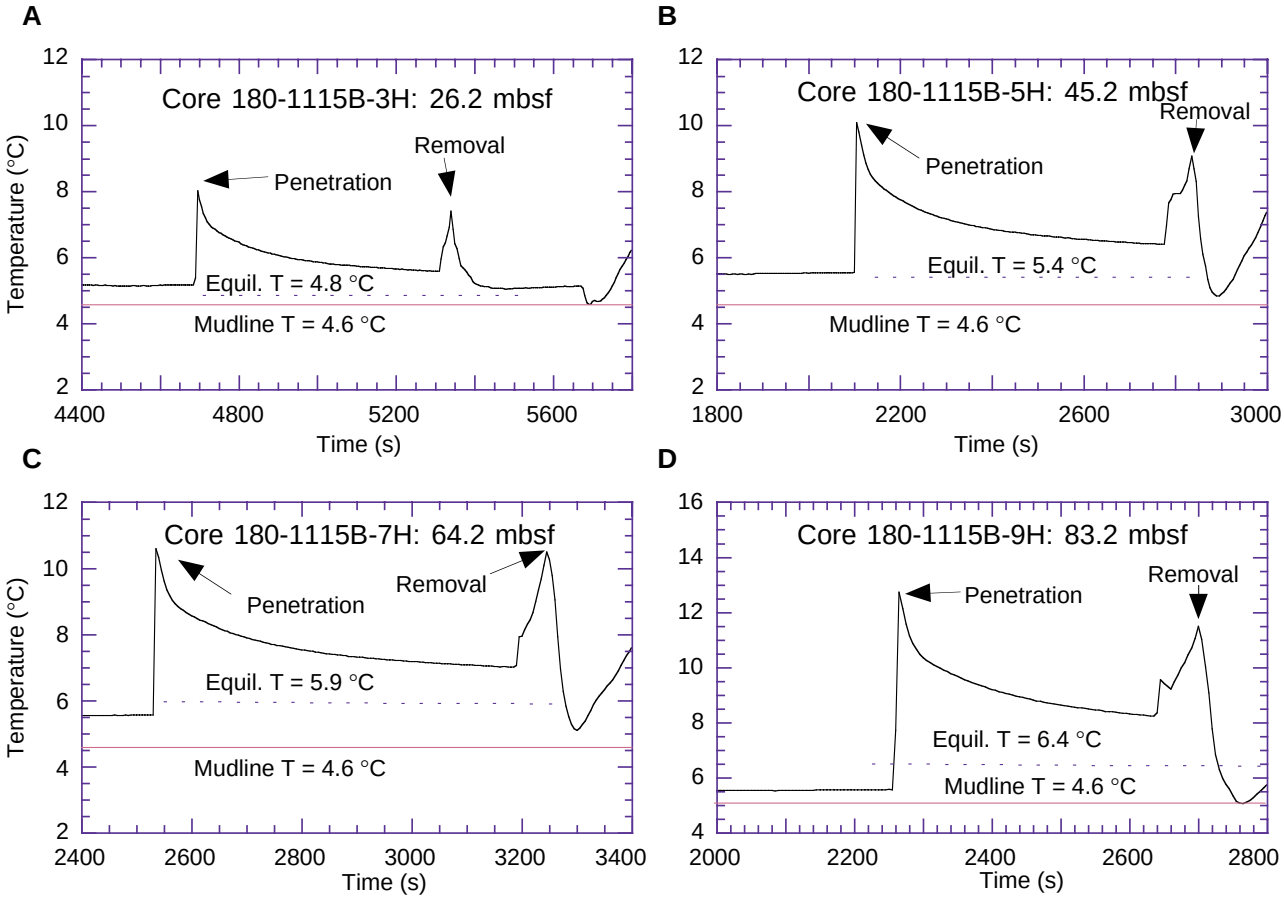

Figure F77. Temperature as a function of time for the DVTP temperature run at 226.9 mbsf. Data from tip thermistor was used. Estimated mudline temperature is marked by a solid line, whereas extrapolated equilibrium temperature is marked by a dashed line.

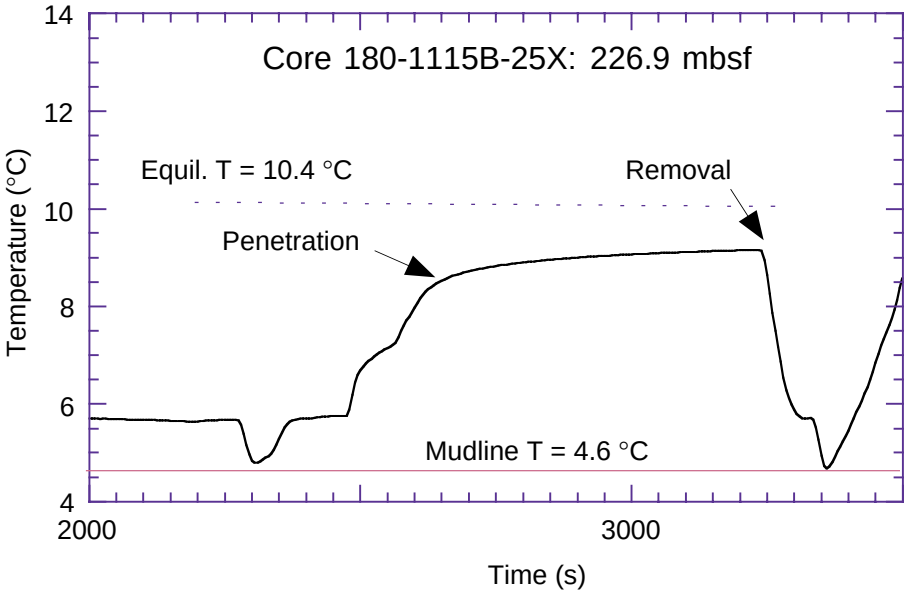

Figure F78. Estimated temperatures as a function of depth and best-fit linear regression with the mudline measurement (open square) excluded. Open circles = Adara measurements. Solid circle = DVTP measurement. Computed thermal gradient is the slope of the linear regression line.

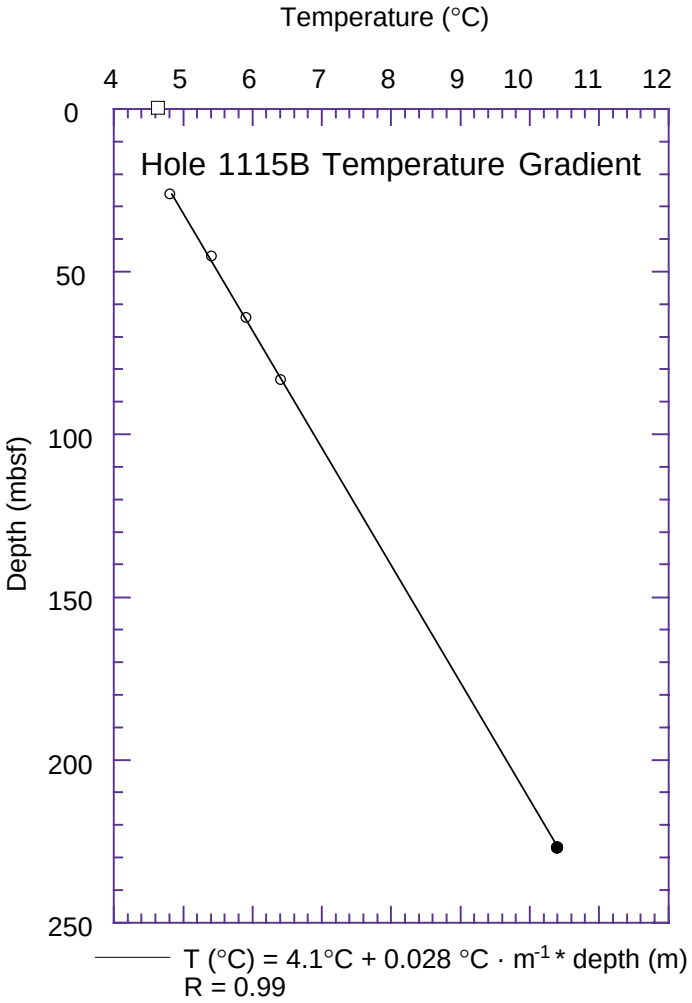

Figure F79. Depth vs. transit time for the Site 1115 VSP. The interval velocity was derived by fitting a straight line through the points and calculating the gradient.

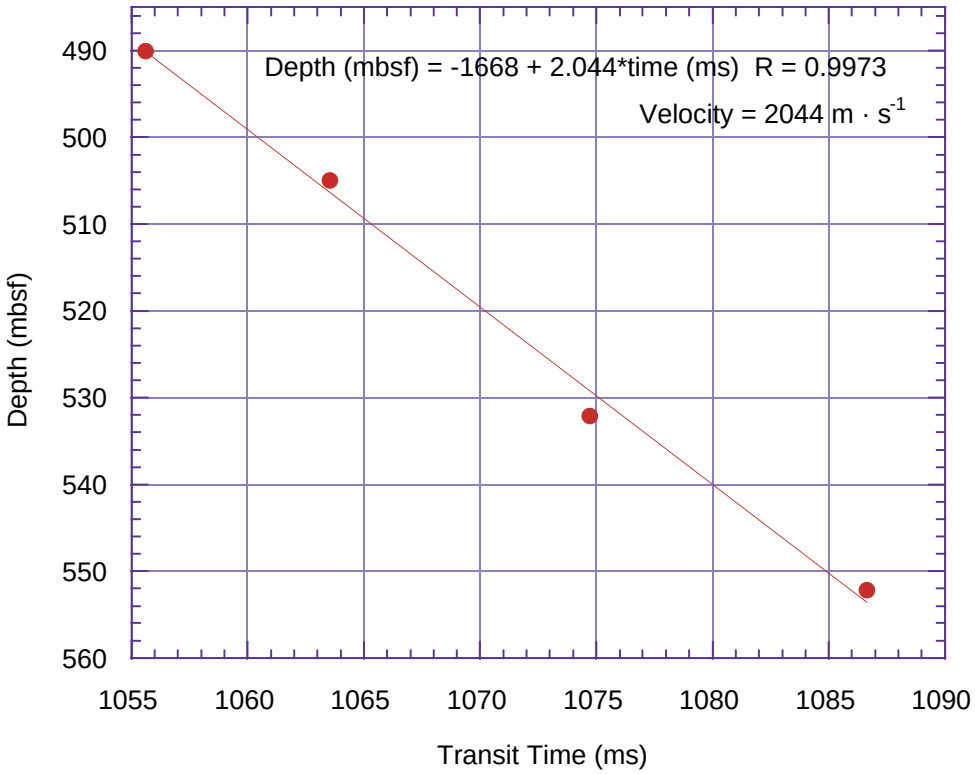

Figure F80. The velocity vs. depth function for Site 1115. Dots are sonic log velocities and crosses are from laboratory measurements. The black line defines the velocity function used.

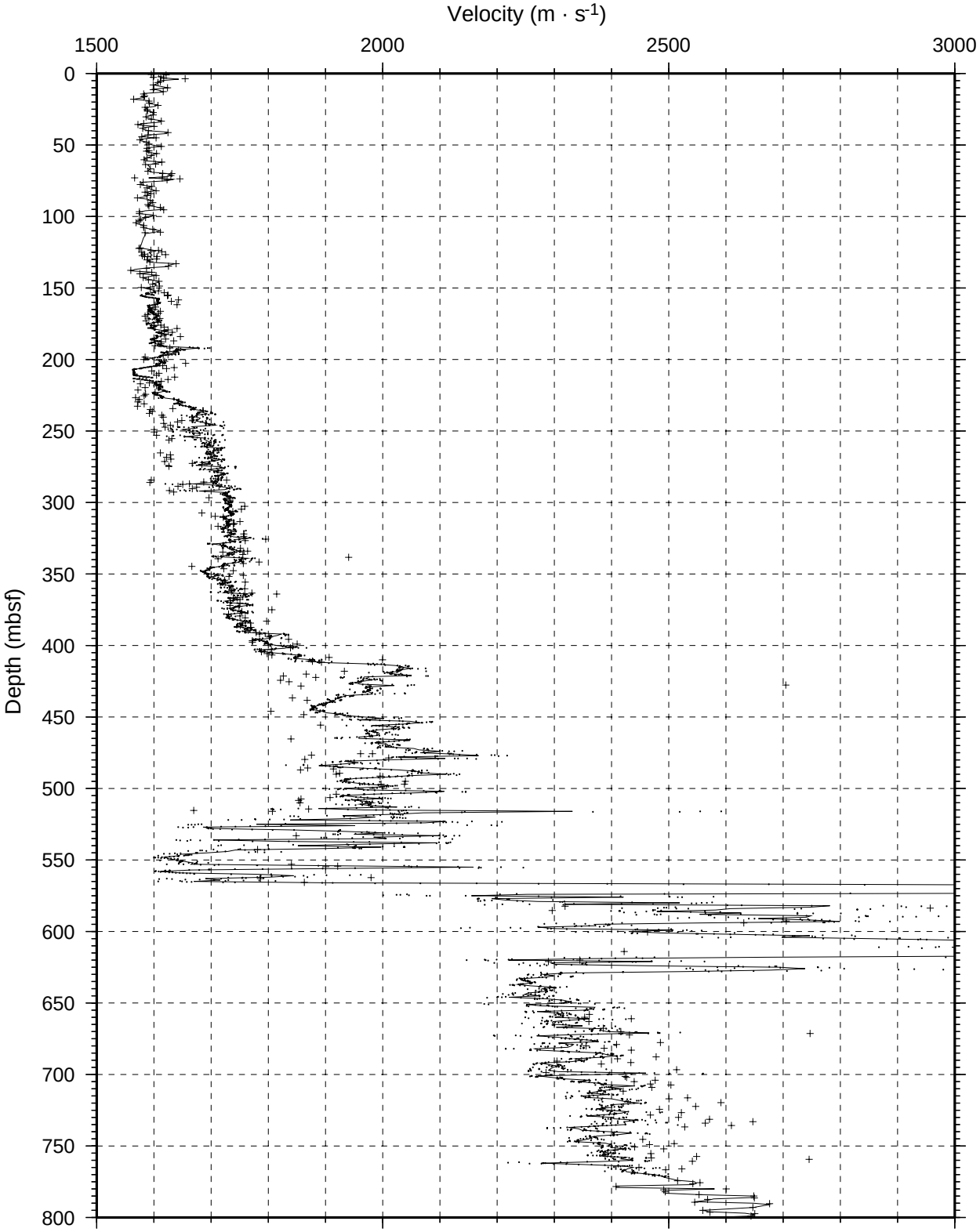

Figure F81. The density vs. depth function for Site 1115. Dots are log densities and crosses are from laboratory measurements. The black line defines the density function used.

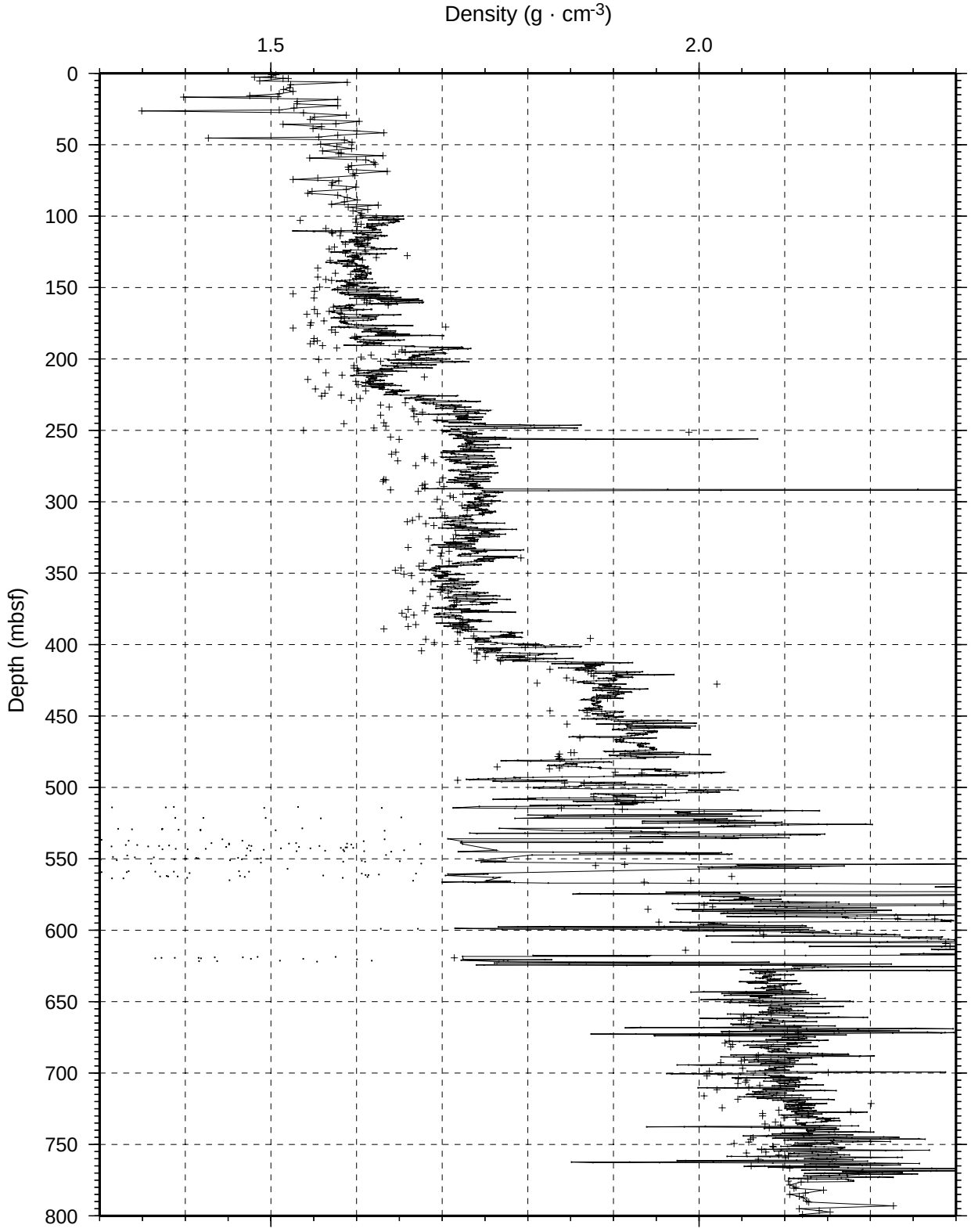

Figure F82. Depth-converted MCS data (left), synthetic seismic trace (syn), and reflection coefficient (rc). This compilation of data is derived from the density (blue/left) and velocity (red/right) data shown on the right.

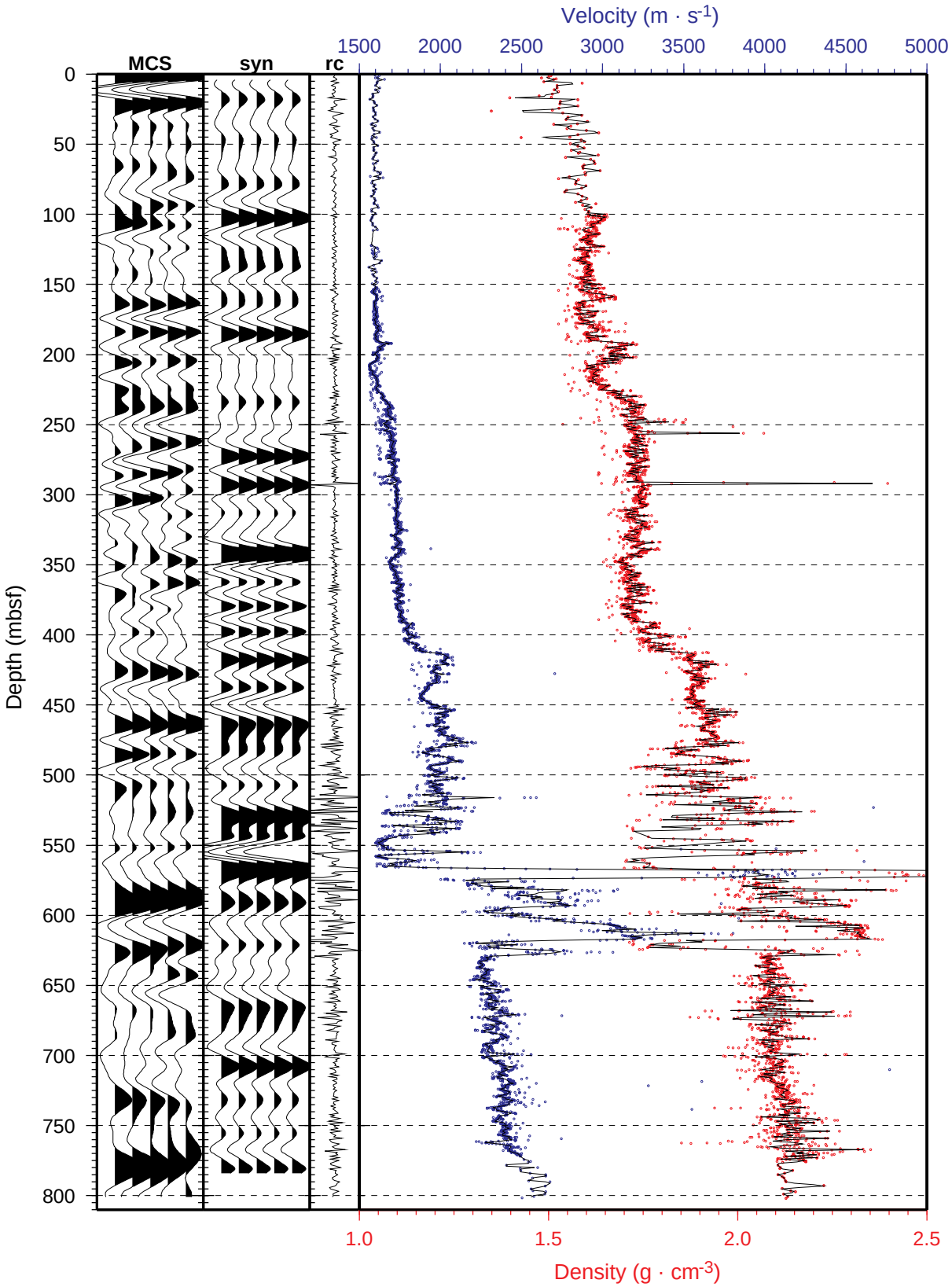

Figure F83. MCS Line EW9510-1366 cut at Site 1115. The five far right MCS traces have been depth converted and are displayed to the right with the lithostratigraphic column. Lines linking the time and depth data are spaced every 30 m. CMP = common midpoint.

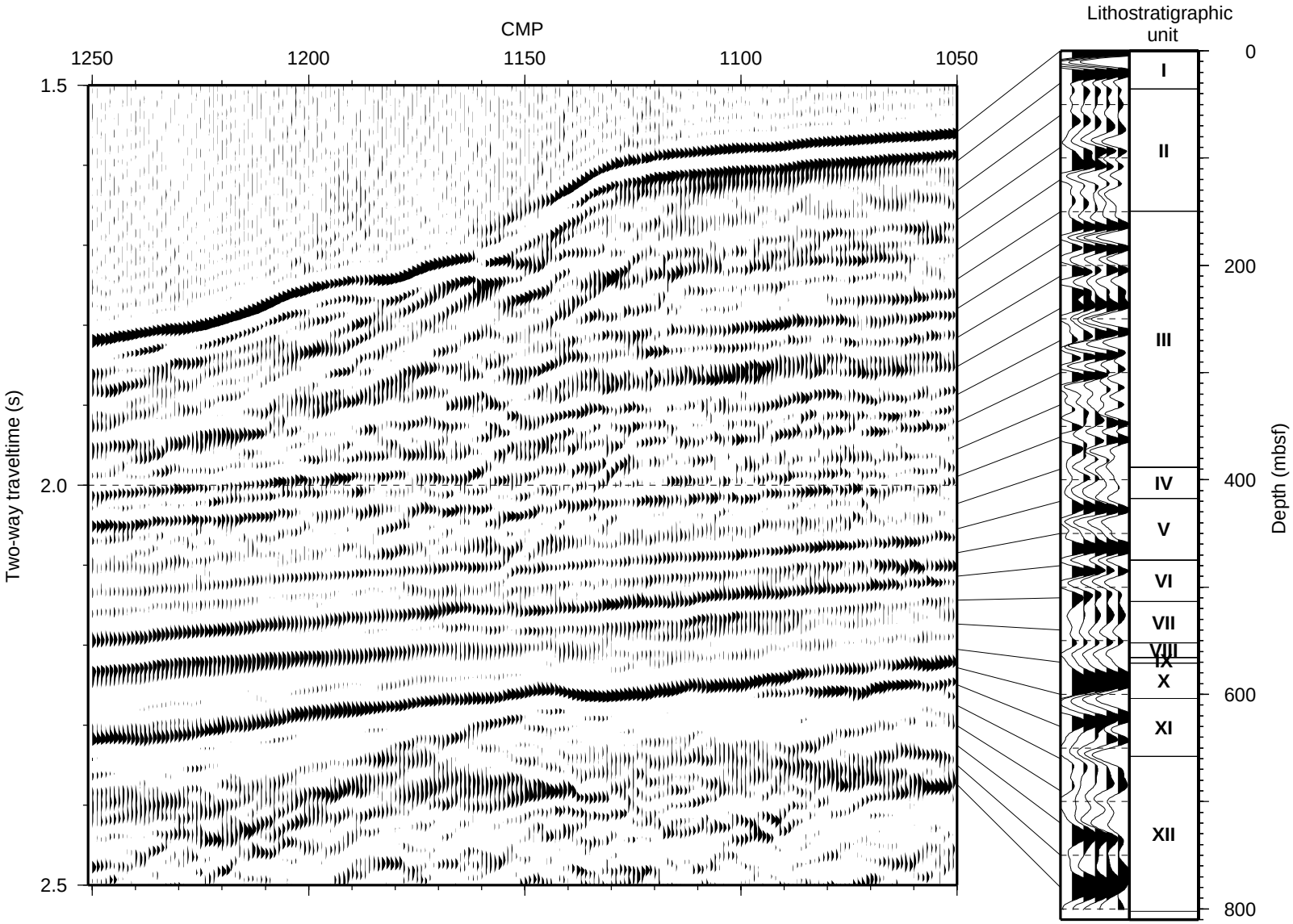

Table T1. Site 1115 coring summary. (Continued on next two pages.)

Hole 1115A

Latitude: 9°11.389′S
Longitude: 151°34.450′E
Seafloor (drill-pipe measurement from rig floor, mbrf): 1161.1
Distance between rig floor and sea level (m): 11.5
Water depth (drill-pipe measurement from sea level, m): 1149.6
Total depth (from rig floor, mbrf): 1165.5
Penetration (mbsf): 4.4
Total number of cores: 1
Total length of cored section (m): 4.4
Total core recovered (m): 4.43
Core recovery (%): 101

Core	Date (July 1998)	Time (UTC +10 hr)	Depth (mbsf)	Length cored (m)	Length recovered (m)	Recovery (%)	Comments
180-1115A-							
1H	16	1525	0.0-4.4	4.40	4.43	100.7	
Totals:				4.40	4.43	100.7	

Hole 1115B

Latitude: 9°11.382′S
Longitude: 151°34.437′E
Seafloor (drill-pipe measurement from rig floor, mbrf): 1160.3
Distance between rig floor and sea level (m): 11.5
Water depth (drill-pipe measurement from sea level, m): 1148.8
Total depth (from rig floor, mbrf): 1453.4
Penetration (mbsf): 293.1
Total number of cores: 1
Total length of cored section (m): 293.1
Total core recovered (m): 286.84
Core recovery (%): 98

Core	Date (July 1998)	Time (UTC +10 hr)	Depth (mbsf)	Length cored (m)	Length recovered (m)	Recovery (%)	Comments
180-1115B-							
1H	16	1550	0.0-7.2	7.2	7.14	99.2	
2H	16	1630	7.2-16.7	9.5	10.03	105.6	
3H	16	1730	16.7-26.2	9.5	10.21	107.5	
4H	16	1800	26.2-35.7	9.5	9.97	105.0	Tensor
5H	16	1850	35.7-45.2	9.5	10.13	106.6	Adara, Tensor
6H	16	1920	45.2-54.7	9.5	10.02	105.5	Tensor
7H	16	2025	54.7-64.2	9.5	9.99	105.2	Adara, Tensor
8H	16	2050	64.2-73.7	9.5	9.96	104.8	Tensor
9H	16	2130	73.7-83.2	9.5	10.07	106	Adara
10H	16	2205	83.2-92.7	9.5	9.75	102.6	Tensor
11H	16	2245	92.7-102.2	9.5	9.94	104.6	Tensor
12H	16	2320	102.2-111.7	9.5	9.70	102.1	Tensor
13H	17	0	111.7-121.2	9.5	9.86	103.8	Tensor
14H	17	30	121.2-130.7	9.5	9.82	103.4	Tensor
15H	17	105	130.7-140.2	9.5	9.85	103.7	Tensor
16H	17	135	140.2-149.7	9.5	10.02	105.5	Tensor
17H	17	210	149.7-159.2	9.5	10.00	105.3	Tensor
18H	17	240	159.2-168.7	9.5	9.99	105.2	Tensor
19H	17	310	168.7-178.2	9.5	9.98	105.1	Tensor
20H	17	350	178.2-187.7	9.5	9.98	105.1	Tensor
21H	17	420	187.7-197.2	9.5	9.72	102.3	Tensor
22H	17	450	197.2-206.7	9.5	9.59	101.0	Full stroke not indicated.
23H	17	530	206.7-216.2	9.5	9.95	104.7	Last Tensor, Last piston core.
24X	17	640	216.2-225.8	9.6	9.84	102.5	
25X	17	815	225.8-235.4	9.6	9.51	99.1	
26X	17	850	235.4-245.0	9.6	9.65	100.5	
27X	17	930	245.0-254.6	9.6	8.69	90.5	
28X	17	1025	254.6-264.3	9.7	2.24	23.1	Core dropped. Section 5A, 45-85 cm dropped and replaced in liner.
29X	17	1110	264.3-273.9	9.6	9.81	102.2	
30X	17	1210	273.9-283.5	9.6	1.53	15.9	
31X	17	1255	283.5-293.1	9.6	9.90	103.1	
Totals:				293.1	286.84	97.9	

Table T1 (continued).

Hole 1115C

Latitude: 9°11.383′S
Longitude: 151°34.422′E
Seafloor (drill-pipe measurement from rig floor, mbrf): 1160.3
Distance between rig floor and sea level (m): 11.6
Water depth (drill-pipe measurement from sea level, m): 1148.7
Total depth (from rig floor, mbrf): 1679.6
Penetration (mbsf): 802.5 (drilled without coring to 283.5 mbsf)
Total number of cores: 54
Total length of cored section (m): 519.3
Total core recovered (m): 291.63
Core recovery (%): 56

Core	Date (July 1998)	Time (UTC +10 hr)	Depth (mbsf)	Length cored (m)	Length recovered (m)	Recovery (%)	Comments
180-1115C-							
		*****Drilled from 0 to 283.2 mbsf*****					Drilled without coring
1R	18	0505	283.2-292.8	9.6	6.46	67.3	
2R	18	0610	292.8-302.5	9.7	6.40	66.0	
3R	18	0635	302.5-312.1	9.6	8.58	89.4	
4R	18	0735	312.1-321.7	9.6	5.27	54.9	
5R	18	0810	321.7-331.4	9.7	5.35	55.2	
6R	18	0850	331.4-341.0	9.6	8.89	92.6	
7R	18	0945	341.0-350.6	9.6	7.14	74.4	
8R	18	1030	350.6-359.9	9.3	6.95	74.7	
9R	18	1115	359.9-369.5	9.6	8.97	93.4	
10R	18	1155	369.5-379.1	9.6	8.76	91.3	
11R	18	1235	379.1-388.5	9.4	8.72	92.8	
12R	18	1320	388.5-398.1	9.6	9.36	97.5	
13R	18	1410	398.1-407.7	9.6	9.24	96.3	
14R	18	1450	407.7-417.3	9.6	4.40	45.8	
15R	18	1535	417.3-426.9	9.6	8.54	89.0	
16R	18	1620	426.9-436.5	9.6	1.78	18.5	
17R	18	1705	436.5-446.1	9.6	2.54	26.5	
18R	18	1755	446.1-455.6	9.5	2.65	27.9	
19R	18	1820	455.6-465.2	9.6	0.55	5.7	
20R	18	1925	465.2-474.9	9.7	0.74	7.6	
21R	18	2010	474.9-484.5	9.6	5.47	57.0	
22R	18	2105	484.5-494.1	9.6	7.07	73.7	
23R	18	2155	494.1-503.8	9.7	3.87	39.9	
24R	18	2240	503.8-513.4	9.6	7.30	76.0	
25R	18	2335	513.4-523.0	9.6	2.98	31.0	
26R	19	0025	523.0-532.6	9.6	0.65	6.8	
27R	19	0115	532.6-542.2	9.6	0.63	6.6	
28R	19	0220	542.2-551.8	9.6	0.95	9.9	
29R	19	0340	551.8-561.4	9.6	3.52	36.7	
30R	19	0600	561.4-571.0	9.6	5.60	58.3	
31R	19	0735	571.0-580.6	9.6	1.28	13.3	
32R	19	0900	580.6-590.2	9.6	4.91	51.2	
33R	19	1015	590.2-599.8	9.6	4.18	43.5	
34R	19	1115	599.8-609.4	9.6	4.29	44.7	
35R	19	1220	609.4-619.1	9.7	5.57	57.4	
36R	19	1415	619.1-628.8	9.7	2.91	30.0	
37R	19	1540	628.8-638.4	9.6	0.20	2.1	
38R	19	1720	638.4-648.1	9.7	0.00	0.0	No recovery
39R	19	1840	648.1-657.8	9.7	0.07	0.7	
40R	19	2035	657.8-667.4	9.6	6.41	66.8	
41R	19	2250	667.4-677.1	9.7	5.57	57.4	
42R	20	0015	677.1-686.8	9.7	5.96	61.4	
43R	20	0145	686.8-696.5	9.7	6.28	64.7	
44R	20	0315	696.5-706.1	9.6	9.45	98.4	
45R	20	0430	706.1-715.7	9.6	6.38	66.5	
46R	20	0610	715.7-725.4	9.7	9.39	96.8	
47R	20	0745	725.4-735.1	9.7	9.96	102.7	
48R	20	0910	735.1-744.7	9.6	3.89	40.5	
49R	20	1125	744.7-754.3	9.6	9.27	96.6	
50R	20	1335	754.3-763.9	9.6	6.64	69.2	
51R	20	1505	763.9-773.6	9.7	3.27	33.7	
52R	20	1710	773.6-783.2	9.6	9.33	97.2	
53R	20	1855	783.2-792.8	9.6	7.73	80.5	

Table T1 (continued).

Core	Date (July 1998)	Time (UTC +10 hr)	Depth (mbsf)	Length cored (m)	Length recovered (m)	Recovery (%)	Comments
54R	20	2100	792.8-802.5	9.7	9.36	96.5	
Totals:				519.3	291.63	56.2	

Note: UTC = Universal Time Coordinated.

Table T2. Site 1115 coring summary by section (continued on next 14 pages).

Core	Date (July 1998)	Time (UTC +10 hr)	Core depth (mbsf) Top	Core depth (mbsf) Bottom	Length (m) Cored	Length (m) Recovered	Recovery (%)	Section	Length (m) Liner	Length (m) Curated	Section depth (mbsf) Top	Section depth (mbsf) Bottom	Catwalk samples	Comment
180-1115A														
1H	16	1525	0.0	4.4	4.4	4.43	100.7							
								1	0.28	0.28	0.00	0.28	IW, WEL	
								2	1.22	1.22	0.28	1.50	WROG, WRMB	
								3	1.50	1.50	1.50	3.00	HS, IW, WEL	
								4	1.20	1.20	3.00	4.20	IW, WEL	
								CC	0.23	0.23	4.20	4.43	PAL	
									4.43	4.43				
				Totals:	4.4	4.43	100.7							
180-1115B														
1H	16	1550	0.0	7.2	7.2	7.14	99.2							
								1	1.50	1.50	0.00	1.50		
								2	1.50	1.50	1.50	3.00		
								3	1.50	1.50	3.00	4.50		
								4	1.50	1.50	4.50	6.00		
								5	0.97	0.97	6.00	6.97		
								CC	0.17	0.17	6.97	7.14	PAL	
									7.14	7.14				
2H	16	1630	7.2	16.7	9.5	10.03	105.6							
								1	1.50	1.50	7.20	8.70	IW	
								2	1.50	1.50	8.70	10.20	WEL	
								3	1.50	1.50	10.20	11.70	HS	
								4	1.50	1.50	11.70	13.20		
								5	1.50	1.50	13.20	14.70		
								6	1.50	1.50	14.70	16.20		
								7	0.68	0.68	16.20	16.88		
								CC	0.35	0.35	16.88	17.23	PAL	
									10.03	10.03				
3H	16	1730	16.7	26.2	9.5	10.21	107.5							
								1	1.50	1.50	16.70	18.20		
								2	1.50	1.50	18.20	19.70		
								3	1.50	1.50	19.70	21.20	IW, WROG, WRMB	
								4	1.50	1.50	21.20	22.70	WEL	
								5	1.50	1.50	22.70	24.20		
								6	1.50	1.50	24.20	25.70	HS	
								7	0.75	0.75	25.70	26.45		
								CC	0.46	0.46	26.45	26.91	PAL	
									10.21	10.21				
4H	16	1800	26.2	35.7	9.5	9.97	104.9							
								1	1.50	1.50	26.20	27.70	IW	
								2	1.50	1.50	27.70	29.20	HS, WEL	
								3	1.50	1.50	29.20	30.70		
								4	1.50	1.50	30.70	32.20		
								5	1.50	1.50	32.20	33.70		
								6	1.50	1.50	33.70	35.20		
								7	0.71	0.71	35.20	35.91		
								CC	0.26	0.26	35.91	36.17	PAL	
									9.97	9.97				

Table T2 (continued).

Core	Date (July 1998)	Time (UTC +10 hr)	Core depth (mbsf) Top	Core depth (mbsf) Bottom	Length (m) Cored	Length (m) Recovered	Recovery (%)	Section	Length (m) Liner	Length (m) Curated	Section depth (mbsf) Top	Section depth (mbsf) Bottom	Catwalk samples	Comment
5H	16	1850	35.7	45.2	9.5	10.13	106.6							
								1	1.50	1.50	35.70	37.20	IW	
								2	1.50	1.50	37.20	38.70	HS, WEL	
								3	1.50	1.50	38.70	40.20		
								4	1.50	1.50	40.20	41.70		
								5	1.50	1.50	41.70	43.20		
								6	1.50	1.50	43.20	44.70		
								7	0.70	0.70	44.70	45.40		
								CC	0.43	0.43	45.40	45.83	PAL	
									10.13	10.13				
6H	16	1920	45.2	54.7	9.5	10.02	105.5							
								1	1.50	1.50	45.20	46.70	IW	
								2	1.50	1.50	46.70	48.20	HS, WEL	
								3	1.50	1.50	48.20	49.70		
								4	1.50	1.50	49.70	51.20		
								5	1.50	1.50	51.20	52.70		
								6	1.50	1.50	52.70	54.20		
								7	0.76	0.76	54.20	54.96		
								CC	0.26	0.26	54.96	55.22	PAL	
									10.02	10.02				
7H	16	2025	54.7	64.2	9.5	9.99	105.2							
								1	1.50	1.50	54.70	56.20	IW	
								2	1.50	1.50	56.20	57.70	HS, WEL	
								3	1.50	1.50	57.70	59.20		
								4	1.50	1.50	59.20	60.70		
								5	1.50	1.50	60.70	62.20		
								6	1.50	1.50	62.20	63.70		
								7	0.54	0.54	63.70	64.24		
								CC	0.45	0.45	64.24	64.69	PAL	
									9.99	9.99				
8H	16	2050	64.2	73.7	9.5	9.96	104.8							
								1	1.50	1.50	64.20	65.70	IW	
								2	1.50	1.50	65.70	67.20	HS, WEL	
								3	1.50	1.50	67.20	68.70		
								4	1.50	1.50	68.70	70.20		
								5	1.50	1.50	70.20	71.70		
								6	1.50	1.50	71.70	73.20		
								7	0.65	0.65	73.20	73.85		
								CC	0.31	0.31	73.85	74.16	PAL	
									9.96	9.96				
9H	16	2130	73.7	83.2	9.5	10.07	106.0							
								1	1.50	1.50	73.70	75.20		
								2	1.50	1.50	75.20	76.70		
								3	1.50	1.50	76.70	78.20	HS, IW	
								4	1.50	1.50	78.20	79.70	WEL	
								5	1.50	1.50	79.70	81.20		
								6	1.50	1.50	81.20	82.70		
								7	0.63	0.63	82.70	83.33		

Table T2 (continued).

Core	Date (July 1998)	Time (UTC +10 hr)	Core depth (mbsf) Top	Core depth (mbsf) Bottom	Length (m) Cored	Length (m) Recovered	Recovery (%)	Section	Length (m) Liner	Length (m) Curated	Section depth (mbsf) Top	Section depth (mbsf) Bottom	Catwalk samples	Comment
								CC	0.44	0.44	83.33	83.77	PAL	
									10.07	10.07				
10H	16	2205	83.2	92.7	9.5	9.75	102.6							
								1	1.50	1.50	83.20	84.70		
								2	1.50	1.50	84.70	86.20		
								3	1.50	1.50	86.20	87.70	WROG, WRMB, IW	
								4	1.50	1.50	87.70	89.20	HS, WEL	
								5	1.50	1.50	89.20	90.70		
								6	1.50	1.50	90.70	92.20		
								7	0.46	0.46	92.20	92.66		
								CC	0.29	0.29	92.66	92.95	PAL	
									9.75	9.75				
11H	16	2245	92.7	102.2	9.5	9.94	104.6							
								1	1.50	1.50	92.70	94.20	IW	
								2	1.50	1.50	94.20	95.70	HS	
								3	1.50	1.50	95.70	97.20		
								4	1.50	1.50	97.20	98.70		
								5	1.50	1.50	98.70	100.20		
								6	1.50	1.50	100.20	101.70	WRSCR	
								7	0.60	0.60	101.70	102.30		
								CC	0.34	0.34	102.30	102.64	PAL	
									9.94	9.94				
12H	16	2320	102.2	111.7	9.5	9.70	102.1							
								1	1.50	1.50	102.20	103.70	IW	
								2	1.50	1.50	103.70	105.20	HS, WEL	
								3	1.50	1.50	105.20	106.70		
								4	1.50	1.50	106.70	108.20		
								5	1.50	1.50	108.20	109.70		
								6	1.50	1.50	109.70	111.20		
								7	0.39	0.39	111.20	111.59		
								CC	0.31	0.31	111.59	111.90	PAL	
									9.70	9.70				
13H	17	0000	111.7	121.2	9.5	9.86	103.8							
								1	1.50	1.50	111.70	113.20	IW	
								2	1.50	1.50	113.20	114.70	HS	
								3	1.50	1.50	114.70	116.20		
								4	1.50	1.50	116.20	117.70		
								5	1.50	1.50	117.70	119.20		
								6	1.50	1.50	119.20	120.70		
								7	0.55	0.55	120.70	121.25		
								CC	0.31	0.31	121.25	121.56	PAL	
									9.86	9.86				
14H	17	0030	121.2	130.7	9.5	9.82	103.4							
								1	1.50	1.50	121.20	122.70	IW	
								2	1.50	1.50	122.70	124.20	HS, WEL	
								3	1.50	1.50	124.20	125.70		
								4	1.50	1.50	125.70	127.20		
								5	1.50	1.50	127.20	128.70		

Table T2 (continued).

Core	Date (July 1998)	Time (UTC +10 hr)	Core depth (mbsf) Top	Core depth (mbsf) Bottom	Length (m) Cored	Length (m) Recovered	Recovery (%)	Section	Length (m) Liner	Length (m) Curated	Section depth (mbsf) Top	Section depth (mbsf) Bottom	Catwalk samples	Comment
								6	1.50	1.50	128.70	130.20		
								7	0.60	0.60	130.20	130.80		
								CC	0.22	0.22	130.80	131.02	PAL	
									9.82	9.82				
15H	17	0105	130.7	140.2	9.5	9.85	103.7							
								1	1.50	1.50	130.70	132.20	IW	
								2	1.50	1.50	132.20	133.70	HS	
								3	1.50	1.50	133.70	135.20		
								4	1.50	1.50	135.20	136.70		
								5	1.50	1.50	136.70	138.20		
								6	1.50	1.50	138.20	139.70		
								7	0.66	0.66	139.70	140.36		
								CC	0.19	0.19	140.36	140.55	PAL	
									9.85	9.85				
16H	17	0135	140.2	149.7	9.5	10.02	105.5							
								1	1.50	1.50	140.20	141.70		
								2	1.50	1.50	141.70	143.20	IW	
								3	1.50	1.50	143.20	144.70	HS, WEL	
								4	1.50	1.50	144.70	146.20		
								5	1.50	1.50	146.20	147.70		
								6	1.50	1.50	147.70	149.20		
								7	0.69	0.69	149.20	149.89		
								CC	0.33	0.33	149.89	150.22	PAL	
									10.02	10.02				
17H	17	0210	149.7	159.2	9.5	10.00	105.3							
								1	1.50	1.50	149.70	151.20	IW	
								2	1.50	1.50	151.20	152.70	HS	
								3	1.50	1.50	152.70	154.20		
								4	1.50	1.50	154.20	155.70		
								5	1.50	1.50	155.70	157.20		
								6	1.50	1.50	157.20	158.70		
								7	0.75	0.75	158.70	159.45		
								CC	0.25	0.25	159.45	159.70	PAL	
									10.00	10.00				
18H	17	0240	159.2	168.7	9.5	9.99	105.2							
								1	1.50	1.50	159.20	160.70		
								2	1.50	1.50	160.70	162.20	HS, WROG, WRMB, IW	
								3	1.50	1.50	162.20	163.70	WEL	
								4	1.50	1.50	163.70	165.20		
								5	1.50	1.50	165.20	166.70		
								6	1.50	1.50	166.70	168.20		
								7	0.71	0.71	168.20	168.91		
								CC	0.28	0.28	168.91	169.19	PAL	
									9.99	9.99				
19H	17	0310	168.7	178.2	9.5	9.98	105.1							
								1	1.50	1.50	168.70	170.20	IW	
								2	1.50	1.50	170.20	171.70	HS	
								3	1.50	1.50	171.70	173.20		

Table T2 (continued).

Core	Date (July 1998)	Time (UTC +10 hr)	Core depth (mbsf) Top	Core depth (mbsf) Bottom	Length (m) Cored	Length (m) Recovered	Recovery (%)	Section	Length (m) Liner	Length (m) Curated	Section depth (mbsf) Top	Section depth (mbsf) Bottom	Catwalk samples	Comment
								4	1.50	1.50	173.20	174.70		
								5	1.50	1.50	174.70	176.20		
								6	1.50	1.50	176.20	177.70		
								7	0.74	0.74	177.70	178.44		
								CC	0.24	0.24	178.44	178.68	PAL	
									9.98	9.98				
20H	17	0350	178.2	187.7	9.5	9.98	105.1							
								1	1.50	1.50	178.20	179.70	IW	
								2	1.50	1.50	179.70	181.20	HS, WEL	
								3	1.50	1.50	181.20	182.70		
								4	1.50	1.50	182.70	184.20		
								5	1.50	1.50	184.20	185.70		
								6	1.50	1.50	185.70	187.20		
								7	0.71	0.71	187.20	187.91		
								CC	0.27	0.27	187.91	188.18	PAL	
									9.98	9.98				
21H	17	0420	187.7	197.2	9.5	9.72	102.3							
								1	1.50	1.50	187.70	189.20	IW	
								2	1.50	1.50	189.20	190.70	HS	
								3	1.50	1.50	190.70	192.20		
								4	1.50	1.50	192.20	193.70		
								5	1.50	1.50	193.70	195.20		
								6	1.50	1.50	195.20	196.70		
								7	0.45	0.45	196.70	197.15		
								CC	0.27	0.27	197.15	197.42	PAL	
									9.72	9.72				
22H	17	0450	197.2	206.7	9.5	9.59	100.9							Full stroke not indicated
								1	1.50	1.50	197.20	198.70	IW	
								2	1.50	1.50	198.70	200.20	HS, WEL	
								3	1.50	1.50	200.20	201.70		
								4	1.44	1.44	201.70	203.14	WRSCR	
								5	1.50	1.50	203.14	204.64		
								6	1.50	1.50	204.64	206.14		
								7	0.36	0.36	206.14	206.50		
								CC	0.29	0.29	206.50	206.79	PAL	
									9.59	9.59				
23H	17	0530	206.7	216.2	9.5	9.95	104.7							Last tensor; last APC core
								1	1.50	1.50	206.70	208.20	IW	
								2	1.50	1.50	208.20	209.70	HS	
								3	1.50	1.50	209.70	211.20		
								4	1.50	1.50	211.20	212.70		
								5	1.50	1.50	212.70	214.20		
								6	1.50	1.50	214.20	215.70		
								7	0.68	0.68	215.70	216.38		
								CC	0.27	0.27	216.38	216.65	PAL	
									9.95	9.95				
24X	17	0640	216.2	225.8	9.6	9.84	102.5							
								1	1.50	1.50	216.20	217.70	IW	

Table T2 (continued).

Core	Date (July 1998)	Time (UTC +10 hr)	Core depth (mbsf) Top	Core depth (mbsf) Bottom	Length (m) Cored	Length (m) Recovered	Recovery (%)	Section	Length (m) Liner	Length (m) Curated	Section depth (mbsf) Top	Section depth (mbsf) Bottom	Catwalk samples	Comment
								2	1.50	1.50	217.70	219.20	WEL	
								3	1.30	1.30	219.20	220.50	HS	
								4	1.50	1.50	220.50	222.00		
								5	1.50	1.50	222.00	223.50		
								6	1.20	1.20	223.50	224.70		
								7	0.98	0.98	224.70	225.68		
								CC	0.36	0.36	225.68	226.04	PAL	
									9.84	9.84				
25X	17	0815	225.8	235.4	9.6	9.51	99.1							
								1	1.50	1.50	225.80	227.30	IW	
								2	1.50	1.50	227.30	228.80		
								3	1.50	1.50	228.80	230.30	HS	
								4	1.50	1.50	230.30	231.80		
								5	1.50	1.50	231.80	233.30		
								6	1.50	1.50	233.30	234.80		
								7	0.31	0.31	234.80	235.11		
								CC	0.20	0.20	235.11	235.31	PAL	
									9.51	9.51				
26X	17	0850	235.4	245.0	9.6	9.65	100.5							
								1	1.50	1.50	235.40	236.90	IW, WROG, WRMB	
								2	1.50	1.50	236.90	238.40	WEL	
								3	1.50	1.50	238.40	239.90	HS	
								4	1.50	1.50	239.90	241.40		
								5	1.50	1.50	241.40	242.90		
								6	1.30	1.30	242.90	244.20		
								7	0.51	0.51	244.20	244.71		
								CC	0.34	0.34	244.71	245.05	PAL	
									9.65	9.65				
27X	17	0930	245.0	254.6	9.6	8.69	90.5							
								1	1.50	1.50	245.00	246.50	IW	
								2	1.50	1.50	246.50	248.00	HS	
								3	1.50	1.50	248.00	249.50		
								4	1.50	1.50	249.50	251.00		
								5	1.50	1.50	251.00	252.50		
								6	0.85	0.85	252.50	253.35		
								CC	0.34	0.34	253.35	253.69	PAL	
									8.69	8.69				
28X	17	1025	254.6	264.3	9.7	2.24	23.1							
								1	1.50	1.50	254.60	256.10	HS, IW	
								2	0.45	0.45	256.10	256.55	WEL	
								CC	0.29	0.29	256.55	256.84	PAL	
									2.24	2.24				
29X	17	1110	264.3	273.9	9.6	9.81	102.2							Section 5(A), 45-85 cm, dropped and replaced in liner
								1	1.50	1.50	264.30	265.80	IW	
								2	1.50	1.50	265.80	267.30	HS	
								3	1.50	1.50	267.30	268.80		
								4	1.50	1.50	268.80	270.30		

Table T2 (continued).

Core	Date (July 1998)	Time (UTC +10 hr)	Core depth (mbsf) Top	Core depth (mbsf) Bottom	Length (m) Cored	Length (m) Recovered	Recovery (%)	Section	Length (m) Liner	Length (m) Curated	Section depth (mbsf) Top	Section depth (mbsf) Bottom	Catwalk samples	Comment
								5	1.50	1.50	270.30	271.80		
								6	1.50	1.50	271.80	273.30		
								7	0.46	0.46	273.30	273.76		
								CC	0.35	0.35	273.76	274.11	PAL	
									9.81	9.81				
30X	17	1210	273.9	283.5	9.6	1.53	15.9							
								1	1.07	1.07	273.90	274.97	HS	
								CC	0.46	0.46	274.97	275.43	PAL	
									1.53	1.53				
31X	17	1255	283.5	293.1	9.6	9.90	103.1							
								1	1.50	1.50	283.50	285.00		
								2	1.50	1.50	285.00	286.50	IW	
								3	1.50	1.50	286.50	288.00	WEL	
								4	1.50	1.50	288.00	289.50		
								5	1.50	1.50	289.50	291.00	HS	
								6	1.50	1.50	291.00	292.50		
								7	0.49	0.49	292.50	292.99		
								CC	0.41	0.41	292.99	293.40	PAL	
									9.90	9.90				
				Totals:	293.1	286.84	97.9							
180-1115C														
Drilled from 0.0 to 283.2 mbsf														Drilled interval
1R	18	0505	283.2	292.8	9.6	6.46	67.3							
								1	1.42	1.42	283.20	284.62		
								2	1.46	1.46	284.62	286.08		
								3	1.50	1.50	286.08	287.58		
								4	1.50	1.50	287.58	289.08	HS	
								5	0.41	0.41	289.08	289.49		
								CC	0.17	0.17	289.49	289.66	PAL	
									6.46	6.46				
2R	18	0610	292.8	302.5	9.7	6.40	66.0							
								1	1.50	1.50	292.80	294.30	IW	
								2	1.50	1.50	294.30	295.80	HS	
								3	0.39	0.39	295.80	296.19	WRSCR	
								4	1.50	1.50	296.19	297.69		
								5	1.34	1.34	297.69	299.03		
								CC	0.17	0.17	299.03	299.20	PAL	
									6.40	6.40				
3R	18	0635	302.5	312.1	9.6	8.58	89.4							
								1	1.50	1.50	302.50	304.00		
								2	1.50	1.50	304.00	305.50		
								3	1.50	1.50	305.50	307.00	HS	
								4	1.50	1.50	307.00	308.50		
								5	1.50	1.50	308.50	310.00	IW, WROG, WRMB	
								6	0.71	0.71	310.00	310.71	WEL	
								CC	0.37	0.37	310.71	311.08	PAL	
									8.58	8.58				

Table T2 (continued).

Core	Date (July 1998)	Time (UTC +10 hr)	Core depth (mbsf) Top	Core depth (mbsf) Bottom	Length (m) Cored	Length (m) Recovered	Recovery (%)	Section	Length (m) Liner	Length (m) Curated	Section depth (mbsf) Top	Section depth (mbsf) Bottom	Catwalk samples	Comment
4R	18	0735	312.1	321.7	9.6	5.27	54.9							
								1	1.51	1.51	312.10	313.61	IW	
								2	1.50	1.50	313.61	315.11	HS	
								3	1.35	1.35	315.11	316.46		
								4	0.72	0.72	316.46	317.18		
								CC	0.19	0.19	317.18	317.37	PAL	
									5.27	5.27				
5R	18	0810	321.7	331.4	9.7	5.35	55.2							
								1	1.27	1.27	321.70	322.97	IW	
								2	1.50	1.50	322.97	324.47	WEL	
								3	1.50	1.50	324.47	325.97	HS	
								4	0.88	0.88	325.97	326.85		
								CC	0.20	0.20	326.85	327.05	PAL	
									5.35	5.35				
6R	18	0850	331.4	341.0	9.6	8.89	92.6							
								1	1.50	1.50	331.40	332.90	IW	
								2	1.50	1.50	332.90	334.40	HS	
								3	1.50	1.50	334.40	335.90		
								4	1.50	1.50	335.90	337.40		
								5	1.50	1.50	337.40	338.90		
								6	1.32	1.32	338.90	340.22		
								CC	0.07	0.07	340.22	340.29	PAL	
									8.89	8.89				
7R	18	0945	341.0	350.6	9.6	7.14	74.4							
								1	1.46	1.46	341.00	342.46	IW	
								2	1.46	1.46	342.46	343.92	HS, WEL	
								3	1.43	1.43	343.92	345.35		
								4	1.39	1.39	345.35	346.74		
								5	1.27	1.27	346.74	348.01		
								CC	0.13	0.13	348.01	348.14	PAL	
									7.14	7.14				
8R	18	1030	350.6	359.9	9.3	6.95	74.7							
								1	0.84	0.84	350.60	351.44	IW	
								2	1.50	1.50	351.44	352.94	HS	
								3	1.50	1.50	352.94	354.44		
								4	1.50	1.50	354.44	355.94		
								5	1.48	1.48	355.94	357.42		
								CC	0.13	0.13	357.42	357.55	PAL	
									6.95	6.95				
9R	18	1115	359.9	369.5	9.6	8.97	93.4							
								1	1.19	1.19	359.90	361.09	IW	
								2	1.28	1.28	361.09	362.37	HS, WEL	
								3	1.34	1.34	362.37	363.71		
								4	1.50	1.50	363.71	365.21		
								5	1.36	1.36	365.21	366.57		
								6	1.30	1.30	366.57	367.87		
								7	0.81	0.81	367.87	368.68		

Table T2 (continued).

Core	Date (July 1998)	Time (UTC +10 hr)	Core depth (mbsf) Top	Core depth (mbsf) Bottom	Length (m) Cored	Length (m) Recovered	Recovery (%)	Section	Length (m) Liner	Length (m) Curated	Section depth (mbsf) Top	Section depth (mbsf) Bottom	Catwalk samples	Comment
								CC	0.19	0.19	368.68	368.87	PAL	
									8.97	8.97				
10R	18	1155	369.5	379.1	9.6	8.76	91.3							
								1	1.50	1.50	369.50	371.00	IW	
								2	1.50	1.50	371.00	372.50	HS	
								3	1.50	1.50	372.50	374.00		
								4	1.50	1.50	374.00	375.50		
								5	1.50	1.50	375.50	377.00		
								6	1.06	1.06	377.00	378.06		
								CC	0.20	0.20	378.06	378.26	PAL	
									8.76	8.76				
11R	18	1235	379.1	388.5	9.4	8.72	92.8							
								1	1.44	1.44	379.10	380.54		
								2	1.48	1.48	380.54	382.02		
								3	1.40	1.40	382.02	383.42	HS, WEL	
								4	1.50	1.50	383.42	384.92	WROG, WRMB, IW	
								5	1.42	1.42	384.92	386.34		
								6	1.22	1.22	386.34	387.56		
								CC	0.26	0.26	387.56	387.82	PAL	
									8.72	8.72				
12R	18	1320	388.5	398.1	9.6	9.36	97.5							
								1	1.50	1.50	388.50	390.00	HS	
								2	1.50	1.50	390.00	391.50		
								3	1.40	1.40	391.50	392.90	IW, WRSCR	
								4	1.50	1.50	392.90	394.40		
								5	1.50	1.50	394.40	395.90		
								6	1.50	1.50	395.90	397.40		
								7	0.24	0.24	397.40	397.64		
								CC	0.22	0.22	397.64	397.86	PAL	
									9.36	9.36				
13R	18	1410	398.1	407.7	9.6	9.24	96.3							
								1	1.50	1.50	398.10	399.60	WEL	
								2	1.37	1.37	399.60	400.97	IW	
								3	1.18	1.18	400.97	402.15	HS	
								4	1.44	1.44	402.15	403.59		
								5	1.44	1.44	403.59	405.03		
								6	1.45	1.45	405.03	406.48		
								7	0.63	0.63	406.48	407.11		
								CC	0.23	0.23	407.11	407.34	PAL	
									9.24	9.24				
14R	18	1450	407.7	417.3	9.6	4.40	45.8							
								1	1.44	1.44	407.70	409.14	HS, IW	
								2	1.15	1.15	409.14	410.29		
								3	0.73	0.73	410.29	411.02		
								4	0.88	0.88	411.02	411.90		
								CC	0.20	0.20	411.90	412.10	PAL	
									4.40	4.40				

Table T2 (continued).

Core	Date (July 1998)	Time (UTC +10 hr)	Core depth (mbsf) Top	Core depth (mbsf) Bottom	Length (m) Cored	Length (m) Recovered	Recovery (%)	Section	Length (m) Liner	Length (m) Curated	Section depth (mbsf) Top	Section depth (mbsf) Bottom	Catwalk samples	Comment
15R	18	1535	417.3	426.9	9.6	8.54	89.0							
								1	1.50	1.50	417.30	418.80		
								2	1.50	1.50	418.80	420.30	IW	
								3	1.50	1.50	420.30	421.80	HS, WEL	
								4	1.50	1.50	421.80	423.30		
								5	1.50	1.50	423.30	424.80		
								6	0.86	0.86	424.80	425.66		
								CC	0.18	0.18	425.66	425.84	PAL	
									8.54	8.54				
16R	18	1620	426.9	436.5	9.6	1.78	18.5							
								1	0.79	0.79	426.90	427.69	IW	
								2	0.86	0.86	427.69	428.55	HS	
								CC	0.13	0.13	428.55	428.68	PAL	
									1.78	1.78				
17R	18	1705	436.5	446.1	9.6	2.54	26.5							
								1	1.19	1.19	436.50	437.69	IW	
								2	1.17	1.17	437.69	438.86	HS, WEL	
								CC	0.18	0.18	438.86	439.04	PAL	
									2.54	2.54				
18R	18	1755	446.1	455.6	9.5	2.65	27.9							
								1	1.48	1.48	446.10	447.58		
								2	1.00	1.00	447.58	448.58	HS	
								CC	0.17	0.17	448.58	448.75	PAL	
									2.65	2.65				
19R	18	1820	455.6	465.2	9.6	0.55	5.7							
								1	0.42	0.42	455.60	456.02	HS	
								CC	0.13	0.13	456.02	456.15	PAL	
									0.55	0.55				
20R	18	1925	465.2	474.9	9.7	0.74	7.6							
								1	0.57	0.57	465.20	465.77	HS	
								CC	0.17	0.17	465.77	465.94	PAL	
									0.74	0.74				
21R	18	2010	474.9	484.5	9.6	5.47	57.0							
								1	0.82	0.82	474.90	475.72		
								2	0.96	0.96	475.72	476.68	WROG, WRMB, IW	
								3	1.32	1.32	476.68	478.00	HS, WEL	
								4	1.50	1.50	478.00	479.50		
								5	0.58	0.58	479.50	480.08		
								CC	0.29	0.29	480.08	480.37	PAL	
									5.47	5.47				
22R	18	2105	484.5	494.1	9.6	7.07	73.6							
								1	1.50	1.50	484.50	486.00	IW	
								2	0.76	0.76	486.00	486.76	HS, WRSCR	
								3	1.50	1.50	486.76	488.26		
								4	1.50	1.50	488.26	489.76		
								5	1.00	1.00	489.76	490.76		
								6	0.58	0.58	490.76	491.34		

Table T2 (continued).

Core	Date (July 1998)	Time (UTC +10 hr)	Core depth (mbsf) Top	Core depth (mbsf) Bottom	Length (m) Cored	Length (m) Recovered	Recovery (%)	Section	Length (m) Liner	Length (m) Curated	Section depth (mbsf) Top	Section depth (mbsf) Bottom	Catwalk samples	Comment
								CC	0.23	0.23	491.34	491.57	PAL	
									7.07	7.07				
23R	18	2155	494.1	503.8	9.7	3.87	39.9							
								1	1.38	1.38	494.10	495.48	IW	
								2	1.50	1.50	495.48	496.98	HS, WEL	
								3	0.72	0.72	496.98	497.70		
								CC	0.27	0.27	497.70	497.97	PAL	
									3.87	3.87				
24R	18	2240	503.8	513.4	9.6	7.30	76.0							
								1	1.50	1.50	503.80	505.30		
								2	1.50	1.50	505.30	506.80		
								3	1.50	1.50	506.80	508.30	HS	
								4	1.50	1.50	508.30	509.80		
								5	0.99	0.99	509.80	510.79		
								CC	0.31	0.31	510.79	511.10	PAL	
									7.30	7.30				
25R	18	2335	513.4	523.0	9.6	2.98	31.0							
								1	1.50	1.50	513.40	514.90	IW	
								2	1.29	1.29	514.90	516.19	HS, WEL	
								CC	0.19	0.19	516.19	516.38	PAL	
									2.98	2.98				
26R	19	0025	523.0	532.6	9.6	0.65	6.8							
								1	0.41	0.41	523.00	523.41	HS	
								CC	0.24	0.24	523.41	523.65	PAL	
									0.65	0.65				
27R	19	0115	532.6	542.2	9.6	0.63	6.6							
								1	0.45	0.45	532.60	533.05	HS	
								CC	0.18	0.18	533.05	533.23	PAL	
									0.63	0.63				
28R	19	0220	542.2	551.8	9.6	0.95	9.9							
								1	0.82	0.82	542.20	543.02	IW, HS	
								CC	0.13	0.13	543.02	543.15	PAL	
									0.95	0.95				
29R	19	0340	551.8	561.4	9.6	3.52	36.7							
								1	1.45	1.45	551.80	553.25		
								2	1.04	1.04	553.25	554.29	HS	
								3	0.78	0.78	554.29	555.07	WROG, WRMB, WEL	
								CC	0.25	0.25	555.07	555.32	PAL	
									3.52	3.52				
30R	19	0600	561.4	571.0	9.6	5.27	54.9							
								1	0.53	0.53	561.40	561.93	WRSCR	
								2	1.04	1.04	561.93	562.97		
								3	1.50	1.50	562.97	564.47		
								4	1.21	1.21	564.47	565.68	HS	
								5	0.72	0.72	565.68	566.40		
								CC	0.27	0.27	566.40	566.67	PAL	
									5.27	5.27				

Table T2 (continued).

Core	Date (July 1998)	Time (UTC +10 hr)	Core depth (mbsf) Top	Core depth (mbsf) Bottom	Length (m) Cored	Length (m) Recovered	Recovery (%)	Section	Length (m) Liner	Length (m) Curated	Section depth (mbsf) Top	Section depth (mbsf) Bottom	Catwalk samples	Comment
31R	19	0735	571.0	580.6	9.6	1.28	13.3							
								1	1.08	1.08	571.00	572.08		
								CC	0.20	0.20	572.08	572.28	PAL	
									1.28	1.28				
32R	19	0900	580.6	590.2	9.6	4.85	50.5							
								1	1.41	1.41	580.60	582.01		
								2	0.94	0.94	582.01	582.95		
								3	1.26	1.26	582.95	584.21	HS, IW, WEL	
								4	1.04	1.04	584.21	585.25		
								CC	0.20	0.20	585.25	585.45	PAL	
									4.85	4.85				
33R	19	1015	590.2	599.8	9.6	4.18	43.5							
								1	1.46	1.46	590.20	591.66		
								2	1.40	1.40	591.66	593.06		
								3	1.15	1.15	593.06	594.21	HS	
								CC	0.17	0.17	594.21	594.38	PAL	
									4.18	4.18				
34R	19	1115	599.8	609.4	9.6	4.29	44.7							
								1	1.48	1.48	599.80	601.28	HS, IW, WEL	
								2	1.50	1.50	601.28	602.78		
								3	1.07	1.07	602.78	603.85		
								CC	0.24	0.24	603.85	604.09		
									4.29	4.29				
35R	19	1220	609.4	619.1	9.7	5.57	57.4							
								1	1.38	1.38	609.40	610.78		
								2	1.43	1.43	610.78	612.21	HS	
								3	1.46	1.46	612.21	613.67		
								4	1.04	1.04	613.67	614.71		
								CC	0.26	0.26	614.71	614.97	PAL	
									5.57	5.57				
36R	19	1415	619.1	628.8	9.7	2.91	30.0							
								1	1.40	1.40	619.10	620.50		
								2	1.34	1.34	620.50	621.84	HS	
								CC	0.17	0.17	621.84	622.01	PAL	
									2.91	2.91				
37R	19	1540	628.8	638.4	9.6	0.20	2.1							
								CC	0.20	0.20	628.80	629.00	PAL	
									0.20	0.20				
38R	19	1720	638.4	648.1	9.7	0.00	0.0							
								1	0.00	0.00				
									0.00	0.00				
39R	19	1840	648.1	657.8	9.7	0.07	0.7							
								CC	0.07	0.07	648.10	648.17	PAL, HS	
									0.07	0.07				
40R	19	2035	657.8	667.4	9.6	6.41	66.8							
								1	1.50	1.50	657.80	659.30		
								2	1.50	1.50	659.30	660.80	IW, WROG, WRMB	
								3	1.50	1.50	660.80	662.30	WEL	

Table T2 (continued).

Core	Date (July 1998)	Time (UTC +10 hr)	Core depth (mbsf) Top	Core depth (mbsf) Bottom	Length (m) Cored	Length (m) Recovered	Recovery (%)	Section	Length (m) Liner	Length (m) Curated	Section depth (mbsf) Top	Section depth (mbsf) Bottom	Catwalk samples	Comment
								4	1.50	1.50	662.30	663.80	HS	
								5	0.41	0.41	663.80	664.21	PAL	
									6.41	6.41				
41R	19	2250	667.4	677.1	9.7	5.57	57.4							
								1	1.46	1.46	667.40	668.86		
								2	1.50	1.50	668.86	670.36	HS	
								3	1.50	1.50	670.36	671.86		
								4	0.86	0.86	671.86	672.72		
								CC	0.25	0.25	672.72	672.97	PAL	
									5.57	5.57				
42R	20	0015	677.1	686.8	9.7	5.96	61.4							
								1	0.79	0.79	677.10	677.89	WRSCR	
								2	1.50	1.50	677.89	679.39		
								3	1.50	1.50	679.39	680.89	IW	
								4	1.38	1.38	680.89	682.27	HS, WEL	
								5	0.79	0.79	682.27	683.06	PAL	
									5.96	5.96				
43R	20	0145	686.8	696.5	9.7	6.22	64.1							
								1	1.50	1.50	686.80	688.30		
								2	1.50	1.50	688.30	689.80		
								3	1.23	1.23	689.80	691.03	HS	
								4	1.17	1.17	691.03	692.20		
								5	0.67	0.67	692.20	692.87		
								CC	0.21	0.21	692.87	693.08	PAL	
									6.28	6.28				
44R	20	0315	696.5	706.1	9.6	9.45	98.4							
								1	1.08	1.08	696.50	697.58	IW	
								2	1.50	1.50	697.58	699.08	HS, WEL	
								3	1.40	1.40	699.08	700.48		
								4	1.30	1.30	700.48	701.78		
								5	1.41	1.41	701.78	703.19		
								6	1.35	1.35	703.19	704.54		
								7	1.27	1.27	704.54	705.81		
								CC	0.14	0.14	705.81	705.95	PAL	
									9.45	9.45				
45R	20	0430	706.1	715.7	9.6	6.38	66.5							
								1	1.24	1.24	706.10	707.34		
								2	1.27	1.27	707.34	708.61		
								3	1.43	1.43	708.61	710.04	HS	
								4	1.47	1.47	710.04	711.51		
								5	0.78	0.78	711.51	712.29		
								CC	0.19	0.19	712.29	712.48	PAL	
									6.38	6.38				
46R	20	0610	715.7	725.4	9.7	9.39	96.8							
								1	1.15	1.15	715.70	716.85	IW	
								2	1.39	1.39	716.85	718.24	HS, WEL	
								3	1.32	1.32	718.24	719.56		
								4	1.46	1.46	719.56	721.02		

Table T2 (continued).

Core	Date (July 1998)	Time (UTC +10 hr)	Core depth (mbsf) Top	Core depth (mbsf) Bottom	Length (m) Cored	Length (m) Recovered	Recovery (%)	Section	Length (m) Liner	Length (m) Curated	Section depth (mbsf) Top	Section depth (mbsf) Bottom	Catwalk samples	Comment
								5	1.42	1.42	721.02	722.44		
								6	1.47	1.47	722.44	723.91		
								7	0.99	0.99	723.91	724.90		
								CC	0.19	0.19	724.90	725.09	PAL	
									9.39	9.39				
47R	20	0745	725.4	735.1	9.7	9.96	102.7							
								1	1.36	1.36	725.40	726.76		
								2	1.46	1.46	726.76	728.22	HS	
								3	1.32	1.32	728.22	729.54		
								4	1.50	1.50	729.54	731.04		
								5	1.21	1.21	731.04	732.25		
								6	1.50	1.50	732.25	733.75		
								7	1.20	1.20	733.75	734.95		
								CC	0.41	0.41	734.95	735.36	PAL	
									9.96	9.96				
48R	20	0910	735.1	744.7	9.6	3.89	40.5							
								1	1.18	1.18	735.10	736.28	WROG, WRMB, IW	
								2	1.37	1.37	736.28	737.65	WEL	
								3	1.10	1.10	737.65	738.75	HS	
								CC	0.24	0.24	738.75	738.99	PAL	
									3.89	3.89				
49R	20	1125	744.7	754.3	9.6	9.27	96.6							
								1	1.29	1.29	744.70	745.99		
								2	1.30	1.30	745.99	747.29		
								3	1.51	1.51	747.29	748.80		
								4	1.47	1.47	748.80	750.27		
								5	1.31	1.31	750.27	751.58		
								6	1.50	1.50	751.58	753.08	HS	
								7	0.72	0.72	753.08	753.80		
								CC	0.17	0.17	753.80	753.97	PAL	
									9.27	9.27				
50R	20	1335	754.3	763.9	9.6	6.64	69.2							
								1	1.40	1.40	754.30	755.70		
								2	1.29	1.29	755.70	756.99		
								3	1.00	1.00	756.99	757.99		
								4	1.24	1.24	757.99	759.23		
								5	1.02	1.02	759.23	760.25	IW, WEL	
								6	0.45	0.45	760.25	760.70	HS	
								CC	0.24	0.24	760.70	760.94	PAL	
									6.64	6.64				
51R	20	1505	763.9	773.6	9.7	3.27	33.7							
								1	1.32	1.32	763.90	765.22		
								2	1.11	1.11	765.22	766.33		
								3	0.71	0.71	766.33	767.04	WRSCR, HS	
								CC	0.13	0.13	767.04	767.17	PAL	
									3.27	3.27				
52R	20	1710	773.6	783.2	9.6	9.38	97.7							
								1	1.13	1.13	773.60	774.73	IW	

Table T2 (continued).

Core	Date (July 1998)	Time (UTC +10 hr)	Core depth (mbsf) Top	Core depth (mbsf) Bottom	Length (m) Cored	Length (m) Recovered	Recovery (%)	Section	Length (m) Liner	Length (m) Curated	Section depth (mbsf) Top	Section depth (mbsf) Bottom	Catwalk samples	Comment
								2	1.42	1.42	774.73	776.15	HS, WEL	
								3	1.50	1.50	776.15	777.65		
								4	1.42	1.42	777.65	779.07		
								5	1.46	1.46	779.07	780.53		
								6	1.17	1.17	780.53	781.70		
								7	1.05	1.05	781.70	782.75		
								CC	0.18	0.18	782.75	782.93	PAL	
									9.33	9.33				
53R	20	1855	783.2	792.8	9.6	7.73	80.5							
								1	1.50	1.50	783.20	784.70		
								2	1.34	1.34	784.70	786.04		
								3	1.20	1.20	786.04	787.24		
								4	1.27	1.27	787.24	788.51		
								5	1.42	1.42	788.51	789.93	HS	
								6	1.00	1.00	789.93	790.93	PAL	
									7.73	7.73				
54R	20	2100	792.8	802.5	9.7	9.36	96.5							
								1	1.08	1.08	792.80	793.88		
								2	1.36	1.36	793.88	795.24		
								3	1.50	1.50	795.24	796.74		
								4	1.50	1.50	796.74	798.24	IW, WROG, WRMB	
								5	1.37	1.37	798.24	799.61	HS	
								6	1.22	1.22	799.61	800.83		
								7	1.13	1.13	800.83	801.96	WEL	
								CC	0.20	0.20	801.96	802.16	PAL	
									9.36	9.36				
				Cored:	519.3	291.63	56.2							
				Drilled:	283.2									
				Total:	802.5									

Note: IW = interstitial water; WEL = Wellsbury microbiology; WROG = whole-round organic geochemistry; WRMB = whole-round microbiology; HS = headspace; PAL = paleontology.

Table T3. Results of X-ray diffraction analysis of bulk fine-grained sediments, Site 1115. (Continued on next page.)

Core, section, interval (cm)	Depth (mbsf)	Description	XRD identification: major (minor) minerals
180-1115A-			
1H-3, 133.5-134.5	2.84	Foraminifer-bearing nannofossil ooze	Calcite (aragonite, quartz)
180-1115B-			
1H-2, 135-136	2.85	Foraminifer-bearing nannofossil ooze	Calcite (aragonite, quartz)
1H-5, 85-86	6.85	Foraminifer-bearing nannofossil ooze	Calcite (aragonite, quartz)
2H-2, 73-74	9.43	Silty clay nannofossil ooze	Calcite (quartz, aragonite)
3H-1, 51-52	17.21	Silty clay nannofossil ooze	Calcite (quartz, aragonite)
4H-1, 69-70	26.89	Clay nannofossil ooze	Calcite (quartz, amphibole)
5H-2, 57-58	37.77	Nannofossil clay	Calcite (quartz, amphibole)
6H-1, 43.5-44	45.63	Nannofossil clay	Calcite (quartz, plagioclase)
7H-1, 49-49.5	55.19	Calcareous clay	Calcite (aragonite, quartz, plagioclase)
8H-1, 65-66	64.85	Calcareous clay	Calcite (quartz, aragonite, plagioclase)
9H-6, 92-93	82.12	Calcareous clay	Calcite (quartz, aragonite, plagioclase)
10H-4, 142.5-144	89.13	Nannofossil-rich silty clay	Calcite (aragonite, quartz, plagioclase)
11H-2, 128-130	95.48	Nannofossil-rich silty clay	Calcite (aragonite, quartz, plagioclase)
12H-4, 139-140	108.09	Nannofossil-rich silty clay	Calcite (aragonite, quartz, plagioclase)
13H-6, 127-128	120.47	Nannofossil-rich silty clay	Calcite (quartz, plagioclase)
14H-4, 62.5-63.5	126.32	Nannofossil-rich silty clay	Calcite (plagioclase, quartz)
15H-4, 113-114	136.33	Nannofossil-rich silty clay	Calcite (plagioclase)
16H-1, 58-59	140.78	Nannofossil-rich silty clay	Calcite (plagioclase, quartz)
17H-2, 49-50	151.69	Nannofossil-rich silty clay	Calcite (plagioclase, quartz)
18H-1, 42-44	159.62	Calcareous clay	Calcite (quartz, plagioclase, chlorite)
19H-1, 26-27	168.96	Calcareous clay	Calcite (quartz, plagioclase, illite)
20H-1, 32-33	178.52	Calcareous clay	Calcite (quartz, plagioclase, illite)
21H-1, 33-33.5	188.03	Calcareous clay	Calcite (quartz, plagioclase, illite)
22H-1, 32-33	197.52	Calcareous clay	Calcite (quartz, plagioclase, illite, chlorite, amphibole)
23H-1, 29-30	206.99	Calcareous clay	Calcite (quartz, plagioclase, illite)
24X-3, 117-118	220.37	Nannofossil-bearing silty clay	Calcite (quartz, plagioclase, illite)
25X-3, 118-120	229.98	Nannofossil-bearing silty clay	Calcite (quartz, plagioclase, dolomite)
26X-4, 66-67	240.56	Nannofossil-rich silty clay	Dolomite, ?ankerite, calcite, plagioclase (quartz, illite)
27X-4, 58-59	250.08	Nannofossil-rich silty clay	Calcite, plagioclase (illite, chlorite)
28X-1, 83.5-84.5	255.43	Calcareous silty clay	Calcite, plagioclase, quartz, dolomite, illite (amphibole)
29X-7, 19-20	273.49	Nannofossil-rich silty clay	Calcite, plagioclase, quartz, illite (amphibole)
31X-1, 28-29	283.78	Calcareous silty clay	Calcite, plagioclase, quartz, illite, amphibole (pyroxene)
180-1115C-			
1R-1, 30-31	283.50	Silty calcareous clay	Calcite, plagioclase, quartz, illite (amphibole, pyrite)
2R-1, 9-11	292.89	Silty calcareous claystone	Dolomite (plagioclase, quartz, illite)
2R-1, 38-40	293.18	Silty calcareous claystone	Calcite, plagioclase, quartz, illite, amphibole (pyrite)
3R-1, 19-20	302.69	Calcareous claystone	Calcite, plagioclase, quartz (illite, amphibole, pyrite)
4R-1, 107-109	313.17	Calcareous claystone	Calcite, plagioclase, quartz (illite, amphibole, pyrite)
5R-1, 39-41	322.09	Calcareous silty claystone	Calcite, quartz, plagioclase (illite, amphibole, pyrite)
6R-1, 31-32	331.71	Calcareous silty claystone	Calcite, quartz, plagioclase (illite, amphibole, pyrite)
7R-1, 78.5-80	341.79	Silty claystone	Calcite, quartz, plagioclase (illite, amphibole, pyrite)
8R-2, 18-20	351.62	Calcareous silty claystone	Calcite, quartz, plagioclase (illite, pyrite)
9R-4, 35-36	364.06	Silty claystone	Calcite, quartz, plagioclase (illite, amphibole, pyrite)
10R-4, 113.5-115.5	375.14	Calcareous silty claystone	Calcite, quartz, plagioclase (illite, amphibole, pyrite)
11R-1, 14-16	379.24	Calcareous silty claystone	Calcite, quartz, plagioclase (illite, amphibole, pyrite)
12R-1, 30-32	388.80	Calcareous silty claystone	Calcite, quartz, plagioclase, illite, amphibole, pyrite
13R-1, 78-79	398.88	Calcareous sandy silty claystone	Calcite, quartz, plagioclase, illite (amphibole, pyrite)
14R-1, 53-54	408.23	Calcareous sandy silty claystone	Calcite, quartz, plagioclase (illite, amphibole)
15R-1, 59-60	417.89	Silty sandstone	Calcite, plagioclase, quartz (aragonite, illite)
16R-CC, 3-4	428.58	Sandstone	Plagioclase, calcite, quartz (illite, amphibole, pyrite)
17R-2, 55.5-56	438.24	Calcareous silty sandstone	Plagioclase, quartz, calcite, pyroxene (illite, amphibole, pyrite, aragonite)
18R-2, 66-68	448.24	Mixed silty sandstone	Quartz, plagioclase, calcite, illite, pyrite (amphibole)
19R-1, 18.5-19	455.79	Sandstone	Quartz, plagioclase, calcite, illite (pyrite, amphibole, chlorite))
21R-1, 10-11	475.00	Siltstone-claystone	Calcite, plagioclase, quartz, illite, aragonite (amphibole, chlorite)
21R-2, 8-9	475.80	Foraminifer-bearing siltstone-sandstone	Calcite, plagioclase, quartz, illite (chlorite)
22R-5, 11.5-12	489.87	Silty sandstone	Calcite, plagioclase, quartz, illite (aragonite, pyrite)
23R-2, 145-147	496.93	Silty sandstone	Calcite, plagioclase, quartz, illite
24R-1, 111-112	504.91	Sandy siltstone	Plagioclase, quartz, calcite, illite (chlorite)
25R-2, 43-44	515.33	Sandstone	Plagioclase, quartz (illite, calcite, pyrite)
26R-1, 13-15	523.13	Sandstone (limestone?)	Calcite, plagioclase, quartz (amphibole)
27R-1, 19-20	532.79	Silty sand	Plagioclase, quartz (aragonite, amphibole)
29R-1, 78-80	552.58	Sandstone	Calcite (plagioclase, k-feldspar, quartz)
29R-1, 127-128	553.07	Sandstone	Plagioclase, quartz, amphibole, smectite?
29R-2, 99-100	554.24	Silty claystone	Quartz, plagioclase, smectite?
30R-2, 125-126	563.18	Organic-rich silty claystone	Pyrite, quartz, plagioclase, smectite?

Table T3 (continued).

Core, section, interval (cm)	Depth (mbsf)	Description	XRD identification: major (minor) minerals
30R-4, 56-57	565.36	Silty claystone	Plagioclase, quartz (smectite?)
31R-1, 101-101.5	572.01	Calcareous siltstone	Calcite, plagioclase
32R-1, 45-46	581.05	Silty claystone	Pyroxene, plagioclase, smectite?
33R-1, 21-23	590.41	Siltstone	Pyroxene, plagioclase, zeolite (hematite, smectite?, illite)
34R-1, 51-51.5	600.31	Siltstone	Plagioclase, calcite, zeolite, pyroxene, hematite, smectite? (illite, amphibole)
35R-4, 24-25	613.91	Silty claystone	Pyroxene, plagioclase
36R-1, 83-84	619.93	Claystone-siltstone	Pyroxene, plagioclase, zeolite, Fe-oxide minerals, smectite?
40R-3, 83-84	661.63	Calcareous silty sandstone	Plagioclase (calcite, quartz, zeolite, smectite?)
41R-4, 6-7	671.92	Calcareous silty sandstone	Plagioclase, calcite, quartz, smectite? (zeolite)
42R-4, 70-71	681.59	Sandy siltstone	Plagioclase, calcite (quartz, smectite?, zeolite)
43R-2, 53-55	688.83	Silty sandstone	Plagioclase, calcite (pyroxene, quartz, smectite?, zeolite)
44R-1, 30-32	696.80	Calcareous sandy siltstone	Plagioclase, calcite, pyroxene (quartz, smectite?, zeolite)
45R-1, 49-50	706.59	Siltstone	Plagioclase, calcite (quartz, zeolite, smectite?)
46R-2, 7-9	716.92	Siltstone	Plagioclase, calcite, quartz, pyroxene (zeolite, smectite?)
47R-2, 3-5	726.79	Siltstone-sandstone	Plagioclase, pyroxene (quartz, zeolite, smectite?)
48R-1, 41-43	735.51	Siltstone	Plagioclase, calcite (quartz, zeolite, smectite?)
49R-2, 22-23	746.21	Siltstone	Plagioclase, calcite, quartz (smectite?, zeolite)
50R-1, 28-29	754.58	Siltstone	Plagioclase, calcite, pyroxene, quartz (smectite, zeolite, chlorite)
51R-2, 63-65	765.85	Siltstone	Plagioclase, calcite, quartz (smectite, zeolite, chlorite)
53R-3, 16-17	786.20	Calcareous silty sand	Plagioclase, calcite, pyroxene (chlorite, smectite?, zeolite)
54R-7, 104-105	801.87	Sandy siltstone	Plagioclase, calcite, quartz (chlorite, smectite?)

Note: See **"Lithostratigraphy,"** p. 5, for discussion.

Table T4. Range chart showing the distribution of selected calcareous nannofossil species. **A.** Holes 1115A and 1115B. (Continued on next page.)

Core, section, interval (cm)	Depth (mbsf)	Abundance	Preservation	*Calcidiscus leptoporus*	*Calcidiscus macintyrei*	*Ceratolithus cristatus*	*Coccolithus pelagicus*	*Discoaster asymmetricus*	*Discoaster brouweri*	*Discoaster decorus*	*Discoaster pentaradiatus*	*Discoaster surculus*	*Discoaster tamalis*	*Discoaster variabilis*	*Emiliania huxleyi*	*Gephyrocapsa oceanica*	*Helicosphaera carteri*	*Helicosphaera sellii*	*Pseudoemiliania lacunosa*	*Reticulofenestra minutula*	*Scyphosphaera apsteinii*	*Sphenolithus abies*	*Thoracosphaera heimii*	*Thoracosphaera saxea*	*Umbilicosphaera sibogae*
180-1115A-																									
1H-CC, 20-23	4.40	A	G	C											R	A	C		r						
180-1115B-																									
1H-CC, 14-17	7.11	A	G	C	r										R	A	C								
2H-1, 99-101	8.19																								
2H-5, 96-98	14.16																								
2H-CC, 32-35	17.20	A	G	F												C	F		R						
3H-CC, 43-46	26.88	A	G	F												A	F		F						
4H-CC, 23-26	36.14	A	G	F												C	F		F						
5H-CC, 30-33	45.70	A	G	C												F	C		F						
6H-CC, 23-26	55.19	A	G	F			R									F	F		F						
7H-CC, 42-45	64.66	A	G	C			R									F	C		C						
8H-CC, 28-31	74.13			F			R									F	C		C						
9H-4, 95-97	79.15								r									R							
9H-6, 95-97	82.15								r																
9H-7, 10-12	82.80				R				r									R							
9H-CC, 41-44	83.74	A	G	F	R		R		r							F	C	R	C						
10H-CC, 26-29	92.92			F	R		F									F	C		C						
11H-CC, 31-34	102.61	A	G	F	R		F										C	R	C						
12H-1, 96-98	103.16								r																
12H-3, 96-97	106.16								R																
12H-CC, 28-31	111.87	A	G	F	R		F		R								C	R	C						
13H-4, 77-78	116.97								R																
13H-7, 29-30	120.99								R																
13H-CC, 28-31	121.53	C	G	F		R	F		F								F		C	C	R				
14H-CC, 20-22	131.00	C	G	R		R	F		F								F		F	C				R	R
15H-CC, 16-19	140.52	C	M	R		R	R		F								F	R	F		R				
16H-3, 93-95	144.13																								
16H-5, 95-97	147.15										R														
16H-CC, 30-33	150.19	C	G	R			R		F		F						F			C					
17H-CC, 22-25	159.67	C	G	R	R		F	R	C		F									C					
18H-CC, 25-28	169.16	C	G	R	R				C		F										F				
19H-5, 95-97	175.65																								
19H-CC, 19-24	178.63	C	G	R			F	R	C		C	R					F		F	C					
20H-CC, 24-27	188.15	C	G	R				R	C	R	C	R	R				C		C		F				
21H-CC, 24-27	197.39	C	G	R			F		C	R	C	R	R	R			F		C	C		R			
22H-CC, 26-29	206.76	C	G	R			R	R	C		C	R	R				F		F	C	F	R			
23H-CC, 24-27	216.62	C	G	F	R		F	R	C	R	C	R	R				F		F	C		R	R		
24X-CC, 33-36	226.01	C	G		R		F	R	C		C		R				F		C	C		R		R	
25X-CC, 17-20	235.28	C	G	R	R		F	R	F		F						F		F	C		R			
26X-CC, 31-34	245.02	C	G	F	R		F		C		C		R							C		R	R		
27X-CC, 31-34	253.66	C	G		R		F		F		F									C		F			
28X-CC, 11-14	256.66	C	M						F		F						F			C		R			
29X-CC, 32-35	274.08	C	M	F	R		R	R	F	R	F	R					C	R		C	R	R	R	R	
30X-CC, 43-46	275.40	B																							
31X-CC, 38-41	293.37	C	M	F			F	R	F		F	R					C					R			

Notes: Abundance (number specimens of a species per field of view): A = abundant (10–100); C = common (1–10); B = barren. Preservation: G = good; M = moderate. Distribution: C = common; F = few; R = rare; r = reworked.

Table T4 (continued). B. Hole 1115C.

Core, section, interval (cm)	Depth (mbsf)	Abundance	Preservation	*Braarudosphaera bigelowii*	*Calcidiscus leptoporus*	*Calcidiscus macintyrei*	*Ceratolithus armatus*	*Ceratolithus rugosus*	*Coccolithus miopelagicus*	*Coccolithus pelagicus*	*Cyclicargolithus floridanus*	*Discoaster asymmetricus*	*Discoaster brouweri*	*Discoaster decorus*	*Discoaster deflandrei*	*Discoaster exilis*	*Discoaster pentaradiatus*	*Discoaster quinqueramus*	*Discoaster surculus*	*Discoaster tamalis*	*Discoaster variabilis*	*Helicosphaera carteri*	*Helicosphaera sellii*	*Pseudoemiliania lacunosa*	*Reticulofenestra pseudoumbilicus*	*Reticulofenestra minutula*	*Scyphosphaera apsteinii*	*Sphenolithus abies*	*Sphenolithus heteromorphus*	*Sphenolithus moniformis*	*Thoracosphaera heimii*	*Thoracosphaera saxea*
180-1115C-																															
1R-CC, 14-17	289.63	C	G		R					R			F				F					C				C	R			R	
2R-CC, 14-17	299.17	C	G		R								F				F			R		C				C	R				
3R-CC, 34-37	311.05	C	G										F				F		R												
4R-CC, 16-19	317.34	C	M		F							R	F				F		F	R		C				C					
5R-CC, 17-20	327.02	C	G		R					R			F				F			R		F				C					
6R-CC, 3-7	340.25	C	G				R			R		R	F	R			F			R		F									
7R-CC, 10-13	348.11	C	G									R	F				F		R	R		F				C	R				R
8R-CC, 10-13	357.52	C	M		F	R								R						R		F		R		C		F				
9R-CC, 16-19	368.84	C	M									R	F	R			F		R		F	R				C	R	R				
10R-CC, 17-20	378.23	C	M		F								F				F		R	R		F									
11R-CC, 23-26	387.79				F	R		R		R			F				F		R			F									
12R-CC, 19-22	397.83				F	R						R	F				F			R		F									
13R-CC, 20-23	407.31	C	M		F							R	F				F		R	R		F									
14R-CC, 17-20	412.07	C	M									R	F				F	r	R			F									
15R-CC, 15-18	425.81	C	M		F							R	F				F					F			R						
16R-CC, 10-13	428.65	C	P		R								F				F	r				F									
17R-CC, 15-18	439.01	C	M		R								F				R					F			F			F			
18R-CC, 14-17	448.72	C	P										R				R					R			R			F			
19R-CC, 2-5	456.04	C	M		R			R					F				R					R			R			R			
20R-CC, 14-17	465.91	C	M		R								F				R					F			R			F			
21R-CC, 26-29	480.34	F	P		R								F				R		R			R						F			
22R-CC, 20-23	491.54	C	P		R																	R			R			F			
23R-CC, 25-27	497.95	C	M										R									R						F			
24R-CC, 29-31	511.08	F	P										R									R						R			
25R-1, 89-91	514.29												R				F		R		R							C			
25R-CC, 18-19	516.37	F	P															R				R						R			
26R-CC, 21-24	523.62	F	M															F				R	R		R	F		F			
27R-CC, 15-18	533.20	R	M															R								R					
28R-CC, 10-13	543.12	R	P															R								R					
29R-CC, 22-25	555.29	R	M						R		R				R			R								R					
30R-CC, 26-27	566.99	B																													
31R-CC, 19-20	572.27	T	P																							R		R			
32R-CC, 19-20	585.50	R	P	R							R		R		R	R					R	R				R					
33R-CC, 14-17	594.35	R	P								R														R						
34R-1, 31-33	600.11	F	P								F					R									F				R	R	
35R-CC, 24-26	614.95	B																													
36R-CC, 14-17	621.98	R	P								R											R			R						
37R-CC, 18-20	628.98	F	M		R						F											F			R						
39R-CC, 6-7	648.16	F	M							R	R											R									
40R-5, 40-41	664.20	F	M							R	R											F			R				F		
41R-CC, 24-25	672.96	F	M								F											R							R		
42R-5, 78-79	683.05	T	P																												
43R-CC, 18-21	692.99	C	P								C				R	R						F							F	R	
44R-CC, 11-14	705.92	C	P							R	C																		F	F	
45R-CC, 10-12	712.39	F	P							R	F																		F	R	R
46R-CC, 12-15	725.02	F	P								F																		R	R	
47R-CC, 37-41	735.32	F	P								F																		F	R	
48R-CC, 23-24	738.98	C	M								C																		F	F	
49R-CC, 14-17	753.94	C	M								F																		R		
50R-CC, 21-24	760.91	C	M								F																		F		
51R-CC, 10-13	767.14	C	M								F											F							F		
52R-CC, 16-18	782.96	C	M								C											F							F		
53R-6, 98-100	790.91										F											F							F		
54R-CC, 18-20	802.14	C	M								F											R							F		

Notes: Abundance (number specimens of a species per field of view): C = common (1–10); F = few (1 per 10 fields of view); R = rare (<1 per 10 fields of view); B = barren; T = trace (<1 per transect of slide). Preservation: G = good; M = moderate; P = poor. Distribution: C = common; F = few; R = rare; r = reworked.

Table T5. Range chart showing the distribution of planktonic foraminifers. **A.** Holes 1115A and 1115B. (Continued on next page.)

Core, section, interval (cm)	Depth (mbsf)	Abundance	Preservation	*Bolliella calida*	*Candeina nitida*	*Dentoglobigerina altispira*	*Globigerina bulloides*	*Globigerinella siphonifera*	*Globigerinoides conglobatus*	*Globigerinoides extremus*	*Globigerinoides fistulosus*	*Globigerinoides quadrilobatus*	*Globigerinoides ruber*	*Globigerinoides ruber* (pink)	*Globigerinoides sacculifer*	*Globigerinoides trilobus*	*Globoquadrina pseudofoliata*	*Globoquadrina venzuelana*	*Globorotalia crassaformis*	*Globorotalia inflata*	*Globorotalia menardii*	*Globorotalia scitula*	*Globorotalia tosaensis*	*Globorotalia truncatulinoides*	*Globorotalia tumida*	*Globorotalia tumida flexuosa*	*Neogloboquadrina acostaensis*	*Neogloboquadrina dutertrei*	*Neogloboquadrina humerosa*	*Orbulina bilobata*	*Orbulina universa*	*Pulleniatina obliquiloculata*	*Pulleniatina praecursor*	*Pulleniatina primalis*	*Sphaeroidinella dehiscens*	*Sphaeroidinella dehiscens* s.l.	*Sphaeroidinellopsis paenedehiscens*	*Zeaglobigerina rubescens*
180-1115A-																																					
1H-CC, 20-23	4.40	A	G	R			F	A	F			F	A	F	F	F			F	F	F	F		F	F			A	A			F			F			F
180-1115B-																																						
1H-CC, 14-17	7.11	A	G	R			F	A	A			A	A	A	A	A					F			F	F			A			F	F		F			F
2H-CC, 32-35	17.20	A	G		F			A				A	A		A	A			R	R	A			F	A			A			F	A					
3H-CC, 43-46	26.88				R			F	F			A	A		A	A			F		F	R		F	F	F		A			F	F		F			
4H-CC, 23-26	36.14	A	G					A	A			A	A		A	A			F		A			A	F			A	A		R			F			
5H-CC, 30-33	45.70	A	G				F		F			A	A		A	A			F		F	R		F	F			A		R	F	F		R			
6H-CC, 23-26	55.19	A	G				F	A	F			A	A		A	A			F			R	F	F	F	F		A	A		R	F		R			
7H-CC, 42-45	64.66	A	G		R				F			A	A		A	A			F		F		F	F	F	F		A	A		F	F		F			
8H-CC, 28-31	74.13	A	G					F	F			A	A		A	A			F		F	F	F	F	F	F		F	F		F	F		F			
9H-CC, 41-44	83.74	A	G						F			A	A		A	A			R		F		F	F	F			A	A		F			F			
10H-1, 95-97	84.15	A	G		R			F	F			A	A		A	A			F		F		F	F	F	F		F	A		F	F		F			
10H-2, 95-97	85.65	A	G					F	F	F		A	A		A	A	R		F		F		F	R	F	R		A	A		R	F		F			
10H-4, 65-67	88.35	A	G					F	F		F	A	A		A	A			F		F	R	F	F	F			A	A		F	F		F			
10H-CC, 26-29	92.92	A	G						F		F	A	A			A			R		F		F	F	F			A	A		R	F		R			
11H-CC, 31-34	102.61	A	G					F	A	F	A	A	A		A	A			A		A		A		A	A		A	F		F	A		F			
12H-CC, 28-31	111.87	A	G					A	A	A	A	A	A		A	A			A		A		F	F	A	A		A	A		F	A		A			
13H-CC, 28-31	121.53	A	G					A	A	F	A	A	A		A	A			F		A		R	R	A	A	A	A	A		A	A		A			
14H-CC, 20-22	131.00	A	G					A	A	F		A	A		A	A			A		A		R	R	A		F	A	A		A	A	F	A			
15H-CC, 16-19	140.52	A	G					A	A	A	F	A	A		A	A			A		A		A		A			A	A		A	A		A			
16H-CC, 30-33	150.19	A	G					A	A	A	A	A	A		A	A			A		A		A	R	A		A	A	A		A	A		A			
17H-CC, 22-25	159.67	A	G					A	F	A	A	A	A		A	F			A		A		A		A		F	F	F		F	A		F			
18H-CC, 25-28	169.16	A	G					A	F	F	A	A	A		A	A			A		A		R		A		F	F	A		F	A		F			
19H-CC, 19-24	178.63	A	G					F	F	A	A	A	A		A	F			F		A		R		F				A		R	F		F			
20H-CC, 24-27	188.15	A	G					F	F	A	A	A	A		A	F			F		A		R		F				A		R	A		F			
21H-CC, 24-27	197.39	A	G			A		A	F	F	A	A	A		A	F			A		A		A		F				A		R	A		A			
22H-CC, 26-29	206.76	A	G			A			F	F	A	A	F		F	F			A		A		A		F				F		F	A		F			
23H-CC, 24-27	216.62	A	G			A		F	F	F	F	A	A		A				F		A		F		A				F		F	A		A			
24X-CC, 33-36	226.01	A	G			A		F	F	F	F	A	A		A	F			A		A		R		F		F		A		F	A		F			
25X-CC, 17-20	235.28	A	G			A		F	F	F		A	F		A	F			A		A				F		R		A		F	F		F			
26X-CC, 31-34	245.02	A	G			A		F	F	F		A	A		F	F			F		A				F		F		F		F	A		A			
27X-CC, 31-34	253.66	A	M			A		F	F	F		A	A		A	F			F		A				F		F		F		F	A		F			
28X-CC, 11-14	256.66	A	M			A		F	F	F		A	A		F	F			F		A				F		F		F		F	F	F	R	F		
29X-CC, 32-35	274.08	A	M			A		F	F	F		A	A			F			F		A				F		A		F		F				F		R
30X-CC, 43-46	275.40	R	P										R			R					R											R			R			
31X-CC, 38-41	293.37	R	P			F		F	F	F		A	A		A	A		R	F		F				F		A		A		F	R	F		F	F		

Notes: Abundance (number of specimens per field of view): A = abundant (2–9); R = rare (1–3 per tray). Preservation: G = good; M = moderate; P = poor.

Table T5 (continued). B. Hole 1115C.

Core, section, interval (cm)	Depth (mbsf)	Abundance	Preservation	*Candeina nitida*	*Cassigerinella chipolensis*	*Dentoglobigerina altispira*	*Dentoglobigerina globosa*	*Globigerina bulloides*	*Globigerinella siphonifera*	*Globigerinita glutinata*	*Globigerinoides bollii*	*Globigerinoides conglobatus*	*Globigerinoides extremus*	*Globigerinoides obliquus*	*Globigerinoides quadrilobatus*	*Globigerinoides ruber*	*Globigerinoides sacculifer*	*Globigerinoides subquadratus*	*Globigerinoides trilobus*	*Globoquadrina baroemoenensis*	*Globoquadrina dehiscens*	*Globoquadrina venzuelana*	*Globorotalia archeomenardii*	*Globorotalia crassaformis*	*Globorotalia lenguaensis*	*Globorotalia margaritae*	*Globorotalia menardii*	*Globorotalia peripheroronda*	*Globorotalia praemenardii*	*Globorotalia scitula*	*Globorotalia tumida*	*Globorotalia tumida flexuosa*	*Jenkinsella mayeri*	*Neogloboquadrina acostaensis*	*Neogloboquadrina continuosa*	*Neogloboquadrina humerosa*	*Neogloboquadrina mayeri*	*Orbulina bilobata*	*Orbulina suturalis*	*Orbulina universa*	*Pulleniatina obliquiloculata*	*Pulleniatina praecursor*	*Pulleniatina primalis*	*Sphaeroidinella dehiscens*	*Sphaeroidinella dehiscens* s.l.	*Sphaeroidinellopsis paenedehiscens*	*Sphaeroidinellopsis seminulina*	*Sphaeroidinellopsis subdehiscens*
180-1115C-																																													
1R-CC, 14-17	289.63	A	G			A			F			F	F		A	A	A		F					A		A			A				A	A				A	F	F		F			
2R-CC, 14-17	299.17	A	G			A			A			A	A		A	A	A		A					A		A			A				A	A				F	A			A		R	
3R-CC, 34-37	311.05	A	G			A			F			A	A		A	A	A		F					F		A			A				A	A				F	A			A		F	
4R-CC, 16-19	317.34	A	G			A			F			F	A		A	A	A		F					F		A			A				A	A				F	F	F		A			
5R-CC, 17-20	327.02	A	G			A			F			F	A		A	A	A		F					F		A			A				A					A	A			A			
6R-CC, 3-7	340.25	A	G			A			F			F	F		A	A	A		F					F		A			A				A	F				A		F		A			
7R-CC, 10-13	348.11	A	M			A			F			F	F		A	A	A		F					R		A			F				F	F				A	A			A			
8R-CC, 10-13	357.52	A	M			A			F			F	F		A	A	A		F					A		A			A				A					F	A			A			
9R-CC, 16-19	368.84	A	G			A			F			A	A		A	A	A		F					F		A			A				A	A				F	A			A			
10R-CC, 17-20	378.23	A	G			F						A	A		A	A	A		A					R		R	F		F		F		F	F				F		F		F	F		
11R-CC, 23-26	387.79	A	G			F	F					F	A		A	A	A		A					R		R	F		F		F		F	F				F		F					
12R-CC, 19-22	397.83	A	G			F	F					A	A		A	A	A		A					R			F		F		F		F	F				F		F		F	F	F	
13R-CC, 20-23	407.31	A	G			F	F					R	A		A	A	A		A					R			F		F		F		F	F				F		F			F	F	F
14R-CC, 17-20	412.07	A	G			F			R			F	A		A	A	A		A								F		F		F			F					R				R	R
15R-CC, 15-18	425.81	A	G	R		F			F			F					F									R	F			F				F					F		F			R		
16R-CC, 10-13	428.65	A	G			F			F	A			F				F		F							F	R			R				F					R		F					
17R-CC, 15-18	439.01	C	G			F			R				F		F		F		F								R			R			F	R				R		F					
18R-CC, 14-17	448.72	F	G										F		F		F		F								R			R												R			
19R-CC, 2-5	456.04	F	G			R			R				F				F		F								R															R			
20R-CC, 14-17	465.91	F	G			R							F				F		F								R		R					F											
21R-CC, 26-29	480.34	R	G											R																																
22R-CC, 20-23	491.54	R	M												R																															
23R-CC, 25-27	497.95	R	M										F		F												R																		
24R-CC, 29-31	511.08	R	M																F																										
25R-CC, 18-19	516.37																																												
26R-CC, 21-24	523.62																																												
27R-CC, 15-18	533.2																																												
28R-CC, 10-13	543.12																																												
29R-CC, 22-25	555.29																																												
30R-CC, 26-27	566.99																																												
31R-CC, 19-20	572.27	C	P			F									R				R										R											R						P
32R-CC, 19-20	585.5	R	P			F									R																														
33R-CC, 14-17	594.35	A	M		R	F		R	F							A			A	R					F				F									A		A					
35R-CC, 24-26	614.95	C	P			F					F							F	F																			R		F					
36R-CC, 14-17	621.98																																												
37R-CC, 18-20	628.98	F	P						R					R					R														R						R						
39R-CC, 6-7	648.16	R	M																R																										
41R-CC, 24-25	672.96	F	M		F	F								F					F										R									R		F				R	
42R-5, 78-79	683.05	T	P																																				P					
43R-CC, 18-21	693.05	C	P																				R				R												A	F					
44R-CC, 11-14	705.92	C	P																														F						R	R					
45R-CC, 10-12	712.39	C	P			F																											F	F				F	F					
46R-CC, 12-15	725.02	C	P			F																	R						R										F	F					
47R-CC, 37-41	735.32	F	P			F																																	R	R					
48R-CC, 23-24	738.98	C	P			F													F		F																		R	R					
49R-CC, 14-17	753.94	F	M			F								F					F			R					R							R			F		F					
50R-CC, 21-24	760.91	F	M			R								F					F	R																	R		F					
51R-CC, 10-13	767.14	F	M			R								F					F	R																	R		F					
52R-CC, 16-18	782.96	F	P											R					F	R		R					R																	
53R-6, 98-100	790.91	F	M			R								F					F		F	R					R								F				R					
54R-CC, 18-20	802.14	F	M											F					F																				R						

Notes: Abundance (number of specimens per field of view): A = abundant (2–9); C = common (lower range of abundant); F = few (0.5–1.0); R = rare (1–3 per tray); T = trace (<1 per transect of slide). Preservation: G = good; M = moderate; P = poor.

Table T6. Tensor tool orientation data for cores, Hole 1115B.

Core	Inclination angle (°)	Mean MTF (°)
180-1115B-		
3H	1.3	140.5
4H	1.5	284.8
5H	1.2	250.9
6H	1.3	40.0
7H	1.1	158.8
8H	1.2	49.3
9H	1.1	16.9
10H	0.95	110.6
11H	0.7	179.8
12H	1.0	351.2
13H	0.98	324.2
14H	0.88	297.7
15H	0.73	114.7
16H	0.75	112.7
17H	0.8	83.7
18H	0.61	173.4
19H	0.84	352.4
20H	0.65	206.9
21H	0.9	68.0
22H	1.3	19.9
23H	1.1	275.7

Notes: Inclination angle = drift of z-axis of core from true vertical (Local declination anomaly is 8°E). Orientation parameter (MTF) = angle in degrees between magnetic north and the double line (+x direction) marked on the center of working half of core.

Table T7. Interstitial water geochemistry, Site 1115.

Core, section, interval (cm)	Depth (mbsf)	pH	Alkalinity (mM)	Salinity	Cl (T) (mM)	Cl (IC) (mM)	SO_4 (mM)	Na (mM)	K (mM)	Mg (mM)	Ca (mM)	Ca/Mg	Li (µM)	NH_4 (µM)	Sr (µM)	SiO_2 (µM)
180-1115A-																
1H-1, 23-28	0.23	7.91	3.126	34.5	553	550	28.4	473	11.1	52.0	10.4	0.20	28	0	96	291
1H-3, 145-150	2.95	7.78	3.472	34.5	558	554	28.9	474	12.1	52.4	10.2	0.19	27	0	96	399
1H-4, 115-120	4.15	7.78	3.58	34.5	549	552	27.6	472	12.2	51.8	9.9	0.19	27	0	134	454
180-1115B-																
2H-1, 145-150	8.65	7.78	3.894	34	549	552	27.1	479	12.4	51.6	9.4	0.18	27	181	146	471
3H-3, 145-150	21.15	7.70	4.693	35	553	555	26.0	481	12.4	51.6	8.9	0.17	27	332	216	520
4H-1, 145-150	27.65	7.78	4.809	34	554	559	24.8	481	12.2	50.6	8.3	0.16	25	351	243	493
5H-1, 145-150	37.15	7.76	5.096	34	555	561	23.0	480	12.6	49.0	7.7	0.16	25	565	293	528
6H-1, 145-150	46.65	7.86	5.542	34	553	562	22.8	484	12.7	48.9	7.6	0.16	26	685	317	520
7H-1, 145-150	56.15	7.74	5.887	34	554	557	18.5	482	12.3	46.3	6.9	0.15	26	741	328	530
8H-1, 145-150	65.65	7.86	5.959	34	552	559	16.6	481	12.1	44.7	6.5	0.15	25	927	338	540
9H-3, 145-150	78.15	7.81	5.564	33	551	558	14.5	479	12.7	42.3	5.5	0.13	26	1028	296	501
10H-3, 145-150	87.65	7.92	6.096	32	548	557	12.3	467	12.0	40.9	5.5	0.13	24	1174	300	518
11H-1, 145-150	94.15	7.92	5.719	32	548	555	11.0	470	12.2	40.3	5.3	0.13	24	1163	283	547
12H-1, 145-150	103.65	7.85	6.179	32	542	559	9.1	467	11.4	39.1	5.4	0.14	24	1210	267	557
13H-1, 145-150	113.15	7.55	5.874	32	542	558	7.7	468	11.6	38.4	5.2	0.14	23	1326	249	533
14H-1, 145-150	122.65	7.86	5.626	32	544	558	6.8	466	11.3	37.9	5.4	0.14	24	1288	239	444
15H-1, 145-150	132.15	7.88	5.85	32	543	557	5.9	463	11.1	37.3	5.1	0.14	24	1347	229	486
16H-2, 145-150	143.15	7.83	5.232	32	540	556	4.6	459	11.0	36.5	5.2	0.14	24	1386	215	434
17H-1, 145-150	151.15	7.85	5.008	32	542	557	3.7	460	11.0	36.1	5.5	0.15	24	1486	210	432
18H-2, 145-150	162.15	7.79	4.779	31	545	556	2.8	457	11.3	34.6	5.7	0.17	24	1514	209	392
19H-1, 145-150	170.15	7.88	5.142	31	544	553	2.2	452	10.5	34.4	5.5	0.16	24	1391	206	510
20H-1, 145-150	179.65	7.92	5.185	30	538	556	1.5	451	10.5	34.1	5.6	0.16	24	1660	205	543
21H-1, 145-150	189.15	7.9	5.162	30	535	552	0.9	452	10.4	33.1	5.5	0.17	24	1580	198	510
22H-1, 145-150	198.65	7.85	5.176	30	534	553	0.0	451	10.5	32.0	5.4	0.17	24	1610	192	390
23H-1, 145-150	208.15	7.88	5.159	30	538	531	0.0	433	10.4	31.5	5.7	0.18	23	1636	188	510
24X-1, 145-150	217.65	7.85	5.373	30	536	537	1.2	451	10.6	33.4	6.2	0.19	23	1379	183	663
25X-1, 145-150	227.25	7.83	5.815	30	538	527	0.6	433	10.1	31.1	6.2	0.20	25	1665	192	715
26X-1, 115-120	236.55	7.69	5.848	30	528	526	0.7	433	10.3	31.0	6.6	0.21	30	1792	183	767
27X-1, 145-150	246.45	7.92	6.068	30	526	521	0.1	425	9.9	30.7	6.8	0.22	36	1792	185	757
28X-1, 145-150	256.05	7.92	6.385	30	522	526	0.0	424	9.9	31.2	7.8	0.25	39	1749	195	760
29X-1, 145-150	265.75	7.48	6.489	30	523	520	1.0	426	10.1	32.5	7.6	0.24	47	1792	193	893
31X-2, 145-150	286.45	8	5.842	30	523	523	0.7	422	10.4	32.4	7.9	0.24	49	1983	212	720
180-1115C-																
2R-1, 144-150	294.24	7.86	6.709	30	530	532	0.1	424	9.6	33.6	9.0	0.27	51	1851	225	751
3R-5, 115-120	309.65	7.58	5.8	30	530	534	0.2	425	9.6	34.1	9.4	0.27	55	1780	234	795
4R-1, 146-151	313.56	7.86	5.863	30	533	534	1.7	427	9.2	35.4	10.0	0.28	52	1773	234	751
5R-1, 120-127	322.90	7.8	5.535	30	528	534	0.5	424	9.2	34.8	10.0	0.29	53	1879	244	773
6R-1, 140-145	332.80	7.73	5.404	30	534	537	0.6	432	9.0	36.7	10.5	0.29	54	1757	256	766
7R-1, 141-146	342.41	7.79	5.003	30	536	543	1.2	430	8.8	35.6	10.6	0.30	52	1784	263	768
8R-1, 79-84	351.39	7.76	3.437	30	539	542	0.0	427	8.9	35.0	10.7	0.31	52	1853	282	610
9R-1, 113-119	361.03	7.76	3.778	30.5	538	546	1.0	429	8.5	37.1	13.0	0.35	51	1857	305	686
10R-1, 145-150	370.95	7.79	3.966	30.5	542	552	0.3	424	8.0	36.9	12.7	0.34	53	1763	343	859
11R-4, 30-41	383.72	7.78	3.226	31	539	555	0.9	426	7.6	37.4	13.2	0.35	47	1684	348	730
12R-3, 130-140	392.80	8.01	1.989	31	544	559	0.0	428	7.7	36.6	13.4	0.37	46	1744	351	588
13R-2, 0-4	399.60	8.03	1.892	31	546	560	0.1	421	6.9	37.1	14.5	0.39	45	1719	361	591
14R-1, 135-144	409.05	8.26	1.342	31	546	563	0.0	422	6.5	37.1	15.2	0.41	46	1617	369	508
15R-2, 140-150	420.20	8.14	1.273	31	548	571	0.2	422	5.5	37.8	17.6	0.47	48	1608	362	135
16R-1, 69-79	427.59	8.37	0.824	31	548	572	0.0	423	5.1	36.2	19.1	0.53	49	1645	366	94
17R-1, 109-119	437.59	8.42	0.967	31	550	568	0.0	418	4.1	35.8	21.7	0.60	51	1592	355	121
21R-2, 86-96	476.58	8.71	0.911	32	551	550	0.9	409	2.7	32.1	35.9	1.12	46	1252	379	233
22R-1, 140-150	485.90	8.46	0.751	32	552	553	0.2	407	2.5	30.2	40.0	1.32	43	1172	403	260
23R-1, 123-138	495.33	8.49	0.716	32	554	556	0.4	404	2.3	29.1	43.0	1.48	45	1050	366	510
25R-1, 140-150	514.80	8.41	0.903	32	545	546	2.5	401	2.0	26.6	48.6	1.83	39	906	400	262
28R-1, 20-30	542.40	8.59	0.842	32	556	560	0.4	397	1.7	21.9	60.1	2.75	32	894	400	128
32R-3, 116-126	584.11	8.9	0.809	34	561	568	0.9	370	1.4	8.5	94.5	11.19	18	845	324	116
34R-1, 138-148	601.18	9.08	0.928	35.5	587	589	0.1	397	1.2	3.5	120.9	34.45	18	1144	318	88
40R-2, 140-150	660.70	8.97	1.001	36.5	607	619	0.3	370	1.1	2.6	128.5	49.71	23	1394	106	96
42R-3, 140-150	680.79	9.08	1.172	37	603	615	0.3	369	1.1	2.9	124.4	42.31	25	1651	61	84
44R-1, 98-108	697.48			37	603	618	0.8	373	1.1	2.5	124.7	50.39	28	1693	45	109
46R-1, 105-115	716.75	9	1.155	37	605	621	1.2	381	1.2	2.8	121.6	43.43	30	1829	30	138
48R-1, 78-88	735.88			37	605	620	1.4	385	1.2	3.1	120.0	38.88	35	1721	24	113
50R-5, 90-102	760.13	8.94	1.636	37	611	629	0.5	387	1.2	2.8	121.2	43.53	41	1848	21	105
52R-1, 103-113	774.63				607	626	1.6	394	1.3	3.2	115.8	35.90	39		19	
54R-4, 140-150	798.14			38	636	639	0.3	395	1.1	2.1	121.4	58.78	38	2326	18	101

Notes: Cl (T) = chloride by titration, Cl (IC) = chloride by chromatography. Blank spaces = not detected.

Table T8. Composition of headspace gas in sediments, Site 1115. (Continued on next page.)

Core, section, interval (cm)	Depth (mbsf)	C_1	C_2	C_3	C_1/C_2
180-1115A-					
1H-3, 0-5	1.50				
180-1115B-					
2H-3, 0-5	10.20	2			
3H-6, 0-5	24.20	2			
4H-2, 0-5	27.70	2			
5H-2, 0-5	37.20	2			
6H-2, 0-5	46.70	2			
7H-2, 0-5	56.20	2			
8H-2, 0-5	65.70	2			
9H-3, 0-5	76.70	2			
10H-4, 0-5	87.70	2			
11H-2, 0-5	94.20	2			
12H-2, 0-5	103.70	2			
13H-2, 0-5	113.20	2			
14H-2, 0-5	122.70	2			
15H-2, 0-5	132.20	2			
16H-3, 0-5	143.20	2			
17H-2, 0-5	151.20	3			
18H-2, 0-5	160.70	2			
19H-2, 0-5	170.20	2			
20H-2, 0-5	179.70	3			
21H-2, 0-5	189.20	3			
22H-2, 0-5	198.70	2			
23H-2, 0-5	208.20	4			
24X-3, 0-5	219.20	265			
25X-3, 0-5	228.80	849			
26X-3, 0-5	238.40	961			
27X-2, 0-5	246.50	1,208			
28X-1, 145-150	256.05	1,767			
29X-2, 0-5	265.80	1,548			
30X-1, 102-107	274.92	2,025			
31X-5, 0-5	289.50	2,434	1		3,477
180-1115C-					
1R-4, 0-5	287.58	3,210	1		3,210
2R-2, 0-2	294.30	1,871			
3R-3, 0-2	305.50	1,749			
4R-2, 0-2	313.61	2,841			
5R-3, 0-2	324.47	1,922			
6R-2, 0-2	332.90	1,857			
7R-2, 0-2	342.46	1,526			
8R-2, 0-2	351.44	1,579			
9R-2, 0-2	361.09	1,164			
10R-2, 0-2	371.00	2,404	1		2,404
11R-3, 0-2	382.02	2,774	1		2,522
12R-1, 0-2	388.50	1,850	1		2,313
13R-3, 0-2	400.97	2,108	1		2,108
14R-1, 134-135	409.04	1,434			
15R-3, 0-2	420.30	974			
16R-2, 0-2	427.69	1,332			
17R-2, 0-2	437.69	2,015	1		1,832
18R-2, 0-2	447.58	1,287	1		1,609
19R-1, 0-2	455.60	668			
20R-1, 54-57	465.74	305			
21R-3, 0-2	476.68	436			
22R-2, 0-2	486.00	180			
23R-2, 0-2	495.48	25			
24R-3, 0-2	506.80	9			
25R-2, 0-2	514.90	3			
26R-1, 39-41	523.39	2			
27R-1, 0-2	532.60	3			
28R-1, 0-2	542.20	3			
29R-2, 0-2	553.25	877			
30R-4, 0-2	564.78	1,017			
32R-3, 114-115	584.09	14,767	2		7,032
33R-3, 113-115	594.19	21,056	4		5,264
34R-1, 136-138	601.16	37,313	7		5,182
35R-2, 0-2	610.78	21,451	4		5,363

Table T8 (continued).

Core, section, interval (cm)	Depth (mbsf)	C_1	C_2	C_3	C_1/C_2
36R-2, 132-134	621.82	18,952	3		5,743
39R-CC, 0-1	648.10	16,619	5		3,324
40R-4, 0-1	662.30	46,800	9		5,143
41R-2, 0-2	668.86	16,641	4		4,160
42R-4, 0-2	680.89	31,554	6		5,009
43R-3, 0-1	689.80	12,267	5		2,610
44R-2, 0-1	697.58	21,290	4		5,459
45R-3, 0-1	708.61	41,487	7		5,843
46R-2, 0-2	716.85	62,461	11		5,527
47R-2, 0-2	726.76	37,682	7		5,624
48R-3, 0-2	737.65	40,163	8		4,958
49R-6, 0-2	751.58	9,121	2		3,800
50R-6, 0-2	760.25	28,289	6		4,420
51R-3, 0-2	766.33	38,019	7		5,280
52R-2, 0-2	774.73	44,398	8		5,842
53R-5, 0-2	788.51	17,072	3	1	5,887
54R-5, 0-2	798.24	27,479	5		5,089

Notes: All concentrations are reported in parts per million by volume. Blanks indicate values below detection limit, except for C_1/C_2 ratio where blanks indicate an undefined value.

Table T9. Calcium carbonate, carbon, nitrogen, and sulfur contents in sediments, Site 1115. (Continued on next page.)

Core, section, interval (cm)	Depth (mbsf)	Inorganic carbon (wt%)	$CaCO_3$ (wt%)	Organic carbon (wt%)	Total nitrogen (wt%)	C/N	Total sulfur (wt%)
180-1115A-							
1H-3, 131.5-132.5	2.82	8.78	73.20	0.07	0.05	1	0.12
180-1115B-							
1H-2, 131-132	2.81	8.76	73.00				0.10
1H-5, 87-88	6.87	9.29	77.40		0.01		0.08
2H-2, 71-73	9.41	7.96	66.30	0.08			0.13
3H-1, 50-51	17.20	7.51	62.60				0.08
4H-1, 66-67	26.86	7.47	62.20	0.12			0.08
6H-1, 43-43.5	45.63	7.78	64.90				0.22
7H-1, 48-48.5	55.18	5.95	49.60				
8H-1, 66-67	64.86	7.34	61.20				0.53
9H-6, 90-91	82.10	6.88	57.30	0.03			0.16
10H-4, 142.5-144	89.13	6.67	55.60	0.02			0.19
11H-2, 127-129	95.47	7.74	64.50	0.11			
12H-4, 140-141	108.10	7.06	58.80	0.03			0.18
13H-6, 129-130	120.49	6.61	55.10	0.13			
14H-4, 59.5-60.5	126.29	4.23	35.30				0.09
15H-4, 115-116	136.35	5.83	48.60				0.09
16H-1, 54-56	140.74	4.22	35.20	0.12			0.18
17H-2, 50-51	151.70	5.22	43.50	0.05			
18H-1, 43-44	159.63	5.63	46.90	0.06			0.09
19H-1, 26-27	168.96	5.87	48.90				
20H-1, 32-33	178.52	4.76	39.70	0.28			
21H-1, 34.5-35	188.04	5.02	41.90	0.30			
22H-1, 31-32	197.51	4.21	35.10	0.42			0.10
23H-1, 28-29	206.98	4.41	36.80	0.29			
24X-3, 118-119	220.38	3.10	25.90	0.36			1.29
25X-3, 118-120	229.98	3.59	29.90	0.53			1.46
26X-4, 67.5-68.5	240.57	5.43	45.30	0.27			0.61
27X-4, 60-61	250.10	2.42	20.20	0.41			0.78
28X-1, 84-85	255.44	2.81	23.40	0.29			0.67
29X-7, 18-19	273.48	2.16	18.00	0.41	0.01	41	0.43
31X-1, 32-33	283.82	2.45	20.50	0.47			0.28
180-1115C-							
1R-1, 30-31	283.50	2.22	18.60	0.37			0.61
2R-1, 12-13	292.92	9.00	75.00	0.24			0.16
2R-1, 38-40	293.18	1.92	16.00	0.68			0.62
3R-1, 19-20	302.69	2.27	19.00	0.68			0.47
4R-1, 107-109	313.17	2.39	20.00	0.42			0.39
5R-1, 39-41	322.09	2.73	22.80	0.46			
6R-1, 32-33	331.72	2.47	20.60	0.43	0.03	14	0.54
7R-1, 79-81	341.79	2.59	21.60	0.66	0.04	17	0.47
8R-2, 18-20	351.62	2.66	22.20	0.84	0.06	14	0.59
9R-4, 34-35	364.05	2.69	22.40	0.43	0.02	22	0.13
10R-4, 113.5-115.5	375.14	2.47	20.60	0.44			
1R-1, 14-16	379.24	2.86	23.90	0.52	0.04	13	0.39
12R-1, 30-32	388.80	2.11	17.60	0.40			0.21
13R-1, 77-78	398.87	2.81	23.40	0.60	0.02	30	0.29
14R-1, 53-54	408.23	3.53	29.50	0.28	0.02	14	
15R-1, 59-60	417.89	4.72	39.30	0.45	0.03	15	
16R-CC, 5-6	428.60	4.05	33.80	0.22			
17R-2, 54-55.5	438.23	1.89	15.80	0.32			
18R-2, 66-68	448.24	1.73	14.50	0.32			
19R-CC, 8-9	456.10	6.28	52.30	0.22			
21R-1, 11-12	475.01	2.36	19.70	0.08			
21R-2, 7-8	475.79	2.54	21.20	0.24			
22R-5, 12-13	489.88	2.83	23.60	0.36	0.02	18	
23R-2, 143-144	496.91	2.94	24.50	0.33	0.01	33	
24R-1, 112-113	504.92	1.17	9.80	0.23			
25R-2, 43-44	515.33	0.03	0.30	0.66	0.03	22	0.24
26R-1, 13-14	523.13	4.63	38.60	0.23			
27R-1, 19-20	532.79	2.35	19.60				
28R-1, 67-68	542.87	4.92	41.00	0.26			
29R-1, 78-80	552.58	6.38	53.20	0.15			
29R-1, 124-125	553.04	0.18	1.50	0.02			
29R-2, 99-100	554.24	0.10	0.80	0.12			

Table T9 (continued).

Core, section, interval (cm)	Depth (mbsf)	Inorganic carbon (wt%)	$CaCO_3$ (wt%)	Organic carbon (wt%)	Total nitrogen (wt%)	C/N	Total sulfur (wt%)
30R-2, 125-126	563.18	0.03	0.30	3.84			6.52
30R-4, 56-57	565.36	0.03	0.30	0.04			1.49
31R-1, 101.5-102	572.02	4.87	40.60	0.02			0.89
32R-1, 46-47	581.06	0.09	0.80	0.08			0.36
33R-1, 22-23	590.42	0.20	1.70	0.03			0.07
34R-1, 50-51	600.30	1.10	9.20	0.13			0.32
35R-4, 24-25	613.91	0.19	1.60	0.11			0.27
36R-1, 85-86	619.95	0.21	1.80	0.01			1.64
40R-3, 84-85	661.64	0.82	6.90	0.69			0.31
41R-4, 7-8	671.93	1.22	10.20	0.80			0.40
42R-4, 69-70	681.58	1.01	8.50	0.63			0.45
43R-2, 53-55	688.83	1.05	8.80	0.58			0.27
44R-1, 30-32	696.80	1.06	8.90	0.66			0.57
45R-1, 49-50	706.59	1.15	9.70	0.61			0.27
46R-2, 7-9	716.92	1.13	9.40	0.54			0.33
47R-2, 3-5	726.79	0.62	5.20	0.23			
48R-1, 41-43	735.51	0.87	7.30	0.54			0.33
49R-2, 21-22	746.20	0.85	7.10	0.80			0.46
50R-1, 29-30	754.59	1.05	8.80	0.85			0.50
51R-2, 62-63	765.84	0.89	7.50	0.33			0.56
53R-3, 15-16	786.19	0.95	8.00	0.45			0.23
54R-7, 105-106	801.88	1.01	8.50	0.51			0.19

Note: Blanks indicate values below detection limit, except for C/N ratio where blanks indicate an undefined value.

Table T10. Total bacterial populations and numbers of dividing and divided cells in sediments, Site 1115.

Depth (mbsf)	Total bacterial population (log cells/cm^3)	Dividing and divided cells (log cells/cm^3)
0.01	8.451	7.382
1.50	7.633	6.524
3.00	7.512	6.424
8.70	7.108	5.928
21.20	7.019	5.931
27.70	7.004	5.669
37.20	7.056	5.406
46.70	6.972	5.415
56.20	6.788	5.390
65.70	6.893	5.185
78.20	6.726	5.377
87.70	6.718	5.375
103.70	6.591	5.336
122.70	6.596	5.411
143.20	6.516	5.174
162.20	6.688	5.226
179.70	6.519	4.866
198.70	6.304	4.813
217.70	6.266	4.803
236.90	6.467	5.166
256.10	6.454	5.454
286.50	6.511	5.199
310.00	6.249	4.757
322.97	6.290	4.785
342.46	6.293	4.774
361.09	6.278	5.074
383.41	6.201	4.738
399.59	6.238	4.807
420.30	6.264	5.133
437.69	6.119	4.776
476.68	6.170	4.739
495.48	6.005	4.644
514.90	6.050	4.635
555.06	5.948	4.587
584.10	6.235	4.633
601.15	5.977	4.579
660.80	5.927	4.605
680.89	5.877	4.555
697.58	5.812	4.858
716.85	5.687	4.541
736.28	5.818	4.841
760.12	5.693	4.489
774.73	5.633	4.170
800.83	5.545	0.000

Table T11. Index properties measured in cores, Site 1115. (Continued on next eight pages. See table note.)

Leg	Site	Hole	Core	Type	Section	Top (cm)	Bottom (cm)	Depth (mbsf)	Water content (bulk)	Water content (dry)	Bulk density ($g \cdot cm^{-3}$)	Dry density ($g \cdot cm^{-3}$)	Grain density ($g \cdot cm^{-3}$)	Porosity (%)	Void ratio
180	1115	A	1	H	2	65	67	0.93	45.7	84.3	1.501	0.814	2.469	67.0	2.03
180	1115	A	1	H	3	108	110	2.58	48.8	95.2	1.481	0.759	2.578	70.6	2.40
180	1115	A	1	H	4	60	62	3.60	46.2	85.9	1.514	0.814	2.569	68.3	2.16
180	1115	B	1	H	1	107	109	1.07	48.0	92.5	1.506	0.782	2.666	70.6	2.41
180	1115	B	1	H	2	83	85	2.33	47.1	88.9	1.500	0.794	2.557	68.9	2.22
180	1115	B	1	H	3	52	54	3.52	47.5	90.6	1.520	0.798	2.707	70.5	2.39
180	1115	B	1	H	4	97	99	5.47	49.6	98.4	1.487	0.750	2.678	72.0	2.57
180	1115	B	1	H	5	28	30	6.28	41.3	70.5	1.589	0.932	2.603	64.2	1.79
180	1115	B	2	H	1	82	84	8.02	47.3	89.8	1.523	0.803	2.707	70.4	2.37
180	1115	B	2	H	2	122	124	9.92	46.5	86.9	1.522	0.814	2.638	69.1	2.24
180	1115	B	2	H	3	109	111	11.29	46.9	88.2	1.515	0.805	2.628	69.4	2.26
180	1115	B	2	H	4	89	91	12.59	47.6	90.8	1.526	0.799	2.749	70.9	2.44
180	1115	B	2	H	5	104	106	14.24	49.0	96.1	1.510	0.770	2.778	72.3	2.61
180	1115	B	2	H	6	94	96	15.64	50.4	101.4	1.475	0.732	2.667	72.5	2.64
180	1115	B	2	H	7	21	23	16.41	48.2	93.1	1.508	0.781	2.695	71.0	2.45
180	1115	B	3	H	1	4	6	16.74	56.1	128.0	1.398	0.613	2.623	76.6	3.28
180	1115	B	3	H	2	4	6	18.24	44.1	78.8	1.578	0.883	2.750	67.9	2.12
180	1115	B	3	H	3	4	6	19.74	47.4	90.0	1.531	0.806	2.763	70.8	2.43
180	1115	B	3	H	4	4	6	21.24	46.4	86.6	1.530	0.820	2.676	69.3	2.26
180	1115	B	3	H	5	4	6	22.74	43.3	76.4	1.578	0.895	2.693	66.8	2.01
180	1115	B	3	H	6	4	6	24.24	46.4	86.7	1.527	0.818	2.659	69.2	2.25
180	1115	B	3	H	7	4	6	25.74	47.2	89.4	1.510	0.797	2.621	69.6	2.29
180	1115	B	4	H	1	8	10	26.28	54.9	121.6	1.349	0.609	2.195	72.3	2.61
180	1115	B	4	H	2	8	10	27.78	45.7	84.1	1.538	0.836	2.663	68.6	2.19
180	1115	B	4	H	3	8	10	29.28	43.5	77.0	1.588	0.897	2.757	67.5	2.07
180	1115	B	4	H	4	8	10	30.78	45.3	82.7	1.551	0.849	2.701	68.6	2.18
180	1115	B	4	H	5	8	10	32.28	45.8	84.5	1.546	0.838	2.718	69.2	2.24
180	1115	B	4	H	6	8	10	33.78	42.9	75.2	1.603	0.915	2.787	67.2	2.05
180	1115	B	4	H	7	8	10	35.28	43.0	75.5	1.576	0.898	2.660	66.2	1.96
180	1115	B	5	H	1	4	6	35.74	48.0	92.2	1.514	0.788	2.710	70.9	2.44
180	1115	B	5	H	2	4	6	37.24	45.4	83.2	1.559	0.851	2.761	69.2	2.24
180	1115	B	5	H	3	4	6	38.74	45.4	83.1	1.549	0.846	2.701	68.7	2.19
180	1115	B	5	H	4	4	6	40.24	43.1	75.8	1.600	0.910	2.788	67.4	2.06
180	1115	B	5	H	5	4	6	41.74	40.7	68.8	1.632	0.967	2.757	64.9	1.85
180	1115	B	5	H	6	4	6	43.24	44.0	78.6	1.578	0.884	2.749	67.9	2.11
180	1115	B	5	H	7	4	6	44.74	44.5	80.2	1.556	0.864	2.665	67.6	2.09
180	1115	B	6	H	1	5	7	45.25	54.3	118.6	1.427	0.653	2.679	75.6	3.10
180	1115	B	6	H	2	5	7	46.75	43.9	78.1	1.586	0.890	2.774	67.9	2.12
180	1115	B	6	H	3	5	7	48.25	42.0	72.4	1.595	0.925	2.673	65.4	1.89
180	1115	B	6	H	4	5	7	49.75	44.2	79.2	1.558	0.870	2.654	67.2	2.05
180	1115	B	6	H	5	5	7	51.25	44.3	79.6	1.577	0.878	2.767	68.3	2.15
180	1115	B	6	H	6	5	7	52.75	43.2	76.2	1.594	0.905	2.768	67.3	2.06
180	1115	B	6	H	7	5	7	54.25	44.3	79.5	1.560	0.869	2.673	67.5	2.08
180	1115	B	7	H	1	90	92	55.60	43.5	76.9	1.582	0.895	2.723	67.1	2.04
180	1115	B	7	H	2	4	6	56.24	44.2	79.1	1.579	0.882	2.764	68.1	2.14
180	1115	B	7	H	3	4	6	57.74	37.5	60.0	1.631	1.019	2.530	59.7	1.48
180	1115	B	7	H	4	4	6	59.24	45.4	83.2	1.545	0.844	2.680	68.5	2.18
180	1115	B	7	H	5	4	6	60.74	42.2	72.9	1.611	0.931	2.766	66.3	1.97

Table T11 (continued).

Leg	Site	Hole	Core	Type	Section	Top (cm)	Bottom (cm)	Depth (mbsf)	Water content (bulk)	Water content (dry)	Bulk density (g·cm^{-3})	Dry density (g·cm^{-3})	Grain density (g·cm^{-3})	Porosity (%)	Void ratio
180	1115	B	7	H	6	4	6	62.24	38.0	61.3	1.620	1.004	2.518	60.1	1.51
180	1115	B	7	H	7	4	6	63.74	41.2	70.2	1.622	0.953	2.748	65.3	1.88
180	1115	B	8	H	1	60	62	64.80	42.2	73.1	1.594	0.921	2.688	65.7	1.92
180	1115	B	8	H	2	5	7	65.75	43.4	76.7	1.590	0.900	2.759	67.4	2.07
180	1115	B	8	H	3	5	7	67.25	42.6	74.1	1.591	0.914	2.696	66.1	1.95
180	1115	B	8	H	4	5	7	68.75	40.4	67.8	1.636	0.975	2.752	64.6	1.82
180	1115	B	8	H	5	5	7	70.25	41.5	71.1	1.596	0.933	2.648	64.8	1.84
180	1115	B	8	H	6	5	7	71.75	43.5	76.9	1.598	0.903	2.811	67.9	2.11
180	1115	B	8	H	7	5	7	73.25	45.1	82.1	1.555	0.854	2.707	68.5	2.17
180	1115	B	9	H	1	80	82	74.50	46.9	88.2	1.526	0.811	2.686	69.8	2.31
180	1115	B	9	H	2	4	6	75.24	44.0	78.6	1.579	0.884	2.754	67.9	2.12
180	1115	B	9	H	3	4	6	76.74	43.6	77.4	1.572	0.886	2.683	67.0	2.03
180	1115	B	9	H	4	4	6	78.24	43.3	76.3	1.571	0.891	2.652	66.4	1.98
180	1115	B	9	H	5	4	6	79.74	42.3	73.2	1.599	0.924	2.716	66.0	1.94
180	1115	B	9	H	6	4	6	81.24	42.1	72.6	1.588	0.920	2.647	65.2	1.88
180	1115	B	9	H	7	4	6	82.74	45.1	82.1	1.548	0.851	2.671	68.2	2.14
180	1115	B	10	H	1	88	90	84.08	44.9	81.6	1.543	0.850	2.634	67.7	2.10
180	1115	B	10	H	2	67	69	85.37	42.5	73.8	1.578	0.908	2.626	65.4	1.89
180	1115	B	10	H	3	77	79	86.97	41.8	71.7	1.589	0.925	2.629	64.8	1.84
180	1115	B	10	H	4	90	92	88.60	41.9	72.0	1.601	0.931	2.696	65.5	1.90
180	1115	B	10	H	5	90	92	90.10	43.3	76.5	1.586	0.899	2.734	67.1	2.04
180	1115	B	10	H	6	90	92	91.60	44.2	79.1	1.571	0.877	2.718	67.7	2.10
180	1115	B	10	H	7	23	25	92.43	40.3	67.6	1.625	0.970	2.692	64.0	1.78
180	1115	B	11	H	1	90	92	93.60	42.5	74.0	1.590	0.914	2.694	66.1	1.95
180	1115	B	11	H	2	105	107	95.25	40.0	66.6	1.613	0.968	2.612	62.9	1.70
180	1115	B	11	H	3	77	79	96.47	42.5	73.9	1.596	0.918	2.717	66.2	1.96
180	1115	B	11	H	4	77	79	97.97	40.5	68.0	1.606	0.956	2.618	63.5	1.74
180	1115	B	11	H	5	74	76	99.44	42.7	74.4	1.604	0.920	2.772	66.8	2.01
180	1115	B	11	H	6	54	56	100.74	41.3	70.5	1.623	0.952	2.763	65.5	1.90
180	1115	B	11	H	7	18	20	101.88	42.6	74.2	1.599	0.918	2.742	66.5	1.99
180	1115	B	12	H	1	69	71	102.89	46.5	87.0	1.534	0.820	2.707	69.7	2.30
180	1115	B	12	H	2	61	63	104.31	42.7	74.4	1.599	0.917	2.748	66.6	2.00
180	1115	B	12	H	3	61	63	105.81	42.8	74.8	1.605	0.918	2.792	67.1	2.04
180	1115	B	12	H	4	61	63	107.31	42.1	72.8	1.601	0.926	2.715	65.9	1.93
180	1115	B	12	H	5	61	63	108.81	44.2	79.4	1.564	0.872	2.687	67.6	2.08
180	1115	B	12	H	6	61	63	110.31	43.1	75.8	1.582	0.900	2.696	66.6	2.00
180	1115	B	12	H	7	25	27	111.45	44.1	78.7	1.571	0.879	2.709	67.6	2.08
180	1115	B	13	H	1	44	46	112.14	41.2	70.2	1.572	0.924	2.516	63.3	1.72
180	1115	B	13	H	2	44	46	113.64	42.7	74.4	1.581	0.907	2.658	65.9	1.93
180	1115	B	13	H	3	44	46	115.14	40.1	66.9	1.614	0.967	2.626	63.2	1.72
180	1115	B	13	H	4	44	46	116.64	39.9	66.3	1.613	0.970	2.608	62.8	1.69
180	1115	B	13	H	5	44	46	118.14	41.9	72.2	1.601	0.930	2.700	65.6	1.90
180	1115	B	13	H	6	44	46	119.64	42.6	74.3	1.587	0.911	2.682	66.1	1.95
180	1115	B	13	H	7	44	46	121.14	42.9	75.1	1.602	0.915	2.779	67.1	2.04
180	1115	B	14	H	1	44	46	121.64	40.8	68.8	1.574	0.933	2.498	62.7	1.68
180	1115	B	14	H	2	44	46	123.14	43.3	76.4	1.568	0.889	2.638	66.3	1.97
180	1115	B	14	H	3	44	46	124.64	38.1	61.6	1.610	0.996	2.487	59.9	1.50
180	1115	B	14	H	4	44	46	126.14	39.8	66.0	1.587	0.956	2.491	61.6	1.61

Table T11 (continued).

Leg	Site	Hole	Core	Type	Section	Top (cm)	Bottom (cm)	Depth (mbsf)	Water content (bulk)	Water content (dry)	Bulk density (g·cm^{-3})	Dry density (g·cm^{-3})	Grain density (g·cm^{-3})	Porosity (%)	Void ratio
180	1115	B	14	H	5	44	46	127.64	38.0	61.3	1.659	1.029	2.676	61.6	1.60
180	1115	B	14	H	6	44	46	129.14	39.3	64.7	1.623	0.985	2.611	62.3	1.65
180	1115	B	14	H	7	44	46	130.64	39.8	66.2	1.607	0.967	2.580	62.5	1.67
180	1115	B	15	H	1	44	46	131.14	42.3	73.4	1.569	0.905	2.576	64.9	1.85
180	1115	B	15	H	2	44	46	132.64	41.9	72.2	1.595	0.926	2.670	65.3	1.88
180	1115	B	15	H	3	44	46	134.14	39.7	65.8	1.589	0.959	2.494	61.6	1.60
180	1115	B	15	H	4	103	105	136.23	43.8	78.1	1.555	0.873	2.613	66.6	1.99
180	1115	B	15	H	5	36	38	137.06	41.6	71.3	1.613	0.941	2.732	65.5	1.90
180	1115	B	15	H	6	36	38	138.56	41.7	71.5	1.606	0.937	2.703	65.3	1.89
180	1115	B	15	H	7	36	38	140.06	44.2	79.2	1.575	0.879	2.747	68.0	2.13
180	1115	B	16	H	1	39	41	140.59	42.1	72.6	1.593	0.923	2.670	65.4	1.89
180	1115	B	16	H	2	108	110	142.78	44.8	81.3	1.555	0.858	2.689	68.1	2.13
180	1115	B	16	H	3	97	99	144.17	44.4	79.8	1.564	0.870	2.700	67.8	2.10
180	1115	B	16	H	4	39	41	145.09	44.1	78.8	1.571	0.879	2.714	67.6	2.09
180	1115	B	16	H	5	39	41	146.59	42.7	74.5	1.592	0.913	2.715	66.4	1.97
180	1115	B	16	H	6	38	40	148.08	41.9	72.1	1.597	0.928	2.678	65.3	1.89
180	1115	B	16	H	7	39	41	149.59	45.6	83.7	1.557	0.848	2.760	69.3	2.26
180	1115	B	17	H	1	4	6	149.74	42.6	74.3	1.588	0.911	2.688	66.1	1.95
180	1115	B	17	H	2	4	6	151.24	42.8	74.9	1.578	0.902	2.653	66.0	1.94
180	1115	B	17	H	3	4	6	152.74	44.7	80.7	1.551	0.858	2.656	67.7	2.09
180	1115	B	17	H	4	4	6	154.24	46.6	87.2	1.526	0.815	2.663	69.4	2.27
180	1115	B	17	H	5	4	6	155.74	40.9	69.2	1.640	0.969	2.806	65.5	1.90
180	1115	B	17	H	6	4	6	157.24	45.4	83.3	1.550	0.846	2.710	68.8	2.21
180	1115	B	17	H	7	4	6	158.74	41.0	69.5	1.609	0.949	2.668	64.4	1.81
180	1115	B	18	H	1	5	7	159.25	40.1	66.9	1.616	0.968	2.632	63.2	1.72
180	1115	B	18	H	2	5	7	160.75	41.7	71.7	1.612	0.939	2.740	65.7	1.92
180	1115	B	18	H	3	5	7	162.25	39.8	66.1	1.637	0.986	2.707	63.6	1.75
180	1115	B	18	H	4	5	7	163.75	43.5	77.1	1.573	0.888	2.681	66.9	2.02
180	1115	B	18	H	5	5	7	165.25	44.8	81.1	1.551	0.856	2.660	67.8	2.11
180	1115	B	18	H	6	5	7	166.75	43.8	78.0	1.568	0.881	2.679	67.1	2.04
180	1115	B	18	H	7	5	7	168.25	46.1	85.4	1.554	0.838	2.781	69.9	2.32
180	1115	B	19	H	1	7	9	168.77	46.9	88.5	1.542	0.818	2.792	70.7	2.41
180	1115	B	19	H	2	7	9	170.27	43.5	77.1	1.586	0.896	2.748	67.4	2.07
180	1115	B	19	H	3	7	9	171.77	42.9	75.1	1.582	0.903	2.675	66.2	1.96
180	1115	B	19	H	4	7	9	173.27	44.2	79.1	1.562	0.872	2.672	67.4	2.07
180	1115	B	19	H	5	7	9	174.77	46.5	87.0	1.547	0.827	2.787	70.3	2.37
180	1115	B	19	H	6	7	9	176.27	45.4	83.2	1.546	0.844	2.683	68.5	2.18
180	1115	B	19	H	7	7	9	177.77	33.3	49.9	1.704	1.137	2.547	55.4	1.24
180	1115	B	20	H	1	7	9	178.27	46.8	87.9	1.526	0.812	2.681	69.7	2.30
180	1115	B	20	H	2	7	9	179.77	43.0	75.4	1.571	0.896	2.630	66.0	1.94
180	1115	B	20	H	3	7	9	181.27	42.5	73.8	1.575	0.906	2.614	65.3	1.89
180	1115	B	20	H	4	7	9	182.77	36.7	58.0	1.645	1.041	2.537	59.0	1.44
180	1115	B	20	H	5	7	9	184.27	41.0	69.5	1.598	0.943	2.617	64.0	1.78
180	1115	B	20	H	6	7	9	185.77	44.7	80.8	1.550	0.857	2.653	67.7	2.09
180	1115	B	20	H	7	7	9	187.27	44.9	81.3	1.554	0.857	2.682	68.1	2.13
180	1115	B	21	H	1	7	9	187.77	44.8	81.1	1.550	0.856	2.655	67.8	2.10
180	1115	B	21	H	2	7	9	189.27	46.9	88.4	1.546	0.821	2.816	70.9	2.43
180	1115	B	21	H	3	7	9	190.77	44.6	80.6	1.560	0.864	2.700	68.0	2.13

Table T11 (continued).

Leg	Site	Hole	Core	Type	Section	Top (cm)	Bottom (cm)	Depth (mbsf)	Water content (bulk)	Water content (dry)	Bulk density (g·cm^{-3})	Dry density (g·cm^{-3})	Grain density (g·cm^{-3})	Porosity (%)	Void ratio
180	1115	B	21	H	4	7	9	192.27	42.9	75.2	1.577	0.900	2.655	66.1	1.95
180	1115	B	21	H	5	7	9	193.77	38.6	62.9	1.653	1.015	2.693	62.3	1.65
180	1115	B	21	H	6	7	9	195.27	38.4	62.4	1.657	1.020	2.699	62.2	1.65
180	1115	B	21	H	7	7	9	196.77	39.0	63.8	1.645	1.004	2.684	62.6	1.67
180	1115	B	22	H	1	12	14	197.32	40.4	67.8	1.617	0.964	2.665	63.8	1.76
180	1115	B	22	H	2	12	14	198.82	40.9	69.1	1.605	0.950	2.641	64.1	1.78
180	1115	B	22	H	3	12	14	200.32	44.2	79.2	1.556	0.868	2.642	67.1	2.04
180	1115	B	22	H	4	12	14	201.82	40.2	67.3	1.628	0.973	2.702	64.0	1.78
180	1115	B	22	H	5	12	14	203.26	38.1	61.5	1.664	1.030	2.700	61.8	1.62
180	1115	B	22	H	6	12	14	204.76	41.3	70.3	1.597	0.938	2.633	64.4	1.81
180	1115	B	22	H	7	12	14	206.26	42.5	73.9	1.597	0.918	2.725	66.3	1.97
180	1115	B	23	H	1	4	6	206.74	41.9	72.2	1.601	0.930	2.698	65.5	1.90
180	1115	B	23	H	2	4	6	208.24	42.7	74.4	1.602	0.918	2.760	66.7	2.01
180	1115	B	23	H	3	4	6	209.74	44.6	80.4	1.564	0.867	2.713	68.0	2.13
180	1115	B	23	H	4	4	6	211.24	43.4	76.6	1.583	0.896	2.723	67.1	2.04
180	1115	B	23	H	5	4	6	212.74	36.9	58.4	1.679	1.060	2.680	60.4	1.53
180	1115	B	23	H	6	4	6	214.24	45.7	84.3	1.543	0.837	2.695	68.9	2.22
180	1115	B	23	H	7	4	6	215.74	42.5	73.9	1.599	0.919	2.730	66.3	1.97
180	1115	B	24	X	1	49	51	216.69	39.6	65.5	1.611	0.974	2.578	62.2	1.65
180	1115	B	24	X	2	45	47	218.15	40.8	68.9	1.602	0.948	2.621	63.8	1.76
180	1115	B	24	X	3	45	47	219.65	42.8	74.7	1.568	0.897	2.601	65.5	1.90
180	1115	B	24	X	4	45	47	220.95	44.4	79.8	1.552	0.863	2.638	67.3	2.06
180	1115	B	24	X	5	45	47	222.45	40.3	67.6	1.611	0.961	2.632	63.5	1.74
180	1115	B	24	X	6	59	61	224.09	43.8	77.9	1.563	0.878	2.649	66.8	2.02
180	1115	B	24	X	7	59	61	225.29	42.5	74.0	1.582	0.909	2.651	65.7	1.92
180	1115	B	25	X	1	36	38	226.16	44.2	79.2	1.559	0.870	2.658	67.3	2.06
180	1115	B	25	X	2	36	38	227.66	41.5	71.0	1.604	0.938	2.682	65.0	1.86
180	1115	B	25	X	3	36	38	229.16	40.9	69.2	1.594	0.942	2.591	63.6	1.75
180	1115	B	25	X	4	32	34	230.62	36.5	57.5	1.657	1.052	2.571	59.1	1.44
180	1115	B	25	X	5	50	52	232.30	39.6	65.6	1.628	0.983	2.656	63.0	1.70
180	1115	B	25	X	6	36	38	233.66	38.7	63.1	1.638	1.004	2.634	61.9	1.62
180	1115	B	25	X	7	17	19	234.97	36.8	58.3	1.665	1.052	2.621	59.9	1.49
180	1115	B	26	X	1	83	85	236.23	34.9	53.6	1.667	1.085	2.511	56.8	1.31
180	1115	B	26	X	2	36	38	237.26	33.5	50.4	1.677	1.115	2.473	54.9	1.22
180	1115	B	26	X	3	83	85	239.23	37.8	60.6	1.628	1.014	2.536	60.0	1.50
180	1115	B	26	X	4	36	38	240.26	36.2	56.8	1.667	1.063	2.592	59.0	1.44
180	1115	B	26	X	5	110	112	242.50	33.9	51.2	1.694	1.120	2.548	56.0	1.27
180	1115	B	26	X	6	110	112	244.00	34.0	51.4	1.672	1.104	2.477	55.4	1.24
180	1115	B	26	X	7	38	40	244.58	37.6	60.3	1.632	1.018	2.542	60.0	1.50
180	1115	B	27	X	1	39	41	245.39	42.0	72.4	1.585	0.919	2.628	65.0	1.86
180	1115	B	27	X	2	39	41	246.89	39.3	64.7	1.634	0.992	2.660	62.7	1.68
180	1115	B	27	X	3	39	41	248.39	39.2	64.6	1.620	0.984	2.595	62.1	1.64
180	1115	B	27	X	4	39	41	249.89	45.8	84.5	1.538	0.834	2.671	68.8	2.20
180	1115	B	27	X	5	39	41	251.39	22.3	28.6	1.988	1.545	2.721	43.2	0.76
180	1115	B	27	X	6	39	41	252.89	33.4	50.1	1.735	1.156	2.661	56.6	1.30
180	1115	B	28	X	1	20	22	254.80	38.3	62.2	1.640	1.011	2.622	61.4	1.59
180	1115	B	28	X	2	20	22	256.30	37.5	59.9	1.650	1.032	2.603	60.4	1.52
180	1115	B	29	X	1	96	98	265.26	37.3	59.4	1.646	1.032	2.574	59.9	1.49

Table T11 (continued).

Leg	Site	Hole	Core	Type	Section	Top (cm)	Bottom (cm)	Depth (mbsf)	Water content (bulk)	Water content (dry)	Bulk density (g·cm^{-3})	Dry density (g·cm^{-3})	Grain density (g·cm^{-3})	Porosity (%)	Void ratio
180	1115	B	29	X	2	96	98	266.76	38.5	62.6	1.641	1.009	2.634	61.7	1.61
180	1115	B	29	X	3	96	98	268.26	35.2	54.4	1.680	1.088	2.580	57.8	1.37
180	1115	B	29	X	4	96	98	269.76	35.7	55.6	1.680	1.080	2.608	58.6	1.42
180	1115	B	29	X	5	96	98	271.26	38.4	62.2	1.648	1.016	2.653	61.7	1.61
180	1115	B	29	X	6	96	98	272.76	36.3	56.9	1.690	1.077	2.681	59.8	1.49
180	1115	B	30	X	1	70	72	274.60	37.1	58.9	1.669	1.050	2.652	60.4	1.53
180	1115	B	31	X	1	79	81	284.29	39.1	64.2	1.632	0.994	2.634	62.3	1.65
180	1115	B	31	X	2	79	81	285.79	39.3	64.8	1.631	0.989	2.648	62.6	1.68
180	1115	B	31	X	4	79	81	288.79	36.2	56.8	1.677	1.069	2.631	59.4	1.46
180	1115	B	31	X	5	79	81	290.29	36.0	56.1	1.680	1.076	2.623	59.0	1.44
180	1115	B	31	X	6	79	81	291.79	38.5	62.7	1.640	1.008	2.632	61.7	1.61
180	1115	B	31	X	7	17	19	292.67	36.1	56.5	1.672	1.068	2.605	59.0	1.44
180	1115	C	1	R	1	8	10	283.30	33.4	50.2	1.701	1.132	2.544	55.5	1.25
180	1115	C	1	R	2	8	10	284.72	39.5	65.4	1.634	0.988	2.677	63.1	1.71
180	1115	C	1	R	3	8	10	286.18	34.0	51.6	1.697	1.120	2.567	56.4	1.29
180	1115	C	1	R	4	8	10	287.68	36.3	57.0	1.680	1.070	2.647	59.6	1.47
180	1115	C	1	R	5	8	10	289.18	35.5	55.1	1.702	1.097	2.680	59.1	1.44
180	1115	C	2	R	2	22	24	294.54	34.1	51.8	1.724	1.136	2.671	57.5	1.35
180	1115	C	2	R	3	12	14	295.94	34.0	51.4	1.709	1.129	2.606	56.7	1.31
180	1115	C	2	R	4	75	77	296.96	34.3	52.2	1.713	1.126	2.639	57.3	1.34
180	1115	C	2	R	5	79	81	298.50	35.2	54.2	1.694	1.098	2.626	58.2	1.39
180	1115	C	3	R	1	5	7	302.57	33.6	50.6	1.723	1.144	2.631	56.5	1.30
180	1115	C	3	R	2	99	101	305.01	35.3	54.5	1.698	1.099	2.648	58.5	1.41
180	1115	C	3	R	3	39	41	305.91	34.2	52.1	1.729	1.137	2.695	57.8	1.37
180	1115	C	3	R	4	62	64	307.64	33.7	50.8	1.747	1.159	2.724	57.5	1.35
180	1115	C	3	R	5	105	107	309.57	35.3	54.6	1.703	1.102	2.671	58.8	1.42
180	1115	C	3	R	6	37	39	310.39	36.8	58.2	1.673	1.057	2.650	60.1	1.51
180	1115	C	4	R	1	83	85	312.95	36.5	57.5	1.665	1.057	2.603	59.4	1.46
180	1115	C	4	R	2	53	55	314.16	37.2	59.2	1.659	1.042	2.622	60.3	1.52
180	1115	C	4	R	3	20	22	315.33	36.3	56.9	1.681	1.071	2.648	59.5	1.47
180	1115	C	4	R	4	26	28	316.74	36.0	56.3	1.690	1.081	2.664	59.4	1.47
180	1115	C	5	R	1	48	50	322.20	32.0	47.2	1.736	1.179	2.582	54.3	1.19
180	1115	C	5	R	2	8	10	323.07	34.5	52.6	1.716	1.125	2.662	57.8	1.37
180	1115	C	5	R	3	137	139	325.86	33.9	51.2	1.713	1.133	2.614	56.7	1.31
180	1115	C	5	R	4	4	6	326.03	36.1	56.4	1.684	1.077	2.647	59.3	1.46
180	1115	C	6	R	1	51	53	331.93	37.5	59.9	1.660	1.038	2.645	60.7	1.55
180	1115	C	6	R	2	120	122	334.12	35.8	55.9	1.686	1.081	2.637	59.0	1.44
180	1115	C	6	R	3	28	30	334.70	34.6	52.9	1.708	1.117	2.642	57.7	1.36
180	1115	C	6	R	4	19	21	336.11	35.2	54.4	1.699	1.100	2.648	58.5	1.41
180	1115	C	6	R	5	60	62	338.02	35.3	54.6	1.698	1.098	2.653	58.6	1.42
180	1115	C	6	R	6	30	32	339.22	29.5	41.8	1.792	1.264	2.612	51.6	1.07
180	1115	C	7	R	1	75	77	341.77	35.1	54.0	1.708	1.109	2.673	58.5	1.41
180	1115	C	7	R	2	38	40	342.86	37.0	58.7	1.678	1.057	2.685	60.6	1.54
180	1115	C	7	R	3	91	93	344.85	37.2	59.4	1.673	1.050	2.680	60.8	1.55
180	1115	C	7	R	4	94	96	346.31	38.3	62.0	1.652	1.019	2.664	61.7	1.61
180	1115	C	7	R	5	108	110	347.84	38.3	62.0	1.645	1.015	2.636	61.5	1.60
180	1115	C	8	R	1	19	21	350.81	37.9	61.0	1.655	1.028	2.651	61.2	1.58
180	1115	C	8	R	2	9	11	351.55	37.2	59.2	1.664	1.045	2.640	60.4	1.53

Table T11 (continued).

Leg	Site	Hole	Core	Type	Section	Top (cm)	Bottom (cm)	Depth (mbsf)	Water content (bulk)	Water content (dry)	Bulk density (g·cm^{-3})	Dry density (g·cm^{-3})	Grain density (g·cm^{-3})	Porosity (%)	Void ratio
180	1115	C	8	R	4	140	142	355.86	36.9	58.5	1.677	1.058	2.674	60.4	1.53
180	1115	C	8	R	5	8	10	356.04	35.8	55.7	1.687	1.084	2.639	58.9	1.44
180	1115	C	9	R	1	53	55	360.45	34.9	53.7	1.700	1.106	2.634	58.0	1.38
180	1115	C	9	R	2	110	112	362.21	37.6	60.2	1.666	1.040	2.675	61.1	1.57
180	1115	C	9	R	3	110	112	363.49	35.3	54.4	1.698	1.099	2.647	58.5	1.41
180	1115	C	9	R	4	38	40	364.11	34.7	53.2	1.707	1.114	2.646	57.9	1.37
180	1115	C	9	R	5	119	121	366.42	36.8	58.2	1.686	1.066	2.703	60.6	1.54
180	1115	C	10	R	1	89	91	370.41	34.4	52.5	1.717	1.125	2.663	57.7	1.37
180	1115	C	10	R	2	102	104	372.04	34.3	52.3	1.714	1.126	2.647	57.5	1.35
180	1115	C	10	R	3	16	18	372.68	37.1	59.0	1.681	1.057	2.704	60.9	1.56
180	1115	C	10	R	4	119	121	375.21	37.8	60.7	1.660	1.033	2.664	61.2	1.58
180	1115	C	10	R	5	86	88	376.38	36.6	57.6	1.680	1.066	2.663	60.0	1.50
180	1115	C	10	R	6	97	99	377.99	38.0	61.2	1.653	1.025	2.650	61.3	1.59
180	1115	C	11	R	1	8	10	379.20	36.9	58.5	1.667	1.052	2.636	60.1	1.51
180	1115	C	11	R	2	16	18	380.72	38.5	62.6	1.658	1.020	2.706	62.3	1.65
180	1115	C	11	R	3	88	90	382.92	34.1	51.6	1.724	1.137	2.663	57.3	1.34
180	1115	C	11	R	4	87	89	384.31	35.0	53.9	1.729	1.123	2.752	59.2	1.45
180	1115	C	11	R	5	99	101	385.93	37.0	58.8	1.669	1.052	2.651	60.3	1.52
180	1115	C	11	R	6	98	100	387.34	37.2	59.4	1.660	1.042	2.628	60.4	1.52
180	1115	C	12	R	1	64	66	389.16	36.7	58.0	1.632	1.033	2.488	58.5	1.41
180	1115	C	12	R	2	96	98	390.98	34.6	52.9	1.718	1.124	2.679	58.1	1.38
180	1115	C	12	R	3	31	33	391.83	34.0	51.5	1.721	1.136	2.649	57.1	1.33
180	1115	C	12	R	4	114	116	394.06	33.4	50.1	1.737	1.157	2.668	56.6	1.31
180	1115	C	12	R	5	113	115	395.55	30.5	43.9	1.873	1.302	2.942	55.8	1.26
180	1115	C	12	R	6	56	58	396.48	36.4	57.2	1.681	1.070	2.655	59.7	1.48
180	1115	C	12	R	7	18	20	397.60	34.0	51.4	1.718	1.134	2.637	57.0	1.32
180	1115	C	13	R	1	71	73	398.83	36.3	56.9	1.691	1.078	2.687	59.9	1.49
180	1115	C	13	R	2	102	104	400.64	29.9	42.8	1.809	1.267	2.691	52.9	1.12
180	1115	C	13	R	3	103	105	402.02	30.4	43.7	1.797	1.251	2.680	53.3	1.14
180	1115	C	13	R	4	71	73	402.88	33.7	50.7	1.734	1.150	2.676	57.0	1.33
180	1115	C	13	R	5	77	79	404.38	33.7	50.9	1.676	1.111	2.479	55.2	1.23
180	1115	C	13	R	6	71	73	405.76	33.5	50.5	1.740	1.156	2.688	57.0	1.33
180	1115	C	13	R	7	5	7	406.55	33.0	49.3	1.741	1.166	2.658	56.2	1.28
180	1115	C	14	R	1	58	60	408.30	33.0	49.2	1.750	1.173	2.686	56.3	1.29
180	1115	C	14	R	2	95	97	410.11	30.2	43.3	1.809	1.262	2.707	53.4	1.15
180	1115	C	14	R	3	65	67	410.96	33.2	49.6	1.740	1.163	2.664	56.4	1.29
180	1115	C	14	R	4	79	81	411.83	32.0	47.0	1.768	1.203	2.684	55.2	1.23
180	1115	C	15	R	1	5	7	417.37	28.8	40.4	1.826	1.300	2.672	51.3	1.06
180	1115	C	15	R	2	5	7	418.87	27.0	37.0	1.870	1.365	2.695	49.3	0.97
180	1115	C	15	R	3	5	7	420.37	26.9	36.7	1.874	1.371	2.697	49.2	0.97
180	1115	C	15	R	4	5	7	421.87	26.7	36.4	1.877	1.376	2.694	48.9	0.96
180	1115	C	15	R	5	5	7	423.37	27.9	38.6	1.845	1.331	2.672	50.2	1.01
180	1115	C	15	R	6	5	7	424.87	27.9	38.7	1.853	1.336	2.701	50.5	1.02
180	1115	C	16	R	1	8	10	427.00	29.7	42.2	1.811	1.273	2.682	52.5	1.11
180	1115	C	16	R	2	8	10	427.79	20.2	25.3	2.021	1.613	2.680	39.8	0.66
180	1115	C	17	R	1	10	12	436.62	26.2	35.5	1.880	1.388	2.674	48.1	0.93
180	1115	C	17	R	2	10	12	437.81	26.2	35.6	1.893	1.396	2.713	48.5	0.94
180	1115	C	18	R	1	22	24	446.34	27.8	38.5	1.826	1.319	2.614	49.5	0.98

Table T11 (continued).

Leg	Site	Hole	Core	Type	Section	Top (cm)	Bottom (cm)	Depth (mbsf)	Water content (bulk)	Water content (dry)	Bulk density (g·cm^{-3})	Dry density (g·cm^{-3})	Grain density (g·cm^{-3})	Porosity (%)	Void ratio
180	1115	C	18	R	2	22	24	447.82	25.8	34.7	1.869	1.387	2.618	47.0	0.89
180	1115	C	19	R	1	8	10	455.70	27.0	37.0	1.846	1.348	2.627	48.7	0.95
180	1115	C	20	R	1	16	18	465.38	26.1	35.2	1.861	1.376	2.613	47.3	0.90
180	1115	C	21	R	1	64	66	475.56	26.4	35.9	1.854	1.364	2.616	47.8	0.92
180	1115	C	21	R	2	2	4	475.76	27.0	37.1	1.850	1.350	2.639	48.9	0.96
180	1115	C	21	R	3	10	12	476.80	27.4	37.8	1.837	1.333	2.623	49.2	0.97
180	1115	C	21	R	4	40	42	478.42	27.9	38.8	1.835	1.322	2.647	50.1	1.00
180	1115	C	21	R	5	24	26	479.76	27.5	37.9	1.837	1.332	2.628	49.3	0.97
180	1115	C	22	R	1	122	124	485.74	30.5	43.9	1.764	1.226	2.584	52.6	1.11
180	1115	C	22	R	2	31	33	486.33	27.5	37.8	1.837	1.332	2.625	49.2	0.97
180	1115	C	22	R	3	26	28	487.04	27.4	37.7	1.825	1.325	2.587	48.8	0.95
180	1115	C	22	R	4	108	110	489.36	24.7	32.8	1.902	1.432	2.648	45.9	0.85
180	1115	C	22	R	5	19	21	489.97	23.7	31.0	1.933	1.476	2.669	44.7	0.81
180	1115	C	22	R	6	37	39	491.15	21.7	27.6	1.973	1.546	2.652	41.7	0.72
180	1115	C	23	R	1	89	91	495.01	33.7	50.8	1.718	1.139	2.619	56.5	1.30
180	1115	C	23	R	2	139	141	496.89	26.1	35.3	1.866	1.379	2.631	47.6	0.91
180	1115	C	23	R	3	11	13	497.11	27.0	37.1	1.843	1.344	2.619	48.7	0.95
180	1115	C	24	R	1	28	30	504.10	23.0	29.8	1.961	1.510	2.696	44.0	0.79
180	1115	C	24	R	2	91	93	506.23	26.3	35.7	1.877	1.383	2.670	48.2	0.93
180	1115	C	24	R	3	42	44	507.24	23.1	30.0	1.950	1.500	2.675	43.9	0.78
180	1115	C	24	R	4	19	21	508.51	24.7	32.8	1.904	1.434	2.654	46.0	0.85
180	1115	C	24	R	5	31	33	510.13	23.8	31.2	1.925	1.468	2.654	44.7	0.81
180	1115	C	25	R	1	98	100	514.40	27.6	38.2	1.839	1.331	2.643	49.6	0.99
180	1115	C	25	R	2	32	34	515.24	24.6	32.7	1.910	1.440	2.663	45.9	0.85
180	1115	C	27	R	1	34	36	532.96	23.1	30.1	1.960	1.506	2.702	44.3	0.79
180	1115	C	28	R	1	39	41	542.61	24.6	32.6	1.915	1.445	2.673	46.0	0.85
180	1115	C	29	R	2	69	71	553.96	25.4	34.0	1.913	1.428	2.716	47.4	0.90
180	1115	C	29	R	3	40	42	554.71	26.3	35.6	1.879	1.385	2.675	48.2	0.93
180	1115	C	30	R	2	33	35	562.28	21.0	26.6	2.038	1.610	2.768	41.8	0.72
180	1115	C	30	R	4	47	49	565.29	21.3	27.1	1.990	1.565	2.674	41.5	0.71
180	1115	C	30	R	5	20	22	566.23	24.4	32.2	1.936	1.464	2.715	46.1	0.85
180	1115	C	31	R	CC	7	9	572.17	7.2	7.8	2.438	2.262	2.732	17.2	0.21
180	1115	C	32	R	1	79	81	581.41	13.0	14.9	2.285	1.988	2.798	28.9	0.41
180	1115	C	32	R	2	38	40	582.47	19.9	24.8	2.006	1.607	2.632	39.0	0.64
180	1115	C	32	R	3	65	67	583.68	19.5	24.2	2.016	1.623	2.634	38.4	0.62
180	1115	C	32	R	4	101	103	585.30	22.9	29.6	1.940	1.496	2.640	43.3	0.76
180	1115	C	33	R	1	134	136	591.56	14.5	17.0	2.232	1.908	2.793	31.7	0.46
180	1115	C	33	R	2	27	29	591.95	13.4	15.5	2.275	1.970	2.805	29.8	0.42
180	1115	C	33	R	3	111	113	594.19	23.4	30.6	1.953	1.496	2.702	44.6	0.81
180	1115	C	34	R	1	45	47	600.27	18.8	23.2	2.071	1.682	2.715	38.1	0.61
180	1115	C	34	R	2	83	85	602.13	15.3	18.0	2.184	1.850	2.745	32.6	0.48
180	1115	C	34	R	3	15	17	602.95	19.0	23.4	2.075	1.682	2.731	38.4	0.62
180	1115	C	35	R	1	7	9	609.49	12.4	14.2	2.288	2.003	2.773	27.8	0.38
180	1115	C	35	R	2	13	15	610.93	11.9	13.5	2.293	2.020	2.755	26.7	0.36
180	1115	C	35	R	3	4	6	612.27	11.5	13.0	2.309	2.043	2.760	26.0	0.35
180	1115	C	35	R	4	31	33	614.00	22.0	28.3	1.984	1.547	2.700	42.7	0.75
180	1115	C	36	R	1	12	14	619.24	34.9	53.5	1.714	1.117	2.681	58.3	1.40
180	1115	C	36	R	2	64	66	621.16	2.6	2.6	2.513	2.448	2.614	6.3	0.07

Table T11 (continued).

Leg	Site	Hole	Core	Type	Section	Top (cm)	Bottom (cm)	Depth (mbsf)	Water content (bulk)	Water content (dry)	Bulk density ($g \cdot cm^{-3}$)	Dry density ($g \cdot cm^{-3}$)	Grain density ($g \cdot cm^{-3}$)	Porosity (%)	Void ratio
180	1115	C	40	R	1	14	16	657.96	17.8	21.6	2.084	1.714	2.684	36.2	0.57
180	1115	C	40	R	2	84	86	660.16	19.6	24.3	2.052	1.650	2.715	39.2	0.65
180	1115	C	40	R	3	8	10	660.90	19.2	23.7	2.061	1.666	2.712	38.6	0.63
180	1115	C	40	R	4	76	78	663.08	19.0	23.4	2.049	1.661	2.677	38.0	0.61
180	1115	C	40	R	5	9	11	663.91	18.9	23.2	2.060	1.671	2.693	37.9	0.61
180	1115	C	41	R	1	40	42	667.82	18.7	23.0	2.059	1.675	2.683	37.6	0.60
180	1115	C	41	R	2	95	97	669.83	17.0	20.5	2.103	1.745	2.681	34.9	0.54
180	1115	C	41	R	3	117	119	671.55	16.7	20.0	2.116	1.764	2.689	34.4	0.53
180	1115	C	41	R	4	49	51	672.37	19.2	23.7	2.035	1.645	2.657	38.1	0.62
180	1115	C	42	R	1	46	48	677.58	19.1	23.6	2.035	1.646	2.654	38.0	0.61
180	1115	C	42	R	2	100	102	678.91	19.1	23.7	2.030	1.642	2.645	37.9	0.61
180	1115	C	42	R	3	49	51	679.90	19.0	23.5	2.039	1.651	2.657	37.9	0.61
180	1115	C	42	R	4	65	67	681.56	19.0	23.5	2.037	1.649	2.654	37.9	0.61
180	1115	C	42	R	5	66	68	682.95	17.8	21.6	2.081	1.711	2.679	36.1	0.57
180	1115	C	43	R	1	91	93	687.73	17.7	21.5	2.069	1.703	2.651	35.8	0.56
180	1115	C	43	R	2	50	52	688.82	18.2	22.3	2.067	1.691	2.674	36.8	0.58
180	1115	C	43	R	3	94	96	690.76	18.5	22.7	2.053	1.674	2.658	37.0	0.59
180	1115	C	43	R	4	56	58	691.61	18.6	22.8	2.049	1.669	2.656	37.2	0.59
180	1115	C	43	R	5	34	36	692.56	19.6	24.4	2.025	1.627	2.660	38.8	0.64
180	1115	C	44	R	1	21	23	696.73	18.7	23.0	2.051	1.667	2.668	37.5	0.60
180	1115	C	44	R	2	106	108	698.66	20.4	25.6	2.012	1.602	2.672	40.0	0.67
180	1115	C	44	R	3	65	67	699.75	14.8	17.4	2.151	1.832	2.660	31.1	0.45
180	1115	C	44	R	4	74	76	701.24	19.2	23.8	2.027	1.638	2.641	38.0	0.61
180	1115	C	44	R	5	32	34	702.12	19.9	24.8	2.009	1.610	2.639	39.0	0.64
180	1115	C	44	R	6	95	97	704.16	18.9	23.2	2.046	1.660	2.664	37.7	0.60
180	1115	C	44	R	7	46	48	705.02	19.0	23.5	2.056	1.665	2.692	38.2	0.62
180	1115	C	45	R	1	34	36	706.46	19.5	24.3	2.054	1.653	2.718	39.2	0.64
180	1115	C	45	R	2	6	8	707.42	19.6	24.4	2.045	1.644	2.701	39.2	0.64
180	1115	C	45	R	3	5	7	708.68	18.8	23.1	2.071	1.682	2.710	37.9	0.61
180	1115	C	45	R	4	6	8	710.12	19.2	23.7	2.058	1.664	2.707	38.5	0.63
180	1115	C	45	R	5	2	4	711.55	21.0	26.5	2.021	1.597	2.724	41.4	0.71
180	1115	C	46	R	1	33	35	716.05	21.2	26.9	2.006	1.582	2.703	41.5	0.71
180	1115	C	46	R	3	17	19	718.43	19.2	23.8	2.045	1.652	2.681	38.4	0.62
180	1115	C	46	R	5	23	25	721.27	19.4	24.0	2.201	1.775	3.041	41.6	0.71
180	1115	C	46	R	7	37	39	724.30	20.2	25.3	2.027	1.618	2.694	39.9	0.67
180	1115	C	47	R	1	66	68	726.08	17.6	21.3	2.093	1.725	2.693	35.9	0.56
180	1115	C	47	R	2	7	9	726.85	15.1	17.7	2.177	1.849	2.721	32.0	0.47
180	1115	C	47	R	3	13	15	728.37	17.9	21.8	2.074	1.703	2.670	36.2	0.57
180	1115	C	47	R	4	52	54	730.08	17.6	21.3	2.074	1.709	2.653	35.6	0.55
180	1115	C	47	R	5	34	36	731.40	16.9	20.3	2.099	1.744	2.667	34.6	0.53
180	1115	C	47	R	6	81	83	733.08	16.4	19.6	2.113	1.766	2.670	33.9	0.51
180	1115	C	47	R	7	40	42	734.17	17.2	20.8	2.089	1.730	2.666	35.1	0.54
180	1115	C	48	R	1	38	40	735.50	17.4	21.0	2.077	1.716	2.651	35.3	0.55
180	1115	C	48	R	2	18	20	736.48	17.1	20.6	2.095	1.738	2.670	34.9	0.54
180	1115	C	48	R	3	76	78	738.43	17.8	21.6	2.082	1.712	2.682	36.2	0.57
180	1115	C	49	R	1	67	69	745.39	19.0	23.4	2.063	1.671	2.706	38.3	0.62
180	1115	C	49	R	2	27	29	746.28	18.7	23.0	2.060	1.675	2.687	37.7	0.60
180	1115	C	49	R	3	87	89	748.18	18.9	23.4	2.058	1.668	2.695	38.1	0.62

Table T11 (continued).

Leg	Site	Hole	Core	Type	Section	Top (cm)	Bottom (cm)	Depth (mbsf)	Water content (bulk)	Water content (dry)	Bulk density ($g \cdot cm^{-3}$)	Dry density ($g \cdot cm^{-3}$)	Grain density ($g \cdot cm^{-3}$)	Porosity (%)	Void ratio
180	1115	C	49	R	4	65	67	749.47	19.0	23.5	2.041	1.652	2.664	38.0	0.61
180	1115	C	49	R	5	118	120	751.47	18.4	22.6	2.086	1.702	2.724	37.5	0.60
180	1115	C	49	R	6	2	4	751.62	18.3	22.5	2.087	1.704	2.722	37.4	0.60
180	1115	C	49	R	7	64	66	753.74	18.4	22.5	2.073	1.692	2.694	37.2	0.59
180	1115	C	50	R	1	89	91	755.21	17.9	21.8	2.078	1.707	2.679	36.3	0.57
180	1115	C	50	R	2	13	15	755.85	18.7	23.1	2.055	1.670	2.677	37.6	0.60
180	1115	C	50	R	3	42	44	757.43	17.8	21.6	2.093	1.721	2.702	36.3	0.57
180	1115	C	50	R	4	2	4	758.03	17.0	20.5	2.104	1.746	2.684	34.9	0.54
180	1115	C	50	R	5	15	17	759.40	17.1	20.6	2.101	1.742	2.682	35.1	0.54
180	1115	C	50	R	6	3	5	760.30	17.7	21.5	2.069	1.702	2.651	35.8	0.56
180	1115	C	51	R	1	113	115	765.05	19.1	23.5	2.061	1.669	2.707	38.3	0.62
180	1115	C	51	R	2	67	69	765.91	17.6	21.3	2.098	1.729	2.704	36.0	0.56
180	1115	C	51	R	3	45	47	766.80	17.0	20.5	2.106	1.748	2.686	34.9	0.54
180	1115	C	52	R	1	61	63	774.23	16.6	19.9	2.127	1.774	2.708	34.5	0.53
180	1115	C	52	R	2	83	85	775.58	17.1	20.6	2.104	1.745	2.689	35.1	0.54
180	1115	C	52	R	3	3	5	776.20	16.8	20.1	2.119	1.764	2.701	34.7	0.53
180	1115	C	52	R	4	60	62	778.27	17.6	21.4	2.106	1.735	2.722	36.2	0.57
180	1115	C	52	R	5	89	91	779.98	17.0	20.5	2.113	1.754	2.702	35.1	0.54
180	1115	C	52	R	6	4	6	780.59	17.3	20.9	2.111	1.745	2.713	35.7	0.55
180	1115	C	52	R	7	27	29	781.99	16.5	19.7	2.145	1.792	2.734	34.5	0.53
180	1115	C	53	R	1	83	85	784.05	16.6	19.9	2.124	1.772	2.701	34.4	0.52
180	1115	C	53	R	2	32	34	785.04	16.6	19.8	2.106	1.758	2.665	34.0	0.52
180	1115	C	53	R	3	17	19	786.23	16.6	19.9	2.117	1.765	2.688	34.4	0.52
180	1115	C	53	R	4	6	8	787.32	16.4	19.6	2.122	1.775	2.687	34.0	0.51
180	1115	C	53	R	5	100	102	789.53	16.4	19.7	2.126	1.777	2.698	34.1	0.52
180	1115	C	53	R	6	22	24	790.17	16.1	19.2	2.128	1.785	2.686	33.5	0.51
180	1115	C	54	R	1	7	9	792.89	17.3	21.0	2.227	1.841	2.953	37.7	0.60
180	1115	C	54	R	2	106	108	794.96	16.7	20.1	2.117	1.762	2.694	34.6	0.53
180	1115	C	54	R	3	120	122	796.46	16.2	19.3	2.140	1.793	2.711	33.9	0.51
180	1115	C	54	R	4	47	49	797.23	16.4	19.7	2.153	1.799	2.750	34.6	0.53
180	1115	C	54	R	5	76	78	799.02	16.6	19.8	2.121	1.769	2.693	34.3	0.52
180	1115	C	54	R	6	90	92	800.53	15.9	18.9	2.133	1.794	2.682	33.1	0.50
180	1115	C	54	R	7	90	92	801.75	16.8	20.2	2.127	1.769	2.721	35.0	0.54

Note: This table is also available in ASCII format in the **TABLES** directory.

Table T12. Longitudinal (z) and transverse (x and y) velocities for cores, Site 1115. (Continued on next six pages. See table note.)

Leg	Site	Hole	Core	Type	Section	Top (cm)	Bottom (cm)	Depth (mbsf)	x-velocity ($m \cdot s^{-1}$)	y-velocity ($m \cdot s^{-1}$)	z-velocity ($m \cdot s^{-1}$)
180	1115	A	1	H	2	54.0	54.0	0.82		1611.93	
180	1115	A	1	H	2	54.1	54.1	0.82			1555.42
180	1115	A	1	H	3	105.6	105.6	2.56		1551.65	1558.58
180	1115	A	1	H	4	58.3	58.3	3.58		1568.41	1614.81
180	1115	B	1	H	1	110.5	110.5	1.11		1581.22	1581.52
180	1115	B	1	H	2	85.5	85.5	2.36		1576.92	1571.74
180	1115	B	1	H	3	50.0	50.0	3.50		1578.35	1577.22
180	1115	B	1	H	4	100.4	100.4	5.50		1568.41	1570.85
180	1115	B	1	H	5	26.4	26.4	6.26		1575.50	1566.86
180	1115	B	2	H	1	80.0	80.0	8.00			1559.14
180	1115	B	2	H	1	80.1	80.1	8.00		1571.24	
180	1115	B	2	H	2	121.0	121.0	9.91		1551.65	1583.96
180	1115	B	2	H	3	107.2	107.2	11.27		1557.19	1559.14
180	1115	B	2	H	4	91.4	91.4	12.61		1571.24	1576.08
180	1115	B	2	H	5	105.8	105.8	14.26		1535.24	1541.88
180	1115	B	2	H	6	91.7	91.7	15.62		1536.60	1543.94
180	1115	B	2	H	7	18.8	18.8	16.39		1525.83	1541.88
180	1115	B	3	H	1	128.5	128.5	17.99		1506.05	
180	1115	B	3	H	1	128.7	128.7	17.99			1524.34
180	1115	B	3	H	2	128.9	128.9	19.49		1551.37	1551.02
180	1115	B	3	H	3	98.8	98.8	20.69		1557.82	1551.88
180	1115	B	3	H	4	123.3	123.3	22.43			1566.86
180	1115	B	3	H	4	123.4	123.4	22.43		1548.89	
180	1115	B	3	H	5	113.0	113.0	23.83		1494.43	1544.62
180	1115	B	3	H	6	123.5	123.5	25.44		1533.89	1547.78
180	1115	B	3	H	7	54.1	54.1	26.24		1558.45	1548.95
180	1115	B	4	H	1	115.1	115.1	27.35		1550.27	
180	1115	B	4	H	1	115.2	115.2	27.35			1558.44
180	1115	B	4	H	2	123.4	123.4	28.93			1558.44
180	1115	B	4	H	2	123.5	123.5	28.94		1568.41	
180	1115	B	4	H	3	123.2	123.2	30.43		1515.22	1545.99
180	1115	B	4	H	4	123.4	123.4	31.93		1558.59	1555.69
180	1115	B	4	H	5	123.4	123.4	33.43		1557.75	1573.23
180	1115	B	4	H	6	123.4	123.4	34.93		1542.72	1541.88
180	1115	B	4	H	7	52.0	52.0	35.72		1531.80	1532.39
180	1115	B	5	H	1	124.3	124.3	36.94		1540.67	1560.16
180	1115	B	5	H	2	124.3	124.3	38.44			1540.52
180	1115	B	5	H	2	124.4	124.4	38.44		1523.23	
180	1115	B	5	H	3	132.5	132.5	40.03		1547.51	1550.12
180	1115	B	5	H	4	124.4	124.4	41.44		1554.42	1584.50
180	1115	B	5	H	5	124.3	124.3	42.94		1537.95	1549.43
180	1115	B	5	H	6	124.3	124.3	44.44		1531.20	1539.16
180	1115	B	5	H	7	40.9	40.9	45.11		1555.80	1564.04
180	1115	B	6	H	1	115.8	115.8	46.36		1519.18	1535.09
180	1115	B	6	H	2	115.9	115.9	47.86		1553.03	1547.37
180	1115	B	6	H	3	121.3	121.3	49.41		1516.54	1551.50
180	1115	B	6	H	4	115.2	115.2	50.85		1588.42	1572.52
180	1115	B	6	H	5	117.4	117.4	52.37		1535.24	1547.64
180	1115	B	6	H	6	117.2	117.2	53.87		1559.98	1551.50
180	1115	B	6	H	7	16.7	16.7	54.37			1547.37
180	1115	B	6	H	7	16.8	16.8	54.37		1544.77	
180	1115	B	7	H	1	120.0	120.0	55.90		1558.59	
180	1115	B	7	H	1	120.1	120.1	55.90			1564.75
180	1115	B	7	H	2	128.4	128.4	57.48		1554.28	1555.66
180	1115	B	7	H	3	120.0	120.0	58.90		1539.31	1548.05
180	1115	B	7	H	4	120.0	120.0	60.40		1540.67	1542.57
180	1115	B	7	H	5	120.0	120.0	61.90		1540.67	1573.94
180	1115	B	7	H	6	120.0	120.0	63.40		1547.51	1562.64
180	1115	B	7	H	7	11.3	11.3	63.81		1555.80	1545.31
180	1115	B	7	H	7	48.6	48.6	64.19	1586.94		
180	1115	B	8	H	1	114.2	114.2	65.34		1523.83	
180	1115	B	8	H	1	125.6	125.6	65.46	1599.31		
180	1115	B	8	H	2	112.0	112.0	66.82		1548.89	1553.58
180	1115	B	8	H	2	136.6	136.6	67.07	1610.80		
180	1115	B	8	H	3	119.6	119.6	68.40			1549.43
180	1115	B	8	H	3	119.8	119.8	68.40		1553.03	
180	1115	B	8	H	3	143.0	143.0	68.63	1641.19		
180	1115	B	8	H	4	113.4	113.4	69.83			1575.12

Table T12 (continued).

Leg	Site	Hole	Core	Type	Section	Top (cm)	Bottom (cm)	Depth (mbsf)	x-velocity ($m \cdot s^{-1}$)	y-velocity ($m \cdot s^{-1}$)	z-velocity ($m \cdot s^{-1}$)
180	1115	B	8	H	4	113.6	113.6	69.84		1532.54	
180	1115	B	8	H	4	138.2	138.2	70.08	1631.05		
180	1115	B	8	H	5	117.0	117.0	71.37			1569.68
180	1115	B	8	H	5	117.1	117.1	71.37		1562.78	
180	1115	B	8	H	6	121.7	121.7	72.92			1573.98
180	1115	B	8	H	6	121.9	121.9	72.92		1566.01	
180	1115	B	8	H	6	140.6	140.6	73.11	1614.52		
180	1115	B	8	H	7	49.6	49.6	73.70			1555.66
180	1115	B	8	H	7	52.3	52.3	73.72		1539.31	
180	1115	B	8	H	7	61.2	61.2	73.81	1645.61		
180	1115	B	9	H	1	47.4	47.4	74.17		1543.40	1562.64
180	1115	B	9	H	1	57.3	57.3	74.27	1622.98		
180	1115	B	9	H	2	87.1	87.1	76.07		1532.54	1545.31
180	1115	B	9	H	2	94.5	94.5	76.15	1581.29		
180	1115	B	9	H	3	83.3	83.3	77.53		1546.14	1545.89
180	1115	B	9	H	3	92.2	92.2	77.62	1576.27		
180	1115	B	9	H	4	55.1	55.1	78.75		1537.95	1555.66
180	1115	B	9	H	4	63.8	63.8	78.84	1595.95		
180	1115	B	9	H	5	34.2	34.2	80.04		1559.98	1573.69
180	1115	B	9	H	5	42.4	42.4	80.12	1587.68		
180	1115	B	9	H	6	67.9	67.9	81.88		1559.98	1569.68
180	1115	B	9	H	6	76.2	76.2	81.96	1603.44		
180	1115	B	9	H	7	19.8	19.8	82.90		1539.31	1564.75
180	1115	B	9	H	7	27.1	27.1	82.97	1584.87		
180	1115	B	10	H	1	87.1	87.1	84.07		1535.24	1548.05
180	1115	B	10	H	1	96.3	96.3	84.16	1594.21		
180	1115	B	10	H	2	56.6	56.6	85.27	1588.15		
180	1115	B	10	H	2	66.2	66.2	85.36		1532.54	
180	1115	B	10	H	2	66.3	66.3	85.36			1547.37
180	1115	B	10	H	3	75.8	75.8	86.96			1542.57
180	1115	B	10	H	3	75.9	75.9	86.96		1535.24	
180	1115	B	10	H	3	82.1	82.1	87.02	1571.49		
180	1115	B	10	H	4	92.3	92.3	88.62		1554.42	1554.97
180	1115	B	10	H	4	100.0	100.0	88.70	1594.03		
180	1115	B	10	H	5	92.3	92.3	90.12		1524.50	1548.74
180	1115	B	10	H	5	98.9	98.9	90.19	1598.19		
180	1115	B	10	H	6	92.3	92.3	91.62		1531.20	1543.25
180	1115	B	10	H	6	99.6	99.6	91.70	1589.52		
180	1115	B	10	H	7	24.1	24.1	92.44		1553.03	1564.04
180	1115	B	10	H	7	31.9	31.9	92.52	1591.10		
180	1115	B	11	H	1	83.3	83.3	93.53	1610.95	1537.95	1556.36
180	1115	B	11	H	2	103.5	103.5	95.24		1547.51	1557.75
180	1115	B	11	H	2	110.4	110.4	95.30	1617.04		
180	1115	B	11	H	3	75.8	75.8	96.46		1524.50	1526.34
180	1115	B	11	H	3	83.5	83.5	96.54	1574.63		
180	1115	B	11	H	4	75.8	75.8	97.96	1574.54	1542.04	1549.43
180	1115	B	11	H	5	73.3	73.3	99.43		1548.89	1559.84
180	1115	B	11	H	5	73.4	73.4	99.43	1599.03		
180	1115	B	11	H	6	53.0	53.0	100.73	1585.50	1544.77	1553.58
180	1115	B	11	H	7	15.9	15.9	101.86	1577.44	1527.17	1545.31
180	1115	B	12	H	1	67.0	67.0	102.87		1525.83	1519.68
180	1115	B	12	H	1	67.0	67.0	102.87	1574.52		
180	1115	B	12	H	2	61.1	61.1	104.31	1568.74		
180	1115	B	12	H	3	102.5	102.5	106.23	1581.73		
180	1115	B	12	H	4	102.5	102.5	107.73	1582.21		
180	1115	B	12	H	5	69.4	69.4	108.89	1598.06		
180	1115	B	12	H	6	129.7	129.7	111.00	1610.92		
180	1115	B	12	H	7	24.8	24.8	111.45	1585.00		
180	1115	B	14	H	1	89.9	89.9	122.10	1576.21		
180	1115	B	14	H	1	107.6	107.6	122.28	1574.16		
180	1115	B	14	H	2	99.3	99.3	123.69	1594.31		
180	1115	B	14	H	2	107.2	107.2	123.77	1607.70		
180	1115	B	14	H	3	47.2	47.2	124.67	1613.81		
180	1115	B	14	H	3	94.4	94.4	125.14	1578.67		
180	1115	B	14	H	4	69.8	69.8	126.40	1583.33		
180	1115	B	14	H	4	95.9	95.9	126.66	1620.03		
180	1115	B	14	H	5	24.0	24.0	127.44	1579.28		
180	1115	B	14	H	5	80.0	80.0	128.00	1605.17		
180	1115	B	14	H	5	83.7	83.7	128.04	1589.54		

Table T12 (continued).

Leg	Site	Hole	Core	Type	Section	Top (cm)	Bottom (cm)	Depth (mbsf)	x-velocity ($m \cdot s^{-1}$)	y-velocity ($m \cdot s^{-1}$)	z-velocity ($m \cdot s^{-1}$)
180	1115	B	14	H	5	96.0	96.0	128.16	1583.80		
180	1115	B	14	H	6	107.2	107.2	129.77	1604.48		
180	1115	B	14	H	7	17.9	17.9	130.38	1587.67		
180	1115	B	15	H	1	105.5	105.5	131.76	1592.93		
180	1115	B	15	H	2	90.0	90.0	133.10	1638.39		
180	1115	B	15	H	3	95.6	95.6	134.66	1625.01		
180	1115	B	15	H	4	106.1	106.1	136.26	1587.06		
180	1115	B	15	H	5	92.2	92.2	137.62	1559.74		
180	1115	B	15	H	6	93.0	93.0	139.13	1596.49		
180	1115	B	15	H	7	41.0	41.0	140.11	1575.80		
180	1115	B	16	H	1	97.2	97.2	141.17	1603.86		
180	1115	B	16	H	2	110.6	110.6	142.81	1581.04		
180	1115	B	16	H	3	98.7	98.7	144.19	1590.58		
180	1115	B	16	H	4	69.8	69.8	145.40	1608.53		
180	1115	B	16	H	5	117.9	117.9	147.38	1598.15		
180	1115	B	16	H	6	90.0	90.0	148.60	1609.58		
180	1115	B	16	H	7	36.0	36.0	149.56	1577.65		
180	1115	B	17	H	1	84.8	84.8	150.55	1593.94		
180	1115	B	17	H	2	89.9	89.9	152.10	1608.28		
180	1115	B	17	H	3	76.1	76.1	153.46	1617.60		
180	1115	B	17	H	4	90.8	90.8	155.11	1624.41		
180	1115	B	17	H	4	102.1	102.1	155.22	1623.91		
180	1115	B	17	H	6	97.3	97.3	158.17	1643.20		
180	1115	B	17	H	7	53.7	53.7	159.24	1630.10		
180	1115	B	18	H	1	92.1	92.1	160.12	1606.18		
180	1115	B	18	H	2	89.7	89.7	161.60	1640.12		
180	1115	B	18	H	3	111.3	111.3	163.31	1602.52		
180	1115	B	18	H	4	120.1	120.1	164.90	1600.19		
180	1115	B	18	H	5	104.8	104.8	166.25	1611.60		
180	1115	B	18	H	6	95.5	95.5	167.66	1608.29		
180	1115	B	18	H	7	50.4	50.4	168.70	1588.83		
180	1115	B	19	H	1	93.1	93.1	169.63	1584.54		
180	1115	B	19	H	2	107.0	107.0	171.27	1610.52		
180	1115	B	19	H	3	116.9	116.9	172.87	1586.31		
180	1115	B	19	H	4	95.7	95.7	174.16	1606.73		
180	1115	B	19	H	5	118.0	118.0	175.88	1611.85		
180	1115	B	19	H	6	107.9	107.9	177.28	1617.79		
180	1115	B	19	H	7	56.7	56.7	178.27	1640.55		
180	1115	B	20	H	1	123.1	123.1	179.43	1624.17		
180	1115	B	20	H	2	121.4	121.4	180.91	1632.39		
180	1115	B	20	H	3	128.4	128.4	182.48	1618.05		
180	1115	B	20	H	4	132.7	132.7	184.03	1645.89		
180	1115	B	20	H	5	131.3	131.3	185.51	1620.41		
180	1115	B	20	H	6	126.4	126.4	186.96	1634.35		
180	1115	B	20	H	7	59.7	59.7	187.80	1613.29		
180	1115	B	21	H	1	125.6	125.6	188.96	1611.82		
180	1115	B	21	H	2	128.3	128.3	190.48	1602.46		
180	1115	B	21	H	3	121.9	121.9	191.92	1628.11		
180	1115	B	21	H	4	128.0	128.0	193.48	1643.01		
180	1115	B	21	H	5	128.8	128.8	194.99	1637.79		
180	1115	B	21	H	6	138.7	138.7	196.59	1624.55		
180	1115	B	21	H	7	36.5	36.5	197.07	1616.31		
180	1115	B	22	H	1	119.1	119.1	198.39	1584.42		
180	1115	B	22	H	2	130.6	130.6	200.01	1582.13		
180	1115	B	22	H	3	124.0	124.0	201.44	1618.99		
180	1115	B	22	H	4	111.3	111.3	202.81	1655.29		
180	1115	B	22	H	5	121.0	121.0	204.35	1615.57		
180	1115	B	22	H	6	118.1	118.1	205.82	1635.49		
180	1115	B	22	H	7	28.4	28.4	206.42	1622.25		
180	1115	B	23	H	1	129.9	129.9	208.00	1596.65		
180	1115	B	23	H	2	136.9	136.9	209.57	1608.60		
180	1115	B	23	H	3	129.1	129.1	210.99	1604.94		
180	1115	B	23	H	4	127.6	127.6	212.48	1636.09		
180	1115	B	23	H	5	133.4	133.4	214.03	1624.81		
180	1115	B	23	H	6	127.1	127.1	215.47	1613.27		
180	1115	B	23	H	7	56.1	56.1	216.26	1592.34		
180	1115	B	24	X	1	90.5	90.5	217.11	1575.85		
180	1115	B	24	X	2	55.1	55.1	218.25	1604.72		
180	1115	B	24	X	3	48.8	48.8	219.69	1584.28		

Table T12 (continued).

Leg	Site	Hole	Core	Type	Section	Top (cm)	Bottom (cm)	Depth (mbsf)	x-velocity ($m \cdot s^{-1}$)	y-velocity ($m \cdot s^{-1}$)	z-velocity ($m \cdot s^{-1}$)
180	1115	B	24	X	4	87.3	87.3	221.37	1572.41		
180	1115	B	24	X	5	87.9	87.9	222.88	1602.17		
180	1115	B	24	X	6	76.9	76.9	224.27	1585.18		
180	1115	B	24	X	7	63.6	63.6	225.34	1583.18		
180	1115	B	25	X	1	92.7	92.7	226.73	1567.85		
180	1115	B	25	X	2	84.3	84.3	228.14	1574.17		
180	1115	B	25	X	3	73.2	73.2	229.53	1572.06		
180	1115	B	25	X	4	78.9	78.9	231.09	1582.98		
180	1115	B	25	X	5	72.2	72.2	232.52	1570.97		
180	1115	B	25	X	6	89.4	89.4	234.19	1632.52		
180	1115	B	25	X	7	20.6	20.6	235.01	1593.92		
180	1115	B	26	X	1	83.8	83.8	236.24	1597.47		
180	1115	B	26	X	2	90.3	90.3	237.80	1592.17		
180	1115	B	26	X	3	64.4	64.4	239.04	1613.44		
180	1115	B	26	X	4	32.6	32.6	240.23	1616.37		
180	1115	B	26	X	5	110.3	110.3	242.50	1648.57		
180	1115	B	26	X	6	89.2	89.2	243.79	1641.35		
180	1115	B	26	X	7	38.9	38.9	244.59	1616.75		
180	1115	B	27	X	1	90.3	90.3	245.90	1628.60		
180	1115	B	27	X	2	94.9	94.9	247.45	1619.79		
180	1115	B	27	X	3	89.8	89.8	248.90	1600.67		
180	1115	B	27	X	4	106.9	106.9	250.57	1600.53		
180	1115	B	27	X	6	58.2	58.2	253.08	1604.52		
180	1115	B	28	X	1	76.7	76.7	255.37	1630.89		
180	1115	B	28	X	2	22.0	22.0	256.32	1626.04		
180	1115	B	29	X	1	94.8	94.8	265.25	1611.00		
180	1115	B	29	X	2	94.8	94.8	266.75	1628.79		
180	1115	B	29	X	3	94.8	94.8	268.25	1621.72		
180	1115	B	29	X	4	94.8	94.8	269.75	1629.97		
180	1115	B	29	X	5	94.8	94.8	271.25	1618.49		
180	1115	B	29	X	6	94.8	94.8	272.75	1667.46		
180	1115	B	29	X	7	13.4	13.4	273.43	1683.72		
180	1115	B	30	X	1	66.7	66.7	274.57	1626.43		
180	1115	B	31	X	1	85.0	85.0	284.35	1595.11		
180	1115	B	31	X	2	85.0	85.0	285.85	1592.83		
180	1115	B	31	X	3	80.0	80.0	287.30	1650.59		
180	1115	B	31	X	4	80.0	80.0	288.80	1642.33		
180	1115	B	31	X	5	80.0	80.0	290.30	1667.45		
180	1115	B	31	X	6	80.0	80.0	291.80	1627.37		
180	1115	B	31	X	7	11.0	11.0	292.61	1634.63		
180	1115	C	1	R	1	104.7	104.7	284.25	1727.22		
180	1115	C	1	R	2	110.8	110.8	285.73	1687.46		
180	1115	C	1	R	3	80.5	80.5	286.89	1661.97		
180	1115	C	1	R	4	105.3	105.3	288.63	1713.61		
180	1115	C	1	R	5	17.3	17.3	289.25	1674.89		
180	1115	C	2	R	1	5.0	5.0	292.85		4985.89	5033.24
180	1115	C	2	R	2	90.0	90.0	295.20	1727.96	1731.87	1734.28
180	1115	C	2	R	4	40.0	40.0	296.59	1696.45	1728.79	1739.93
180	1115	C	2	R	5	74.0	74.0	298.43	1732.66	1719.32	1742.49
180	1115	C	3	R	1	9.0	9.0	302.59	1758.82	1754.56	1757.48
180	1115	C	3	R	2	70.0	70.0	304.70	1753.29	1754.13	1762.13
180	1115	C	3	R	3	90.0	90.0	306.40	1738.18	1733.38	1749.08
180	1115	C	3	R	4	25.0	25.0	307.25	1683.88	1683.98	1689.03
180	1115	C	3	R	5	111.0	111.0	309.61	1706.81	1707.95	1705.03
180	1115	C	3	R	6	42.0	42.0	310.42	1721.31	1727.14	1727.74
180	1115	C	4	R	1	107.0	107.0	313.17	1750.17	1752.02	1734.98
180	1115	C	4	R	2	105.0	105.0	314.66	1740.80	1730.83	1712.19
180	1115	C	4	R	3	11.0	11.0	315.22	1738.81	1749.92	1726.84
180	1115	C	4	R	4	5.0	5.0	316.51	1712.48	1715.86	1704.10
180	1115	C	5	R	1	43.0	43.0	322.13	1757.43		1757.95
180	1115	C	5	R	1	43.0	43.0	322.13			1769.39
180	1115	C	5	R	2	76.0	76.0	323.73	1757.26	1744.44	1771.02
180	1115	C	5	R	3	133.0	133.0	325.80	1795.44	1789.39	1865.21
180	1115	C	5	R	4	76.0	76.0	326.73	1759.89	1747.83	1746.15
180	1115	C	6	R	1	57.0	57.0	331.97	1750.87	1748.66	1738.30
180	1115	C	6	R	2	126.0	126.0	334.16	1763.88	1762.57	1754.93
180	1115	C	6	R	3	39.0	39.0	334.79	1720.70	1738.66	1763.91
180	1115	C	6	R	4	29.0	29.0	336.19	1755.09	1774.47	1761.69
180	1115	C	6	R	5	108.0	108.0	338.48	1940.44	1942.32	1871.55

Table T12 (continued).

Leg	Site	Hole	Core	Type	Section	Top (cm)	Bottom (cm)	Depth (mbsf)	x-velocity ($m \cdot s^{-1}$)	y-velocity ($m \cdot s^{-1}$)	z-velocity ($m \cdot s^{-1}$)
180	1115	C	6	R	6	29.0	29.0	339.19	1711.85	1737.39	1768.60
180	1115	C	7	R	1	79.0	79.0	341.79	1784.05	1795.25	1801.07
180	1115	C	7	R	2	35.0	35.0	342.81	1756.51	1754.93	1737.51
180	1115	C	7	R	3	89.0	89.0	344.81	1665.87	1732.17	1721.53
180	1115	C	7	R	4	104.0	104.0	346.39	1722.35	1719.78	1691.72
180	1115	C	7	R	5	105.0	105.0	347.79	1738.74	1715.11	1701.56
180	1115	C	8	R	1	24.0	24.0	350.84	1756.10	1743.30	1697.38
180	1115	C	8	R	2	19.0	19.0	351.63	1730.95	1730.20	1701.27
180	1115	C	8	R	3	131.0	131.0	354.25	1723.55	1729.24	1721.81
180	1115	C	8	R	4	137.0	137.0	355.81	1759.43	1750.34	1728.56
180	1115	C	8	R	5	14.0	14.0	356.08	1724.21	1719.88	1701.10
180	1115	C	9	R	1	46.0	46.0	360.36	1758.37	1766.29	1741.25
180	1115	C	9	R	2	109.0	109.0	362.18	1735.80	1735.42	1712.96
180	1115	C	9	R	3	110.0	110.0	363.47	1771.42	1805.10	1791.66
180	1115	C	9	R	4	35.0	35.0	364.06	1814.49	1812.46	1805.56
180	1115	C	9	R	5	131.0	131.0	366.52	1745.66	1727.29	1718.34
180	1115	C	9	R	6	22.0	22.0	366.79	1738.66	1736.30	1729.00
180	1115	C	9	R	7	64.0	64.0	368.51	1733.51	1752.00	1721.36
180	1115	C	10	R	1	83.0	83.0	370.33	1750.06	1742.99	1748.80
180	1115	C	10	R	2	96.0	96.0	371.96	1733.03	1745.45	1756.31
180	1115	C	10	R	3	20.0	20.0	372.70	1748.44	1779.94	1723.63
180	1115	C	10	R	4	114.0	114.0	375.14	1806.29	1765.60	1814.73
180	1115	C	10	R	5	92.0	92.0	376.42	1753.76	1734.79	1753.81
180	1115	C	10	R	6	91.0	91.0	377.91	1730.43	1724.45	1672.39
180	1115	C	11	R	1	15.0	15.0	379.25	1750.31	1760.45	1740.36
180	1115	C	11	R	2	13.0	13.0	380.67	1759.57	1764.66	1731.34
180	1115	C	11	R	3	85.0	85.0	382.87	1797.24	1782.68	1809.21
180	1115	C	11	R	4	82.0	82.0	384.24	1768.74	1778.42	1786.01
180	1115	C	11	R	5	97.0	97.0	385.89	1751.27	1758.73	1765.50
180	1115	C	11	R	6	96.0	96.0	387.30	1769.76	1773.08	1773.08
180	1115	C	12	R	1	70.0	70.0	389.20		1773.24	1780.12
180	1115	C	12	R	1	96.0	96.0	389.46	1764.66		
180	1115	C	12	R	2	93.0	93.0	390.93	1778.93	1790.61	1791.47
180	1115	C	12	R	3	37.0	37.0	391.87	1784.54	1797.79	1808.55
180	1115	C	12	R	4	119.0	119.0	394.09	1801.85	1809.21	1818.34
180	1115	C	12	R	5	111.0	111.0	395.51	1835.63	1831.11	1850.07
180	1115	C	12	R	6	61.0	61.0	396.51	1771.95	1774.93	1775.87
180	1115	C	12	R	7	14.0	14.0	397.54	1772.43	1767.24	1781.82
180	1115	C	13	R	1	79.0	79.0	398.89	1850.29	1806.78	1793.71
180	1115	C	13	R	2	69.0	69.0	400.29	1843.05	1866.45	1869.66
180	1115	C	13	R	3	72.0	72.0	401.69	1838.73	1866.34	1891.16
180	1115	C	13	R	4	76.0	76.0	402.91	1805.42	1824.44	1854.04
180	1115	C	13	R	5	82.0	82.0	404.41	1787.72	1821.58	1796.61
180	1115	C	13	R	6	75.0	75.0	405.78	1798.22	1787.11	1809.38
180	1115	C	13	R	7	13.0	13.0	406.61	1806.42	1805.56	1808.84
180	1115	C	14	R	1	55.0	55.0	408.25	1906.09	1902.29	1908.74
180	1115	C	14	R	2	90.0	90.0	410.04	1999.61	2025.92	2093.14
180	1115	C	14	R	3	72.0	72.0	411.01	1876.96	1878.80	1880.70
180	1115	C	14	R	4	73.0	73.0	411.75	1893.02	1906.59	1922.09
180	1115	C	15	R	1	60.0	60.0	417.90	1932.98	1892.68	1948.36
180	1115	C	15	R	2	113.0	113.0	419.93	1866.63	1845.07	1863.63
180	1115	C	15	R	3	93.0	93.0	421.23	1826.08	1858.41	1851.16
180	1115	C	15	R	4	65.0	65.0	422.45	1882.67	1900.66	1865.19
180	1115	C	15	R	5	119.0	119.0	424.49	1820.92	1816.50	1854.25
180	1115	C	15	R	6	37.0	37.0	425.17	1836.05	1802.50	1812.25
180	1115	C	16	R	2	5.0	5.0	427.74	2704.31	2815.56	2678.21
180	1115	C	16	R	2	53.0	53.0	428.22	1856.95	1827.87	1833.45
180	1115	C	17	R	1	4.0	4.0	436.54	1841.71	1850.90	1889.20
180	1115	C	17	R	2	53.0	53.0	438.22	1867.78	1886.86	1875.89
180	1115	C	18	R	1	5.0	5.0	446.15	1804.97	1804.36	1790.42
180	1115	C	18	R	2	68.0	68.0	448.26	1862.49	1878.83	1887.85
180	1115	C	19	R	1	19.0	19.0	455.79	1890.88	1879.73	1897.54
180	1115	C	20	R	1	13.0	13.0	465.33	1839.61	1842.01	1852.22
180	1115	C	21	R	1	71.0	71.0	475.61	1981.77	1974.72	2036.81
180	1115	C	21	R	2	8.0	8.0	475.80	1961.40	1978.81	1986.38
180	1115	C	21	R	3	6.0	6.0	476.74	1875.72	1923.32	1925.68
180	1115	C	21	R	4	58.0	58.0	478.58	2010.24	1885.35	1879.70
180	1115	C	21	R	5	11.0	11.0	479.61	1864.06	1868.39	1871.92
180	1115	C	22	R	1	120.0	120.0	485.70	1868.65	1872.15	1837.18

Table T12 (continued).

Leg	Site	Hole	Core	Type	Section	Top (cm)	Bottom (cm)	Depth (mbsf)	x-velocity ($m \cdot s^{-1}$)	y-velocity ($m \cdot s^{-1}$)	z-velocity ($m \cdot s^{-1}$)
180	1115	C	22	R	2	28.0	28.0	486.28	1913.80	1888.55	1899.40
180	1115	C	22	R	3	23.0	23.0	486.99	1855.93	1872.54	1869.64
180	1115	C	22	R	4	116.0	116.0	489.42	1924.51	1939.97	1915.48
180	1115	C	22	R	5	15.0	15.0	489.91	1918.42	1899.39	1903.73
180	1115	C	22	R	6	42.0	42.0	491.18	1995.69	1989.56	2034.44
180	1115	C	23	R	1	94.0	94.0	495.04	2039.86	2023.37	2021.73
180	1115	C	23	R	2	146.0	146.0	496.94	2038.15	2038.44	2025.91
180	1115	C	23	R	3	8.0	8.0	497.06	1997.23	1992.99	1950.11
180	1115	C	24	R	1	33.0	33.0	504.13	1918.89	1936.11	1918.45
180	1115	C	24	R	2	96.0	96.0	506.26	1907.99	1867.30	1878.99
180	1115	C	24	R	3	47.0	47.0	507.27	1857.42	1866.87	1874.44
180	1115	C	24	R	4	15.0	15.0	508.45	1853.32	1890.06	1899.13
180	1115	C	24	R	5	26.0	26.0	510.06	1855.11	1857.96	1877.52
180	1115	C	25	R	1	104.0	104.0	514.44	1870.27	1848.88	1820.80
180	1115	C	25	R	2	44.0	44.0	515.34	1669.49	1744.32	1895.83
180	1115	C	25	R	2	114.8	114.8	516.05	1806.71		
180	1115	C	26	R	1	13.0	13.0	523.13	4671.18	4588.16	4702.80
180	1115	C	27	R	1	25.0	25.0	532.85	1849.11		
180	1115	C	28	R	1	37.3	37.3	542.57	1780.91		
180	1115	C	29	R	1	79.0	79.0	552.59	4070.98	4100.93	3924.33
180	1115	C	29	R	1	88.1	88.1	552.68	3483.24		
180	1115	C	29	R	1	104.1	104.1	552.84	1840.43		
180	1115	C	29	R	2	101.0	101.0	554.26	1921.20	1922.23	1875.67
180	1115	C	29	R	3	45.0	45.0	554.74	1900.10	1884.94	1876.57
180	1115	C	30	R	1	22.0	22.0	561.62	4612.24	4711.73	4902.46
180	1115	C	30	R	2	31.0	31.0	562.24	1979.95	1940.10	1940.22
180	1115	C	30	R	2	120.0	120.0	563.13	1786.03	1791.25	1717.92
180	1115	C	30	R	4	82.2	82.2	565.62	1863.31		
180	1115	C	30	R	5	68.0	68.0	566.69	5148.01	5415.60	5277.78
180	1115	C	31	R	CC	7.0	7.0	572.15	4047.26	4245.31	4041.94
180	1115	C	32	R	1	84.0	84.0	581.44	3091.24	3212.99	3188.52
180	1115	C	32	R	2	43.0	43.0	582.50	2319.05	2330.25	2065.18
180	1115	C	32	R	3	79.0	79.0	583.80	2957.32	2826.09	2591.77
180	1115	C	32	R	4	94.0	94.0	585.21	2296.50	2299.37	2180.97
180	1115	C	33	R	1	131.0	131.0	591.51	3731.76	3159.00	3641.08
180	1115	C	33	R	2	96.0	96.0	592.62	2705.44	2371.22	2347.64
180	1115	C	33	R	3	107.0	107.0	594.13	2631.40	3177.02	3161.82
180	1115	C	34	R	1	50.0	50.0	600.30	2462.93	2483.55	2380.15
180	1115	C	34	R	2	89.0	89.0	602.17	3839.21	3379.72	3670.54
180	1115	C	34	R	3	19.0	19.0	602.97	3046.04	3146.39	3139.93
180	1115	C	35	R	1	12.0	12.0	609.52	3048.72	3142.39	3127.12
180	1115	C	35	R	2	10.0	10.0	610.88	3450.42	3652.85	3574.55
180	1115	C	35	R	3	11.0	11.0	612.32	3058.49	3178.54	3089.55
180	1115	C	35	R	4	34.0	34.0	614.01	2421.69	2395.60	2383.38
180	1115	C	36	R	1	87.0	87.0	619.97	2344.80	2308.53	2123.19
180	1115	C	36	R	2	40.0	40.0	620.90	2289.23	2438.80	2250.86
180	1115	C	40	R	1	18.0	18.0	657.98	2360.98	2400.59	2374.89
180	1115	C	40	R	2	82.0	82.0	660.12	2352.85	2369.25	2332.09
180	1115	C	40	R	3	14.0	14.0	660.94	2434.45	2426.90	2366.65
180	1115	C	40	R	4	81.0	81.0	663.11	2360.78	2398.31	2370.96
180	1115	C	40	R	5	15.0	15.0	663.95		2438.60	2415.06
180	1115	C	41	R	1	36.0	36.0	667.76	2385.53	2443.44	2334.58
180	1115	C	41	R	2	99.0	99.0	669.85	2416.57	2379.01	2526.35
180	1115	C	41	R	3	99.0	99.0	671.35		2685.47	
180	1115	C	41	R	3	114.0	114.0	671.50	2746.96		2696.90
180	1115	C	41	R	4	46.0	46.0	672.32	2431.65	2401.05	2393.74
180	1115	C	42	R	1	42.0	42.0	677.52	2485.74	2472.85	2273.51
180	1115	C	42	R	2	96.0	96.0	678.85	2409.12	2398.63	2238.29
180	1115	C	42	R	3	54.0	54.0	679.93	2355.24	2274.64	2369.88
180	1115	C	42	R	4	70.0	70.0	681.59	2387.01	2406.31	2326.94
180	1115	C	42	R	5	64.0	64.0	682.91	2434.27	2479.93	2391.48
180	1115	C	43	R	1	96.0	96.0	687.76	2478.16	2477.68	2386.81
180	1115	C	43	R	2	55.0	55.0	688.85	2410.10	2370.38	2381.17
180	1115	C	43	R	3	92.0	92.0	690.72	2304.41	2477.68	2368.72
180	1115	C	43	R	4	52.0	52.0	691.55	2433.61	2514.30	2392.61
180	1115	C	43	R	5	44.0	44.0	692.64	2382.34	2385.64	2327.33
180	1115	C	44	R	1	18.0	18.0	696.68	2513.47	2522.25	2343.19
180	1115	C	44	R	2	104.0	104.0	698.62	2285.53	2315.67	2267.40
180	1115	C	44	R	3	71.0	71.0	699.79	4168.85	4092.75	3877.92

Table T12 (continued).

Leg	Site	Hole	Core	Type	Section	Top (cm)	Bottom (cm)	Depth (mbsf)	x-velocity ($m \cdot s^{-1}$)	y-velocity ($m \cdot s^{-1}$)	z-velocity ($m \cdot s^{-1}$)
180	1115	C	44	R	4	71.0	71.0	701.19	2423.89	2414.86	2335.47
180	1115	C	44	R	5	29.0	29.0	702.07	2426.32	2435.13	2297.99
180	1115	C	44	R	6	93.0	93.0	704.12	2476.46	2462.58	2377.95
180	1115	C	44	R	7	50.0	50.0	705.04	2439.24	2369.25	2323.63
180	1115	C	45	R	1	50.0	50.0	706.60	2468.22	2434.82	2373.76
180	1115	C	45	R	2	2.0	2.0	707.36	2503.98	2558.11	2456.14
180	1115	C	45	R	3	35.0	35.0	708.96	2470.14	2503.56	2462.44
180	1115	C	45	R	4	10.0	10.0	710.14	4770.00	4657.29	4623.94
180	1115	C	45	R	5	6.0	6.0	711.57	2420.59	2478.28	2460.03
180	1115	C	46	R	1	52.0	52.0	716.22	2533.13	2548.81	2444.60
180	1115	C	46	R	2	8.0	8.0	716.93	2500.00	2470.77	2393.90
180	1115	C	46	R	3	21.0	21.0	718.45	3610.27	3715.39	3097.56
180	1115	C	46	R	4	21.0	21.0	719.77	2590.96	2579.74	2546.31
180	1115	C	46	R	5	53.0	53.0	721.55	3281.66	2590.31	2432.37
180	1115	C	46	R	6	2.0	2.0	722.46	2547.18	2624.64	2444.96
180	1115	C	46	R	7	41.0	41.0	724.32	2483.96	2497.63	2448.79
180	1115	C	46	R	7	41.0	41.0	724.32		2448.79	2495.26
180	1115	C	47	R	1	61.0	61.0	726.01	2545.89	2551.23	2474.28
180	1115	C	47	R	2	4.0	4.0	726.80	2521.95	2528.87	2507.15
180	1115	C	47	R	3	4.0	4.0	728.26	2468.24	2652.96	2464.76
180	1115	C	47	R	4	58.0	58.0	730.12	2517.16	2588.09	2452.72
180	1115	C	47	R	5	30.0	30.0	731.34	2571.66	2596.05	2523.26
180	1115	C	47	R	6	78.0	78.0	733.03	2646.80	2695.36	2612.50
180	1115	C	47	R	7	35.0	35.0	734.10	2563.45	2597.91	2490.57
180	1115	C	48	R	1	51.0	51.0	735.61	2609.33	2647.95	2464.32
180	1115	C	48	R	2	23.0	23.0	736.51	2527.80	2528.87	2450.89
180	1115	C	48	R	3	85.0	85.0	738.50	3549.37	3796.50	3390.52
180	1115	C	49	R	1	64.0	64.0	745.34	2454.80	2419.45	2342.04
180	1115	C	49	R	2	22.0	22.0	746.21		2512.53	2547.99
180	1115	C	49	R	2	22.0	22.0	746.21			2532.67
180	1115	C	49	R	3	95.0	95.0	748.24	2509.47	2534.26	2496.44
180	1115	C	49	R	4	36.0	36.0	749.16	2466.21	2458.94	2276.51
180	1115	C	49	R	5	29.0	29.0	750.56	2440.55	2406.42	
180	1115	C	49	R	6	37.0	37.0	751.95	2490.96	2556.92	2414.86
180	1115	C	49	R	7	6.0	6.0	753.14	2405.85	2404.34	2370.08
180	1115	C	50	R	1	96.0	96.0	755.26	2469.15	2494.04	2399.44
180	1115	C	50	R	2	52.0	52.0	756.22	2388.57	2418.50	2407.77
180	1115	C	50	R	3	34.0	34.0	757.33	2548.81	2529.95	2430.37
180	1115	C	50	R	4	40.0	40.0	758.39	2469.99	2529.47	2436.00
180	1115	C	50	R	5	20.0	20.0	759.43	2745.41	2689.87	2585.89
180	1115	C	50	R	6	26.0	26.0	760.51	2541.33	2505.94	2403.94
180	1115	C	51	R	1	118.0	118.0	765.08	2447.86	2471.94	2384.43
180	1115	C	51	R	2	64.0	64.0	765.86	2523.12	2508.95	2408.48
180	1115	C	51	R	3	42.0	42.0	766.75	2494.98	2592.00	2519.01
180	1115	C	52	R	1	66.0	66.0	774.26	2515.42	2544.51	2480.12
180	1115	C	52	R	2	80.0	80.0	775.53	2554.65	2565.45	2450.02
180	1115	C	52	R	3	7.0	7.0	776.30	2542.29	2610.26	2465.04
180	1115	C	52	R	4	71.0	71.0	778.41	2408.18	2362.14	2288.20
180	1115	C	52	R	5	94.0	94.0	780.06	2600.46	2558.31	2448.08
180	1115	C	52	R	6	8.0	8.0	780.66	2491.12	2448.86	2327.63
180	1115	C	52	R	7	25.0	25.0	782.00	2493.46	2601.79	2424.03
180	1115	C	53	R	1	88.0	88.0	784.08	2552.62	2576.16	2477.78
180	1115	C	53	R	2	37.0	37.0	785.07	2648.81	2700.71	2529.23
180	1115	C	53	R	3	16.0	16.0	786.20	2649.37	2631.65	2519.17
180	1115	C	53	R	4	10.0	10.0	787.34	2568.22	2585.87	2448.49
180	1115	C	53	R	5	97.0	97.0	789.48	2545.12	2559.52	2496.46
180	1115	C	53	R	6	27.0	27.0	790.20	2676.25	2718.11	2566.21
180	1115	C	54	R	1	27.0	27.0	793.07	2647.30	2606.51	2525.65
180	1115	C	54	R	2	111.0	111.0	794.99	2559.26	2579.63	2460.67
180	1115	C	54	R	3	124.0	124.0	796.48	2571.68	2567.18	2485.40
180	1115	C	54	R	4	43.0	43.0	797.17	2650.07	2637.35	2555.25
180	1115	C	54	R	5	74.0	74.0	798.98	2643.42	2693.88	2472.63
180	1115	C	54	R	6	88.0	88.0	800.49	2576.76	2602.26	2471.48
180	1115	C	54	R	7	86.0	86.0	801.69	2503.49	2494.39	2419.58

Note: This table is also available in ASCII format in the **TABLES** directory.

Table T13. Thermal conductivity values in cores, Site 1115. (Continued on next eight pages. See table note.)

Leg	Site	Hole	Core	Type	Section	Top interval (cm)	Bottom interval (cm)	Top depth (mbsf)	Bottom depth (mbsf)	Middle depth (mbsf)	Thermal conductivity ($W \cdot m^{-1} \cdot °C^{-1}$)	Thermal conductivity average ($W \cdot m^{-1} \cdot °C^{-1}$)
180	1115	A	1	H	2	45	45	0.73	0.73	0.73	0.92	
180	1115	A	1	H	2	45	45	0.73	0.73	0.73	0.94	
180	1115	A	1	H	2	45	45	0.73	0.73	0.73	0.91	0.93
180	1115	A	1	H	4	58	58	3.58	3.58	3.58	0.95	
180	1115	A	1	H	4	58	58	3.58	3.58	3.58	0.95	
180	1115	A	1	H	4	58	58	3.58	3.58	3.58	0.95	0.95
180	1115	B	1	H	2	75	75	2.25	2.25	2.25	0.93	
180	1115	B	1	H	2	75	75	2.25	2.25	2.25	0.96	
180	1115	B	1	H	2	75	75	2.25	2.25	2.25	0.93	0.94
180	1115	B	1	H	4	75	75	5.25	5.25	5.25	1.00	
180	1115	B	1	H	4	75	75	5.25	5.25	5.25	1.00	
180	1115	B	1	H	4	75	75	5.25	5.25	5.25	0.98	0.99
180	1115	B	2	H	2	75	75	9.45	9.45	9.45	0.97	
180	1115	B	2	H	2	75	75	9.45	9.45	9.45	0.96	
180	1115	B	2	H	2	75	75	9.45	9.45	9.45	0.94	0.96
180	1115	B	2	H	4	75	75	12.45	12.45	12.45	0.96	
180	1115	B	2	H	4	75	75	12.45	12.45	12.45	0.96	
180	1115	B	2	H	4	75	75	12.45	12.45	12.45	0.97	0.96
180	1115	B	2	H	6	75	75	15.45	15.45	15.45	0.99	
180	1115	B	2	H	6	75	75	15.45	15.45	15.45	0.99	0.99
180	1115	B	3	H	2	75	75	18.95	18.95	18.95	1.02	
180	1115	B	3	H	2	75	75	18.95	18.95	18.95	1.03	1.02
180	1115	B	3	H	4	75	75	21.95	21.95	21.95	1.02	
180	1115	B	3	H	4	75	75	21.95	21.95	21.95	1.01	1.01
180	1115	B	3	H	6	75	75	24.95	24.95	24.95	1.01	
180	1115	B	3	H	6	75	75	24.95	24.95	24.95	0.98	0.99
180	1115	B	4	H	4	75	75	31.45	31.45	31.45	0.97	
180	1115	B	4	H	4	75	75	31.45	31.45	31.45	0.97	0.97
180	1115	B	4	H	2	75	75	28.45	28.45	28.45	1.01	
180	1115	B	4	H	2	75	75	28.45	28.45	28.45	1.03	1.02
180	1115	B	4	H	6	75	75	34.45	34.45	34.45	0.97	
180	1115	B	4	H	6	75	75	34.45	34.45	34.45	0.96	0.97
180	1115	B	5	H	1	75	75	36.45	36.45	36.45	0.93	
180	1115	B	5	H	1	75	75	36.45	36.45	36.45	0.93	0.93
180	1115	B	5	H	4	75	75	40.95	40.95	40.95	1.05	
180	1115	B	5	H	4	75	75	40.95	40.95	40.95	1.07	1.06
180	1115	B	5	H	6	75	75	43.95	43.95	43.95	0.99	
180	1115	B	5	H	6	75	75	43.95	43.95	43.95	1.02	1.01
180	1115	B	6	H	2	75	75	47.45	47.45	47.45	1.03	
180	1115	B	6	H	2	75	75	47.45	47.45	47.45	0.99	
180	1115	B	6	H	2	75	75	47.45	47.45	47.45	0.96	
180	1115	B	6	H	2	75	75	47.45	47.45	47.45	0.97	0.99
180	1115	B	6	H	4	75	75	50.45	50.45	50.45	1.02	
180	1115	B	6	H	4	75	75	50.45	50.45	50.45	0.96	0.99
180	1115	B	6	H	6	75	75	53.45	53.45	53.45	0.95	
180	1115	B	6	H	6	75	75	53.45	53.45	53.45	0.94	0.94
180	1115	B	7	H	2	75	75	56.95	56.95	56.95	1.02	
180	1115	B	7	H	2	75	75	56.95	56.95	56.95	1.00	1.01

Table T13 (continued).

Leg	Site	Hole	Core	Type	Section	Top interval (cm)	Bottom interval (cm)	Top depth (mbsf)	Bottom depth (mbsf)	Middle depth (mbsf)	Thermal conductivity ($W \cdot m^{-1} \cdot °C^{-1}$)	Thermal conductivity average ($W \cdot m^{-1} \cdot °C^{-1}$)
180	1115	B	7	H	4	75	75	59.95	59.95	59.95	1.02	
180	1115	B	7	H	4	75	75	59.95	59.95	59.95	1.02	1.02
180	1115	B	7	H	6	75	75	62.95	62.95	62.95	1.02	
180	1115	B	7	H	6	75	75	62.95	62.95	62.95	1.09	1.05
180	1115	B	8	H	1	75	75	64.95	64.95	64.95	1.04	
180	1115	B	8	H	1	75	75	64.95	64.95	64.95	1.06	1.05
180	1115	B	8	H	3	75	75	67.95	67.95	67.95	1.01	
180	1115	B	8	H	3	75	75	67.95	67.95	67.95	1.00	1.00
180	1115	B	8	H	5	75	75	70.95	70.95	70.95	0.94	
180	1115	B	8	H	5	75	75	70.95	70.95	70.95	1.02	0.98
180	1115	B	8	H	7	30	30	73.50	73.50	73.50	0.89	
180	1115	B	8	H	7	30	30	73.50	73.50	73.50	0.88	0.88
180	1115	B	9	H	1	75	75	74.45	74.45	74.45	0.95	
180	1115	B	9	H	1	75	75	74.45	74.45	74.45	0.96	0.95
180	1115	B	9	H	3	75	75	77.45	77.45	77.45	0.99	
180	1115	B	9	H	3	75	75	77.45	77.45	77.45	0.97	0.98
180	1115	B	9	H	5	75	75	80.45	80.45	80.45	0.91	
180	1115	B	9	H	5	75	75	80.45	80.45	80.45	0.84	0.88
180	1115	B	9	H	7	30	30	83.00	83.00	83.00	0.91	
180	1115	B	9	H	7	30	30	83.00	83.00	83.00	0.93	0.92
180	1115	B	10	H	1	75	75	83.95	83.95	83.95	1.02	
180	1115	B	10	H	1	75	75	83.95	83.95	83.95	0.99	1.01
180	1115	B	10	H	3	75	75	86.95	86.95	86.95	1.04	
180	1115	B	10	H	3	75	75	86.95	86.95	86.95	1.08	1.06
180	1115	B	10	H	5	75	75	89.95	89.95	89.95	1.04	
180	1115	B	10	H	5	75	75	89.95	89.95	89.95	0.96	1.00
180	1115	B	10	H	7	30	30	92.50	92.50	92.50	0.93	
180	1115	B	10	H	7	30	30	92.50	92.50	92.50	0.86	0.89
180	1115	B	11	H	2	75	75	94.95	94.95	94.95	1.02	
180	1115	B	11	H	2	75	75	94.95	94.95	94.95	1.00	
180	1115	B	11	H	2	75	75	94.95	94.95	94.95	1.01	1.01
180	1115	B	11	H	4	75	75	97.95	97.95	97.95	0.99	
180	1115	B	11	H	4	75	75	97.95	97.95	97.95	1.00	1.00
180	1115	B	11	H	6	75	75	100.95	100.95	100.95	1.07	
180	1115	B	11	H	6	75	75	100.95	100.95	100.95	1.07	1.07
180	1115	B	12	H	4	75	75	107.45	107.45	107.45	1.05	
180	1115	B	12	H	4	75	75	107.45	107.45	107.45	1.02	
180	1115	B	12	H	4	75	75	107.45	107.45	107.45	0.98	1.02
180	1115	B	12	H	2	75	75	104.45	104.45	104.45	1.06	
180	1115	B	12	H	2	75	75	104.45	104.45	104.45	1.04	1.05
180	1115	B	12	H	6	75	75	110.45	110.45	110.45	1.03	
180	1115	B	12	H	6	75	75	110.45	110.45	110.45	1.00	
180	1115	B	12	H	6	75	75	110.45	110.45	110.45	1.02	1.02
180	1115	B	13	H	2	75	75	113.95	113.95	113.95	1.03	
180	1115	B	13	H	2	75	75	113.95	113.95	113.95	1.02	1.03
180	1115	B	13	H	6	75	75	119.95	119.95	119.95	1.02	
180	1115	B	13	H	6	75	75	119.95	119.95	119.95	1.01	

Table T13 (continued).

Leg	Site	Hole	Core	Type	Section	Top interval (cm)	Bottom interval (cm)	Top depth (mbsf)	Bottom depth (mbsf)	Middle depth (mbsf)	Thermal conductivity ($W \cdot m^{-1} \cdot °C^{-1}$)	Thermal conductivity average ($W \cdot m^{-1} \cdot °C^{-1}$)
180	1115	B	13	H	6	75	75	119.95	119.95	119.95	1.01	1.01
180	1115	B	13	H	4	75	75	116.95	116.95	116.95	1.06	
180	1115	B	13	H	4	75	75	116.95	116.95	116.95	1.04	1.05
180	1115	B	14	H	6	75	75	129.45	129.45	129.45	0.99	
180	1115	B	14	H	6	75	75	129.45	129.45	129.45	1.00	0.99
180	1115	B	14	H	2	75	75	123.45	123.45	123.45	1.02	
180	1115	B	14	H	2	75	75	123.45	123.45	123.45	1.01	
180	1115	B	14	H	2	75	75	123.45	123.45	123.45	1.03	1.02
180	1115	B	14	H	4	75	75	126.45	126.45	126.45	0.97	
180	1115	B	14	H	4	75	75	126.45	126.45	126.45	0.94	
180	1115	B	14	H	4	75	75	126.45	126.45	126.45	0.95	0.95
180	1115	B	15	H	2	75	75	132.95	132.95	132.95	1.00	
180	1115	B	15	H	2	75	75	132.95	132.95	132.95	0.99	1.00
180	1115	B	15	H	4	75	75	135.95	135.95	135.95	0.98	
180	1115	B	15	H	4	75	75	135.95	135.95	135.95	0.99	
180	1115	B	15	H	4	75	75	135.95	135.95	135.95	0.98	0.98
180	1115	B	15	H	6	75	75	138.95	138.95	138.95	0.97	
180	1115	B	15	H	6	75	75	138.95	138.95	138.95	0.98	0.98
180	1115	B	16	H	2	75	75	142.45	142.45	142.45	0.96	
180	1115	B	16	H	2	75	75	142.45	142.45	142.45	0.91	
180	1115	B	16	H	2	75	75	142.45	142.45	142.45	0.92	0.93
180	1115	B	16	H	4	75	75	145.45	145.45	145.45	0.97	
180	1115	B	16	H	4	75	75	145.45	145.45	145.45	0.97	0.97
180	1115	B	16	H	6	75	75	148.45	148.45	148.45	1.00	
180	1115	B	16	H	6	75	75	148.45	148.45	148.45	1.02	1.01
180	1115	B	17	H	2	75	75	151.95	151.95	151.95	0.98	
180	1115	B	17	H	2	75	75	151.95	151.95	151.95	0.95	0.97
180	1115	B	17	H	4	85	85	155.05	155.05	155.05	0.92	0.92
180	1115	B	18	H	1	75	75	159.95	159.95	159.95	1.04	
180	1115	B	18	H	1	75	75	159.95	159.95	159.95	1.05	
180	1115	B	18	H	1	75	75	159.95	159.95	159.95	1.05	1.05
180	1115	B	18	H	4	75	75	164.45	164.45	164.45	0.94	
180	1115	B	18	H	4	75	75	164.45	164.45	164.45	0.90	0.92
180	1115	B	19	H	1	75	75	169.45	169.45	169.45	0.91	
180	1115	B	19	H	1	75	75	169.45	169.45	169.45	0.88	0.89
180	1115	B	19	H	4	75	75	173.95	173.95	173.95	0.90	
180	1115	B	19	H	4	75	75	173.95	173.95	173.95	0.93	0.92
180	1115	B	20	H	2	75	75	180.45	180.45	180.45	0.97	
180	1115	B	20	H	2	75	75	180.45	180.45	180.45	0.98	0.98
180	1115	B	20	H	6	75	75	186.45	186.45	186.45	0.92	
180	1115	B	20	H	6	75	75	186.45	186.45	186.45	0.94	0.93
180	1115	B	20	H	4	75	75	183.45	183.45	183.45	0.76	
180	1115	B	20	H	4	75	75	183.45	183.45	183.45	0.85	0.81
180	1115	B	21	H	6	75	75	195.95	195.95	195.95	0.87	
180	1115	B	21	H	6	75	75	195.95	195.95	195.95	0.96	0.91
180	1115	B	21	H	2	75	75	189.95	189.95	189.95	0.98	
180	1115	B	21	H	2	75	75	189.95	189.95	189.95	1.01	1.00

Table T13 (continued).

Leg	Site	Hole	Core	Type	Section	Top interval (cm)	Bottom interval (cm)	Top depth (mbsf)	Bottom depth (mbsf)	Middle depth (mbsf)	Thermal conductivity ($W \cdot m^{-1} \cdot °C^{-1}$)	Thermal conductivity average ($W \cdot m^{-1} \cdot °C^{-1}$)
180	1115	B	22	H	5	75	75	203.89	203.89	203.89	0.87	
180	1115	B	22	H	5	75	75	203.89	203.89	203.89	0.86	0.86
180	1115	B	22	H	2	75	75	199.45	199.45	199.45	0.96	
180	1115	B	22	H	2	75	75	199.45	199.45	199.45	0.98	0.97
180	1115	B	23	H	2	75	75	208.95	208.95	208.95	0.95	
180	1115	B	23	H	2	75	75	208.95	208.95	208.95	0.95	0.95
180	1115	B	23	H	4	75	75	211.95	211.95	211.95	0.99	
180	1115	B	23	H	4	75	75	211.95	211.95	211.95	0.94	0.96
180	1115	B	23	H	6	75	75	214.95	214.95	214.95	0.96	
180	1115	B	23	H	6	75	75	214.95	214.95	214.95	0.96	0.96
180	1115	B	24	X	6	75	75	224.25	224.25	224.25	0.65	
180	1115	B	24	X	6	75	75	224.25	224.25	224.25	0.68	0.66
180	1115	C	1	R	1	137	138	284.57	284.58	284.58	1.00	
180	1115	C	1	R	1	137	138	284.57	284.58	284.58	1.00	
180	1115	C	1	R	1	137	138	284.57	284.58	284.58	1.01	
180	1115	C	1	R	1	137	138	284.57	284.58	284.58	1.00	1.00
180	1115	C	2	R	4	42	44	296.61	296.63	296.62	1.03	
180	1115	C	2	R	4	42	44	296.61	296.63	296.62	1.04	
180	1115	C	2	R	4	42	44	296.61	296.63	296.62	1.05	
180	1115	C	2	R	4	42	44	296.61	296.63	296.62	0.99	1.03
180	1115	C	2	R	1	0	2	292.80	292.82	292.81	1.36	
180	1115	C	2	R	1	0	2	292.80	292.82	292.81	1.30	
180	1115	C	2	R	1	0	2	292.80	292.82	292.81	1.37	
180	1115	C	2	R	1	0	2	292.80	292.82	292.81	1.31	1.34
180	1115	C	3	R	2	67	68	304.67	304.68	304.68	0.96	
180	1115	C	3	R	2	67	68	304.67	304.68	304.68	1.03	
180	1115	C	3	R	2	67	68	304.67	304.68	304.68	1.03	
180	1115	C	3	R	2	67	68	304.67	304.68	304.68	1.02	1.01
180	1115	C	3	R	4	27	29	307.27	307.29	307.28	1.04	
180	1115	C	3	R	4	27	29	307.27	307.29	307.28	1.07	
180	1115	C	3	R	4	27	29	307.27	307.29	307.28	1.06	
180	1115	C	3	R	4	27	29	307.27	307.29	307.28	1.06	
180	1115	C	3	R	4	27	29	307.27	307.29	307.28	1.06	1.06
180	1115	C	3	R	6	44	46	310.44	310.46	310.45	0.95	
180	1115	C	3	R	6	44	46	310.44	310.46	310.45	1.01	
180	1115	C	3	R	6	44	46	310.44	310.46	310.45	1.00	
180	1115	C	3	R	6	44	46	310.44	310.46	310.45	1.01	0.99
180	1115	C	4	R	4	7	8	316.53	316.54	316.54	0.73	
180	1115	C	4	R	4	7	8	316.53	316.54	316.54	1.00	
180	1115	C	4	R	4	7	8	316.53	316.54	316.54	0.97	
180	1115	C	4	R	4	7	8	316.53	316.54	316.54	0.99	0.92
180	1115	C	4	R	2	105	106	314.66	314.67	314.67	0.73	
180	1115	C	4	R	2	105	106	314.66	314.67	314.67	1.04	
180	1115	C	4	R	2	105	106	314.66	314.67	314.67	0.95	
180	1115	C	4	R	2	105	106	314.66	314.67	314.67	0.97	0.92
180	1115	C	5	R	1	41	42	322.11	322.12	322.12	1.02	
180	1115	C	5	R	1	41	42	322.11	322.12	322.12	1.03	

Table T13 (continued).

Leg	Site	Hole	Core	Type	Section	Top interval (cm)	Bottom interval (cm)	Top depth (mbsf)	Bottom depth (mbsf)	Middle depth (mbsf)	Thermal conductivity ($W \cdot m^{-1} \cdot °C^{-1}$)	Thermal conductivity average ($W \cdot m^{-1} \cdot °C^{-1}$)
180	1115	C	5	R	1	41	42	322.11	322.12	322.12	1.03	1.03
180	1115	C	5	R	4	10	11	326.07	326.08	326.08	0.80	
180	1115	C	5	R	4	10	11	326.07	326.08	326.08	1.02	
180	1115	C	5	R	4	10	11	326.07	326.08	326.08	1.03	
180	1115	C	5	R	4	10	11	326.07	326.08	326.08	1.03	0.97
180	1115	C	6	R	2	123	124	334.13	334.14	334.14	1.05	
180	1115	C	6	R	2	123	124	334.13	334.14	334.14	1.03	
180	1115	C	6	R	2	123	124	334.13	334.14	334.14	1.03	
180	1115	C	6	R	2	123	124	334.13	334.14	334.14	1.01	1.03
180	1115	C	6	R	4	30	31	336.20	336.21	336.21	1.00	
180	1115	C	6	R	4	30	31	336.20	336.21	336.21	1.03	1.01
180	1115	C	6	R	1	68	70	332.08	332.10	332.09	0.83	
180	1115	C	6	R	1	68	70	332.08	332.10	332.09	0.98	
180	1115	C	6	R	1	68	70	332.08	332.10	332.09	1.03	
180	1115	C	6	R	1	68	70	332.08	332.10	332.09	1.04	0.97
180	1115	C	7	R	1	80	82	341.80	341.82	341.81	1.06	
180	1115	C	7	R	1	80	82	341.80	341.82	341.81	1.04	1.05
180	1115	C	7	R	5	86	87	347.60	347.61	347.61	0.96	
180	1115	C	7	R	5	86	87	347.60	347.61	347.61	0.99	0.97
180	1115	C	7	R	3	87	88	344.79	344.80	344.80	1.03	
180	1115	C	7	R	3	87	88	344.79	344.80	344.80	1.03	1.03
180	1115	C	8	R	3	132	133	354.26	354.27	354.27	1.15	
180	1115	C	8	R	3	132	133	354.26	354.27	354.27	1.03	1.09
180	1115	C	8	R	1	26	27	350.86	350.87	350.87	0.99	
180	1115	C	8	R	1	26	27	350.86	350.87	350.87	1.01	1.00
180	1115	C	8	R	5	18	19	356.12	356.13	356.13	0.96	
180	1115	C	8	R	5	18	19	356.12	356.13	356.13	0.99	0.97
180	1115	C	9	R	1	59	60	360.49	360.50	360.50	0.99	
180	1115	C	9	R	1	59	60	360.49	360.50	360.50	1.02	1.00
180	1115	C	9	R	3	108	109	363.45	363.46	363.46	1.00	
180	1115	C	9	R	3	108	109	363.45	363.46	363.46	1.03	1.02
180	1115	C	9	R	5	129	130	366.50	366.51	366.51	0.97	
180	1115	C	9	R	5	129	130	366.50	366.51	366.51	1.04	1.00
180	1115	C	9	R	7	62	63	368.49	368.50	368.50	0.97	
180	1115	C	9	R	7	62	63	368.49	368.50	368.50	0.95	0.96
180	1115	C	10	R	1	85	86	370.35	370.36	370.36	0.95	
180	1115	C	10	R	1	85	86	370.35	370.36	370.36	0.96	0.96
180	1115	C	10	R	3	22	23	372.72	372.73	372.73	1.04	
180	1115	C	10	R	3	22	23	372.72	372.73	372.73	1.02	1.03
180	1115	C	10	R	5	94	95	376.44	376.45	376.45	1.03	
180	1115	C	10	R	5	94	95	376.44	376.45	376.45	1.05	
180	1115	C	10	R	5	94	95	376.44	376.45	376.45	0.98	376.45
180	1115	C	11	R	1	14	15	379.24	379.25	379.25	1.19	
180	1115	C	11	R	1	14	15	379.24	379.25	379.25	1.15	1.17
180	1115	C	11	R	3	83	84	382.85	382.86	382.86	0.41	
180	1115	C	11	R	3	83	84	382.85	382.86	382.86	1.01	
180	1115	C	11	R	3	83	84	382.85	382.86	382.86	1.05	382.86

Table T13 (continued).

Leg	Site	Hole	Core	Type	Section	Top interval (cm)	Bottom interval (cm)	Top depth (mbsf)	Bottom depth (mbsf)	Middle depth (mbsf)	Thermal conductivity ($W \cdot m^{-1} \cdot °C^{-1}$)	Thermal conductivity average ($W \cdot m^{-1} \cdot °C^{-1}$)
180	1115	C	11	R	5	95	96	385.87	385.88	385.88	0.99	
180	1115	C	11	R	5	95	96	385.87	385.88	385.88	1.00	1.00
180	1115	C	12	R	1	68	69	389.18	389.19	389.19	0.99	
180	1115	C	12	R	1	68	69	389.18	389.19	389.19	1.02	1.00
180	1115	C	12	R	3	35	36	391.85	391.86	391.86	1.02	
180	1115	C	12	R	3	35	36	391.85	391.86	391.86	1.01	1.01
180	1115	C	12	R	5	108	109	395.48	395.49	395.49	0.53	
180	1115	C	12	R	5	108	109	395.48	395.49	395.49	0.94	
180	1115	C	12	R	5	108	109	395.48	395.49	395.49	1.01	395.49
180	1115	C	12	R	7	15	16	397.55	397.56	397.56	0.73	
180	1115	C	12	R	7	15	16	397.55	397.56	397.56	1.03	
180	1115	C	12	R	7	15	16	397.55	397.56	397.56	1.02	
180	1115	C	12	R	7	15	16	397.55	397.56	397.56	1.02	0.95
180	1115	C	13	R	6	76	77	405.79	405.80	405.80	1.02	
180	1115	C	13	R	6	76	77	405.79	405.80	405.80	1.04	1.03
180	1115	C	13	R	2	71	72	400.31	400.32	400.32	1.10	
180	1115	C	13	R	2	71	72	400.31	400.32	400.32	1.12	1.11
180	1115	C	13	R	4	74	75	402.89	402.90	402.90	1.07	
180	1115	C	13	R	4	74	75	402.89	402.90	402.90	1.07	1.07
180	1115	C	14	R	3	72	73	411.01	411.02	411.02	0.85	
180	1115	C	14	R	3	72	73	411.01	411.02	411.02	1.04	0.94
180	1115	C	14	R	1	51	52	408.21	408.22	408.22	0.75	
180	1115	C	14	R	1	51	52	408.21	408.22	408.22	1.09	
180	1115	C	14	R	1	51	52	408.21	408.22	408.22	1.11	
180	1115	C	14	R	1	51	52	408.21	408.22	408.22	1.05	1.00
180	1115	C	15	R	2	110	111	419.90	419.91	419.91	0.98	
180	1115	C	15	R	2	110	111	419.90	419.91	419.91	1.22	1.10
180	1115	C	15	R	6	36	37	425.16	425.17	425.17	1.10	
180	1115	C	15	R	6	36	37	425.16	425.17	425.17	0.99	1.04
180	1115	C	15	R	4	62	63	422.42	422.43	422.43	1.16	
180	1115	C	15	R	4	62	63	422.42	422.43	422.43	1.17	1.16
180	1115	C	16	R	2	6	7	427.75	427.76	427.76	1.41	
180	1115	C	16	R	2	6	7	427.75	427.76	427.76	1.30	1.35
180	1115	C	17	R	1	2	3	436.52	436.53	436.53	1.18	
180	1115	C	17	R	1	2	3	436.52	436.53	436.53	1.18	1.18
180	1115	C	18	R	1	19	20	446.29	446.30	446.30	1.13	
180	1115	C	18	R	1	19	20	446.29	446.30	446.30	1.14	1.14
180	1115	C	19	R	1	20	21	455.80	455.81	455.81	1.18	
180	1115	C	19	R	1	20	21	455.80	455.81	455.81	1.17	1.18
180	1115	C	20	R	1	10	11	465.30	465.31	465.31	1.13	
180	1115	C	20	R	1	10	11	465.30	465.31	465.31	1.12	1.12
180	1115	C	21	R	3	7	8	476.75	476.76	476.76	1.12	
180	1115	C	21	R	3	7	8	476.75	476.76	476.76	1.17	1.15
180	1115	C	21	R	1	69	70	475.59	475.60	475.60	1.32	
180	1115	C	21	R	1	69	70	475.59	475.60	475.60	1.16	
180	1115	C	21	R	1	69	70	475.59	475.60	475.60	1.12	
180	1115	C	21	R	1	69	70	475.59	475.60	475.60	1.09	1.17

Table T13 (continued).

Leg	Site	Hole	Core	Type	Section	Top interval (cm)	Bottom interval (cm)	Top depth (mbsf)	Bottom depth (mbsf)	Middle depth (mbsf)	Thermal conductivity ($W \cdot m^{-1} \cdot °C^{-1}$)	Thermal conductivity average ($W \cdot m^{-1} \cdot °C^{-1}$)
180	1115	C	22	R	1	117	118	485.67	485.68	485.68	1.02	
180	1115	C	22	R	1	117	118	485.67	485.68	485.68	1.03	1.02
180	1115	C	22	R	3	21	22	486.97	486.98	486.98	1.07	
180	1115	C	22	R	3	21	22	486.97	486.98	486.98	1.07	
180	1115	C	22	R	3	21	22	486.97	486.98	486.98	1.06	1.07
180	1115	C	22	R	5	16	17	489.92	489.93	489.93	1.10	
180	1115	C	22	R	5	16	17	489.92	489.93	489.93	1.07	1.08
180	1115	C	23	R	1	91	92	495.01	495.02	495.02	1.06	
180	1115	C	23	R	1	91	92	495.01	495.02	495.02	1.04	1.05
180	1115	C	23	R	3	4	5	497.02	497.03	497.03	1.14	
180	1115	C	23	R	3	4	5	497.02	497.03	497.03	1.14	1.14
180	1115	C	24	R	3	48	49	507.28	507.29	507.29	1.13	
180	1115	C	24	R	3	48	49	507.28	507.29	507.29	1.10	1.11
180	1115	C	24	R	5	27	28	510.07	510.08	510.08	1.01	
180	1115	C	24	R	5	27	28	510.07	510.08	510.08	1.05	1.03
180	1115	C	24	R	1	31	32	504.11	504.12	504.12	1.18	
180	1115	C	24	R	1	31	32	504.11	504.12	504.12	0.99	
180	1115	C	24	R	1	31	32	504.11	504.12	504.12	1.31	1.16
180	1115	C	25	R	1	106	107	514.46	514.47	514.47	0.93	
180	1115	C	25	R	1	106	107	514.46	514.47	514.47	1.09	1.01
180	1115	C	29	R	1	50	51	552.30	552.31	552.31	1.02	
180	1115	C	29	R	1	50	51	552.30	552.31	552.31	1.05	1.03
180	1115	C	29	R	1	80	81	552.60	552.61	552.61	1.64	
180	1115	C	29	R	1	80	81	552.60	552.61	552.61	1.53	1.59
180	1115	C	30	R	1	23	24	561.63	561.64	561.64	1.49	
180	1115	C	30	R	1	23	24	561.63	561.64	561.64	1.69	1.59
180	1115	C	30	R	2	28	29	562.21	562.22	562.22	1.09	
180	1115	C	30	R	2	28	29	562.21	562.22	562.22	1.11	1.10
180	1115	C	30	R	2	122	123	563.15	563.16	563.16	0.76	
180	1115	C	30	R	2	122	123	563.15	563.16	563.16	0.92	0.84
180	1115	C	30	R	5	69	70	566.70	566.71	566.71	1.62	
180	1115	C	30	R	5	69	70	566.70	566.71	566.71	1.73	1.68
180	1115	C	31	R	1	100	108	572.00	572.08	572.04	1.63	
180	1115	C	31	R	1	100	108	572.00	572.08	572.04	1.53	1.58
180	1115	C	32	R	1	85	86	581.45	581.46	581.46	1.31	
180	1115	C	32	R	1	85	86	581.45	581.46	581.46	1.40	1.36
180	1115	C	32	R	3	77	78	583.78	583.79	583.79	1.03	
180	1115	C	32	R	3	77	78	583.78	583.79	583.79	1.10	1.07
180	1115	C	33	R	3	105	106	594.11	594.12	594.12	0.70	
180	1115	C	33	R	3	105	106	594.11	594.12	594.12	1.24	0.97
180	1115	C	33	R	1	131	132	591.51	591.52	591.52	1.25	
180	1115	C	33	R	1	131	132	591.51	591.52	591.52	1.36	1.30
180	1115	C	34	R	2	92	93	602.20	602.21	602.21	1.42	
180	1115	C	34	R	2	92	93	602.20	602.21	602.21	1.62	1.52
180	1115	C	35	R	1	10	11	609.50	609.51	609.51	2.12	
180	1115	C	35	R	1	10	11	609.50	609.51	609.51	1.65	1.89
180	1115	C	35	R	3	11	12	612.32	612.33	612.33	1.25	

Table T13 (continued).

Leg	Site	Hole	Core	Type	Section	Top interval (cm)	Bottom interval (cm)	Top depth (mbsf)	Bottom depth (mbsf)	Middle depth (mbsf)	Thermal conductivity ($W \cdot m^{-1} \cdot °C^{-1}$)	Thermal conductivity average ($W \cdot m^{-1} \cdot °C^{-1}$)
180	1115	C	35	R	3	11	12	612.32	612.33	612.33	1.23	1.24
180	1115	C	36	R	2	38	39	620.88	620.89	620.89	1.09	
180	1115	C	36	R	2	38	39	620.88	620.89	620.89	1.16	1.12
180	1115	C	40	R	1	16	17	657.96	657.97	657.97	1.06	
180	1115	C	40	R	1	16	17	657.96	657.97	657.97	1.13	1.09
180	1115	C	40	R	3	11	12	660.91	660.92	660.92	1.13	
180	1115	C	40	R	3	11	12	660.91	660.92	660.92	1.15	1.14
180	1115	C	40	R	5	13	14	663.93	663.94	663.94	1.10	
180	1115	C	40	R	5	13	14	663.93	663.94	663.94	1.09	1.09
180	1115	C	41	R	1	38	39	667.78	667.79	667.79	1.12	
180	1115	C	41	R	1	38	39	667.78	667.79	667.79	1.12	1.12
180	1115	C	41	R	3	111	112	671.47	671.48	671.48	1.24	1.24
180	1115	C	42	R	3	57	58	679.96	679.97	679.97	0.80	
180	1115	C	42	R	3	57	58	679.96	679.97	679.97	1.07	0.93
180	1115	C	42	R	1	44	45	677.54	677.55	677.55	1.10	
180	1115	C	42	R	1	44	45	677.54	677.55	677.55	1.16	1.13
180	1115	C	42	R	5	61	62	682.88	682.89	682.89	1.11	
180	1115	C	42	R	5	61	62	682.88	682.89	682.89	1.14	1.12
180	1115	C	43	R	1	97	98	687.77	687.78	687.78	1.06	
180	1115	C	43	R	1	97	98	687.77	687.78	687.78	1.14	1.10
180	1115	C	43	R	5	34	36	692.54	692.56	692.55	1.19	
180	1115	C	43	R	5	34	36	692.54	692.56	692.55	1.09	1.14
180	1115	C	43	R	3	89	90	690.69	690.70	690.70	1.14	
180	1115	C	43	R	3	89	90	690.69	690.70	690.70	1.13	1.14
180	1115	C	44	R	5	26	27	702.04	702.05	702.05	1.08	
180	1115	C	44	R	5	26	27	702.04	702.05	702.05	1.09	1.08
180	1115	C	44	R	1	16	17	696.66	696.67	696.67	1.09	
180	1115	C	44	R	1	16	17	696.66	696.67	696.67	1.09	1.09
180	1115	C	44	R	7	51	52	705.05	705.06	705.06	1.08	
180	1115	C	44	R	7	51	52	705.05	705.06	705.06	1.08	1.08
180	1115	C	44	R	3	68	69	699.76	699.77	699.77	1.23	
180	1115	C	44	R	3	68	69	699.76	699.77	699.77	1.30	1.26
180	1115	C	45	R	4	12	13	710.16	710.17	710.17	1.54	
180	1115	C	45	R	4	12	13	710.16	710.17	710.17	1.70	1.62
180	1115	C	45	R	2	0	1	707.34	707.35	707.35	1.10	
180	1115	C	45	R	2	0	1	707.34	707.35	707.35	1.16	1.13
180	1115	C	46	R	6	0	1	722.44	722.45	722.45	1.11	
180	1115	C	46	R	6	0	1	722.44	722.45	722.45	1.15	1.13
180	1115	C	46	R	4	24	25	719.80	719.81	719.81	1.02	
180	1115	C	46	R	4	24	25	719.80	719.81	719.81	0.99	1.00
180	1115	C	46	R	2	11	12	716.96	716.97	716.97	1.03	
180	1115	C	46	R	2	11	12	716.96	716.97	716.97	1.03	1.03
180	1115	C	47	R	2	0	1	726.76	726.77	726.77	1.20	
180	1115	C	47	R	2	0	1	726.76	726.77	726.77	1.25	1.22
180	1115	C	47	R	4	56	57	730.10	730.11	730.11	1.19	1.22
180	1115	C	47	R	6	76	77	733.01	733.02	733.02	1.17	
180	1115	C	47	R	6	76	77	733.01	733.02	733.02	1.20	1.18
180	1115	C	48	R	1	41	42	735.51	735.52	735.52	1.06	

Table T13 (continued).

Leg	Site	Hole	Core	Type	Section	Top interval (cm)	Bottom interval (cm)	Top depth (mbsf)	Bottom depth (mbsf)	Middle depth (mbsf)	Thermal conductivity ($W \cdot m^{-1} \cdot °C^{-1}$)	Thermal conductivity average ($W \cdot m^{-1} \cdot °C^{-1}$)
180	1115	C	48	R	1	41	42	735.51	735.52	735.52	1.09	1.07
180	1115	C	48	R	3	85	86	738.50	738.51	738.51	1.18	
180	1115	C	48	R	3	85	86	738.50	738.51	738.51	1.18	
180	1115	C	48	R	3	85	86	738.50	738.51	738.51	1.19	1.19
180	1115	C	49	R	6	38	39	751.96	751.97	751.97	0.70	
180	1115	C	49	R	6	38	39	751.96	751.97	751.97	1.14	
180	1115	C	49	R	6	38	39	751.96	751.97	751.97	1.14	1.00
180	1115	C	49	R	4	34	35	749.14	749.15	749.15	0.94	
180	1115	C	49	R	4	34	35	749.14	749.15	749.15	0.93	0.94
180	1115	C	49	R	2	24	25	746.23	746.24	746.24	1.01	
180	1115	C	49	R	2	24	25	746.23	746.24	746.24	1.17	1.09
180	1115	C	50	R	4	38	39	758.37	758.38	758.38	1.10	
180	1115	C	50	R	4	38	39	758.37	758.38	758.38	1.17	1.14
180	1115	C	50	R	6	24	25	760.49	760.50	760.50	1.10	
180	1115	C	50	R	6	24	25	760.49	760.50	760.50	1.16	1.13
180	1115	C	50	R	2	53	54	756.23	756.24	756.24	1.04	
180	1115	C	50	R	2	53	54	756.23	756.24	756.24	1.07	1.06
180	1115	C	51	R	3	43	44	766.76	766.77	766.77	1.15	
180	1115	C	51	R	3	43	44	766.76	766.77	766.77	1.18	1.16
180	1115	C	51	R	1	119	120	765.09	765.10	765.10	1.02	
180	1115	C	51	R	1	119	120	765.09	765.10	765.10	1.09	1.06
180	1115	C	52	R	7	26	27	781.96	781.97	781.97	1.15	
180	1115	C	52	R	7	26	27	781.96	781.97	781.97	1.15	1.15
180	1115	C	52	R	5	95	96	780.02	780.03	780.03	1.17	
180	1115	C	52	R	5	95	96	780.02	780.03	780.03	1.19	1.18
180	1115	C	52	R	1	64	65	774.24	774.25	774.25	1.20	
180	1115	C	52	R	1	64	65	774.24	774.25	774.25	1.19	1.19
180	1115	C	52	R	3	11	12	776.26	776.27	776.27	1.14	
180	1115	C	52	R	3	11	12	776.26	776.27	776.27	1.17	1.16
180	1115	C	53	R	1	87	88	784.07	784.08	784.08	1.16	
180	1115	C	53	R	1	87	88	784.07	784.08	784.08	1.23	1.19
180	1115	C	53	R	5	94	95	789.45	789.46	789.46	1.18	
180	1115	C	53	R	3	13	14	786.17	786.18	786.18	1.12	
180	1115	C	53	R	3	13	14	786.17	786.18	786.18	1.19	1.15
180	1115	C	54	R	1	28	29	793.08	793.09	793.09	1.21	
180	1115	C	54	R	1	28	29	793.08	793.09	793.09	1.27	1.24
180	1115	C	54	R	3	125	126	796.49	796.50	796.50	1.22	
180	1115	C	54	R	3	125	126	796.49	796.50	796.50	1.22	1.22
180	1115	C	54	R	5	72	73	798.96	798.97	798.97	1.13	
180	1115	C	54	R	5	72	73	798.96	798.97	798.97	1.18	1.16
180	1115	C	54	R	7	88	89	801.71	801.72	801.72	1.22	
180	1115	C	54	R	7	88	89	801.71	801.72	801.72	1.23	1.23

Note: This table is also available in ASCII format in the **TABLES** directory.

Table T14. Unconfined compressive strength and vane shear strength, Site 1115. (Continued on next four pages. See table note.)

Leg	Site	Hole	Core	Type	Section	Top interval (cm)	Bottom interval (cm)	Depth (mbsf)	Unconfined compressive strength (kPa)	Vane shear strength (kPa)
180	1115	A	1	H	2	54.0	54.0	0.82	5.0	
180	1115	A	1	H	3	105.6	105.6	2.56		7.0
180	1115	A	1	H	4	58.3	58.3	3.58		5.2
180	1115	B	1	H	1	110.5	110.5	1.11		5.0
180	1115	B	1	H	2	85.5	85.5	2.36		7.8
180	1115	B	1	H	3	50.0	50.0	3.50		6.4
180	1115	B	1	H	3	64.0	64.0	3.64	12.5	
180	1115	B	1	H	4	100.4	100.4	5.50		7.4
180	1115	B	1	H	5	26.4	26.4	6.26		9.0
180	1115	B	1	H	5	64.0	64.0	6.64	20.0	
180	1115	B	2	H	1	80.0	80.0	8.00		8.5
180	1115	B	2	H	2	121.0	121.0	9.91		14.3
180	1115	B	2	H	3	107.2	107.2	11.27		6.2
180	1115	B	2	H	3	107.2	107.2	11.27	10.0	
180	1115	B	2	H	4	91.4	91.4	12.61		13.5
180	1115	B	2	H	4	91.4	91.4	12.61	30.0	
180	1115	B	2	H	5	105.8	105.8	14.26		16.3
180	1115	B	2	H	6	91.7	91.7	15.62		17.1
180	1115	B	2	H	7	18.8	18.8	16.39		13.6
180	1115	B	3	H	1	90.0	90.0	17.60	15.0	
180	1115	B	3	H	1	142.9	142.9	18.13		19.9
180	1115	B	3	H	2	90.0	90.0	19.10	20.0	
180	1115	B	3	H	2	138.3	138.3	19.58		22.8
180	1115	B	3	H	3	90.0	90.0	20.60	25.0	
180	1115	B	3	H	3	108.1	108.1	20.78		28.5
180	1115	B	3	H	4	90.0	90.0	22.10	25.0	
180	1115	B	3	H	4	135.9	135.9	22.56		36.9
180	1115	B	3	H	5	90.0	90.0	23.60	22.5	
180	1115	B	3	H	5	134.3	134.3	24.04		38.3
180	1115	B	3	H	6	90.0	90.0	25.10	20.0	
180	1115	B	3	H	6	136.8	136.8	25.57		35.5
180	1115	B	3	H	7	66.1	66.1	26.36		48.2
180	1115	B	3	H	7	70.0	70.0	26.40	30.0	
180	1115	B	4	H	1	60.0	60.0	26.80	25.0	
180	1115	B	4	H	1	130.0	130.0	27.50		34.6
180	1115	B	4	H	2	60.0	60.0	28.30	30.0	
180	1115	B	4	H	2	135.1	135.1	29.05		29.4
180	1115	B	4	H	3	60.0	60.0	29.80	35.0	
180	1115	B	4	H	3	137.6	137.6	30.58		25.1
180	1115	B	4	H	4	60.0	60.0	31.30	50.0	
180	1115	B	4	H	4	134.5	134.5	32.04		51.4
180	1115	B	4	H	5	60.0	60.0	32.80	45.0	
180	1115	B	4	H	5	133.6	133.6	33.54		44.8
180	1115	B	4	H	6	60.0	60.0	34.30	40.0	
180	1115	B	4	H	6	135.3	135.3	35.05		54.8
180	1115	B	4	H	7	60.0	60.0	35.80	40.0	
180	1115	B	4	H	7	63.1	63.1	35.83		38.5
180	1115	B	4	H	7	63.1	63.1	35.83		38.5
180	1115	B	5	H	1	25.0	25.0	35.95	40.0	
180	1115	B	5	H	1	133.6	133.6	37.04		54.4
180	1115	B	5	H	2	25.0	25.0	37.45	50.0	
180	1115	B	5	H	2	136.0	136.0	38.56		34.6
180	1115	B	5	H	3	25.0	25.0	38.95	50.0	
180	1115	B	5	H	3	141.9	141.9	40.12		49.2
180	1115	B	5	H	4	25.0	25.0	40.45	25.0	
180	1115	B	5	H	4	137.1	137.1	41.57		66.0
180	1115	B	5	H	5	25.0	25.0	41.95	30.0	
180	1115	B	5	H	5	138.3	138.3	43.08		44.5
180	1115	B	5	H	6	25.0	25.0	43.45	37.5	
180	1115	B	5	H	6	136.3	136.3	44.56		50.3
180	1115	B	5	H	7	25.0	25.0	44.95	55.0	
180	1115	B	6	H	1	40.0	40.0	45.60	80.0	
180	1115	B	6	H	1	125.9	125.9	46.46		43.2
180	1115	B	6	H	2	40.0	40.0	47.10	55.0	
180	1115	B	6	H	2	123.7	123.7	47.94		35.9
180	1115	B	6	H	3	50.0	50.0	48.70	70.0	
180	1115	B	6	H	3	135.1	135.1	49.55		57.8

Table T14 (continued).

Leg	Site	Hole	Core	Type	Section	Top interval (cm)	Bottom interval (cm)	Depth (mbsf)	Unconfined compressive strength (kPa)	Vane shear strength (kPa)
180	1115	B	6	H	4	50.0	50.0	50.20	65.0	
180	1115	B	6	H	4	130.1	130.1	51.00		48.6
180	1115	B	6	H	5	50.0	50.0	51.70	57.5	
180	1115	B	6	H	5	129.0	129.0	52.49		49.5
180	1115	B	6	H	6	50.0	50.0	53.20	50.0	
180	1115	B	6	H	6	134.8	134.8	54.05		57.2
180	1115	B	6	H	6	134.8	134.8	54.05		57.2
180	1115	B	6	H	7	66.1	66.1	54.86		40.6
180	1115	B	7	H	1	40.0	40.0	55.10	50.0	
180	1115	B	7	H	1	100.0	100.0	55.70	55.0	
180	1115	B	7	H	1	131.2	131.2	56.01		51.5
180	1115	B	7	H	2	50.0	50.0	56.70	85.0	
180	1115	B	7	H	2	139.5	139.5	57.60	65.0	32.2
180	1115	B	7	H	3	40.0	40.0	58.10	65.0	
180	1115	B	7	H	3	136.4	136.4	59.06	65.0	56.7
180	1115	B	7	H	4	40.0	40.0	59.60	27.5	
180	1115	B	7	H	4	133.3	133.3	60.53	45.0	66.6
180	1115	B	7	H	5	40.0	40.0	61.10	50.0	
180	1115	B	7	H	5	132.7	132.7	62.03	65.0	69.3
180	1115	B	7	H	6	40.0	40.0	62.60	87.5	
180	1115	B	7	H	6	100.0	100.0	63.20	70.0	
180	1115	B	7	H	6	132.8	132.8	63.53	65.0	78.3
180	1115	B	7	H	7	40.0	40.0	64.10	75.0	
180	1115	B	8	H	1	40.0	40.0	64.60	130.0	
180	1115	B	8	H	1	110.0	110.0	65.30	60.0	
180	1115	B	8	H	2	40.0	40.0	66.10	80.0	
180	1115	B	8	H	3	40.0	40.0	67.60	65.0	
180	1115	B	8	H	3	100.0	100.0	68.20	45.0	
180	1115	B	8	H	4	40.0	40.0	69.10	70.0	
180	1115	B	8	H	4	100.0	100.0	69.70	65.0	
180	1115	B	8	H	5	40.0	40.0	70.60	95.0	
180	1115	B	8	H	5	100.0	100.0	71.20	90.0	
180	1115	B	8	H	6	40.0	40.0	72.10	85.0	
180	1115	B	8	H	7	30.0	30.0	73.50	87.5	
180	1115	B	9	H	1	46.0	46.0	74.16	45.0	
180	1115	B	9	H	2	98.0	98.0	76.18	50.0	
180	1115	B	9	H	3	103.0	103.0	77.73	75.0	
180	1115	B	9	H	4	40.0	40.0	78.60	87.5	
180	1115	B	9	H	4	100.0	100.0	79.20	100.0	
180	1115	B	9	H	5	40.0	40.0	80.10	87.5	
180	1115	B	9	H	5	100.0	100.0	80.70	125.0	
180	1115	B	9	H	6	40.0	40.0	81.60	80.0	
180	1115	B	9	H	6	100.0	100.0	82.20	95.0	
180	1115	B	9	H	7	40.0	40.0	83.10	112.5	
180	1115	B	10	H	1	40.0	40.0	83.60	50.0	
180	1115	B	10	H	1	100.0	100.0	84.20	55.0	
180	1115	B	10	H	2	40.0	40.0	85.10	90.0	
180	1115	B	10	H	2	100.0	100.0	85.70	80.0	
180	1115	B	10	H	3	40.0	40.0	86.60	75.0	
180	1115	B	10	H	3	100.0	100.0	87.20	65.0	
180	1115	B	10	H	4	40.0	40.0	88.10	100.0	
180	1115	B	10	H	4	100.0	100.0	88.70	87.5	
180	1115	B	10	H	5	40.0	40.0	89.60	112.5	
180	1115	B	10	H	5	100.0	100.0	90.20	65.0	
180	1115	B	10	H	6	40.0	40.0	91.10	95.0	
180	1115	B	10	H	6	100.0	100.0	91.70	100.0	
180	1115	B	10	H	7	40.0	40.0	92.60	105.0	
180	1115	B	11	H	1	40.0	40.0	93.10	45.0	
180	1115	B	11	H	1	100.0	100.0	93.70	70.0	
180	1115	B	11	H	2	40.0	40.0	94.60	45.0	
180	1115	B	11	H	2	100.0	100.0	95.20	65.0	
180	1115	B	11	H	3	40.0	40.0	96.10	90.0	
180	1115	B	11	H	3	100.0	100.0	96.70	100.0	
180	1115	B	11	H	4	40.0	40.0	97.60	87.5	
180	1115	B	11	H	4	100.0	100.0	98.20	130.0	
180	1115	B	11	H	5	40.0	40.0	99.10	125.0	
180	1115	B	11	H	5	100.0	100.0	99.70	100.0	
180	1115	B	11	H	6	40.0	40.0	100.60	110.0	

Table T14 (continued).

Leg	Site	Hole	Core	Type	Section	Top interval (cm)	Bottom interval (cm)	Depth (mbsf)	Unconfined compressive strength (kPa)	Vane shear strength (kPa)
180	1115	B	11	H	6	100.0	100.0	101.20	105.0	
180	1115	B	11	H	7	50.0	50.0	102.20	105.0	
180	1115	B	12	H	1	40.0	40.0	102.60	65.0	
180	1115	B	12	H	1	100.0	100.0	103.20	90.0	
180	1115	B	12	H	2	40.0	40.0	104.10	80.0	
180	1115	B	12	H	2	100.0	100.0	104.70	70.0	
180	1115	B	12	H	3	40.0	40.0	105.60	95.0	
180	1115	B	12	H	3	100.0	100.0	106.20	87.5	
180	1115	B	12	H	4	40.0	40.0	107.10	112.5	
180	1115	B	12	H	4	100.0	100.0	107.70	90.0	
180	1115	B	12	H	5	40.0	40.0	108.60	112.5	
180	1115	B	12	H	5	100.0	100.0	109.20	125.0	
180	1115	B	12	H	6	40.0	40.0	110.10	112.5	
180	1115	B	12	H	6	100.0	100.0	110.70	162.5	
180	1115	B	12	H	7	34.0	34.0	111.54	115.0	
180	1115	B	13	H	1	40.0	40.0	112.10	70.0	
180	1115	B	13	H	1	100.0	100.0	112.70	87.5	
180	1115	B	13	H	2	40.0	40.0	113.60	122.5	
180	1115	B	13	H	2	102.0	102.0	114.22	85.0	
180	1115	B	13	H	3	40.0	40.0	115.10	125.0	
180	1115	B	13	H	3	100.0	100.0	115.70	120.0	
180	1115	B	13	H	4	40.0	40.0	116.60	137.5	
180	1115	B	13	H	4	100.0	100.0	117.20	145.0	
180	1115	B	13	H	5	40.0	40.0	118.10	140.0	
180	1115	B	13	H	5	100.0	100.0	118.70	157.5	
180	1115	B	13	H	6	40.0	40.0	119.60	145.0	
180	1115	B	13	H	6	100.0	100.0	120.20	145.0	
180	1115	B	13	H	7	40.0	40.0	121.10	115.0	
180	1115	B	14	H	1	40.0	40.0	121.60	85.0	
180	1115	B	14	H	1	100.0	100.0	122.20	100.0	
180	1115	B	14	H	2	40.0	40.0	123.10	100.0	
180	1115	B	14	H	2	100.0	100.0	123.70	80.0	
180	1115	B	14	H	3	35.0	35.0	124.55	97.5	
180	1115	B	14	H	3	102.0	102.0	125.22	125.0	
180	1115	B	14	H	4	40.0	40.0	126.10	125.0	
180	1115	B	14	H	4	100.0	100.0	126.70	150.0	
180	1115	B	14	H	5	40.0	40.0	127.60	205.0	
180	1115	B	14	H	5	100.0	100.0	128.20	187.5	
180	1115	B	14	H	6	40.0	40.0	129.10	180.0	
180	1115	B	14	H	6	100.0	100.0	129.70	162.5	
180	1115	B	14	H	7	40.0	40.0	130.60	175.0	
180	1115	B	15	H	1	40.0	40.0	131.10	75.0	
180	1115	B	15	H	1	100.0	100.0	131.70	80.0	
180	1115	B	15	H	2	40.0	40.0	132.60	110.0	
180	1115	B	15	H	2	100.0	100.0	133.20	125.0	
180	1115	B	15	H	3	50.0	50.0	134.20	82.5	
180	1115	B	15	H	3	100.0	100.0	134.70	115.0	
180	1115	B	15	H	4	40.0	40.0	135.60	210.0	
180	1115	B	15	H	4	100.0	100.0	136.20	170.0	
180	1115	B	15	H	5	40.0	40.0	137.10	162.5	
180	1115	B	15	H	5	100.0	100.0	137.70	160.0	
180	1115	B	15	H	6	40.0	40.0	138.60	190.0	
180	1115	B	15	H	6	100.0	100.0	139.20	162.5	
180	1115	B	15	H	7	40.0	40.0	140.10	160.0	
180	1115	B	16	H	1	40.0	40.0	140.60	120.0	
180	1115	B	16	H	1	100.0	100.0	141.20	112.5	
180	1115	B	16	H	2	60.0	60.0	142.30	150.0	
180	1115	B	16	H	2	110.0	110.0	142.80	87.5	
180	1115	B	16	H	3	40.0	40.0	143.60	112.5	
180	1115	B	16	H	3	105.0	105.0	144.25	112.5	
180	1115	B	16	H	4	70.0	70.0	145.40	180.0	
180	1115	B	16	H	4	130.0	130.0	146.00	175.0	
180	1115	B	16	H	5	40.0	40.0	146.60	215.0	
180	1115	B	16	H	5	100.0	100.0	147.20	150.0	
180	1115	B	16	H	6	40.0	40.0	148.10	170.0	
180	1115	B	16	H	6	100.0	100.0	148.70	200.0	
180	1115	B	16	H	7	40.0	40.0	149.60	140.0	
180	1115	B	17	H	1	40.0	40.0	150.10	125.0	

Table T14 (continued).

Leg	Site	Hole	Core	Type	Section	Top interval (cm)	Bottom interval (cm)	Depth (mbsf)	Unconfined compressive strength (kPa)	Vane shear strength (kPa)
180	1115	B	17	H	2	40.0	40.0	151.60	130.0	
180	1115	B	17	H	3	40.0	40.0	153.10	112.5	
180	1115	B	17	H	4	40.0	40.0	154.60	112.5	
180	1115	B	17	H	5	40.0	40.0	156.10	212.5	
180	1115	B	17	H	6	40.0	40.0	157.60	155.0	
180	1115	B	17	H	7	40.0	40.0	159.10	140.0	
180	1115	B	18	H	1	40.0	40.0	159.60	125.0	
180	1115	B	18	H	1	120.0	120.0	160.40	112.5	
180	1115	B	18	H	2	30.0	30.0	161.00	105.0	
180	1115	B	18	H	2	40.0	40.0	161.10	105.0	
180	1115	B	18	H	2	50.0	50.0	161.20	50.0	
180	1115	B	18	H	2	60.0	60.0	161.30	180.0	
180	1115	B	18	H	3	40.0	40.0	162.60	135.0	
180	1115	B	18	H	3	120.0	120.0	163.40	185.0	
180	1115	B	18	H	4	50.0	50.0	164.20	185.0	
180	1115	B	18	H	5	60.0	60.0	165.80	185.0	
180	1115	B	18	H	6	60.0	60.0	167.30	195.0	
180	1115	B	18	H	7	30.0	30.0	168.50	182.5	
180	1115	B	19	H	1	30.0	30.0	169.00	95.0	
180	1115	B	19	H	2	30.0	30.0	170.50	115.0	
180	1115	B	19	H	3	30.0	30.0	172.00	135.0	
180	1115	B	19	H	4	30.0	30.0	173.50	145.0	
180	1115	B	19	H	5	30.0	30.0	175.00	190.0	
180	1115	B	19	H	6	30.0	30.0	176.50	195.0	
180	1115	B	19	H	7	30.0	30.0	178.00	157.5	
180	1115	B	20	H	1	40.0	40.0	178.60	105.0	
180	1115	B	20	H	1	110.0	110.0	179.30	145.0	
180	1115	B	20	H	2	40.0	40.0	180.10	132.5	
180	1115	B	20	H	2	110.0	110.0	180.80	125.0	
180	1115	B	20	H	3	40.0	40.0	181.60	125.0	
180	1115	B	20	H	3	110.0	110.0	182.30	107.5	
180	1115	B	20	H	4	40.0	40.0	183.10	162.5	
180	1115	B	20	H	4	110.0	110.0	183.80	175.0	
180	1115	B	20	H	5	40.0	40.0	184.60	175.0	
180	1115	B	20	H	6	40.0	40.0	186.10	200.0	
180	1115	B	20	H	7	40.0	40.0	187.60	175.0	
180	1115	B	21	H	1	50.0	50.0	188.20	150.0	
180	1115	B	21	H	2	50.0	50.0	189.70	200.0	
180	1115	B	21	H	3	50.0	50.0	191.20	185.0	
180	1115	B	21	H	4	50.0	50.0	192.70	175.0	
180	1115	B	21	H	5	50.0	50.0	194.20	175.0	
180	1115	B	21	H	5	100.0	100.0	194.70	175.0	
180	1115	B	21	H	6	50.0	50.0	195.70	175.0	
180	1115	B	21	H	6	100.0	100.0	196.20	175.0	
180	1115	B	21	H	7	20.0	20.0	196.90	185.0	
180	1115	B	21	H	7	40.0	40.0	197.10	175.0	
180	1115	B	22	H	1	124.0	124.0	198.44	165.0	
180	1115	B	22	H	2	124.0	124.0	199.94	165.0	
180	1115	B	22	H	3	123.0	123.0	201.43	205.0	
180	1115	B	22	H	4	124.0	124.0	202.94	200.0	
180	1115	B	22	H	5	124.0	124.0	204.38	200.0	
180	1115	B	22	H	6	124.0	124.0	205.88	200.0	
180	1115	B	23	H	1	124.0	124.0	207.94	175.0	
180	1115	B	23	H	2	124.0	124.0	209.44	225.0	
180	1115	B	23	H	3	124.0	124.0	210.94	225.0	
180	1115	B	23	H	4	120.0	120.0	212.40	200.0	
180	1115	B	23	H	6	124.0	124.0	215.44	200.0	
180	1115	B	23	H	7	60.0	60.0	216.30	200.0	
180	1115	B	24	X	1	48.0	48.0	216.68	90.0	
180	1115	B	24	X	3	60.0	60.0	219.80	60.0	
180	1115	B	24	X	4	87.0	87.0	221.37	100.0	
180	1115	B	24	X	5	90.0	90.0	222.90	110.0	
180	1115	B	24	X	6	80.0	80.0	224.30	115.0	
180	1115	B	24	X	7	40.0	40.0	225.10	195.0	
180	1115	B	25	X	1	55.0	55.0	226.35	55.0	
180	1115	B	25	X	2	40.0	40.0	227.70	140.0	
180	1115	B	26	X	1	44.0	44.0	235.84	25.0	
180	1115	B	26	X	1	100.0	100.0	236.40	112.5	

Table T14 (continued).

Leg	Site	Hole	Core	Type	Section	Top interval (cm)	Bottom interval (cm)	Depth (mbsf)	Unconfined compressive strength (kPa)	Vane shear strength (kPa)
180	1115	B	26	X	2	40.0	40.0	237.30	90.0	
180	1115	B	26	X	2	100.0	100.0	237.90	50.0	
180	1115	B	26	X	3	20.0	20.0	238.60	200.0	

Note: This table is also available in ASCII format in the **TABLES** directory.

Table T15. Summary of logging operations, Hole 1115C.

Logging			Mudline depth (mbrf)		Pipe depth (mbsf)		Logged interval (mbsf)	
Run	Tool string	Pass	Drill pipe	Wireline	Drill pipe	Wireline	Bottom	Top
1	Triple combo	Down	1160.3		99.7			102.0
1	Triple combo	Up	1160.3	1161.0	79.7	79.2	784.2	–38.4
2	FMS-sonic	Up 1	1160.3		99.7		787.0	726.0
2	FMS-sonic	Up 2	1160.3	1162.5	79.7		784.0	152.4
2	FMS-sonic	Up 3	1160.3	1162.5	79.7	79.0	787.0	42.0

Table T16. Break times, transit times, depths, and interval velocities for each station occupied during the VSP experiment.

Station	Depth (mbsf)	Hydrophone break time (ms)	Geophone break time (ms)	Transit time (ms)	Interval velocity ($m \cdot s^{-1}$)
8	490.1	74.67	1130.29	1055.62	1881.31
7	505.0	73.66	1137.20	1063.54	2426.14
6	532.1	73.66	1148.36	1074.71	1683.72
5	552.2	73.67	1160.31	1086.65	

Table T17. A comparison of VSP check-shot data with depth estimates derived from physical properties and logging measurements.

VSP depth (mbsf)	VSP TWT (ms)	VSP TWT (ms bsf)	Predicted depth (m)	Error (m)
490.10	2119.7	561.9	485.83	4.17
505.00	2135.5	577.7	502.38	2.72
532.10	2157.8	600.0	524.57	7.53
552.20	2181.7	623.9	547.17	5.03

Note: VSP two-way traveltime (TWT) is converted to two-way traveltime below seafloor (bsf) in column three for comparison to depth measurements made relative to the seafloor.